Taking charge of the surface

Unlocking the potential of InP-based quantum dots

Stam, M.

DOI

10.4233/uuid:b0cb1ce3-2527-421b-a68b-6cce490e713a

Publication date

2025

Document Version

Final published version

Important note

To cite this publication, please use the final published version (if applicable).
Please check the document version above.

Taking charge of the surface

Unlocking the potential of InP-based quantum dots

Maarten Stam

Taking charge of the surface

Unlocking the potential of InP-based quantum dots

Dissertation

for the purpose of obtaining the degree of doctor
at Delft University of Technology
by the authority of the Rector Magnificus, Prof. dr. ir. T. H. J. J. van der Hagen
chair of the Board of Doctorates

to be defended publicly on
Tuesday 7 January 2025 at 15:00 o'clock

By

Maarten STAM

Master of Science in Chemistry
Leiden University, the Netherlands
born in Oud-Beijerland, the Netherlands

This dissertation has been approved by the promotors.

Composition of the doctoral committee:

Rector Magnificus,	chairperson
Prof. dr. A.J. Houtepen	Delft University of Technology, promotor
Dr. ir. T.J. Savenije	Delft University of Technology, promotor

Independent members:

Prof. dr. P. Dorenbos	Delft University of Technology
Prof. dr. F.C. Grozema	Delft University of Technology
Prof. dr. L. Protesescu	University of Groningen
Dr. S. Er	Dutch Institute for Fundamental Energy Research
Prof. J.J. Geuchies	Leiden University

What is a scientist after all? It is a curious person looking through a keyhole, the keyhole of nature, trying to know what's going on.

Jacques-Yves Cousteau

Table of Contents

1

Introduction

1

1.1 Introduction to InP Quantum Dots

Semiconductor technologies have revolutionized our civilization over the past 50 years, in particular through electronic and optical applications. One of the most well-known examples of this revolution is the development of transistors, which operate at key positions in almost all modern electronic devices. Other important examples include the development of solar cells and LEDs, which play a significant role in the development of sustainable energy consumption. Another prominent feature of semiconductors is that their electronic and optical properties depend not only on their composition and structure but also on their size and shape when confined to the nanometer scale, due to quantum mechanical effects.[1-6] By virtue of their tunable energy landscapes, quantized signatures and efficient luminescence, semiconductor nanostructures (also known as quantum dots (QDs), wires or wells) have been widely explored at a fundamental level and can be found in electronic and optical technologies as common as transistors or light-emitting diodes (LEDs).

Surfactant-assisted syntheses of colloidal nanocrystals have enabled the fabrication of an enormous variety of semiconductor nanostructures with remarkable precision in terms of composition, structure and morphology and in high yields. Their freestanding colloidal form also confers great versatility for further integration into devices.[7-11] As the design, stability, performance and functionality of colloidal QDs, wires and wells have evolved over the past three decades, they have become valuable materials for a growing number of optical technologies such as lighting, displays, lasers, quantum information, solar energy converters, infrared cameras, security inks and theranostics.[11-25]

Cd-based QDs are the benchmark for QDs to meet the stringent requirements for optical applications. Cd-based QDs have been developed that exhibit unity efficiency,[26-28] single exponential photoluminescence decay[27, 28] and strong photobleaching[29, 30] and electrochemical stability.[31] However, the use of Cd in electrical and electronic equipment is limited in the European Union through the Restriction of Hazardous Substances (RoHS) directive (Directive 2011/65/EU of the European Parliament).

InP-based QDs have raised considerable interest as alternative for Cd-based QDs in optical technologies operating in the visible and near-infrared (NIR) regions, because of their compliance with the RoHS directive. Additionally, InP-based have wide spectral tunability, strong light absorption, efficient luminescence and high carrier mobility. Advances in their synthesis and design have considerably improved their quality.[32, 33] InP-based QDs can already be found integrated as down-converting phosphors in commercial displays and are being considered for other applications as their qualities improve and expand, such as for gain media or visible and NIR light sources and detectors.[34, 35]

This thesis deals with the surface chemistry of InP QDs and the properties of InP-based QD films upon charging in the context of developing down-converting phosphors for lighting applications. In this Introduction Chapter, the growing field of InP-based QDs from its genesis in the mid-1990s to date is introduced, providing a comprehensive account of its progress and challenges and drawing on relevant knowledge from other types of QDs and from III–V semiconductors as a whole for a more complete picture. The Chapter covers the electronic and optical properties of InP QDs, their synthesis and the occurrence

and passivation of electronic defects. Further, a discussion is provided about the types of QD heterostructures on the basis of InP and about the various optical applications of these systems. Intriguingly, a large body of literature on InP QDs is not always coherent, owing to the structural complexity that these systems can have. Therefore, a critical cross-analysis is included to provide structure, clarity and guidance to the field.

1.2 General Properties of InP

InP is a semiconductor that usually crystallizes in the zinc blende structure. It is considered a relatively covalent semiconductor and has a direct band gap of approximately 1.35 eV in its bulk form (Table 1.1).[36] The band gap is formed between valence orbitals with bonding character and conduction orbitals with antibonding character. Specifically, its valence band edge is characterized by a strong contribution from P3p orbitals, whereas the conduction band edge has a more mixed character, with the largest contribution coming from the In 5s orbitals, as well as a lower density of states as shown in Figure 1.1a.[37] Its band structure is characterized by direct transitions from light, heavy and split-off hole states,[38-40] and its absorption coefficient is relatively strong (>10^4 cm^{-1} at 1.4 eV) as shown in Figure 1.1b.

Table 1.1 Structural, mechanical and optoelectronic properties of selected bulk semiconductors in the zinc-blende or wurtzite (w) structure.[56-61] Lattice constant (a), band gap (E_g), valence band energy (E_{VB}) vs. vacuum, effective density of states (DOS) at the valence band (VB) and conduction band (CB), effective mass of electrons (m_e) and holes (m_h), absorption coefficient (α) at 2.50 eV, Debye temperature (T_D), bulk modulus (B_s) and the Phillips iconicity (PI, a larger or smaller value characterizes a more ionic or more covalent lattice, respectively). For GaP, two m_e values are given (longitudinal and transversal) because the surfaces of equal energies are ellipsoids. lh, light hole; hh, heavy hole.

Material	a (A)	E_g (eV)	E_{VB} (eV)	DOS (VB) (#/eV)	DOS (CB) (#/eV)	m_e	m_h (lh/hh)	α ($\times 10^5$ cm^{-1})	T_D (K)	B_s (GPa)	PI
InN(w)	3.53 /5.69	2	6.43	5.3 x10^{19}	9.0 x10^{17}	0.11	0.27/1.63	1.21	660	140	
GaP	5.45	2.26	5.51	1.9 x10^{19}	1.8 x10^{19}	1.12 /0.22	0.14/0.79	0.01	445	88	0.33
InP	5.87	1.34	5.17	1.1 x10^{19}	5.7 x10^{17}	0.08	0.6/0.089	1.30	425	71	0.42
GaAs	5.65	1.42	4.98	9.0 x10^{17}	4.7 x10^{17}	0.063	0.51/0.082	0.99	360	75	0.31
InAs	6.06	0.35	4.69	6.6 x10^{18}	8.7 x10^{16}	0.023	0.41/0.026	4.53	280	58	0.36
CdSe	4.30	1.7	4.75			0.13	0.45	1.21			0.70
ZnSe	5.67	2.82	5.98			0.14	0.6	-			0.63
ZnS	5.41	3.68	6.53			0.28	-	-			0.62

Owing to the quantum size effect,[1-6] the band gap of InP can be tuned from the NIR (1.3 eV) up to the violet (approximately 2.7 eV) by confining InP to a fraction of its Bohr radius (around 10 nm). The relationship between band gap and volume for InP QDs is displayed in Figure 1.1c.[41] Although the individual band edge shifts are not fully established, it has

1

been suggested that the conduction band levels are more sensitive to quantum confinement than the valence levels, based on simple effective mass arguments and confirmed by more advanced computations (see Table 1.1 for effective masses).[42-44]

At room temperature, luminescence linewidths of approximately 50 meV have been observed from a single InP QD emitting in the red, and around 80 meV for smaller green-emitting dots as shown in Figure 1.1d.[41] [41] For applications such as displays, narrow emission linewidths from CQD ensembles are required. Although the emission linewidth of a single QD is size-dependent and limited by ultrafast structural dynamics and electron-phonon coupling,[45-53] which are, in turn, exacerbated by the presence of electronic traps,[54, 55] the linewidths of an ensemble of QDs is further broadened by its size distribution. Narrower linewidths may be obtainable in QDs with higher quantum yields as well as in core-shell structures.
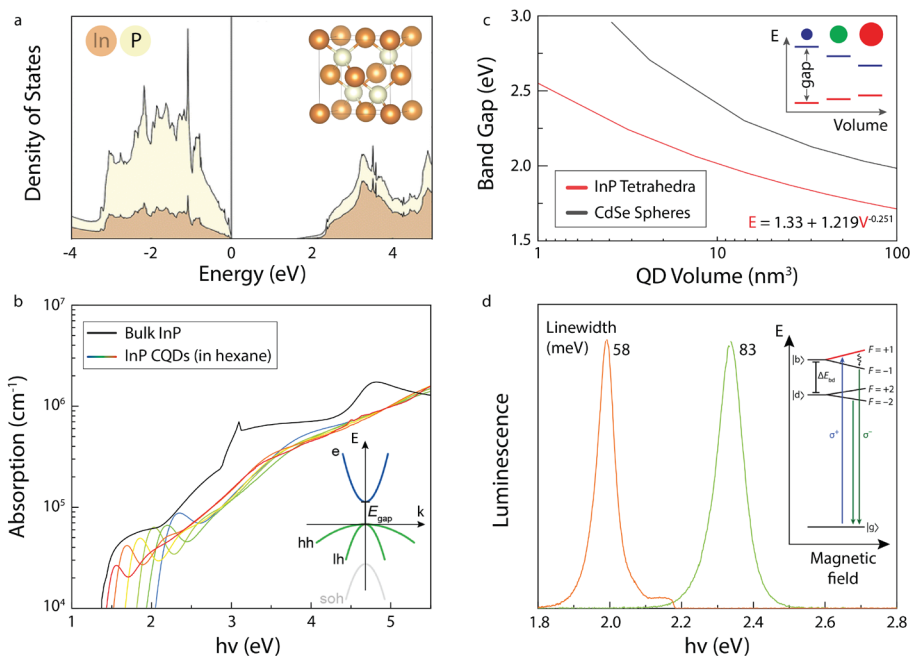
Figure 1.1 Optoelectronic properties of InP: (a) Bulk density of states. The inset shows the zinc-blende unit cell.[37] (b) Absorption coefficients of bulk InP and of InP QDs with edge lengths ranging from 1.5 to 4.0 nm. The inset shows a simplified band structure.[41] (c) Band gap vs. QD volume for InP tetrahedra and CdSe spheres. The inset illustrates the shift of the band edge levels of InP with quantum confinement.[41] (d) Room temperature photoluminescence spectra of single InP QDs emitting in the red and in the green exhibiting linewidths of approximately 58 and 83 meV, respectively. The inset shows fine structure splitting at 4 K. lh, light hole; hh, heavy hole; soh, split-off hole.[41, 63]

In QDs, the electron-hole exchange interaction causes the splitting of degenerate electron-hole pair configurations into various states.[62] Briefly, in zinc-blende QDs like InP, the

4

conduction band edge is formed by a double degenerate electron level, while the valence band edge is formed by a fourfold degenerate hole level. Exchange interactions between these levels, combined with shape anisotropy, gives rise to an exciton fine structure, with an $F = \pm2$ dark lowest exciton state, separated by 2-9 meV from a $F = \pm1$ bright state (depicted in the inset of Figure 1.1d, data from core-shell QDs).[62-64] At room temperature the emission comes from the thermally populated high energy bright exciton state. In principle, this fine-structure splitting is similar to that observed in other tetrahedral binary semiconductors such as CdSe. However, it has been shown that the fine structure in InP QDs is particularly insensitive to shape anisotropy. This phenomenon is attributed to the particular ratio of the light hole over the heavy hole effective mass.[64, 65] In InP, this ratio is 0.149, close to the value of 0.14 in which the exciton fine structure is predicted to be least sensitive to shape anisotropy.[66] As a consequence, the exciton remains nearly isotropic even for prolate or oblate InP QDs. This explains why mixing of the low energy dark exciton with the higher energy bright exciton does not occur in magnetic fields,[65] and why the bright exciton is found to consist of a doublet in single-particle cryogenic PL measurements.[64]

The luminescence of InP QDs is typically limited by electronic traps arising from structural defects and also by Auger processes that take place in the multi-exciton and charged regimes (of relevance for applications such as LEDs or lasers).[13, 67] There has been great progress in mitigating trap-related losses in InP QDs but much less so in solving Auger losses. Non-radiative Auger processes are extremely relevant as InP QDs emitting in the visible exhibit bi-exciton lifetimes of 5–60 ps, three to four orders of magnitude shorter than the single exciton lifetime.[41] In addition, Auger processes produce energetic carriers that can lead to irreversible redox chemistry and device degradation.

Finally, particular applications (such as coherent single-photon emission) require QDs with relatively long coherence times. Although it is known that the coherence times of QDs can be limited by structural dynamics and electron-phonon coupling,[45, 47, 68, 69] and also by fine-structure related transitions,[62, 70-72] no studies of the coherence time have been conducted on InP QDs.

Although we discuss the relationship between structure and optoelectronic properties of InP-based QDs in the following sections, we note that this link is not always straightforward to assess. The QDs in ensembles are not all exactly the same in terms of size, shape, composition, structure and surface coverage, which leads to a distribution in optoelectronic properties. In addition, there are difficulties inherent to physical characterization at such small scales.

1.3 Synthesis of Colloidal InP QDs

Various protocols have been proposed to synthesize InP QDs.[73-92] InP QDs are generally produced by reacting an In^{3+} salt with a P^{3-} source in a liquid medium and in presence of ions and/or molecules (termed ligands) that bind to the surface of the formed QDs, providing colloidal stability. Alternatively, the P^{3-} ion may also be formed in-situ by reducing a phosphorus compound in a higher oxidation state. Of all the methods, two surfactant-assisted syntheses in nonpolar solvents have become the most popular and are

1

currently used in industrial-scale manufacturing.

In one synthesis, described in Figure 1.2a, indium(III) carboxylates of general formula In(RCOO)$_3$ (R = alkyl chain, typically C$_{14-18}$) are reacted with an organic silyl phosphine of general formula P(SiR$_3$)$_3$ (R=alkyl or aryl, typically CH$_3$) at temperatures up to 300 °C.[76, 93-96] This path leads to QDs capped by carboxylates (whether SiR$_3$ groups are also present on the surface remains unclear).[97] When the synthesis is carried out at more elevated temperatures, it delivers the most monodisperse InP QDs of all methods, and impressively narrow linewidths can be obtained by adding trioctylphosphine (TOP, *vide infra*) to the synthesis, as shown in Figures 2b and 2c.[84-86] However, this route is prone to several unwanted side reactions. For instance, free carboxylic acids left from the preparation of the indium carboxylate precursor can react with InP QDs, forming PH$_3$[98]; react with P(SiR$_3$)$_3$ leading to a series of phosphorus precursors of varying reactivity[99, 100]; or condense into ketones releasing water which can then oxidize InP QDs and/or react with indium carboxylates to form In$_2$O$_3$ particles.[97, 101] These side reactions can be suppressed by adding a base (such as TOP), keeping the temperature low, or purifying the indium carboxylate precursor. Nevertheless, even with these adjustments, indium carboxylates themselves may be prone to other side reactions.[102] In addition, the silyl phosphine precursors used are pyrophoric, making them hard to handle and expensive.
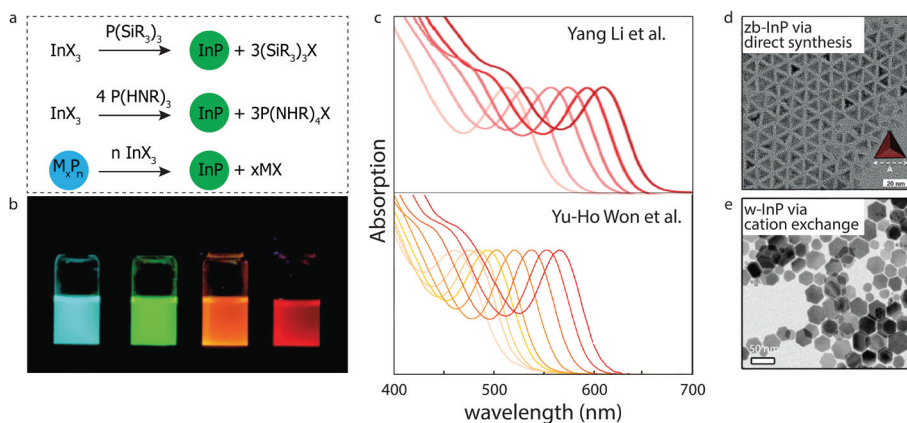
Figure 1.2 (a) InP QDs can be prepared by reacting an InX$_3$ salt (in which X is a generic monovalent anion such as Cl$^-$, RCO$_2$$^-$, etc.) with (top) an organic silyl phosphine P(SiR$_3$)$_3$ or with (middle) an aminophosphine P(HNR)$_3$ in the presence of a reducing agent (such as the aminophosphine itself). Alternatively, InP QDs can also be prepared by transforming (cation exchanging) other metal phosphide nanocrystals into InP QDs. (b) Photograph (under UV light) of samples prepared within our group. (c) Absorption spectra of monodisperse InP QDs with band gaps spanning the visible range prepared using silyl phosphines.[86, 102] (d) Electron micrographs of zinc-blende InP QDs with tetrahedral shape.[89] (e) Electron micrograph of wurtzite InP QDs in the form of platelets.[103]

The other common route to prepare InP QDs, also displayed in Figure 1.2a, is based on the reaction of indium(III) halides (typically InCl$_3$) with aminophosphines of general

formula $P(HNR)_3$ (typically formed in-situ by the reaction of primary alkyl amines RNH_2 with $P(NR_2)_3$ precursors). The aminophosphines act simultaneously as a P-source (in an oxidation state of +3) and as reducing agent (to reduce P to -3).[88-90] This method forms QDs capped by halide ions and alkylamines. Alternatively, indium(I) halides and/or PX_3 (X = Cl, Br or I) may be used as precursors.[104-106] Compared with the first route, this route has been less studied and cannot yet produce QDs as monodisperse,[107] but it is definitely more cost-attractive owing to its cheaper precursors.

It is not well understood how the different chemicals used in each of these synthetic routes affect the growth mechanism, reaction kinetics or morphology of the resulting InP QDs. Studying the growth kinetics has long been complicated by oxidation of InP QDs during the synthesis, which was only recently circumvented by using reducing atmospheres.[108-110] Nevertheless, it is known that the growth of InP QDs using indium carboxylates and $P(SiR_3)_3$ precursors proceeds through the formation and ripening of cluster intermediates[111-117] whose structure has been identified[118] and also that these clusters can be employed as single-source precursors for synthesizing InP QDs.[85, 112] Other noteworthy advances include preliminary studies on the determination and control of the reaction kinetics using various aminophosphines,[119] the investigation of nucleation and growth through computational methods,[120] and the successful development of continuous production methods.[121-127]

Shape-wise, both routes yield InP QDs that appear in electron micrographs to adopt a triangular pyramidal shape, as shown in Figure 1.2d. Large InP QDs synthesized by the aminophosphine route have been found to derive their eventual tetrahedral shape from smaller, early-stage tetrapod InP QDs whose arms are enclosed by (110) facets.[128] Interestingly, the tetrapod shape could be controlled to a certain degree by controlling the reaction temperature and amount of precursors. The experimentally observed tetrahedral shape has been rationalized as fulfilling the requirement of charge neutrality with common monovalent ligands, such that (100) facets are unlikely to be expressed in cation-rich InP QDs and a (111) termination is more favourable.[44] Following this line of reasoning, other possible shapes include truncated pyramids and small-sized cuboctahedrons with (100), (111) and (-111) facets. Density functional theory calculations also show that both bare and ligand-terminated (111) facets exhibit a lower surface energy than (100) facets.[129]

Ga-substituted and As-substituted alloys of InP can also be synthesized using variations of the aforementioned routes.[130-134] However, control over morphology and structure of InP-based QDs through direct synthesis remain a challenge.[135] Nonetheless, morphology-controlled InP QDs can still be prepared indirectly, by transforming (cation-exchanging) other metal phosphide nanocrystals into InP QDs while persevering the original phase and morphology, as illustrated in Figure 1.2a. In this way, hexagonal (wurtzite) InP platelets, shown in Figure 1.2e, and InP rods could be successfully prepared from their Cu_3P analogues.[103, 136-138] Control over the exchange rate is important to ensure that single crystalline InP QDs are obtained.[136]

Surface ligands have a key role not only in the synthesis, colloidal stability and self-assembly of QDs but also in many of their optoelectronic properties (such as trap passivation, electron-phonon coupling, carrier delocalization and film conductivity). Ligands also

1

enable post-synthetic surface functionalization. In fact, surface-ligand engineering of QDs has been intensely investigated[134, 139, 140] and reviewed.[10, 141-143]

## 1.4 Defects and Trap Passivation

As-synthesized InP QDs typically exhibit weak luminescence efficiencies, of a few percent at most (often <1%). Defect passivation and shelling approaches allow InP QDs to be prepared with near-unity efficiencies. Various types of defects are possible in InP materials in general (including QDs and thin films), but can be passivated and mitigated with several strategies as displayed in Figure 1.3.

1.4.1 Oxidation and etching.

III-V semiconductors, including InP, are well known to be prone to oxidation which limits their growth and luminescence efficiency.[86, 109, 144-152] Oxygen is known to adsorb dissociatively on (bulk) InP surfaces,[153-156] and at room temperature In-O-P and PO_x species (x > 1) form at oxygen pressures as low as 5 µbar and 5 mbar, respectively, highlighting the strong reactivity of the phosphide anion towards oxidation. Further structural transformations occur at higher temperatures, including the bridging of PO_x units at around 200 °C and the development of a thick indium oxide layer at temperature above 300 °C, underlining the diffusion of oxygen.[155, 157] Water also appears to adsorb dissociatively[155, 158] and to lead to the formation of In-O-P and PO_x species upon mild heating (100 °C). In-O-In species can also form, more likely on exposure to oxygen than to water.[155]

This tendency to oxidize poses difficulties for the synthesis (and shelling) of InP QDs,[99, 101, 108, 159, 160] and indeed hydroxyl groups[161] and oxidized phosphorus have been identified on InP QDs[97, 147, 148, 150, 162, 163] as depicted in Figure 1.3, location A-D. The sources of oxidation and types of oxidative defects are likely various, and their impacts on the electronic structure of InP QDs remain unclear. The absence of oxidized species often appears to be correlated with increased luminescence efficiency,[86, 148-150, 152, 164] although opposite results have also been observed.[159, 165-171]

Computational studies are especially suitable to elucidate the effects of oxidation, even though research has mainly been limited to flat (001) surfaces without ligands.[154, 157, 172, 173, 200-202] Some of these studies report the appearance of traps states upon oxidation,[154, 157, 172, 202, 203] but the underlying mechanisms that lead to trap formation are not entirely understood. For example, Santosh and coworkers reported that only substitutional oxygen atoms produced trap states, while In-O-P and In-O-In moieties formed by oxygen adsorption did not lead to trap formation.[154] In contrast, in their study on oxygen adsorption on (001) GaP and InP surfaces,[172] Wood and coworkers found that strained In-O-In moieties can give rise to hole traps. Additionally, In-O-In, In-OH-In and In-In were found to give electron traps if the In-atoms have unsaturated bonds. In-O-P bridges are generally believed not to lead to trap states,[172, 173] although Wood and coworkers did observe an increased number of energy levels near the valence band edge.[172] This collection of results indicate that trap formation is highly dependent on the exact configuration of the oxidized species. Indeed,computations on ligand passivated QD models by Ubbink and coworkers found that hole traps are formed by PO_2 moieties, but not by PO_3 and PO_4.[98] The effect
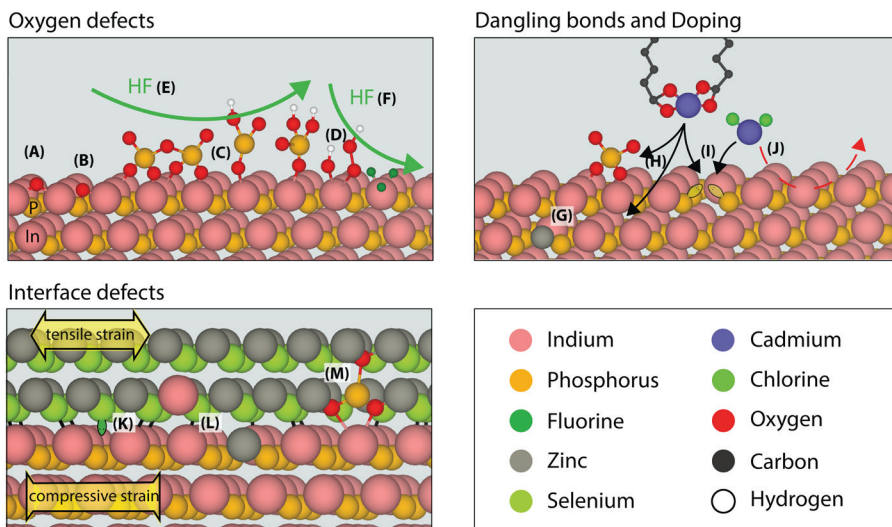
Figure 1.3 Documented structural defects in InP QDs and possible repair mechanisms. Oxygen defects include (A) In-O-In moieties,[154, 155, 172] (B) In-O-P moieties,[154, 155, 157, 158, 172, 173] (C) PO_x moieties,[97, 98, 147, 148, 150, 155, 157, 162, 163] (D) In-OH and In-OOH moieties.[161, 172, 174] Several mechanisms have been proposed for the passivation of oxygen defects using HF including (E) the breaking of PO_x into smaller PO_3 and PO_4 units[98] or (F) the replacement of In-bound hydroxide groups by fluoride anions[174] (G) Lattice doping[91, 149, 175-183] and (H) Incorporation of Cd in surface and subsurface[175]. (I) Dangling phosphorus bonds can be healed via Z-type passivation[44, 98, 184-187] but (J) Z-type exchange is also possible.[164, 188] In core-shell structures, (K) strain-induced interfacial defects,[177, 189-194] (L) mixed interfaces[182, 195-199] and (M) interfacial oxides[97, 147, 166] may also occur.

of polyphosphates remained uncertain due to their unclear oxidation state (leading to n-doping of the QDs) and to the large number of possible surface reconstructions. In addition, Park et al. have investigated the effect of various metal oxide shells around InP QDs and found evidence for localized defect-like states near their surface in InP/InO, InP/GaO, and InP/AlO core-shell systems but not in InP/CdO and InP/ZnO.[204] Although these results do not cover the entire range of possible oxidated species, they do show that oxidation does not necessarily have detrimental effects, which may explain the seemingly contradictory reports on the effects of InP oxidation.

Nevertheless, it is possible to prepare oxide-free InP QDs either under strictly anhydrous and oxygen-free reaction conditions or by using a hydrogen atmosphere as was recently demonstrated.[109, 110] Post-synthetic treatments can also remove oxidative defects. A popular post-synthetic treatment is etching with hydrogen fluoride (HF), as depicted in Figure 1.3 (process E and F). HF etching was used to clean and expose the surface of InP thin films as early as the 1960s[205] and it was later shown to produce a completely oxide-free InP surface, which was unachievable with other etching agents.[206] The application of the HF treatment to InP QD was first reported on by Mićić, *et al.* and an increase in luminescence was observed after the treatment, which was attributed to fluoride ions filling phosphorus

1

vacancies on the surface and replacing oxygen in the oxide layer.[146] Since then, different mechanisms have been proposed for trap passivation by HF. One possible mechanism for the increased luminescence after HF treatment under illumination is through the removal of the phosphor as PF_3, leaving an indium-rich surface that could be better passivated by ligands;[207, 208] elimination of phosphorous dangling bonds by fluoride was also supported by transient absorption results.[151] Alternatively, the increased quantum yield after HF treatment has been ascribed to the passivation of indium dangling bonds. This explanation is supported by observations that after HF treatment, carboxylate ligands exchange for fluoride ions and indium(oxo)hydroxides on the nanocrystal surface are removed.[174] Other studies have suggested that HF removes oxygen as PO_x species, rather than as indium hydroxides.[86, 209] Recently, Ubbink *et al.* found that anhydrous HF reacts with InP forming InF_3 (a Z-type ligand) and PH_3, and breaks up polyphosphate species into smaller PO_4 and PO_3 units. Although removal of polyphosphates was correlated with a higher luminescence efficiency, PO_4 and PO_3 species remained present on the surface of highly luminescent HF-treated samples, indicating that only some oxidized species form traps.[98] Given these varied results, it remains an open question as to which types of oxides can be removed by HF treatment, and in what ways their removal affects the optical properties of nanoscale InP. HF treatment does have downsides: InP itself can be etched, causing unwanted spectral changes, and there are inherent dangers associated with using HF.

Because HF is hazardous, alternative fluorination strategies have also been proposed. Adding fluoride-rich ionic liquids either during the synthesis under microwave illumination, or post-synthetically, can strongly improve the quantum yield of the particles.[188, 210] This effect has been ascribed to the passivation of electron traps when fluoride binds to dangling indium bonds.

1.4.2 Surface states and Z-type passivation.

The main suspect for trap states in QDs has always been dangling bonds – that is, undercoordinated atoms at the surface of nanocrystals. Early theoretical calculations by Fu and Zunger,[185] predicted the existence of both electron and hole traps on the surface of InP QDs as a result of In and P dangling bonds, respectively. The traps appear to become "deeper" as the QD size is reduced, owing to the shift of the band edges. These conclusions are also corroborated by the experimental work of Cho, *et al*.[184] Additionally, it has been shown that the formation of trap states owing to undercoordinated surface atoms depends shape of the QD.[44] In this work, cuboctrahedral and In(111)-terminated tetrahedral models are deprived of a surface capping moiety to simulate undercoordinated surface atoms. For cuboctahedrons, surface reconstruction prevents, in most cases, the formation of hole and electron traps. However, tetrahedral-shaped models are prone to form localized trap states within the band gap resulting from undercoordinated In and P atoms.

Surface anions can be passivated by treating the particles with metal salts, also known as Z-type ligands as shown in Figure 1.3, process I.[164, 175, 186-188] Treatment of InP with various Z-type ligands has been shown to increase the quantum yield (to 19% for Zn carboxylates and 49% for Cd oleate[186] or 11% for $CdCl_2$[187]), which has been attributed to the passivation of dangling phosphor bonds. However, there is also evidence that cadmium

carboxylate Z-type ligands can bind both to phosphor and to phosphate present in the (sub)surface of InP nanoparticles as displayed in Figure 1.3, process H.[175] More recently, it was shown that simple Z-type passivation with InF_3 can increase quantum yields to 50-80% if the QDs are free of oxidized phosphorous species, specifically polyphosphates.[41, 98] In addition, it was also observed that Cd^{2+} or Zn^{2+} can also replace surface In^{3+} ions (Z-type ligand exchange, shown in Figure 1.3, process J), relieving steric pressure on the surface and allowing for a more complete passivation, thus reducing the number of trap states.[188] This exchange mechanism was supported by isothermal titration calorimetry experiments monitoring the treatment of InP with metal halides.[164] These results suggest that the Z-type passivation mechanism may be more involved than previously thought.

Surface reconstructions may also have an important role in the creation or removal of surface states. In bulk solid state physics, it is well known that surfaces directly obtained from cleaving the bulk material are often not stable and will reconstruct.[211] For example, studies on GaAs surfaces have shown that the Ga-terminated (111) facet will reconstruct by creating Ga-vacancies.[212] As-terminated (-1-1-1) facets are more complicated, and different reconstructions based on vacancies[213] or As-trimers have been proposed.[214] Although these reconstructions are relatively well understood for bulk surfaces, it is currently unclear whether they also take place on the QD surface. One study by on CdSe QDs has shown that surface vacancies are necessary for the delocalization of the highest occupied molecular orbital and lowest unoccupied molecular orbital levels,[215] highlighting the need for further studies on QD surfaces.

1.4.3 Doping.

Impurities have long been incorporated into III-V semiconductors for doping purposes.[216] The incorporation of cations (other than group III) into InP QDs, however, has been pursued for two main reasons: optical doping (that is, Stokes-shifted emission) or linewidth narrowing. For instance, doping with Eu^{3+} yields multiple emission lines around the red spectral region.[217] Doping with Cu^+ yields a broad emission in the near-infrared-I window (with photoluminescence efficiencies up to 80%) ascribed to hole localization and to structural relaxation around the Cu site.[218-225]

Zn^{2+} ions are commonly introduced as additives during the synthesis of InP QDs to obtain QDs with narrower (ensemble) linewidths.[176, 177, 226] However, aliovalent impurities such as Zn^{2+} are known dopants for III-V semiconductors,[178-181, 227] and appear to diffuse and be incorporated into InP QDs, as illustrated in Figure 1.3, location G.[175, 228] Various spectroscopic analyses have concluded that the incorporation of Zn ions introduces shallow hole states and associated lattice disorder.[180] Moreover, results by Li et al. and Shen et al. suggest that the incorporation of Zn in the InP core limits the performance of core-shell structures.[149, 182] Nevertheless, PLQYs of approximately 90% have been reported for both InP and In(Zn)P QDs shelled with $ZnSe_{1-x}S_x$, (where In(Zn)P = InP QDs incorporating Zn in the InP lattice).[91, 149, 171, 183, 229-231]

Several questions about doping remain open, including what lattice positions the extrinsic ions occupy, whether electronic doping occurs or whether there are doping compensation mechanisms at play.

1

1.4.4 Heterovalent core-shell interfaces.

Epitaxial growth of II-VI on III-V semiconductors (including InP QDs) has been extensively investigated. The heterovalent nature of such interfaces introduces complexity, and it is worthy to highlight insights from works on lattice matched GaAs/ZnSe (001) polar junctions. First, we note the efforts to reduce the density of stacking faults in the ZnSe overlayers.[232, 233] Second, computational studies have shown that an abrupt interface is thermodynamically unstable and that a mixed and/or a defected interface is energetically favoured (Figure 1.3, location L),[195, 234] and experiments also support the existence of mixed and defected interfaces in samples with a low density of stacking faults.[197] Furthermore, the composition of stable mixed interfaces is known to be orientation dependent.[198]

Coating InP QDs with $ZnSe_{1-x}S_x$ shells enables highly efficient and stable emitters. A few studies have highlighted the importance of achieving a balanced stoichiometry in these III-V/II-VI core-shell systems.[149, 182, 235, 236] In particular, results from Li et al. and Shen et al. strongly suggest that an InP/(In,Zn)P/ZnSe interface boosts the photoluminescence efficiency of $InP/ZnSe_{1-x}S_x$ QDs beyond 90%,[182, 199] and that a selenium-terminated interface might be important to limit the diffusion of zinc[237, 238] and sulfur[149, 236] into the InP cores. Interfaces containing oxidized species have also shown to improve the performance of InP QDs (Figure 1.3, location M).[166, 239]

1.4.5 Strain.

In core-shell QDs, strain can arise from the lattice mismatch between core and shell materials, causing several consequences.[240] It can introduce (strain-relieving) defects as depicted in Figure 1.3, position K,[241] alter band offsets,[242, 243] shift vibrational frequencies,[244] give rise to piezoelectric fields,[245] or even impact the fine structure,[246-248] the electron-phonon coupling,[249] and photon out-coupling.[250]

However, little is known about strain engineering in InP QDs. In bulk InP, a phase transition (to rock salt) closely followed by a direct-to-indirect transition (as the X band crosses under Γ) occurs at lattice contractions of about 3-5 % (approximately 10 GPa),[189, 190] and similar values are found for InP QDs.[191, 192, 251] In $InP/Zn_{1-x}Cd_xSe$ core-shell systems, strain can be tuned from compressive (InP/ZnSe) to tensile (InP/CdSe) with no strain observed when x is approximately 0.4.[193] Computational investigations by Suh et al. suggest that even a thin ZnSe can build considerable tensile strain and could lead to a considerable energy shift of the highest occupied molecular orbital.[177] More pronounced effects are found with ZnS shells, which could be related to not only its smaller lattice constant but also its larger Young modulus (see Table 1.1 for mechanical properties).[194] These computational results also point to a decrease in band gap with increasing tensile strain. However, experimental results have shown the opposite trend: a substantial increase in band gap is observed with increasing tensile strain, which could be of potential interest for piezochromic applications.[191, 192]

### 1.5 Wavefunction Engineering

Control over the energy landscape is fundamental in QD technologies.[13, 14] Although tuning the surface ligands might achieve this control to a limited extent,[174, 252] shape-control

and core-shell structuring are more versatile and robust avenues of control. Core-shell structuring, in particular, has been pivotal in the development of performant and stable QDs. For instance, in type I heterostructures, both the electron and hole wavefunctions are confined to the core, which allows undesirable surface states and reactions to be avoided. In type II heterostructures, the electron and hole wavefunctions are spatially separated, which allows the radiative lifetimes to be increased and the band gap to be reduced. It is important to note that the band offset is one of the key parameters in the classification and design of semiconductor heterostructures (displayed in Figures 4a and 4b). However, determining the band offsets in QD heterostructures is not straightforward because the degree of quantum confinement needs to be taken into account, as well as any interface dipoles.[253] The latter is particularly relevant to heterovalent systems such as $InP/ZnSe_{1-x}S_x$ core-shell structures.[254]

1.5.1 Type I InP/ZnSe1-xSx core-shell structures

Type I $InP/ZnSe_{1-x}S_x$ core-shell QDs have been widely studied and implemented in commercial products. ZnSe and ZnS exhibit complementary properties for shelling InP. On the one hand, ZnSe has a small lattice mismatch to InP (3.4 %) but does not provide a robust type I confinement, especially for smaller InP cores. On the other hand, ZnS ensures a robust type I band alignment (regardless of core size) but has a relative large lattice mismatch (7.8 %), which appears to broaden the emission of the QDs.[255] Finding a balance between the size of the InP core and the composition and structure of the $ZnSe_{1-x}S_x$ shell, can overcome these limitations and highly efficient narrow band emitters can be obtained (see Figures 4c and 4d). For instance, red-emitting InP/ZnSe/ZnS core-shell-shell structures with near-unity photoluminescence efficiency and linewidths of 110-130 meV have been realized (including non-blinking QDs),[86, 149, 209] as have green-emitting $InP/ZnSe_{1-x}S_x/ZnS$ (0.5 < x < 0.67) heterostructures with efficiencies around 90 % and slightly broader linewidths (160-210 meV).[91, 229, 230, 255] Blue emitting systems are, so far, least performant with efficiencies and linewidths of 45% and 260 meV, respectively.[231, 256] It is not yet clear why green-emitting and blue-emitting QDs have lower performance than red, but it could be related to the interfacial defects and strain induced by the increased lattice mismatch of the shell and to the fact that strain is more problematic for smaller structures as they are less able to relax strain within the material.[194] Interfacial strain can be relieved by alloying the $ZnSe_{1-x}S_x$ shell with other divalent cations.[193, 257] In addition, the efficiency of green and blue emitters could be limited by defects in the shell (stacking faults, impurities and so an).[199, 258-264] The broader linewidths likely arise from a combination of synthetic and intrinsic drawbacks inherent to the extremely small sizes of the InP cores (such as size distribution requirements and increased homogeneous linewidths), but can be made more narrow by Zn doping of the cores. Blue-emitting and green-emitting $In(Zn)P/ZnSe_{1-x}S_x$ core-shell QDs with improved quantum yields and narrower linewidths have been demonstrated, although their structures remain unclear and might be quite complex.[91, 149, 171, 183, 229-231]

Despite their remarkable efficiencies and stabilities, these QDs have room for improvement. For instance, the relatively thick $ZnSe_{1-x}S_x$ shells make the QDs less compact, which can undermine phosphor and lasing applications. Another perhaps more pressing limitation is their relatively short bi-exciton lifetimes, preventing efficient operation at high exciton

1
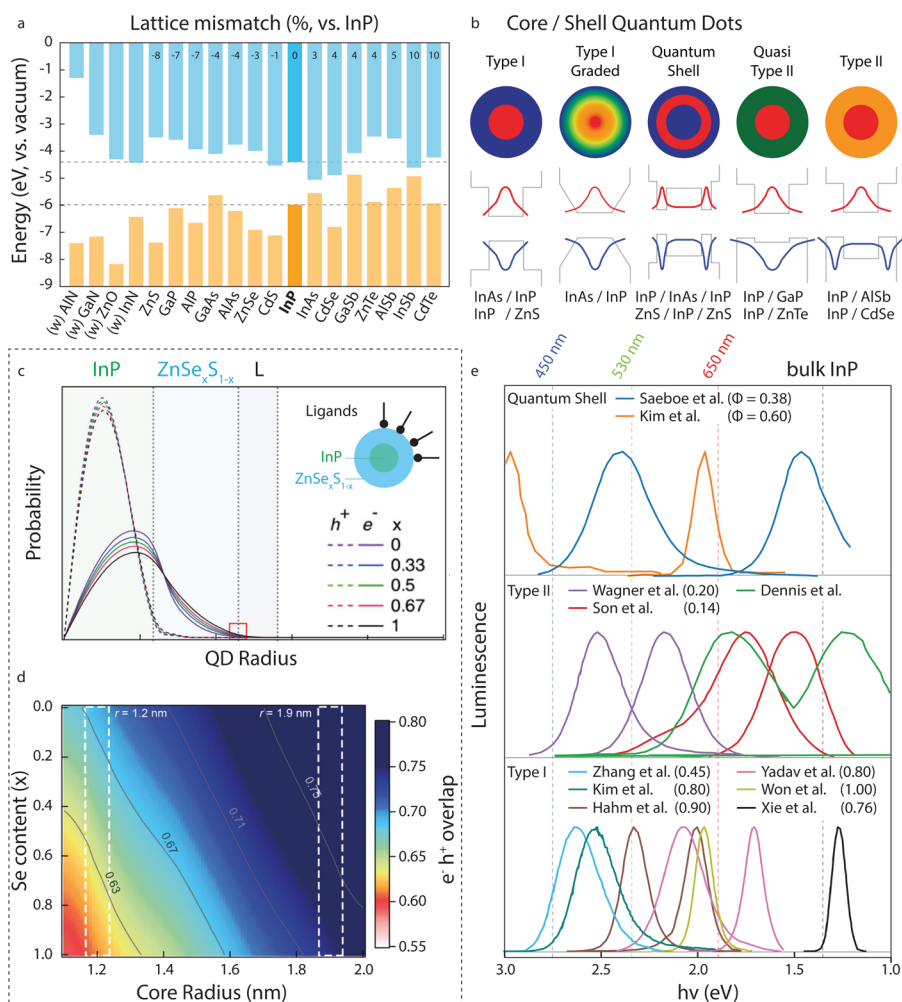
Figure 1.4 InP-based core-shell QDs (a) The band offsets of bulk semiconductors[57, 265] are usually used as a first approximation in the design of core-shell QD structures. (b) Core-shell structures can be classified into various types according to the (de)localization of electron and hole wavefunctions (the electron and hole probability distribution functions are depicted in red and blue, respectively. In fact, quantum confinement also has an important role in the design, and in InP the conduction levels are thought to be more sensitive to it than the valence band levels. For instance, type I confinement in InP/ $ZnSe_xS_{1-x}$ QDs is achieved by (c) employing shells with a large sulfur content and/or (d) by employing larger cores.[255] (e) Photoluminescence spectra of selected InP-based core-shell structures emitting in the visible or near infrared, reported efficiencies Φ in parenthesis.[86, 106, 231, 255, 266-272]

density.[86] For instance, highly efficient red-emitting InP/ZnSe/ZnS core-shell-shell QDs exhibit exciton lifetimes of 13 ns but bi-exciton lifetimes of only 50 ps.[86] In this system, the negative trion is rather long lived (5.3 ns), owing to the delocalization of

the electron wavefunction into the thick ZnSe shell (3.5 nm),[273] suggesting that the short biexciton lifetime results from a sharp hole confinement. Smoothing the confinement potential using compositionally graded core-shell QDs might be an effective approach to mitigate this, as it has found enormous success in II-VI QDs. Graded $ZnSe_{1-x}S_x$ shells grown on InP QDs have not only extended the negative trion lifetimes by approximately four times but also reduced luminescence intermittency (blinking) and spectral diffusion as the grey state appears to originate from the negative trion itself.[91, 274, 275] These type of shells should allow to improve the performance and stability of quantum LEDs (QLEDs) as excess electrons often accumulate in the QD layer owing to the imbalanced charge injection rates; however they do not fix the sharp hole confinement at the core-shell interface and therefore are unlikely to increase bi-exciton lifetimes.[276] This analysis indicated that, at room temperature, gain can be understood as originating from state filling of the lowest electron level with a degeneracy of 2 and of the lowest hole level with an effective degeneracy of 5-10. This effective hole degeneracy is higher than the expected degeneracy of 4, which was attributed to thermal population of higher states in the valence band, perhaps arising from the ZnSe shell. In addition, it was also observed that optical gain was limited to about 10 % of the theoretical maximum value owing to a loss of charge carriers at high exciton density attributed to hole trapping. Hole trapping in this system has also been studied in other works and has been scribed to In atoms in the ZnSe shell.[261, 277]

1.5.2 The quest for all III-V type I core-shell QDs

In principle, shelling InP with a III-V semiconductor should enable QDs with dipole-free interfaces and the graded core-shell structures needed to mitigate Auger-related losses.[278-283] In fact, lasing-quality has been demonstrated using vapor-phase grown InP QDs encapsulated by $Al_xGa_yIn_zP$ layers.[284] However, InP QDs with III-V shells remain rather unexplored for a number of reasons. First, the two evident shelling materials, $In_{1-x}Ga_xP$ and $In_{1-x}Al_xP$, are characterized by a direct-to-indirect crossovers at x = 0.8 and 0.4 respectively, which complicates the prediction of band offsets. Furthermore, it is not clear whether these materials can effectively provide a type I confinement to InP QDs.[285-288] Second, due to their indirect nature, GaP and AlP shells would strongly reduce the absorption cross-section of the QDs. Third, similar to InP, these materials are prone to oxidation and many Ga precursors appear to react with InP QDs to form $In_{1-x}Ga_xP$ alloys, complicating the growth of core-shell structures.[266, 267, 289] The few reports on these structures have been limited to InP/GaP core-shells, mostly in combination with ZnS outer shells.[266, 290-292] Mixed-anion alloys also remain unexplored but could be another avenue to access wide direct gap shelling materials with a type I band alignment. For example, vapour-phase grown $InP/GaAs_{0.6}P_{0.4}$ dot-in-a-well lasers have been demonstrated.[293]

According to bulk band alignments, InP could also be envisaged as a (type I) shell material for infrared emitting InAs QDs. InAs/InP and $InP_{1-x}As_x/InP$ core-shell QDs have been developed to emit in the range of 600-1000 nm.[131, 268] Although their photoluminescence efficiencies were initially quite low (<5%), subsequent shelling with ZnSe allowed for significant improvement (to around 76%). Similarly, for multishell In(Zn)As/In(Zn)P/GaP/ZnS QDs emitting at around 800-1000 nm, the photoluminescence efficiency of the In(Zn)As core (2.5%) increased to 33%, 46% and 75% with each successive shell.[294-296]

1

1.5.3 Reverse core-shell-shell structures

Reverse core-shell-shell structures, also known as quantum shells offer further band gap tunability and room for mitigating Auger losses.[297-301] In this configuration, an InP mid-shell is grown in between a core and an outer shell of wider gaps, with the band gap determined by the core size and the shell thickness. For instance, systems such as ZnSe/InP/ZnS and CdTe/InP/ZnS QDs have been shown to exhibit tunable and efficient emission between 700-900.[269, 270, 302] However, these structures have not been much explored, and whether they can actually mitigate Auger processes remains an open question.

1.5.4 Type II and quasi-type II structures

Type II and quasi-type II structures allow for spatial delocalization and separation of electrons and holes within the dot, which, in turn, reduces the band gap and increases the Stokes shift as well as the carrier lifetimes.[303-305] These structures have found interest for photovoltaic and photo-electrochemical cells,[306-308] photo-catalysis,[309] down-converters for solar concentrators[310] and gain medium[311, 312]. For example, in NIR-emitting InP/CdS core-shell QDs, both the exciton and bi-exciton lifetimes increased with increasing shell thickness, with values up to 702 ns and 7 ns respectively.[271] In addition to this remarkable increase in lifetimes, the charge transfer rate to methylviologen[313] and the multiple exciton generation quantum yield[314] are also not affected by the quasi-type II band alignment, making these QDs interesting for QD-based solar cells. Cd-free alternatives expand their potential to biological applications. For instance, InP/ZnTe/ZnSeS QDs emitting in the NIR have been realized with exciton lifetimes of 387 ns.[272] InP/ZnO QDs have also been proposed for LEDs,[170, 315] solar concentrators[167] and artificial retinas[316] although the exciton lifetimes in these structures appear to be shorter, around 31 ns. The luminescence efficiency of type II QDs can be limited by surface traps, but in principle this can be mitigated by efficient surface passivation or by growing an outer type I shell.[170, 317]

1.6 InP QDs in Optical Technologies

1.6.1 RGB Phosphors

Cyan, green and red QDs with bright, narrow and stable emission are strong contenders for optical down-conversion in display and lighting technologies. Down-converting blue light into red or green through a QD film is a simple and efficient way to upgrade a blue LED array into a full color display (Figure 1.5a). Down-converting blue into both red and green light is also appealing for constructing white emitting diodes using a single blue source (Figure 1.5a), and it circumvents both the poor efficiency of green as well as the high cost of red in the three-diode approach to white light generation. In addition, the tunability of QD phosphors enables the generation of customized spectral outputs.

For QDs to be used as down-converters in high-intensity applications such as LED lamps, they require strong blue absorptivity, narrow emission line (color purity), near-unity quantum yield, stability at elevated temperatures and at high photon fluxes (no droop). Such properties have been obtained for Cd-based type I QDs,[318] but droop remains a major challenge in InP-based QDs.[263] Various design strategies can mitigate Auger recombination in InP QDs, such as trap passivation[151] and incorporating a thick

mid-shell[44] or graded shell[275]. In the latter approach, negative trion Auger recombination can be strongly reduced though potential smoothing in gradient shells, but extended bi-exciton lifetimes remain elusive in these systems. Furthermore, the brightness of InP QDs is limited by the relatively weak blue absorptivity of thick $ZnSe_{1-x}S_x$ shells, so innovative shell engineering solutions such as more compact shells[319] or alternative materials[320] may be required. Smaller InP QDs also exhibit wider linewidths and lower efficiencies, although incorporating Zn into the cores overcomes these limitations.[229]

Commercial use of InP QDs as blue-down-converters in display and lighting technology seems close on the horizon. Red InP QDs have already been shown to be a viable on-chip solution for use in white LEDs using traditional green-yellow phosphors.[321] White LEDs composed fully of InP QDs were also achieved in an early demonstration by avoiding Förster resonance energy transfer processes between QDs of different colors (sizes), in this case red and green.[322] Furthermore, InP QDs are being integrated into up-and-coming μLED displays.[17, 323] Finally, InP QDs may be a solution to the growing interest in cyan phosphors for healthy lightning[324-328] and may be of interest for specialty applications such as custom illumination (for example, indoors or in horticulture), green-house roofs, security inks and so on.

1.6.2 Electroluminescent QLEDs

Theoretically, electroluminescence is a more efficient way to obtain light from QDs compared with down conversion, and there have been many attempts to construct InP QD-based LED devices to this end (Figure 1.5a).[17, 35, 86, 149, 329-336] Electroluminescent QLEDs are particularly appealing for display applications, because the high color purity of red InP and green In(Zn)P QLEDs already closely agrees with the requirements for a wide color space of rec2020 standards (Figure 1.5b).[34] Currently, record efficiencies stand at 22.2% for red[209], 16.3% for green[337] and 2.8% for blue[338, 339] devices. To construct highly efficient LEDs, device structure and materials must be carefully chosen to ensure exciton confinement inside the QDs in order to prevent parasitic or trap emission in the device (this can be achieved by growing a thick type I shell around the InP cores)[330] and balanced electron and hole injection currents. Compared with II-IV materials, the high-lying valence band edge of InP QDs makes electron (hole) injection comparatively hard (easy).[330] Despite the impressive near-limit efficiencies reached in red InP/$ZnSe_{1-x}S_x$ QLEDs, the efficiency droop at higher operation power and the lifetime still need to be improved (Figure 1.5c).

1.6.3 Into the infrared.

Light sources in the far-red and near-infrared range are increasingly required for applications in biology and medicine,[340-344] computer vision[345] and data transmission at both short and long (fiber) ranges.[284, 346-348] Infrared QDs in this range,[349, 350] owing to their small size, tunable surface chemistry and processing versatility, extend the application window of these light sources to miniaturized devices such as μLEDs or photonic chips,[17, 25] nano-imaging,[351] fluorescent (bio) markers,[352] optical sensors, security inks and so on. In addition, infrared QDs with high absorption cross-sections and carrier mobilities are of great interest for infrared detection and imaging technologies[353] and for photovoltaics.[354]

1
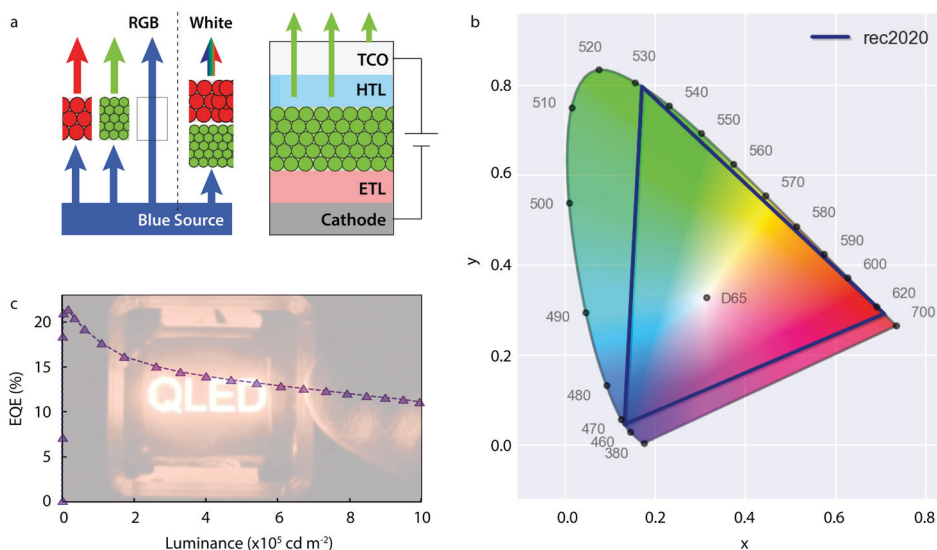
Figure 1.5 InP-based QDs in LEDs. (a) In luminescent down-converting devices, QDs convert blue photons into less energetic photons (such as green or red) shown on the left, whereas in electroluminescent devices QDs convert electrical energy into photons as shown in the right. (b) The high color purity of red InP and green In(Zn)P LEDs is already in close agreement with the requirements for a wide color space of rec2020 standards (the corners of the triangle are the coordinates of highly pure red, green and blue, and D65 represents the coordinates for white light). At low powers, QDs with near-unity photoluminescence efficiencies have been successfully implemented in efficient LEDs. However, at high powers, the efficiency droop remains a problem. This can be clearly seen in (c) the external quantum efficiency of an electroluminescent InP-based QLED as a function of brightness.[86] EQE, external quantum efficency; ETL, electron transporting layer; HTL, hole transporting layer; RGB, red, green and blue; TCO, transparent conducting oxide.

In spite of a bulk band gap of 1.35 eV, and most research being conducted on green and red sizes, InP is still in the competition for far-red to short-wave infrared (<1 eV) applications. Although the synthesis of large-sized InP QDs remains challenging, InP structures emitting in this range have been reported, namely, wurtzite QDs,[137] reverse hetero-structures, $InP_{1-x}As_x$ alloys,[131, 134] doped QDs and InAs-InP core-shell QDs, together with early demonstrations of in vivo imaging, [131, 269, 355] solar cells,[356, 357] LEDs[295, 296] and photo-detectors[358] (see Figure 1.6). In addition, InP QDs have been used in efficient (photon) up-converting systems.[359] Large-sized InP QDs are expected to have higher absorption cross-sections, narrower linewidths, longer bi-exciton lifetimes and higher film mobilities (although still limited to <0.5 cm^2 V^{-1} s^{-1})[140] compared with their smaller counterparts – appealing characteristics that continue to motivate their development.

Broadband infrared sources based on InP QDs can also be envisaged, either by combining

InP QDs emitting at various wavelengths (as in the case of the white LED) or by doping InP with elements such as Cu. Doping with Cu^+ results in a broad emission of impressive efficiency, and it is spectrally tunable with doping concentrations.[218, 223] Given their
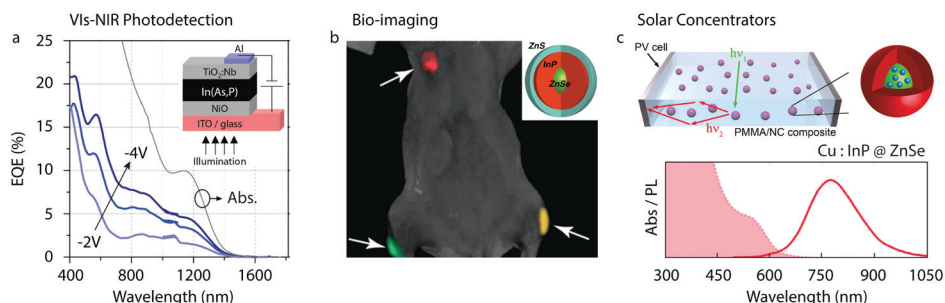
large Stokes shift, Cu-doped InP QDs have also raised interest for luminescent solar concentrators (Figure 1.6c).[167, 222]

Figure 1.6 Near-infrared applications of InP QDs. (a) Photodetectors with high external quantum efficiency.[358] (b) Bio-imaging. In this photograph, QDs are used to probe different parts of a mouse.[269] (c) Solar concentrators. With a large Stokes shift, Cu:doped InP QDs down-convert visible photons to infrared photons, which are then guided by a waveguide, such as a polymethyl methacrylate (PMMA) matrix, to solar panels placed on the side.[222] NC, nanocrystal; NIR, near-infrared; PV, photovoltaic.

1.6.4 Coherent and Quantum Light

QDs are promising active materials for optical amplifiers, super luminescent diodes and lasers.[19] Optical gain and lasing from QDs have been intensely studied over the past two decades,[19, 360] and the development of gain in CdSe is now well understood.[361] Although the physics of gain in InP is expected to be similar to that of CdSe given their similar electronic structures, it remains much less studied in InP QDs. Gain, amplified spontaneous emission and lasing have been observed in $InP/ZnSe_{1-x}S_x$ QDs (see Figure 1.7a-c), but loss processes such as trapping and Auger recombination severely limit gain. In addition, the effective (band edge) degeneracies in $InP/ZnSe_{1-x}S_x$ remain far from understood.[276, 362]

Highly efficient InP-based QDs with robust optical performance in the multi-exciton regime and with well-controlled degeneracies are yet to be achieved. Further studies on size and shape effects, and on compositionally graded and strain-engineered heterostructures, might address this gap.[246-248, 278-283] Alternatively, type II structures allowing for single-exciton gain could also be envisaged.[311]

QDs are also promising emitters for single-photon and entangled-photon sources.[23, 348, 363, 364] For efficient generation of undistinguishable single photons, the optical coherence time needs to approach twice the spontaneous emission lifetime. The generation of entangled photon pairs, instead, can be achieved through the bi-exciton-exciton cascade,[364-367] known to occur in InAs QDs.[368, 369] The development of such light sources using InP QDs is an outstanding challenge, with only few studies observing fast dephasing ascribed to

1

phonons,[370-374] and will require not only improved QD design but also optimized device architectures and efficient fabrication methods. Nevertheless, high-purity single-photon emission was observed in InP/ZnSe QDs under intense continuous wave pumping (Figure 1.7d), owing to the combination of efficient luminescence and efficient Auger recombination of multi-excitons. This result highlights the potential of these systems for on-demand (incoherent) single-photon sources operating at room-temperature.[375]

Finally, super luminescence from QD arrays is an emerging subject of research.[376, 377] Although InP QD arrays, specifically, have not been investigated in this regard, super
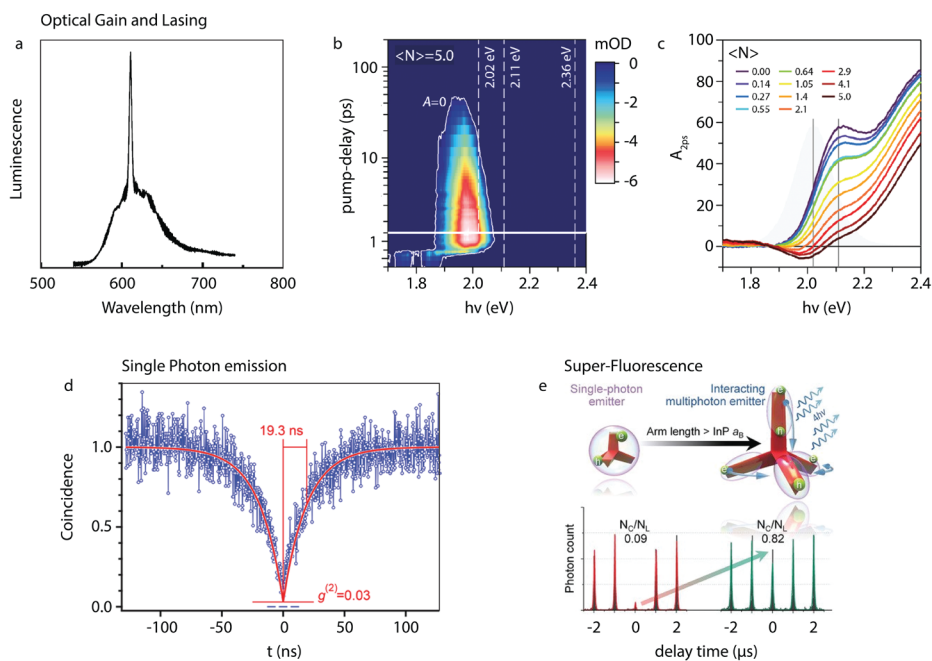
luminescence was observed from a single tetrapod-shaped InP QD with long arms and ascribed to excitons in different arms interacting through quantum tunneling (Figure 1.7e).[378]

Figure 1.7 Coherent and quantum light sources using InP QDs. (a) Lasing using InP QDs has been demonstrated.[362] (b) Ultrafast transient absorption spectroscopy reveals that the multi-excitons remain relatively short-lived.[276] (c) Optical gain is also rather weak (<N> denotes the average number of excitons per dot and A_{2ps} is the absorption at a pump-probe delay of 2 ps).[276] (d) Highly pure (incoherent) single-photon emission has also been demonstrated under continuous-wave excitation.[375] (e) Single InP tetrapods with long arms can emit multiphotons coherently, that is, in a superfluorescent fashion.[378] a.u. arbitraty unit; mOD, milli optical density.

1.7 Outlook
The quality of InP QDs has improved considerably, especially over the past decade.

1

Today, InP QDs emitting in the visible are manufactured at industrial scale for the LED market. However, many aspects of their quality still lag behind those of II-VI or halide perovskite QDs and do not meet expectations for applications, including LEDs. In other words, their current commercial appeal still primarily lies in their compliance, in terms of elemental composition, with regulations on consumer electrons. Improving the quality of InP-based QDs is therefore key to making them more competitive in the technological market. This requires advances on multiple fronts.

First, fundamental understanding about the electronic structure of InP QDs remains scarce, which limits the design of these QDs for specific applications. In addition, their rich but often poorly controlled structure complicates understanding of their structure-property relationships and hence their applicability. Specifically, further investigations are required to understand how their size, shape, phase and composition affect the density of states, exciton fine structure, structural dynamics, electron-phonon coupling and related quantities such as the fundamental linewidths and coherence times, emission lifetimes, Auger recombination of multiple excitons, polarization of the emitted light and so on.

To fill this void, ambitious structure-property studies using state-of-the-art know-how will be required as well as new synthetic methods that produce InP QDs with desired size, shape, phase and composition (in the core, at the surface, at the core-shell interface and also in terms of doping levels). Given the commercial interest of these QDs, safe, robust and scalable methods allowing the production of these QDs at full reaction yields and at reduced costs would also be highly valuable.

The surface of InP QDs also remains largely unexplored and can be engineered towards achieving high brightness, improved stability or highly conductive films. Other functionalities may also be incorporated by modifying the surface such as chirality (such as for polarization-selective photodetectors) or biological activity (such as for theranostics).

The library of core-shell structures must be expanded to surpass current limitations in terms of efficiency, linewidths, brightness, compactness, gain, coherence, stability (chemical, electrochemical, doping, thermal) and so on. So far, $InP/ZnSe_{1-x}S_x$ core-shell QDs have attracted the most popularity, but their performance and range remain limited. Nevertheless, a wide window of interesting opportunities remains rather unexplored, such as all-III-V QDs (including alloys).

Finally, applications beyond visible LEDs should be further explored and optimized. These applications include lasers, infrared technologies, photocatalysis, piezochromism, solution-processed electrons and others.

1.8 Outline of this thesis

This thesis presents a variety of studies that investigate the surface chemistry of InP-based QDs as well as the effect that additional electrons or holes have on their properties and stability. Although the surface of the QD does not contain all atoms of the QD, the properties of the QD are strongly influenced by the atoms, ligands and possible defects on the surface. The role of the experiments, discussed in this thesis, is to understand how the surface of InP-based QDs influences their photoluminescence quantum yield and

1

stability.

In chapter 2, the surface of InP core-only QDs is addressed with the goal to reduce the number of trap states on the surface and thus increase the photoluminescence quantum yield (PLQY). The InP QDs have a PLQY of <1% after the synthesis. This low efficiency is mainly attributed to two surface phenomena: firstly, the formation of oxides on the surface, and secondly, undercoordinated P atoms. The formation of oxides can be prevented by working under strict oxygen-free conditions. The undercoordinated P atoms on the surface can be passivated by providing coordinating ligands. We demonstrate that providing InF_3 as a surface-passivating ligand to InP QDs, under the optimal conditions, leads to a PLQY up to 93%. This increase in PLQY to near-unity values is established while preventing the increase in spectral linewidth of the QDs, which often occurs during the traditional treatment of InP QDs with HF.

Studying QDs at the atomic level is challenging, mainly due to the nm size of QDs. Computational chemistry can be used to simulate what a QD looks like at the atomic level. In Chapter 3, we describe how we use computational chemistry, in the form of Density Functional Theory (DFT) calculations, to understand at the atomic level what happens to InP-based QDs when extra negative charges carriers (electrons) are added to the QDs. The calculations show that, regardless of the shape (tetrahedral or spherical), undercoordinated In in an InP core-only QD reduces when additional electrons are provided. This reduction of In can be prevented by passivating all surface In atoms with a ZnSe shell.

In chapter 4, we measure the response of InP-based QD films when they are charged with positive and negative charge carriers. Applying negative potentials on InP core-only QD films results in charge injection in the film but the charges do not remain in the CB and the observed reactions are related to the surface ligands. Reversible PL quenching is observed for InP/ZnSe/ZnS QD films at negative potentials and after ligand exchange with ethylenediamine (2DA) and sodium sulfide (Na_2S) reversible quenching at positive potentials is observed. Despite the quench in PL, the absorption does not change during the measurements, suggesting that charges are also not remaining in the CB and VB for InP/

References

1. Dingle, R.; Wiegmann, W.; Henry, C. H., Quantum States of Confined Carriers in Very Thin $Al_xGa_{1-x}As$-GaAs-$Al_xGa_{1-x}As$ Heterostructures. *Physical Review Letters* **1974,** *33* (14), 827-830.
2. Sakaki, H., Scattering Suppression and High-Mobility Effect of Size-Quantized Electrons in Ultrafine Semiconductor Wire Structures. *Japanese Journal of Applied Physics* **1980,** *19* (12), 735-738.
3. Ekimov, A.; Onushchenko, A., Quantum size effect in three-dimensional microscopic semiconductor crystals. *Jetp Letters* **1981,** *34*, 345.
4. A. L. Efros; Efros, A. L., Interband Absorption of Light in a Semiconductor Sphere. *Soviet Physics - Semiconductors* **1982,** *16*, 772-775.
5. Brus, L. E., A simple model for the ionization potential, electron affinity, and aqueous redox potentials of small semiconductor crystallites. *The Journal of Chemical Physics* **1983,** *79* (11), 5566-5571.
6. Brus, L. E., Electron–electron and electron-hole interactions in small semiconductor

crystallites: The size dependence of the lowest excited electronic state. *The Journal of Chemical Physics* **1984,** *80* (9), 4403-4409.

7. Meyer, M.; Wallberg, C.; Kurihara, K.; Fendler, J. H., Photosensitized charge separation and hydrogen production in reversed micelle entrapped platinized colloidal cadmium sulphide. *Journal of the Chemical Society, Chemical Communications* **1984,** (2), 90-91.

8. Murray, C. B.; Norris, D. J.; Bawendi, M. G., Synthesis and characterization of nearly monodisperse CdE (E = sulfur, selenium, tellurium) semiconductor nanocrystallites. *Journal of the American Chemical Society* **1993,** *115* (19), 8706-8715.

9. Yin, Y.; Alivisatos, A. P., Colloidal nanocrystal synthesis and the organic–inorganic interface. *Nature* **2005,** *437* (7059), 664-670.

10. Calvin, J. J.; Brewer, A. S.; Alivisatos, A. P., The role of organic ligand shell structures in colloidal nanocrystal synthesis. *Nature Synthesis* **2022,** *1* (2), 127-137.

11. Kovalenko, M. V.; Manna, L.; Cabot, A.; Hens, Z.; Talapin, D. V.; Kagan, C. R.; Klimov, V. I.; Rogach, A. L.; Reiss, P.; Milliron, D. J.; Guyot-Sionnnest, P.; Konstantatos, G.; Parak, W. J.; Hyeon, T.; Korgel, B. A.; Murray, C. B.; Heiss, W., Prospects of Nanoscience with Nanocrystals. *ACS Nano* **2015,** *9* (2), 1012-1057.

12. Efros, A. L.; Brus, L. E., Nanocrystal Quantum Dots: From Discovery to Modern Development. *ACS Nano* **2021,** *15*, 6192–6210.

13. Pietryga, J. M.; Park, Y.-S.; Lim, J.; Fidler, A. F.; Bae, W. K.; Brovelli, S.; Klimov, V. I., Spectroscopic and Device Aspects of Nanocrystal Quantum Dots. *Chemical Reviews* **2016,** *116* (18), 10513-10622.

14. García de Arquer, F. P.; Talapin, D. V.; Klimov, V. I.; Arakawa, Y.; Bayer, M.; Sargent, E. H., Semiconductor quantum dots: Technological progress and future challenges. *Science* **2021,** *373* (6555), eaaz8541.

15. Liu, M.; Yazdani, N.; Yarema, M.; Jansen, M.; Wood, V.; Sargent, E. H., Colloidal quantum dot electronics. *Nature Electronics* **2021,** *4* (8), 548-558.

16. Rhee, S.; Kim, K.; Roh, J.; Kwak, J., Recent Progress in High-Luminance Quantum Dot Light-Emitting Diodes. *Curr. Opt. Photon.* **2020,** *4* (3), 161-173.

17. Liu, Z.; Lin, C.-H.; Hyun, B.-R.; Sher, C.-W.; Lv, Z.; Luo, B.; Jiang, F.; Wu, T.; Ho, C.-H.; Kuo, H.-C.; He, J.-H., Micro-light-emitting diodes with quantum dots in display technology. *Light: Science & Applications* **2020,** *9* (1), 83.

18. Nannen, E.; Frohleiks, J.; Gellner, S., Light-Emitting Electrochemical Cells Based on Color-Tunable Inorganic Colloidal Quantum Dots. *Advanced Functional Materials* **2020,** *30* (33), 1907349.

19. Park, Y.-S.; Roh, J.; Diroll, B. T.; Schaller, R. D.; Klimov, V. I., Colloidal quantum dot lasers. *Nature Reviews Materials* **2021,** *6*, 382-401.

20. Jung, H.; Ahn, N.; Klimov, V. I., Prospects and challenges of colloidal quantum dot laser diodes. *Nature Photonics* **2021,** *15* (9), 643-655.

21. Pejović, V.; Georgitzikis, E.; Lee, J.; Lieberman, I.; Cheyns, D.; Heremans, P.; Malinowski, P. E., Infrared Colloidal Quantum Dot Image Sensors. *IEEE Transactions on Electron Devices* **2022,** *69* (6), 2840-2850.

22. Nakotte, T.; Munyan, S. G.; Murphy, J. W.; Hawks, S. A.; Kang, S.; Han, J.; Hiszpanski, A. M., Colloidal quantum dot based infrared detectors: extending to the mid-infrared and moving from the lab to the field. *Journal of Materials Chemistry C* **2022,** *10* (3), 790-804.

23. Kagan, C. R.; Bassett, L. C.; Murray, C. B.; Thompson, S. M., Colloidal Quantum Dots as Platforms for Quantum Information Science. *Chemical Reviews* **2021,** *121* (5), 3186-3233.

24. Chen, J.; Rong, K., Nanophotonic devices and circuits based on colloidal quantum dots. *Materials Chemistry Frontiers* **2021,** *5* (12), 4502-4537.

25. Chen, M.; Lu, L.; Yu, H.; Li, C.; Zhao, N., Integration of Colloidal Quantum Dots with Photonic Structures for Optoelectronic and Optical Devices. *Advanced Science* **2021,** *8* (18), 2101560.

23

1

ZnSe/ZnS QD films. We propose that either trap states within the bandgap are populated by the injected charges, or that injected charges induce electrochemical reactions once the films become conductive creating trap states.

Zhao, J.; Chen, O.; Vonk, C.; ... Vanmaekelbergh, D.; Bawendi, M. G., Compact high-quality CdSe-CdS core-shell nanocrystals with narrow emission linewidths and suppressed blinking. *Nature Materials* **2013,** *12* (5), 445-451.

27.   Gao, Y.; Peng, X., Photogenerated Excitons in Plain Core CdSe Nanocrystals with Unity Radiative Decay in Single Channel: The Effects of Surface and Ligands. *Journal of the American Chemical Society* **2015,** *137* (12), 4230-4235.

28.   Zhou, J.; Zhu, M.; Meng, R.; Qin, H.; Peng, X., Ideal CdSe/CdS Core/Shell Nanocrystals Enabled by Entropic Ligands and Their Core Size-, Shell Thickness-, and Ligand-Dependent Photoluminescence Properties. *Journal of the American Chemical Society* **2017,** *139* (46), 16556-16567.

29.   Zhong, L.; Liu, W.; Xie, Z.; Liu, J., Biomimetic synthesis of RPL14B-based CdSe quantum dots for the detection of heavy metal copper ions. *RSC Advances* **2024,** *14* (24), 16821-16827.

30.   Zhang, J.; Li, C.; Li, J.; Peng, X., Synthesis of CdSe/ZnSe Core/Shell and CdSe/ZnSe/ZnS Core/Shell/Shell Nanocrystals: Surface-Ligand Strain and CdSe–ZnSe Lattice Strain. *Chemistry of Materials* **2023,** *35* (17), 7049-7059.

31.   van der Stam, W.; Grimaldi, G.; Geuchies, J. J.; Gudjonsdottir, S.; van Uffelen, P. T.; van Overeem, M.; Brynjarsson, B.; Kirkwood, N.; Houtepen, A. J., Electrochemical Modulation of the Photophysics of Surface-Localized Trap States in Core/Shell/(Shell) Quantum Dot Films. *Chemistry of Materials* **2019,** *31* (20), 8484-8493.

32.   Click, S. M.; Rosenthal, S. J., Synthesis, Surface Chemistry, and Fluorescent Properties of InP Quantum Dots. *Chemistry of Materials* **2023,** *35* (3), 822-836.

33.   Kim, Y.; Chang, J. H.; Choi, H.; Kim, Y.-H.; Bae, W. K.; Jeong, S., III–V colloidal nanocrystals: control of covalent surfaces. *Chemical Science* **2020,** *11* (4), 913-922.

34.   Jang, E.; Kim, Y.; Won, Y.-H.; Jang, H.; Choi, S.-M., Environmentally Friendly InP-Based Quantum Dots for Efficient Wide Color Gamut Displays. *ACS Energy Letters* **2020,** *5* (4), 1316-1327.

35.   Wu, Z.; Liu, P.; Zhang, W.; Wang, K.; Sun, X. W., Development of InP Quantum Dot-Based Light-Emitting Diodes. *ACS Energy Letters* **2020,** *5* (4), 1095-1106.

36.   Adachi, S., *Handbook on Physical Properties of Semiconductors*. Springer: 2004; Vol. 2.

37.   Abdollahi, A.; Golzan, M. M.; Aghayar, K., First-principles investigation of electronic properties of AlxIn1−xP semiconductor alloy. *Journal of Materials Science* **2016,** *51* (15), 7343-7354.

38.   Braunstein, R.; Kane, E. O., The valence band structure of the III–V compounds. *Journal of Physics and Chemistry of Solids* **1962,** *23* (10), 1423-1431.

39.   Vurgaftman, I.; Meyer, J. R.; Ram-Mohan, L. R., Band parameters for III–V compound semiconductors and their alloys. *Journal of Applied Physics* **2001,** *89* (11), 5815-5875.

40.   Kim, Y.-S.; Marsman, M.; Kresse, G.; Tran, F.; Blaha, P., Towards efficient band structure and effective mass calculations for III-V direct band-gap semiconductors. *Physical Review B* **2010,** *82* (20), 205212.

41.   Almeida, G.; van der Poll, L.; Evers, W. H.; Szoboszlai, E.; Vonk, S. J. W.; Rabouw, F. T.; Houtepen, A. J., Size-Dependent Optical Properties of InP Colloidal Quantum Dots. *Nano Letters* **2023,** *23* (18), 8697-8703.

42.   Franceschetti, A.; Fu, H.; Wang, L. W.; Zunger, A., Many-body pseudopotential theory of excitons in InP and CdSe quantum dots. *Physical Review B* **1999,** *60* (3), 1819-1829.

43.   Efros, A. L.; Rosen, M., The Electronic Structure of Semiconductor Nanocrystals. *Annual Review of Materials Science* **2000,** *30* (1), 475-521.

44.   Dümbgen, K. C.; Zito, J.; Infante, I.; Hens, Z., Shape, Electronic Structure, and Trap States in Indium Phosphide Quantum Dots. *Chemistry of Materials* **2021,** *33* (17), 6885-6896.

45.   Krauss, T. D.; Wise, F. W., Coherent Acoustic Phonons in a Semiconductor Quantum Dot. *Physical Review Letters* **1997,** *79* (25), 5102-5105.

46. Besombes, L.; Kheng, K.; Marsal, L.; Mariette, H., Acoustic phonon broadening mechanism in single quantum dot emission. *Physical Review B* **2001,** *63* (15), 155307.

47. *Semiconductor Quantum Dots: Physics, Spectroscopy and Applications*. Springer: 2002.

48. Bozyigit, D.; Yazdani, N.; Yarema, M.; Yarema, O.; Lin, W. M. M.; Volk, S.; Vuttivorakulchai, K.; Luisier, M.; Juranyi, F.; Wood, V., Soft surfaces of nanomaterials enable strong phonon interactions. *Nature* **2016,** *531* (7596), 618-622.

49. Cui, J.; Beyler, A. P.; Coropceanu, I.; Cleary, L.; Avila, T. R.; Chen, Y.; Cordero, J. M.; Heathcote, S. L.; Harris, D. K.; Chen, O.; Cao, J.; Bawendi, M. G., Evolution of the Single-Nanocrystal Photoluminescence Linewidth with Size and Shell: Implications for Exciton–Phonon Coupling and the Optimization of Spectral Linewidths. *Nano Letters* **2016,** *16* (1), 289-296.

50. Kirschner, M. S.; Hannah, D. C.; Diroll, B. T.; Zhang, X.; Wagner, M. J.; Hayes, D.; Chang, A. Y.; Rowland, C. E.; Lethiec, C. M.; Schatz, G. C.; Chen, L. X.; Schaller, R. D., Transient Melting and Recrystallization of Semiconductor Nanocrystals Under Multiple Electron–Hole Pair Excitation. *Nano Letters* **2017,** *17* (9), 5314-5320.

51. Yazdani, N.; Bozyigit, D.; Vuttivorakulchai, K.; Luisier, M.; Infante, I.; Wood, V., Tuning Electron–Phonon Interactions in Nanocrystals through Surface Termination. *Nano Letters* **2018,** *18* (4), 2233-2242.

52. Yazdani, N.; Volk, S.; Yarema, O.; Yarema, M.; Wood, V., Size, Ligand, and Defect-Dependent Electron–Phonon Coupling in Chalcogenide and Perovskite Nanocrystals and Its Impact on Luminescence Line Widths. *ACS Photonics* **2020,** *7* (5), 1088-1095.

53. Kang, S.; Kim, Y.; Jang, E.; Kang, Y.; Han, S., Fundamental limit of emission linewidth of quantum dots: ab initio study on CdSe nanocrystals. *ACS Applied Materials & Interfaces* **2020,** *12*, 22012–22018.

54. Guzelturk, B.; Cotts, B. L.; Jasrasaria, D.; Philbin, J. P.; Hanifi, D. A.; Koscher, B. A.; Balan, A. D.; Curling, E.; Zajac, M.; Park, S.; Yazdani, N.; Nyby, C.; Kamysbayev, V.; Fischer, S.; Nett, Z.; Shen, X.; Kozina, M. E.; Lin, M.-F.; Reid, A. H.; Weathersby, S. P.; Schaller, R. D.; Wood, V.; Wang, X.; Dionne, J. A.; Talapin, D. V.; Alivisatos, A. P.; Salleo, A.; Rabani, E.; Lindenberg, A. M., Dynamic lattice distortions driven by surface trapping in semiconductor nanocrystals. *Nature Communications* **2021,** *12* (1), 1860.

55. Monreal, R. C., Electron-phonon interaction in the dynamics of trap filling in quantum dots. *Physical Review B* **2021,** *104* (18), 184304.

56. Kwok, N., *Complete Guide to Semiconductor Devices*. Wiley-IEEE Press: 2002.

57. Van de Walle, C. G.; Neugebauer, J., Universal alignment of hydrogen levels in semiconductors, insulators and solutions. *Nature* **2003,** *423* (6940), 626-628.

58. Adachi, S., *The Handbook on Optical Constants of Semiconductors*. WORLD SCIENTIFIC: 2012; p 632.

59. Catlow, C. R. A.; Stoneham, A. M., Ionicity in solids. *Journal of Physics C: Solid State Physics* **1983,** *16* (22), 4321.

60. Christensen, N. E.; Satpathy, S.; Pawlowska, Z., Bonding and ionicity in semiconductors. *Physical Review B* **1987,** *36* (2), 1032-1050.

61. Tripathy, S. K.; Pattanaik, A., Optical and electronic properties of some semiconductors from energy gaps. *Optical Materials* **2016,** *53*, 123-133.

62. Kim, J.; Wong, C. Y.; Scholes, G. D., Exciton Fine Structure and Spin Relaxation in Semiconductor Colloidal Quantum Dots. *Accounts of Chemical Research* **2009,** *42* (8), 1037-1046.

63. Brodu, A.; Ballottin, M. V.; Buhot, J.; van Harten, E. J.; Dupont, D.; La Porta, A.; Prins, P. T.; Tessier, M. D.; Versteegh, M. A. M.; Zwiller, V.; Bals, S.; Hens, Z.; Rabouw, F. T.; Christianen, P. C. M.; de Mello Donega, C.; Vanmaekelbergh, D., Exciton Fine Structure and Lattice Dynamics in InP/ZnSe Core/Shell Quantum Dots. *ACS Photonics* **2018,** *5* (8), 3353-3362.

64. Brodu, A.; Chandrasekaran, V.; Scarpelli, L.; Buhot, J.; Masia, F.; Ballottin, M. V.; Severijnen,

1

M.; Tessier, M. D.; Dupont, D.; Rabouw, F. T.; Christianen, P. C. M.; de Mello Donega, C.; Vanmaekelbergh, D.; Langbein, W.; Hens, Z., Fine Structure of Nearly Isotropic Bright Excitons in InP/ZnSe Colloidal Quantum Dots. *The Journal of Physical Chemistry Letters* **2019,** *10* (18), 5468-5475.

65. Brodu, A.; Tessier, M. D.; Canneson, D.; Dupont, D.; Ballottin, M. V.; Christianen, P. C. M.; de Mello Donega, C.; Hens, Z.; Yakovlev, D. R.; Bayer, M.; Vanmaekelbergh, D.; Biadala, L., Hyperfine Interactions and Slow Spin Dynamics in Quasi-isotropic InP-based Core/Shell Colloidal Nanocrystals. *ACS Nano* **2019,** *13* (9), 10201-10209.

66. Efros, A. L.; Rosen, M.; Kuno, M.; Nirmal, M.; Norris, D. J.; Bawendi, M., Band-edge exciton in quantum dots of semiconductors with a degenerate valence band: Dark and bright exciton states. *Physical Review B* **1996,** *54* (7), 4843-4856.

67. Melnychuk, C.; Guyot-Sionnest, P., Multicarrier Dynamics in Quantum Dots. *Chemical Reviews* **2021**.

68. Takagahara, T., Electron-phonon interactions and excitonic dephasing in semiconductor nanocrystals. *Physical Review Letters* **1993,** *71* (21), 3577-3580.

69. Borri, P.; Langbein, W.; Woggon, U.; Stavarache, V.; Reuter, D.; Wieck, A. D., Exciton dephasing via phonon interactions in InAs quantum dots: Dependence on quantum confinement. *Physical Review B* **2005,** *71* (11), 115328.

70. Masia, F.; Accanto, N.; Langbein, W.; Borri, P., Spin-Flip Limited Exciton Dephasing in CdSe/ZnS Colloidal Quantum Dots. *Physical Review Letters* **2012,** *108* (8), 087401.

71. Accanto, N.; Masia, F.; Moreels, I.; Hens, Z.; Langbein, W.; Borri, P., Engineering the Spin–Flip Limited Exciton Dephasing in Colloidal CdSe/CdS Quantum Dots. *ACS Nano* **2012,** *6* (6), 5227-5233.

72. Fumani, A. K.; Berezovsky, J., Magnetic-field-dependent spin decoherence and dephasing in room-temperature CdSe nanocrystal quantum dots. *Physical Review B* **2013,** *88* (15), 155316.

73. Micic, O. I.; Curtis, C. J.; Jones, K. M.; Sprague, J. R.; Nozik, A. J., Synthesis and Characterization of InP Quantum Dots. *The Journal of Physical Chemistry* **1994,** *98* (19), 4966-4969.

74. Guzelian, A. A.; Katari, J. E. B.; Kadavanich, A. V.; Banin, U.; Hamad, K.; Juban, E.; Alivisatos, A. P.; Wolters, R. H.; Arnold, C. C.; Heath, J. R., Synthesis of Size-Selected, Surface-Passivated InP Nanocrystals. *The Journal of Physical Chemistry* **1996,** *100* (17), 7212-7219.

75. Mićić, O. I.; Jones, K. M.; Cahill, A.; Nozik, A. J., Optical, Electronic, and Structural Properties of Uncoupled and Close-Packed Arrays of InP Quantum Dots. *The Journal of Physical Chemistry B* **1998,** *102* (49), 9791-9796.

76. Battaglia, D.; Peng, X., Formation of High Quality InP and InAs Nanocrystals in a Noncoordinating Solvent. *Nano Letters* **2002,** *2* (9), 1027-1030.

77. Talapin, D. V.; Rogach, A. L.; Mekis, I.; Haubold, S.; Kornowski, A.; Haase, M.; Weller, H., Synthesis and surface modification of amino-stabilized CdSe, CdTe and InP nanocrystals. *Colloids and Surfaces A: Physicochemical and Engineering Aspects* **2002,** *202* (2), 145-154.

78. Gao, S.; Lu, J.; Chen, N.; Zhao, Y.; Xie, Y., Aqueous synthesis of III–V semiconductor GaP and InP exhibiting pronounced quantum confinement. *Chemical Communications* **2002,** (24), 3064-3065.

79. Jun, K.-W.; Khanna, P. K.; Hong, K.-B.; Baeg, J.-O.; Suh, Y.-D., Synthesis of InP nanocrystals from indium chloride and sodium phosphide by solution route. *Materials Chemistry and Physics* **2006,** *96* (2), 494-497.

80. Gerbec, J. A.; Magana, D.; Washington, A.; Strouse, G. F., Microwave-Enhanced Reaction Rates for Nanoparticle Synthesis. *Journal of the American Chemical Society* **2005,** *127* (45), 15791-15800.

81. Xu, S.; Kumar, S.; Nann, T., Rapid Synthesis of High-Quality InP Nanocrystals. *Journal of the American Chemical Society* **2006,** *128* (4), 1054-1055.

82. Xie, R.; Battaglia, D.; Peng, X., Colloidal InP Nanocrystals as Efficient Emitters Covering Blue to Near-Infrared. *Journal of the American Chemical Society* **2007,** *129* (50), 15432-15433.

1

83. Li, L.; Protière, M.; Reiss, P., Economic Synthesis of High Quality InP Nanocrystals Using Calcium Phosphide as the Phosphorus Precursor. *Chemistry of Materials* **2008,** *20* (8), 2621-2623.

84. Harris, D. K.; Bawendi, M. G., Improved Precursor Chemistry for the Synthesis of III–V Quantum Dots. *Journal of the American Chemical Society* **2012,** *134* (50), 20211-20213.

85. Xu, Z.; Li, Y.; Li, J.; Pu, C.; Zhou, J.; Lv, L.; Peng, X., Formation of Size-Tunable and Nearly Monodisperse InP Nanocrystals: Chemical Reactions and Controlled Synthesis. *Chemistry of Materials* **2019,** *31* (14), 5331-5341.

86. Won, Y.-H.; Cho, O.; Kim, T.; Chung, D.-Y.; Kim, T.; Chung, H.; Jang, H.; Lee, J.; Kim, D.; Jang, E., Highly efficient and stable InP/ZnSe/ZnS quantum dot light-emitting diodes. *Nature* **2019,** *575* (7784), 634-638.

87. Achorn, O. B.; Franke, D.; Bawendi, M. G., Seedless Continuous Injection Synthesis of Indium Phosphide Quantum Dots as a Route to Large Size and Low Size Dispersity. *Chemistry of Materials* **2020,** *32* (15), 6532-6539.

88. Song, W.-S.; Lee, H.-S.; Lee, J. C.; Jang, D. S.; Choi, Y.; Choi, M.; Yang, H. J. J. o. N. R., Amine-derived synthetic approach to color-tunable InP/ZnS quantum dots with high fluorescent qualities. **2013,** *15* (6), 1750.

89. Kim, K.; Yoo, D.; Choi, H.; Tamang, S.; Ko, J.-H.; Kim, S.; Kim, Y.-H.; Jeong, S., Halide–Amine Co-Passivated Indium Phosphide Colloidal Quantum Dots in Tetrahedral Shape. **2016,** *55* (11), 3714-3718.

90. Tessier, M. D.; De Nolf, K.; Dupont, D.; Sinnaeve, D.; De Roo, J.; Hens, Z., Aminophosphines: A Double Role in the Synthesis of Colloidal Indium Phosphide Quantum Dots. *Journal of the American Chemical Society* **2016,** *138* (18), 5923-5929.

91. Jo, J.-H.; Jo, D.-Y.; Lee, S.-H.; Yoon, S.-Y.; Lim, H.-B.; Lee, B.-J.; Do, Y. R.; Yang, H., InP-Based Quantum Dots Having an InP Core, Composition-Gradient ZnSeS Inner Shell, and ZnS Outer Shell with Sharp, Bright Emissivity, and Blue Absorptivity for Display Devices. *ACS Applied Nano Materials* **2020,** *3*, 1972–1980.

92. Liu, Z.; Kumbhar, A.; Xu, D.; Zhang, J.; Sun, Z.; Fang, J., Coreduction Colloidal Synthesis of III–V Nanocrystals: The Case of InP. *Angewandte Chemie International Edition* **2008,** *47* (19), 3540-3542.

93. Joung, S.; Yoon, S.; Han, C.-S.; Kim, Y.; Jeong, S., Facile synthesis of uniform large-sized InP nanocrystal quantum dots using tris(tert-butyldimethylsilyl)phosphine. *Nanoscale Research Letters* **2012,** *7* (1), 93.

94. Gary, D. C.; Glassy, B. A.; Cossairt, B. M., Investigation of Indium Phosphide Quantum Dot Nucleation and Growth Utilizing Triarylsilylphosphine Precursors. *Chemistry of Materials* **2014,** *26* (4), 1734-1744.

95. Chandrasiri, H. B.; Kim, E. B.; Snee, P. T., Sterically Encumbered Tris(trialkylsilyl) Phosphine Precursors for Quantum Dot Synthesis. *Inorganic Chemistry* **2020**.

96. Wells, R. L.; Pitt, C. G.; McPhail, A. T.; Purdy, A. P.; Shafieezad, S.; Hallock, R. B., The use of tris(trimethylsilyl)arsine to prepare gallium arsenide and indium arsenide. *Chemistry of Materials* **1989,** *1* (1), 4-6.

97. Virieux, H.; Le Troedec, M.; Cros-Gagneux, A.; Ojo, W.-S.; Delpech, F.; Nayral, C.; Martinez, H.; Chaudret, B., InP/ZnS Nanocrystals: Coupling NMR and XPS for Fine Surface and Interface Description. *Journal of the American Chemical Society* **2012,** *134* (48), 19701-19708.

98. Ubbink, R. F.; Almeida, G.; Iziyi, H.; du Fossé, I.; Verkleij, R.; Ganapathy, S.; van Eck, E. R. H.; Houtepen, A. J., A Water-Free In Situ HF Treatment for Ultrabright InP Quantum Dots. *Chemistry of Materials* **2022,** *34*, 10093–10103.

99. Gary, D. C.; Cossairt, B. M., Role of Acid in Precursor Conversion During InP Quantum Dot Synthesis. *Chemistry of Materials* **2013,** *25* (12), 2463-2469.

100. Angelé, L.; Dreyfuss, S.; Dubertret, B.; Mézailles, N., Synthesis of Monodisperse InP Quantum Dots: Use of an Acid-Free Indium Carboxylate Precursor. *Inorganic Chemistry* **2021,** *60* (4),

1

2271-2278.

101. Narayanaswamy, A.; Xu, H.; Pradhan, N.; Kim, M.; Peng, X., Formation of Nearly Monodisperse In2O3 Nanodots and Oriented-Attached Nanoflowers: Hydrolysis and Alcoholysis vs Pyrolysis. *Journal of the American Chemical Society* **2006,** *128* (31), 10310-10319.

102. Li, Y.; Hou, X.; Shen, Y.; Dai, N.; Peng, X., Tuning the Reactivity of Indium Alkanoates by Tertiary Organophosphines for the Synthesis of Indium-Based Quantum Dots. *Chemistry of Materials* **2021,** *33* (23), 9348-9356.

103. De Trizio, L.; Gaspari, R.; Bertoni, G.; Kriegel, I.; Moretti, L.; Scotognella, F.; Maserati, L.; Zhang, Y.; Messina, G. C.; Prato, M.; Marras, S.; Cavalli, A.; Manna, L., Cu3-xP Nanocrystals as a Material Platform for Near-Infrared Plasmonics and Cation Exchange Reactions. *Chemistry of Materials* **2015,** *27* (3), 1120-1128.

104. Zhao, T.; Oh, N.; Jishkariani, D.; Zhang, M.; Wang, H.; Li, N.; Lee, J. D.; Zeng, C.; Muduli, M.; Choi, H.-J.; Su, D.; Murray, C. B.; Kagan, C. R., General Synthetic Route to High-Quality Colloidal III–V Semiconductor Quantum Dots Based on Pnictogen Chlorides. *Journal of the American Chemical Society* **2019,** *141* (38), 15145-15152.

105. Ginterseder, M.; Franke, D.; Perkinson, C. F.; Wang, L.; Hansen, E. C.; Bawendi, M. G., Scalable Synthesis of InAs Quantum Dots Mediated through Indium Redox Chemistry. *Journal of the American Chemical Society* **2020,** *142*, 4088-4092.

106. Yadav, R.; Kwon, Y.; Rivaux, C.; Saint-Pierre, C.; Ling, W. L.; Reiss, P., Narrow Near-Infrared Emission from InP QDs Synthesized with Indium(I) Halides and Aminophosphine. *Journal of the American Chemical Society* **2023,** (145), 5070-5891.

107. Valleix, R.; Cisnetti, F.; Okuno, H.; Boutinaud, P.; Chadeyron, G.; Boyer, D., Size-Controlled Indium Phosphide Quantum Dots for Bright and Tunable Light Emission by Simple Hindered Diamine Addition. *ACS Applied Nano Materials* **2021,** *4*, 11105-11114.

108. Xie, L.; Harris, D. K.; Bawendi, M. G.; Jensen, K. F., Effect of Trace Water on the Growth of Indium Phosphide Quantum Dots. *Chemistry of Materials* **2015,** *27* (14), 5058-5063.

109. Baquero, E. A.; Virieux, H.; Swain, R. A.; Gillet, A.; Cros-Gagneux, A.; Coppel, Y.; Chaudret, B.; Nayral, C.; Delpech, F., Synthesis of Oxide-Free InP Quantum Dots: Surface Control and H2-Assisted Growth. *Chemistry of Materials* **2017,** *29* (22), 9623-9627.

110. Calvin, J. J.; Kaufman, T. M.; Sedlak, A. B.; Crook, M. F.; Alivisatos, A. P., Observation of ordered organic capping ligands on semiconducting quantum dots via powder X-ray diffraction. *Nature Communications* **2021,** *12* (1), 2663.

111. Allen, P. M.; Walker, B. J.; Bawendi, M. G., Mechanistic Insights into the Formation of InP Quantum Dots. **2010,** *49* (4), 760-762.

112. Gary, D. C.; Terban, M. W.; Billinge, S. J. L.; Cossairt, B. M., Two-Step Nucleation and Growth of InP Quantum Dots via Magic-Sized Cluster Intermediates. *Chemistry of Materials* **2015,** *27* (4), 1432-1441.

113. Cossairt, B. M., Shining Light on Indium Phosphide Quantum Dots: Understanding the Interplay among Precursor Conversion, Nucleation, and Growth. *Chemistry of Materials* **2016,** *28* (20), 7181-7189.

114. Xie, L.; Shen, Y.; Franke, D.; Sebastián, V.; Bawendi, M. G.; Jensen, K. F., Characterization of Indium Phosphide Quantum Dot Growth Intermediates Using MALDI-TOF Mass Spectrometry. *Journal of the American Chemical Society* **2016,** *138* (41), 13469-13472.

115. Gary, D. C.; Petrone, A.; Li, X.; Cossairt, B. M., Investigating the role of amine in InP nanocrystal synthesis: destabilizing cluster intermediates by Z-type ligand displacement. *Chemical Communications* **2017,** *53* (1), 161-164.

116. Friedfeld, M. R.; Johnson, D. A.; Cossairt, B. M., Conversion of InP Clusters to Quantum Dots. *Inorganic Chemistry* **2019,** *58* (1), 803-810.

117. Kwon, Y.; Oh, J.; Lee, E.; Lee, S. H.; Agnes, A.; Bang, G.; Kim, J.; Kim, D.; Kim, S., Evolution from unimolecular to colloidal-quantum-dot-like character in chlorine or zinc incorporated InP magic size clusters. *Nature Communications* **2020,** *11* (1), 3127.

118. Gary, D. C.; Flowers, S. E.; Kaminsky, W.; Petrone, A.; Li, X.; Cossairt, B. M., Single-Crystal and Electronic Structure of a 1.3 nm Indium Phosphide Nanocluster. *Journal of the American Chemical Society* **2016,** *138* (5), 1510-1513.

119. McMurtry, B. M.; Qian, K.; Teglasi, J. K.; Swarnakar, A. K.; De Roo, J.; Owen, J. S., Continuous Nucleation and Size Dependent Growth Kinetics of Indium Phosphide Nanocrystals. *Chemistry of Materials* **2020.**

120. Zhao, Q.; Kulik, H. J., Electronic Structure Origins of Surface-Dependent Growth in III–V Quantum Dots. *Chemistry of Materials* **2018,** *30* (20), 7154-7165.

121. Baek, J.; Allen, P. M.; Bawendi, M. G.; Jensen, K. F., Investigation of Indium Phosphide Nanocrystal Synthesis Using a High-Temperature and High-Pressure Continuous Flow Microreactor. *Angewandte Chemie International Edition* **2011,** *50* (3), 627-630.

122. Kim, K.; Jeong, S.; Woo, J. Y.; Han, C.-S., Successive and large-scale synthesis of InP/ZnS quantum dots in a hybrid reactor and their application to white LEDs. *Nanotechnology* **2012,** *23* (6), 065602.

123. Ippen, C.; Schneider, B.; Pries, C.; Kröpke, S.; Greco, T.; Holländer, A., Large-scale synthesis of high quality InP quantum dots in a continuous flow-reactor under supercritical conditions. *Nanotechnology* **2015,** *26* (8), 085604.

124. Baek, J.; Shen, Y.; Lignos, I.; Bawendi, M. G.; Jensen, K. F., Multistage Microfluidic Platform for the Continuous Synthesis of III–V Core/Shell Quantum Dots. *Angewandte Chemie International Edition* **2018,** *57* (34), 10915-10918.

125. Vikram, A.; Kumar, V.; Ramesh, U.; Balakrishnan, K.; Oh, N.; Deshpande, K.; Ewers, T.; Trefonas, P.; Shim, M.; Kenis, P. J. A., A Millifluidic Reactor System for Multistep Continuous Synthesis of InP/ZnSeS Nanoparticles. *ChemNanoMat* **2018,** *4* (9), 943-953.

126. Lignos, I.; Mo, Y.; Carayannopoulos, L.; Ginterseder, M.; Bawendi, M. G.; Jensen, K. F., A high-temperature continuous stirred-tank reactor cascade for the multistep synthesis of InP/ZnS quantum dots. *Reaction Chemistry & Engineering* **2021,** *6* (3), 459-464.

127. Okamoto, A.; Toda, S.; Hirakawa, M.; Bai, H.; Tanaka, M.; Seino, S.; Nakagawa, T.; Murakami, H., Narrowing of the Particle Size Distribution of InP Quantum Dots for Green Light Emission by Synthesis in Micro-Flow Reactor. *ChemistrySelect* **2022,** *7* (6), e202104215.

128. Kim, Y.; Choi, H.; Lee, Y.; Koh, W.-k.; Cho, E.; Kim, T.; Kim, H.; Kim, Y.-H.; Jeong, H. Y.; Jeong, S., Tailored growth of single-crystalline InP tetrapods. *Nature Communications* **2021,** *12* (1), 4454.

129. Yoo, H.; Lee, K.-S.; Nahm, S.; Hwang, G. W.; Kim, S., Predicting ligand-dependent nanocrystal shapes of InP quantum dots and their electronic structures. *Applied Surface Science* **2022,** *578*, 151972.

130. Micic, O. I.; Sprague, J. R.; Curtis, C. J.; Jones, K. M.; Machol, J. L.; Nozik, A. J.; Giessen, H.; Fluegel, B.; Mohs, G.; Peyghambarian, N., Synthesis and Characterization of InP, GaP, and GaInP2 Quantum Dots. *The Journal of Physical Chemistry* **1995,** *99* (19), 7754-7759.

131. Kim, S.-W.; Zimmer, J. P.; Ohnishi, S.; Tracy, J. B.; Frangioni, J. V.; Bawendi, M. G., Engineering InAsxP1-x/InP/ZnSe III–V Alloyed Core/Shell Quantum Dots for the Near-Infrared. *Journal of the American Chemical Society* **2005,** *127* (30), 10526-10532.

132. Joo, J.; Choi, Y.; Suh, Y.-H.; Lee, C.-L.; Bae, J.; Park, J., Synthesis and characterization of In1−xGaxP@ZnS alloy core-shell type colloidal quantum dots. *Journal of Industrial and Engineering Chemistry* **2020,** *88*, 106-110.

133. Kim, Y.; Yang, K.; Lee, S., Highly luminescent blue-emitting In1−xGaxP@ZnS quantum dots and their applications in QLEDs with inverted structure. *Journal of Materials Chemistry C* **2020,** *8* (23), 7679-7687.

134. Leemans, J.; Dümbgen, K. C.; Minjauw, M. M.; Zhao, Q.; Vantomme, A.; Infante, I.; Detavernier, C.; Hens, Z., Acid–Base Mediated Ligand Exchange on Near-Infrared Absorbing, Indium-Based III–V Colloidal Quantum Dots. *Journal of the American Chemical Society* **2021,** *143*, 4290–4301.

1

135. Yarema, M.; Kovalenko, M. V., Colloidal Synthesis of InSb Nanocrystals with Controlled Polymorphism Using Indium and Antimony Amides. *Chemistry of Materials* **2013,** *25* (9), 1788-1792.

136. Koh, S.; Kim, W. D.; Bae, W. K.; Lee, Y. K.; Lee, D. C., Controlling Ion-Exchange Balance and Morphology in Cation Exchange from Cu3–xP Nanoplatelets into InP Crystals. *Chemistry of Materials* **2019,** *31* (6), 1990-2001.

137. Stone, D.; Koley, S.; Remennik, S.; Asor, L.; Panfil, Y. E.; Naor, T.; Banin, U., Luminescent Anisotropic Wurtzite InP Nanocrystals. *Nano Letters* **2021,** *21* (23), 10032-10039.

138. Shan, X.; Li, B.; Ji, B., Synthesis of Wurtzite In and Ga Phosphide Quantum Dots Through Cation Exchange Reactions. *Chemistry of Materials* **2021,** *33* (13), 5223-5232.

139. Choi, M.-J.; Sagar, L. K.; Sun, B.; Biondi, M.; Lee, S.; Najjariyan, A. M.; Levina, L.; García de Arquer, F. P.; Sargent, E. H., Ligand Exchange at a Covalent Surface Enables Balanced Stoichiometry in III–V Colloidal Quantum Dots. *Nano Letters* **2021,** *21*, 6057–6063.

140. Zhao, T.; Zhao, Q.; Lee, J.; Yang, S.; Wang, H.; Chuang, M.-Y.; He, Y.; Thompson, S. M.; Liu, G.; Oh, N.; Murray, C. B.; Kagan, C. R., Engineering the Surface Chemistry of Colloidal InP Quantum Dots for Charge Transport. *Chemistry of Materials* **2022,** *34* (18), 8306-8315.

141. Boles, M. A.; Ling, D.; Hyeon, T.; Talapin, D. V., The surface science of nanocrystals. *Nature Materials* **2016,** *15* (2), 141-153.

142. Ghosh, S.; Manna, L., The Many "Facets" of Halide Ions in the Chemistry of Colloidal Inorganic Nanocrystals. *Chemical Reviews* **2018,** *118* (16), 7804-7864.

143. Wang, W.; Zhang, M.; Pan, Z.; Biesold, G. M.; Liang, S.; Rao, H.; Lin, Z.; Zhong, X., Colloidal Inorganic Ligand-Capped Nanocrystals: Fundamentals, Status, and Insights into Advanced Functional Nanodevices. *Chemical Reviews* **2022,** *122* (3), 4091-4162.

144. Rosenberg, A. J., The oxidation of intermetallic compounds—III: The room-temperature oxidation of AIIIBv compounds. *Journal of Physics and Chemistry of Solids* **1960,** *14*, 175-180.

145. Hollinger, G.; Bergignat, E.; Joseph, J.; Robach, Y., On the nature of oxides on InP surfaces. *Journal of Vacuum Science & Technology A* **1985,** *3* (6), 2082-2088.

146. Mićić, O. I.; Sprague, J.; Lu, Z.; Nozik, A. J., Highly efficient band-edge emission from InP quantum dots. *Applied Physics Letters* **1996,** *68* (22), 3150-3152.

147. Cros-Gagneux, A.; Delpech, F.; Nayral, C.; Cornejo, A.; Coppel, Y.; Chaudret, B., Surface Chemistry of InP Quantum Dots: A Comprehensive Study. *Journal of the American Chemical Society* **2010,** *132* (51), 18147-18157.

148. Cossairt, B. M.; Stein, J. L.; Holden, W. M.; Seidler, G. T., 4-1: Invited Paper: Role of Phosphorus Oxidation in Controlling the Luminescent Properties of Indium Phosphide Quantum Dots. **2018,** *49* (1), 21-24.

149. Clarke, M. T.; Viscomi, F. N.; Chamberlain, T. W.; Hondow, N.; Adawi, A. M.; Sturge, J.; Erwin, S. C.; Bouillard, J.-S. G.; Tamang, S.; Stasiuk, G. J., Synthesis of super bright indium phosphide colloidal quantum dots through thermal diffusion. *Communications Chemistry* **2019,** *2* (1), 36.

150. Vikram, A.; Zahid, A.; Bhargava, S. S.; Jang, H.; Sutrisno, A.; Khare, A.; Trefonas, P.; Shim, M.; Kenis, P. J. A., Unraveling the Origin of Interfacial Oxidation of InP-Based Quantum Dots: Implications for Bioimaging and Optoelectronics. *ACS Applied Nano Materials* **2020,** *3* (12), 12325-12333.

151. Yang, W.; Yang, Y.; Kaledin, A. L.; He, S.; Jin, T.; McBride, J. R.; Lian, T., Surface passivation extends single and biexciton lifetimes of InP quantum dots. *Chemical science* **2020,** *11* (22), 5779-5789.

152. Pu, Y.-C.; Fan, H.-C.; Chang, J.-C.; Chen, Y.-H.; Tseng, S.-W., Effects of Interfacial Oxidative Layer Removal on Charge Carrier Recombination Dynamics in InP/ZnSexS1–x Core/Shell Quantum Dots. *The Journal of Physical Chemistry Letters* **2021,** 7194-7200.

153. Chen, G.; Visbeck, S. B.; Law, D. C.; Hicks, R. F., Structure-sensitive oxidation of the indium phosphide (001) surface. *Journal of Applied Physics* **2002,** *91* (11), 9362-9367.

1

154. Santosh, K.; Wang, W.; Dong, H.; Xiong, K.; Longo, R. C.; Wallace, R. M.; Cho, K. J. J. o. A. P., First principles study on InP (001)-(2× 4) surface oxidation. **2013,** *113* (10), 103705.

155. May, M. M.; Lewerenz, H.-J.; Hannappel, T., Optical in Situ Study of InP(100) Surface Chemistry: Dissociative Adsorption of Water and Oxygen. *The Journal of Physical Chemistry C* **2014,** *118* (33), 19032-19041.

156. Ruiz Alvarado, I. A.; Karmo, M.; Runge, E.; Schmidt, W. G., InP and AlInP(001)(2 × 4) Surface Oxidation from Density Functional Theory. *ACS Omega* **2021,** *6* (9), 6297-6304.

157. Zhang, X.; Ogitsu, T.; Wood, B. C.; Pham, T. A.; Ptasinska, S., Oxidation-Induced Polymerization of InP Surface and Implications for Optoelectronic Applications. *The Journal of Physical Chemistry C* **2019,** *123* (51), 30893-30902.

158. Wood, B. C.; Schwegler, E.; Choi, W. I.; Ogitsu, T., Surface Chemistry of GaP(001) and InP(001) in Contact with Water. *The Journal of Physical Chemistry C* **2014,** *118* (2), 1062-1070.

159. Ramasamy, P.; Kim, B.; Lee, M.-S.; Lee, J.-S., Beneficial effects of water in the colloidal synthesis of InP/ZnS core–shell quantum dots for optoelectronic applications. *Nanoscale* **2016,** *8* (39), 17159-17168.

160. Vikram, A.; Zahid, A.; Bhargava, S. S.; Keating, L. P.; Sutrisno, A.; Khare, A.; Trefonas, P.; Shim, M.; Kenis, P. J. A., Mechanistic Insights into Size-Focused Growth of Indium Phosphide Nanocrystals in the Presence of Trace Water. *Chemistry of Materials* **2020,** *32* (8), 3577-3584.

161. Baquero, E. A.; Ojo, W.-S.; Coppel, Y.; Chaudret, B.; Urbaszek, B.; Nayral, C.; Delpech, F., Identifying short surface ligands on metal phosphide quantum dots. *Physical Chemistry Chemical Physics* **2016,** *18* (26), 17330-17334.

162. Tomaselli, M.; Yarger, J. L.; Jr., M. B.; Havlin, R. H.; deGraw, D.; Pines, A.; Alivisatos, A. P., NMR study of InP quantum dots: Surface structure and size effects. *The Journal of Chemical Physics* **1999,** *110* (18), 8861-8864.

163. Stein, J. L.; Holden, W. M.; Venkatesh, A.; Mundy, M. E.; Rossini, A. J.; Seidler, G. T.; Cossairt, B. M., Probing Surface Defects of InP Quantum Dots Using Phosphorus Kα and Kβ X-ray Emission Spectroscopy. *Chemistry of Materials* **2018,** *30* (18), 6377-6388.

164. Calvin, J. J.; Swabeck, J. K.; Sedlak, A. B.; Kim, Y.; Jang, E.; Alivisatos, A. P., Thermodynamic Investigation of Increased Luminescence in Indium Phosphide Quantum Dots by Treatment with Metal Halide Salts. *Journal of the American Chemical Society* **2020,** *142* (44), 18897-18906.

165. Protière, M.; Reiss, P., Amine-induced growth of an In2O3 shell on colloidal InP nanocrystals. *Chemical Communications* **2007,** (23), 2417-2419.

166. Tessier, M. D.; Baquero, E. A.; Dupont, D.; Grigel, V.; Bladt, E.; Bals, S.; Coppel, Y.; Hens, Z.; Nayral, C.; Delpech, F., Interfacial Oxidation and Photoluminescence of InP-Based Core/Shell Quantum Dots. *Chemistry of Materials* **2018,** *30* (19), 6877-6883.

167. Sadeghi, S.; Bahmani Jalali, H.; Melikov, R.; Ganesh Kumar, B.; Mohammadi Aria, M.; Ow-Yang, C. W.; Nizamoglu, S., Stokes-Shift-Engineered Indium Phosphide Quantum Dots for Efficient Luminescent Solar Concentrators. *ACS Applied Materials & Interfaces* **2018,** *10* (15), 12975-12982.

168. Kim, K.; Suh, Y.-H.; Kim, D.; Choi, Y.; Bang, E.; Kim, B. H.; Park, J., Zinc Oxo Clusters Improve the Optoelectronic Properties on Indium Phosphide Quantum Dots. *Chemistry of Materials* **2020,** *32* (7), 2795-2802.

169. Granada-Ramirez, D. A.; Arias-Cerón, J. S.; Pérez-González, M.; Luna-Arias, J. P.; Cruz-Orea, A.; Rodríguez-Fragoso, P.; Herrera-Pérez, J. L.; Gómez-Herrera, M. L.; Tomás, S. A.; Vázquez-Hernández, F.; Durán-Ledezma, A. A.; Mendoza-Alvarez, J. G., Chemical synthesis and optical, structural, and surface characterization of InP-In2O3 quantum dots. *Applied Surface Science* **2020,** *530*, 147294.

170. Eren, G. O.; Sadeghi, S.; Bahmani Jalali, H.; Ritter, M.; Han, M.; Baylam, I.; Melikov, R.; Onal, A.; Oz, F.; Sahin, M.; Ow-Yang, C. W.; Sennaroglu, A.; Lechner, R. T.; Nizamoglu, S., Cadmium-Free and Efficient Type-II InP/ZnO/ZnS Quantum Dots and Their Application for LEDs. *ACS Applied Materials & Interfaces* **2021,** *13*, 32022-32030.

1

171.   Van Avermaet, H.; Schiettecatte, P.; Hinz, S.; Giordano, L.; Ferrari, F.; Nayral, C.; Delpech, F.; Maultzsch, J.; Lange, H.; Hens, Z., Full-Spectrum InP-Based Quantum Dots with Near-Unity Photoluminescence Quantum Efficiency. *ACS Nano* **2022**.

172.   Wood, B. C.; Ogitsu, T.; Schwegler, E., Local structural models of complex oxygen-and hydroxyl-rich GaP/InP (001) surfaces. *The Journal of Chemical Physics* **2012**, *136* (6), 064705.

173.   Zhang, X.; Pham, T. A.; Ogitsu, T.; Wood, B. C.; Ptasinska, S., Modulation of surface bonding topology: Oxygen bridges on OH-terminated InP (001). *The Journal of Physical Chemistry C* **2020**, *124* (5), 3196-3203.

174.   Kim, T.-G.; Zherebetskyy, D.; Bekenstein, Y.; Oh, M. H.; Wang, L.-W.; Jang, E.; Alivisatos, A. P., Trap passivation in indium-based quantum dots through surface fluorination: mechanism and applications. *ACS nano* **2018,** *12* (11), 11529-11540.

175.   Hanrahan, M. P.; Stein, J. L.; Park, N.; Cossairt, B. M.; Rossini, A. J., Elucidating the Location of Cd2+ in Post-synthetically Treated InP Quantum Dots Using Dynamic Nuclear Polarization 31P and 113Cd Solid-State NMR Spectroscopy. *The Journal of Physical Chemistry C* **2021,** *125* (5), 2956-2965.

176.   Thuy, U. T. D.; Reiss, P.; Liem, N. Q., Luminescence properties of In(Zn)P alloy core/ZnS shell quantum dots. *Applied Physics Letters* **2010**, *97* (19), 193104.

177.   Suh, Y.-H.; Lee, S.; Jung, S.-M.; Bang, S. Y.; Yang, J.; Fan, X.-B.; Zhan, S.; Samarakoon, C.; Jo, J.-W.; Kim, Y.; Choi, H. W.; Occhipinti, L. G.; Lee, T. H.; Shin, D.-W.; Kim, J. M., Engineering Core Size of InP Quantum Dot with Incipient ZnS for Blue Emission. *Advanced Optical Materials* **2022,** *10* (7), 2102372.

178.   Mahajan, S.; Bonner, W. A.; Chin, A. K.; Miller, D. C., The characterization of highly-zinc-doped InP crystals. *Applied Physics Letters* **1979,** *35* (2), 165-168.

179.   van Gurp, G. J.; van Dongen, T.; Fontijn, G. M.; Jacobs, J. M.; Tjaden, D. L. A., Interstitial and substitutional Zn in InP and InGaAsP. *Journal of Applied Physics* **1989,** *65* (2), 553-560.

180.   Janke, E. M.; Williams, N. E.; She, C.; Zherebetskyy, D.; Hudson, M. H.; Wang, L.; Gosztola, D. J.; Schaller, R. D.; Lee, B.; Sun, C.; Engel, G. S.; Talapin, D. V., Origin of Broad Emission Spectra in InP Quantum Dots: Contributions from Structural and Electronic Disorder. *Journal of the American Chemical Society* **2018**, *140* (46), 15791-15803.

181.   Asor, L.; Liu, J.; Ossia, Y.; Tripathi, D. C.; Tessler, N.; Frenkel, A. I.; Banin, U., InAs Nanocrystals with Robust p-Type Doping. *Advanced Functional Materials* **2021,** *31* (6), 2007456.

182.   Shen, C.; Zhu, Y.; Li, Z.; Li, J.; Tao, H.; Zou, J.; Xu, X.; Xu, G., Highly luminescent InP–In(Zn) P/ZnSe/ZnS core/shell/shell colloidal quantum dots with tunable emissions synthesized based on growth-doping. *Journal of Materials Chemistry C* **2021**, *9*, 9599-9609.

183.   Yu, P.; Cao, S.; Shan, Y.; Bi, Y.; Hu, Y.; Zeng, R.; Zou, B.; Wang, Y.; Zhao, J., Highly efficient green InP-based quantum dot light-emitting diodes regulated by inner alloyed shell component. *Light: Science & Applications* **2022**, *11* (1), 162.

184.   Cho, E.; Kim, T.; Choi, S.-m.; Jang, H.; Min, K.; Jang, E., Optical Characteristics of the Surface Defects in InP Colloidal Quantum Dots for Highly Efficient Light-Emitting Applications. *ACS Applied Nano Materials* **2018,** *1* (12), 7106-7114.

185.   Fu, H.; Zunger, A., InP quantum dots: Electronic structure, surface effects, and the redshifted emission. *Physical Review B* **1997**, *56* (3), 1496-1508.

186.   Stein, J. L.; Mader, E. A.; Cossairt, B. M., Luminescent InP Quantum Dots with Tunable Emission by Post-Synthetic Modification with Lewis Acids. *The Journal of Physical Chemistry Letters* **2016,** *7* (7), 1315-1320.

187.   Kirkwood, N.; Monchen, J. O. V.; Crisp, R. W.; Grimaldi, G.; Bergstein, H. A. C.; du Fossé, I.; van der Stam, W.; Infante, I.; Houtepen, A. J., Finding and Fixing Traps in II–VI and III–V Colloidal Quantum Dots: The Importance of Z-Type Ligand Passivation. *Journal of the American Chemical Society* **2018,** *140* (46), 15712-15723.

188.   Hughes, K. E.; Stein, J. L.; Friedfeld, M. R.; Cossairt, B. M.; Gamelin, D. R., Effects of Surface Chemistry on the Photophysics of Colloidal InP Nanocrystals. *ACS Nano* **2019,** *13* (12),

14198-14207.

189. Kobayashi, T.; Aoki, K.; Yamamoto, K., Pressure dependence of optical absorption in InP at 77 K. *Physica B+C* **1986,** *139-140*, 537-540.

190. Gorczyca, I.; Christensen, N. E.; Alouani, M., Calculated optical and structural properties of InP under pressure. *Physical Review B* **1989,** *39* (11), 7705-7712.

191. Lee, C.-J.; Mizel, A.; Banin, U.; Cohen, M. L.; Alivisatos, A. P., Observation of pressure-induced direct-to-indirect band gap transition in InP nanocrystals. *The Journal of Chemical Physics* **2000,** *113* (5), 2016-2020.

192. Liu, H.; Wang, Y.; Yang, X.; Zhao, X.; Wang, K.; Wu, M.; Zuo, X.; Yang, W.; Sui, Y.; Zou, B., Pressure-stimulus-responsive behaviors of core–shell InP/ZnSe nanocrystals: remarkable piezochromic luminescence and structural assembly. *Nanoscale* **2022,** *14*, 7530-7537.

193. Rafipoor, M.; Dupont, D.; Tornatzky, H.; Tessier, M. D.; Maultzsch, J.; Hens, Z.; Lange, H., Strain Engineering in InP/(Zn,Cd)Se Core/Shell Quantum Dots. *Chemistry of Materials* **2018,** *30* (13), 4393-4400.

194. Rafipoor, M.; Tornatzky, H.; Dupont, D.; Maultzsch, J.; Tessier, M. D.; Hens, Z.; Lange, H., Strain in InP/ZnSe, S core/shell quantum dots from lattice mismatch and shell thickness—Material stiffness influence. *The Journal of Chemical Physics* **2019,** *151* (15), 154704.

195. Kley, A.; Neugebauer, J., Atomic and electronic structure of the GaAs/ZnSe(001) interface. *Physical Review B* **1994,** *50* (12), 8616-8628.

196. Stroppa, A.; Peressi, M., ZnSe/GaAs (001) heterostructures with defected interfaces: Structural, thermodynamic, and electronic properties. *Physical Review B* **2005,** *72* (24), 245304.

197. Colli, A.; Carlino, E.; Pelucchi, E.; Grillo, V.; Franciosi, A., Local interface composition and native stacking fault density in ZnSe/GaAs(001) heterostructures. *Journal of Applied Physics* **2004,** *96* (5), 2592-2602.

198. Deng, H.-X.; Luo, J.-W.; Wei, S.-H., Chemical trends of stability and band alignment of lattice-matched II-VI/III-V semiconductor interfaces. *Physical Review B* **2015,** *91* (7), 075315.

199. Li, Y.; Hou, X.; Dai, X.; Yao, Z.; Lv, L.; Jin, Y.; Peng, X., Stoichiometry-Controlled InP-Based Quantum Dots: Synthesis, Photoluminescence, and Electroluminescence. *Journal of the American Chemical Society* **2019,** *141* (16), 6448-6452.

200. Wood, B. C.; Schwegler, E.; Choi, W. I.; Ogitsu, T., Surface chemistry of GaP (001) and InP (001) in contact with water. *The Journal of Physical Chemistry C* **2014,** *118* (2), 1062-1070.

201. Pham, T. A.; Zhang, X.; Wood, B. C.; Prendergast, D.; Ptasinska, S.; Ogitsu, T. J. T. J. o. P. C. L., Integrating Ab initio simulations and X-ray photoelectron spectroscopy: Toward a realistic description of oxidized solid/liquid interfaces. **2018,** *9* (1), 194-203.

202. Ruiz Alvarado, I. A.; Karmo, M.; Runge, E.; Schmidt, W. G., InP and AlInP (001)(2× 4) Surface Oxidation from Density Functional Theory. *ACS omega* **2021,** *6* (9), 6297-6304.

203. Berwanger, M.; Schoenhalz, A. L.; Dos Santos, C. L.; Piquini, P., Oxidation of InP nanowires: a first principles molecular dynamics study. *Physical Chemistry Chemical Physics* **2016,** *18* (45), 31101-31106.

204. Park, N.; Beck, R. A.; Hoang, K. K.; Ladd, D. M.; Abramson, J. E.; Rivera-Maldonado, R. A.; Nguyen, H. A.; Monahan, M.; Seidler, G. T.; Toney, M. F.; Li, X.; Cossairt, B. M., Colloidal, Room-Temperature Growth of Metal Oxide Shells on InP Quantum Dots. *Inorganic Chemistry* **2023,** *62* (17), 6674-6687.

205. Gatos, H. C.; Lavine, M. C., Characteristics of the {111} surfaces of the III–V intermetallic compounds. *Journal of the Electrochemical Society* **1960,** *107* (5), 427.

206. Clark, D.; Fok, T.; Roberts, G.; Sykes, R., An investigation by electron spectroscopy for chemical analysis of chemical treatments of the (100) surface of n-type InP epitaxial layers for Langmuir film deposition. *Thin Solid Films* **1980,** *70* (2), 261-283.

207. Adam, S.; Talapin, D.; Borchert, H.; Lobo, A.; McGinley, C.; De Castro, A.; Haase, M.; Weller, H.; Möller, T., The effect of nanocrystal surface structure on the luminescence properties:

1

Photoemission study of HF-etched InP nanocrystals. *The Journal of chemical physics* **2005,** *123* (8), 084706.

208. Talapin, D. V.; Gaponik, N.; Borchert, H.; Rogach, A. L.; Haase, M.; Weller, H., Etching of Colloidal InP Nanocrystals with Fluorides: Photochemical Nature of the Process Resulting in High Photoluminescence Efficiency. *The Journal of Physical Chemistry B* **2002,** *106* (49), 12659-12663.

209. Li, H.; Zhang, W.; Bian, Y.; Ahn, T. K.; Shen, H.; Ji, B., ZnF2-Assisted Synthesis of Highly Luminescent InP/ZnSe/ZnS Quantum Dots for Efficient and Stable Electroluminescence. *Nano Letters* **2022,** *10*, 4067–4073.

210. Lovingood, D. D.; Strouse, G. F., Microwave induced in-situ active ion etching of growing InP nanocrystals. *Nano letters* **2008,** *8* (10), 3394-3397.

211. Duke, C., Semiconductor surface reconstruction: The structural chemistry of two-dimensional surface compounds. *Chemical Reviews* **1996,** *96* (4), 1237-1260.

212. Chadi, D., Vacancy-induced 2× 2 reconstruction of the Ga (111) surface of GaAs. *Physical Review Letters* **1984,** *52* (21), 1911.

213. Chadi, D., Atomic structure of the (2× 2) reconstructed GaAs (1⁻ 1⁻ 1⁻) surface: A multivacancy model. *Physical Review Letters* **1986,** *57* (1), 102.

214. Biegelsen, D.; Bringans, R.; Northrup, J.; Swartz, L., Reconstructions of GaAs (1 1 1) surfaces observed by scanning tunneling microscopy. *Physical Review Letters* **1990,** *65* (4), 452.

215. Voznyy, O.; Sargent, E., Atomistic model of fluorescence intermittency of colloidal quantum dots. *Physical Review Letters* **2014,** *112* (15), 157401.

216. Schubert, E. F., *Doping in III-V Semiconductors.* Cambridge University Press: Cambridge, 1993.

217. Thuy, U. T. D.; Maurice, A.; Liem, N. Q.; Reiss, P., Europium doped In(Zn)P/ZnS colloidal quantum dots. *Dalton Transactions* **2013,** *42* (35), 12606-12610.

218. Xie, R.; Peng, X., Synthesis of Cu-Doped InP Nanocrystals (d-dots) with ZnSe Diffusion Barrier as Efficient and Color-Tunable NIR Emitters. *Journal of the American Chemical Society* **2009,** *131* (30), 10645-10651.

219. Knowles, K. E.; Nelson, H. D.; Kilburn, T. B.; Gamelin, D. R., Singlet–Triplet Splittings in the Luminescent Excited States of Colloidal Cu+:CdSe, Cu+:InP, and CuInS2 Nanocrystals: Charge-Transfer Configurations and Self-Trapped Excitons. *Journal of the American Chemical Society* **2015,** *137* (40), 13138-13147.

220. Hassan, A.; Zhang, X.; Liu, C.; Snee, P. T., Electronic Structure and Dynamics of Copper-Doped Indium Phosphide Nanocrystals Studied with Time-Resolved X-ray Absorption and Large-Scale DFT Calculations. *The Journal of Physical Chemistry C* **2018,** *122* (20), 11145-11151.

221. Kim, H.-J.; Jo, J.-H.; Yoon, S.-Y.; Jo, D.-Y.; Kim, H.-S.; Park, B.; Yang, H., Emission Enhancement of Cu-Doped InP Quantum Dots through Double Shelling Scheme. **2019,** *12* (14), 2267.

222. Sadeghi, S.; Bahmani Jalali, H.; Srivastava, S. B.; Melikov, R.; Baylam, I.; Sennaroglu, A.; Nizamoglu, S., High-Performance, Large-Area, and Ecofriendly Luminescent Solar Concentrators Using Copper-Doped InP Quantum Dots. *iScience* **2020,** *23* (7), 101272.

223. Mundy, M. E.; Eagle, F. W.; Hughes, K. E.; Gamelin, D. R.; Cossairt, B. M., Synthesis and Spectroscopy of Emissive, Surface-Modified, Copper-Doped Indium Phosphide Nanocrystals. *ACS Materials Letters* **2020,** *2* (6), 576-581.

224. Kim, J.; Choi, H. S.; Wedel, A.; Yoon, S.-Y.; Jo, J.-H.; Kim, H.-M.; Han, C.-J.; Song, H.-J.; Yi, J.-M.; Jang, J.-S.; Zschiesche, H.; Lee, B.-J.; Park, K.; Yang, H., Highly luminescent near-infrared Cu-doped InP quantum dots with a Zn–Cu–In–S/ZnS double shell scheme. *Journal of Materials Chemistry C* **2021,** *9* (12), 4330-4337.

225. Prins, P. T.; Spruijt, D. A. W.; Mangnus, M. J. J.; Rabouw, F. T.; Vanmaekelbergh, D.; de Mello Donega, C.; Geiregat, P., Slow Hole Localization and Fast Electron Cooling in Cu-Doped

InP/ZnSe Quantum Dots. *The Journal of Physical Chemistry Letters* **2022**, 9950-9956.

226. Koh, S.; Eom, T.; Kim, W. D.; Lee, K.; Lee, D.; Lee, Y. K.; Kim, H.; Bae, W. K.; Lee, D. C., Zinc–Phosphorus Complex Working as an Atomic Valve for Colloidal Growth of Monodisperse Indium Phosphide Quantum Dots. *Chemistry of Materials* **2017,** *29* (15), 6346-6355.

227. Asor, L.; Liu, J.; Xiang, S.; Tessler, N.; Frenkel, A. I.; Banin, U., Zn-doped P-type InAs Nanocrystal Quantum Dots. *Advanced Materials* **2022,** *35*, 2208332.

228. Kirkwood, N.; De Backer, A.; Altantzis, T.; Winckelmans, N.; Longo, A.; Antolinez, F. V.; Rabouw, F. T.; De Trizio, L.; Geuchies, J. J.; Mulder, J. T.; Renaud, N.; Bals, S.; Manna, L.; Houtepen, A. J., Locating and Controlling the Zn Content in In(Zn)P Quantum Dots. *Chemistry of Materials* **2020,** *32* (1), 557-565.

229. Kim, Y.; Ham, S.; Jang, H.; Min, J. H.; Chung, H.; Lee, J.; Kim, D.; Jang, E., Bright and Uniform Green Light Emitting InP/ZnSe/ZnS Quantum Dots for Wide Color Gamut Displays. *ACS Applied Nano Materials* **2019,** *2* (3), 1496-1504.

230. Liu, P.; Lou, Y.; Ding, S.; Zhang, W.; Wu, Z.; Yang, H.; Xu, B.; Wang, K.; Sun, X. W., Green InP/ZnSeS/ZnS Core Multi-Shelled Quantum Dots Synthesized with Aminophosphine for Effective Display Applications. *Advanced Functional Materials* **2021,** *31*, 2008453.

231. Zhang, W.; Tan, Y.; Duan, X.; Zhao, F.; Liu, H.; Chen, W.; Liu, P.; Liu, X.; Wang, K.; Zhang, Z.; Sun, X. W., High Quantum Yield Blue InP/ZnS/ZnS Quantum Dots Based on Bromine Passivation for Efficient Blue Light-Emitting Diodes. *Advanced Optical Materials* **2022,** *10* (15), 2200685.

232. Heun, S.; Paggel, J. J.; Sorba, L.; Rubini, S.; Franciosi, A.; Bonard, J. M.; Ganière, J. D., Interface composition and stacking fault density in II-VI/III-V heterostructures. *Applied Physics Letters* **1997,** *70* (2), 237-239.

233. Colli, A.; Pelucchi, E.; Franciosi, A., Controlling the native stacking fault density in II-VI/III-V heterostructures. *Applied Physics Letters* **2003,** *83* (1), 81-83.

234. Stroppa, A.; Peressi, M., $\mathrm{Zn}\mathrm{Se}/\mathrm{Ga}\mathrm{As}(001)$ heterostructures with defected interfaces: Structural, thermodynamic, and electronic properties. *Physical Review B* **2005,** *72* (24), 245304.

235. Park, N.; Eagle, F. W.; DeLarme, A. J.; Monahan, M.; LoCurto, T.; Beck, R.; Li, X.; Cossairt, B. M., Tuning the interfacial stoichiometry of InP core and InP/ZnSe core/shell quantum dots. *The Journal of Chemical Physics* **2021,** *155* (8), 084701.

236. Cho, D.-Y.; Xi, L.; Boothroyd, C.; Kardynal, B.; Lam, Y. M., The role of ion exchange in the passivation of In(Zn)P nanocrystals with ZnS. *Scientific Reports* **2016,** *6* (1), 22818.

237. Sun, Z.; Wu, Q.; Wang, S.; Cao, F.; Wang, Y.; Li, L.; Wang, H.; Kong, L.; Yan, L.; Yang, X., Suppressing the Cation Exchange at the Core/Shell Interface of InP Quantum Dots by a Selenium Shielding Layer Enables Efficient Green Light-Emitting Diodes. *ACS Applied Materials & Interfaces* **2022,** *14*, 15401-15406.

238. Wu, Q.; Cao, F.; Wang, S.; Wang, Y.; Sun, Z.; Feng, J.; Liu, Y.; Wang, L.; Cao, Q.; Li, Y.; Wei, B.; Wong, W.-Y.; Yang, X., Quasi-Shell-Growth Strategy Achieves Stable and Efficient Green InP Quantum Dot Light-Emitting Diodes. *Advanced Science* **2022,** *n/a* (n/a), 2200959.

239. Park, N.; Cossairt, B., Colloidal, Room Temperature Growth of Metal Oxide Shells on InP Quantum Dots. *ChemRxiv* **2023**.

240. Jang, Y.; Shapiro, A.; Isarov, M.; Rubin-Brusilovski, A.; Safran, A.; Budniak, A. K.; Horani, F.; Dehnel, J.; Sashchiuk, A.; Lifshitz, E., Interface control of electronic and optical properties in IV–VI and II–VI core/shell colloidal quantum dots: a review. *Chemical Communications* **2017,** *53* (6), 1002-1024.

241. Chen, X.; Lou, Y.; Samia, A. C.; Burda, C., Coherency Strain Effects on the Optical Response of Core/Shell Heteronanostructures. *Nano Letters* **2003,** *3* (6), 799-803.

242. Jing, L.; Kershaw, S. V.; Kipp, T.; Kalytchuk, S.; Ding, K.; Zeng, J.; Jiao, M.; Sun, X.; Mews, A.; Rogach, A. L.; Gao, M., Insight into Strain Effects on Band Alignment Shifts, Carrier Localization and Recombination Kinetics in CdTe/CdS Core/Shell Quantum Dots. *Journal*

of the American Chemical Society **2015,** *137* (5), 2073-2084.

243. Smith, A. M.; Mohs, A. M.; Nie, S., Tuning the optical and electronic properties of colloidal nanocrystals by lattice strain. *Nature Nanotechnology* **2009,** *4* (1), 56-63.

244. Han, P.; Bester, G., Heavy strain conditions in colloidal core-shell quantum dots and their consequences on the vibrational properties from ab initio calculations. *Physical Review B* **2015,** *92* (12), 125438.

245. Park, S.-H.; Cho, Y.-H., Strain and piezoelectric potential effects on optical properties in CdSe/CdS core/shell quantum dots. *Journal of Applied Physics* **2011,** *109* (11), 113103.

246. Yablonovitch, E.; Kane, E., Reduction of lasing threshold current density by the lowering of valence band effective mass. *Journal of Lightwave Technology* **1986,** *4* (5), 504-506.

247. Fan, F.; Voznyy, O.; Sabatini, R. P.; Bicanic, K. T.; Adachi, M. M.; McBride, J. R.; Reid, K. R.; Park, Y.-S.; Li, X.; Jain, A.; Quintero-Bermudez, R.; Saravanapavanantham, M.; Liu, M.; Korkusinski, M.; Hawrylak, P.; Klimov, V. I.; Rosenthal, S. J.; Hoogland, S.; Sargent, E. H., Continuous-wave lasing in colloidal quantum dot solids enabled by facet-selective epitaxy. *Nature* **2017,** *544* (7648), 75-79.

248. Park, Y.-S.; Lim, J.; Klimov, V. I., Asymmetrically strained quantum dots with non-fluctuating single-dot emission spectra and subthermal room-temperature linewidths. *Nature Materials* **2019,** *18* (3), 249-255.

249. Wang, L.; Bai, J.; Zhang, T.; Huang, X.; Hou, T.; Xu, B.; Li, D.; Li, Q.; Jin, X.; Wang, Y.; Zhang, X.; Song, Y., Controlling the emission linewidths of alloy quantum dots with asymmetric strain. *Journal of Colloid and Interface Science* **2022,** *624*, 287-295.

250. Song, Y.; Liu, R.; Wang, Z.; Xu, H.; Ma, Y.; Fan, F.; Voznyy, O.; Du, J., Enhanced emission directivity from asymmetrically strained colloidal quantum dots. *Science Advances 8* (8), eabl8219.

251. Díaz, J. G.; Bryant, G. W.; Jaskólski, W.; Zieliński, M., Theory of InP nanocrystals under pressure. *Physical Review B* **2007,** *75* (24), 245433.

252. Frederick, M. T.; Amin, V. A.; Cass, L. C.; Weiss, E. A., A Molecule to Detect and Perturb the Confinement of Charge Carriers in Quantum Dots. *Nano Letters* **2011,** *11* (12), 5455-5460.

253. Harrison, W. A.; Tersoff, J., Tight-binding theory of heterojunction band lineups and interface dipoles. *Journal of Vacuum Science & Technology B: Microelectronics Processing and Phenomena* **1986,** *4* (4), 1068-1073.

254. Jeong, B. G.; Chang, J. H.; Hahm, D.; Rhee, S.; Park, M.; Lee, S.; Kim, Y.; Shin, D.; Park, J. W.; Lee, C.; Lee, D. C.; Park, K.; Hwang, E.; Bae, W. K., Interface polarization in heterovalent core–shell nanocrystals. *Nature Materials* **2021,** *21*, 246-252.

255. Hahm, D.; Chang, J. H.; Jeong, B. G.; Park, P.; Kim, J.; Lee, S.; Choi, J.; Kim, W. D.; Rhee, S.; Lim, J.; Lee, D. C.; Lee, C.; Char, K.; Bae, W. K., Design Principle for Bright, Robust, and Color-Pure InP/ZnSexS1–x/ZnS Heterostructures. *Chemistry of Materials* **2019,** *31* (9), 3476-3484.

256. Yang, Y.; Li, J.; Li, J.; Huang, J.; Li, Q.; Zhang, Y.; Dai, H.; Yao, J., Optical control of terahertz plasmon-induced transparency based on hybrid CsPbBr3 quantum dot metasurfaces. *Opt. Express* **2020,** *28* (16), 24047-24055.

257. Mulder, J. T.; Kirkwood, N.; De Trizio, L.; Li, C.; Bals, S.; Manna, L.; Houtepen, A. J., Developing Lattice Matched ZnMgSe Shells on InZnP Quantum Dots for Phosphor Applications. *ACS Applied Nano Materials* **2020,** *3* (4), 3859-3867.

258. Orfield, N. J.; McBride, J. R.; Keene, J. D.; Davis, L. M.; Rosenthal, S. J., Correlation of Atomic Structure and Photoluminescence of the Same Quantum Dot: Pinpointing Surface and Internal Defects That Inhibit Photoluminescence. *ACS Nano* **2015,** *9* (1), 831-839.

259. Kim, T.; Kim, K.-H.; Kim, S.; Choi, S.-M.; Jang, H.; Seo, H.-K.; Lee, H.; Chung, D.-Y.; Jang, E., Efficient and stable blue quantum dot light-emitting diode. *Nature* **2020,** *586* (7829), 385-389.

260. Cavanaugh, P.; Jen-La Plante, I.; Ippen, C.; Ma, R.; Kelley, D. F.; Kelley, A. M., Resonance

1

Raman Study of Shell Morphology in InP/ZnSe/ZnS Core/Shell/Shell Nanocrystals. *The Journal of Physical Chemistry C* **2021,** *125* (19), 10549-10557.

261. Nguyen, A. T.; Jen-La Plante, I.; Ippen, C.; Ma, R.; Kelley, D. F., Extremely Slow Trap-Mediated Hole Relaxation in Room-Temperature InP/ZnSe/ZnS Quantum Dots. *The Journal of Physical Chemistry C* **2021,** *125*, 4110-4118.

262. Cavanaugh, P.; Sun, H.; Jen-La Plante, I.; Bautista, M. J.; Ippen, C.; Ma, R.; Kelley, A. M.; Kelley, D. F., Radiative dynamics and delayed emission in pure and doped InP/ZnSe/ZnS quantum dots. *The Journal of Chemical Physics* **2021,** *155* (24), 244705.

263. Nguyen, A. T.; Cavanaugh, P.; Plante, I. J.-L.; Ippen, C.; Ma, R.; Kelley, D. F., Auger dynamics in InP/ZnSe/ZnS quantum dots having pure and doped shells. *The Journal of Physical Chemistry C* **2021,** *125* (28), 15405-15414.

264. Sun, H.; Cavanaugh, P.; Jen-La Plante, I.; Ippen, C.; Bautista, M.; Ma, R.; Kelley, D. F., Biexciton and trion dynamics in InP/ZnSe/ZnS quantum dots. *The Journal of Chemical Physics* **2022,** *156* (5), 054703.

265. Hinuma, Y.; Grüneis, A.; Kresse, G.; Oba, F., Band alignment of semiconductors from density-functional theory and many-body perturbation theory. *Physical Review B* **2014,** *90* (15), 155405.

266. Wegner, K. D.; Pouget, S.; Ling, W. L.; Carrière, M.; Reiss, P., Gallium – a versatile element for tuning the photoluminescence properties of InP quantum dots. *Chemical Communications* **2019,** *55* (11), 1663-1666.

267. Kim, K.-H.; Jo, J.-H.; Jo, D.-Y.; Han, C.-Y.; Yoon, S.-Y.; Kim, Y.; Kim, Y.-H.; Ko, Y. H.; Kim, S. W.; Lee, C.; Yang, H., Cation-Exchange-Derived InGaP Alloy Quantum Dots toward Blue Emissivity. *Chemistry of Materials* **2020,** *32* (8), 3537-3544.

268. Xie, R.; Chen, K.; Chen, X.; Peng, X., InAs/InP/ZnSe core/shell/shell quantum dots as near-infrared emitters: Bright, narrow-band, non-cadmium containing, and biocompatible. *Nano Research* **2008,** *1* (6), 457-464.

269. Saeboe, A. M.; Nikiforov, A. Y.; Toufanian, R.; Kays, J. C.; Chern, M.; Casas, J. P.; Han, K.; Piryatinski, A.; Jones, D.; Dennis, A. M., Extending the Near-Infrared Emission Range of Indium Phosphide Quantum Dots for Multiplexed In Vivo Imaging. *Nano Letters* **2021,** *21* (7), 3271-3279.

270. Kim, S.; Park, J.; Kim, T.; Jang, E.; Jun, S.; Jang, H.; Kim, B.; Kim, S.-W., Reverse Type-I ZnSe/InP/ZnS Core/Shell/Shell Nanocrystals: Cadmium-Free Quantum Dots for Visible Luminescence. *Small* **2011,** *7* (1), 70-73.

271. Dennis, A. M.; Mangum, B. D.; Piryatinski, A.; Park, Y.-S.; Hannah, D. C.; Casson, J. L.; Williams, D. J.; Schaller, R. D.; Htoon, H.; Hollingsworth, J. A., Suppressed Blinking and Auger Recombination in Near-Infrared Type-II InP/CdS Nanocrystal Quantum Dots. *Nano Letters* **2012,** *12* (11), 5545-5551.

272. Son, M.; Kim, S.; Lee, Y.; Bang, J., Synthesis of near-infrared-emitting type-II In(Zn)P/ZnTe (core/shell) quantum dots. *Journal of Alloys and Compounds* **2021,** *886*, 161233.

273. Kim, T.; Won, Y.-H.; Jang, E.; Kim, D., Negative Trion Auger Recombination in Highly Luminescent InP/ZnSe/ZnS Quantum Dots. *Nano Letters* **2021,** *21*, 2111–2116.

274. Lee, S. H.; Kim, Y.; Jang, H.; Min, J. H.; Oh, J.; Jang, E.; Kim, D., The effects of discrete and gradient mid-shell structures on the photoluminescence of single InP quantum dots. *Nanoscale* **2019,** *11* (48), 23251-23258.

275. Lee, Y.; Jo, D.-Y.; Kim, T.; Jo, J.-H.; Park, J.; Yang, H.; Kim, D., Effectual Interface and Defect Engineering for Auger Recombination Suppression in Bright InP/ZnSeS/ZnS Quantum Dots. *ACS Applied Materials & Interfaces* **2022,** *14* (10), 12479-12487.

276. Sousa Velosa, F.; Van Avermaet, H.; Schiettecatte, P.; Mingabudinova, L.; Geiregat, P.; Hens, Z., State Filling and Stimulated Emission by Colloidal InP/ZnSe Core/Shell Quantum Dots. *Advanced Optical Materials* **2022,** *10* (18), 2200328.

277. Kelley, A. M.; Cavanaugh, P.; Sun, H.; Wang, X.; Bautista, M. J.; Jen-La Plante, I.; Ippen, C.;

Kelley, D. F., Identity of the reversible hole traps in InP/ZnSe core/shell quantum dots. *The Journal of Chemical Physics* **2022,** *157* (17), 174701.

278.   Cragg, G. E.; Efros, A. L., Suppression of Auger Processes in Confined Structures. *Nano Letters* **2010,** *10* (1), 313-317.

279.   García-Santamaría, F.; Brovelli, S.; Viswanatha, R.; Hollingsworth, J. A.; Htoon, H.; Crooker, S. A.; Klimov, V. I., Breakdown of Volume Scaling in Auger Recombination in CdSe/CdS Heteronanocrystals: The Role of the Core–Shell Interface. *Nano Letters* **2011,** *11* (2), 687-693.

280.   Park, Y.-S.; Lim, J.; Makarov, N. S.; Klimov, V. I., Effect of Interfacial Alloying versus "Volume Scaling" on Auger Recombination in Compositionally Graded Semiconductor Quantum Dots. *Nano Letters* **2017,** *17* (9), 5607-5613.

281.   Lim, J.; Park, Y.-S.; Wu, K.; Yun, H. J.; Klimov, V. I., Droop-Free Colloidal Quantum Dot Light-Emitting Diodes. *Nano Letters* **2018,** *18* (10), 6645-6653.

282.   Park, Y.-S.; Bae, W. K.; Baker, T.; Lim, J.; Klimov, V. I., Effect of Auger Recombination on Lasing in Heterostructured Quantum Dots with Engineered Core/Shell Interfaces. *Nano Letters* **2015,** *15* (11), 7319-7328.

283.   Roh, J.; Park, Y.-S.; Lim, J.; Klimov, V. I., Optically pumped colloidal-quantum-dot lasing in LED-like devices with an integrated optical cavity. *Nature Communications* **2020,** *11* (1), 271.

284.   Al-Ghamdi, M. S.; Smowton, P. M.; Shutts, S.; Blood, P.; Beanland, R.; Krysa, A. B., Absorption, Gain, and Threshold in InP/AlGaInP Quantum Dot Laser Diodes. *IEEE Journal of Quantum Electronics* **2013,** *49* (4), 389-394.

285.   C. H. Shen, S. A. S., M. J. Peanasky, C. P. Kuo, OMVPE Growth of AlGaInP for HighEfficiency Visible LightEmitting Diodes. In *High Brightness Light Emitting Diodes*, G. Stringfellow, M. C., Ed. Elsevier: 1997; pp 97-149.

286.   Gessmann, T.; Schubert, E. F., High-efficiency AlGaInP light-emitting diodes for solid-state lighting applications. *Journal of Applied Physics* **2004,** *95* (5), 2203-2216.

287.   Meier, L.; Braun, C.; Hannappel, T.; Schmidt, W. G., Band Alignment at Ga x In1–x P/Al y In1–y P Alloy Interfaces from Hybrid Density Functional Theory Calculations. *physica status solidi (b)* **2021,** *258* (2), 2000463.

288.   Zhang, X. H.; Chua, S. J.; Fan, W. J., Band offsets at GaInP/AlGaInP(001) heterostructures lattice matched to GaAs. *Applied Physics Letters* **1998,** *73* (8), 1098-1100.

289.   Srivastava, V.; Kamysbayev, V.; Hong, L.; Dunietz, E.; Klie, R. F.; Talapin, D. V., Colloidal Chemistry in Molten Salts: Synthesis of Luminescent In1–xGaxP and In1–xGaxAs Quantum Dots. *Journal of the American Chemical Society* **2018,** *140* (38), 12144-12151.

290.   Kim, S.; Kim, T.; Kang, M.; Kwak, S. K.; Yoo, T. W.; Park, L. S.; Yang, I.; Hwang, S.; Lee, J. E.; Kim, S. K.; Kim, S.-W., Highly Luminescent InP/GaP/ZnS Nanocrystals and Their Application to White Light-Emitting Diodes. *Journal of the American Chemical Society* **2012,** *134* (8), 3804-3809.

291.   Lee, W. L., C.; Kim, B.; Choi, Y.; Chae, H., Synthesis of Blue-Emissive InP/GaP/ZnS Quantum Dots via Controlling the Reaction Kinetics of Shell Growth and Length of Capping Ligands. *Nanomaterials* **2020,** *10*, 2171.

292.   Xu, Y.; Lv, Y.; Wu, R.; Shen, H.; Yang, H.; Zhang, H.; Li, J.; Li, L. S., Preparation of Highly Stable and Photoluminescent Cadmium-Free InP/GaP/ZnS Core/Shell Quantum Dots and Application to Quantitative Immunoassay. *Particle & Particle Systems Characterization* **2020,** *37*, 1900441.

293.   Luo, W.; Lin, L.; Huang, J.; Lin, Q.; Lau, K. M., Electrically pumped InP/GaAsP quantum dot lasers grown on (001) Si emitting at 750 nm. *Opt. Express* **2022,** *30* (22), 40750-40755.

294.   Enright, M. J.; Jasrasaria, D.; Hanchard, M. M.; Needell, D. R.; Phelan, M. E.; Weinberg, D.; McDowell, B. E.; Hsiao, H.-W.; Akbari, H.; Kottwitz, M.; Potter, M. M.; Wong, J.; Zuo, J.-M.; Atwater, H. A.; Rabani, E.; Nuzzo, R. G., Role of Atomic Structure on Exciton Dynamics and Photoluminescence in NIR Emissive InAs/InP/ZnSe Quantum Dots. *The Journal of Physical Chemistry C* **2022,** *126* (17), 7576-7587.

295. Wijaya, H.; Darwan, D.; Zhao, X.; Ong, E. W. Y.; Lim, K. R. G.; Wang, T.; Lim, L. J.; Khoo, K. H.; Tan, Z.-K., Efficient Near-Infrared Light-Emitting Diodes based on In(Zn)As–In(Zn)P–GaP–ZnS Quantum Dots. *Advanced Functional Materials* **2020,** *30* (4), 1906483.

296. Zhao, X.; Lim, L. J.; Ang, S. S.; Tan, Z.-K., Efficient Short-Wave Infrared Light-Emitting Diodes based on Heavy-Metal-Free Quantum Dots. *Advanced Materials* **2022,** *34*, 2206409.

297. Eychmüller, A.; Mews, A.; Weller, H., A quantum dot quantum well: CdS/HgS/CdS. *Chemical Physics Letters* **1993,** *208* (1), 59-62.

298. Jeong, B. G.; Park, Y.-S.; Chang, J. H.; Cho, I.; Kim, J. K.; Kim, H.; Char, K.; Cho, J.; Klimov, V. I.; Park, P.; Lee, D. C.; Bae, W. K., Colloidal Spherical Quantum Wells with Near-Unity Photoluminescence Quantum Yield and Suppressed Blinking. *ACS Nano* **2016,** *10* (10), 9297-9305.

299. Nagamine, G.; Jeong, B. G.; Ferreira, T. A. C.; Chang, J. H.; Park, K.; Lee, D. C.; Bae, W. K.; Padilha, L. A., Efficient Optical Gain in Spherical Quantum Wells Enabled by Engineering Biexciton Interactions. *ACS Photonics* **2020,** *7* (8), 2252-2264.

300. Rreza, I.; Yang, H.; Hamachi, L.; Campos, M.; Hull, T.; Treadway, J.; Kurtin, J.; Chan, E. M.; Owen, J. S., Performance of Spherical Quantum Well Down Converters in Solid State Lighting. *ACS Applied Materials & Interfaces* **2021,** *13* (10), 12191-12197.

301. Cassidy, J.; Diroll, B. T.; Mondal, N.; Berkinsky, D. B.; Zhao, K.; Harankahage, D.; Porotnikov, D.; Gately, R.; Khon, D.; Proppe, A.; Bawendi, M. G.; Schaller, R. D.; Malko, A. V.; Zamkov, M., Quantum Shells Boost the Optical Gain of Lasing Media. *ACS Nano* **2022,** *16*, 3017–3026.

302. Kim, S.; Shim, W.; Seo, H.; Hyun Bae, J.; Sung, J.; Choi, S. H.; Moon, W. K.; Lee, G.; Lee, B.; Kim, S.-W., Bandgap engineered reverse type-I CdTe/InP/ZnS core–shell nanocrystals for the near-infrared. *Chemical Communications* **2009,** (10), 1267-1269.

303. Kim, S.; Lim, Y. T.; Soltesz, E. G.; De Grand, A. M.; Lee, J.; Nakayama, A.; Parker, J. A.; Mihaljevic, T.; Laurence, R. G.; Dor, D. M.; Cohn, L. H.; Bawendi, M. G.; Frangioni, J. V., Near-infrared fluorescent type II quantum dots for sentinel lymph node mapping. *Nature Biotechnology* **2004,** *22* (1), 93-97.

304. Kim, S.; Fisher, B.; Eisler, H.-J.; Bawendi, M., Type-II Quantum Dots: CdTe/CdSe(Core/Shell) and CdSe/ZnTe(Core/Shell) Heterostructures. *Journal of the American Chemical Society* **2003,** *125* (38), 11466-11467.

305. de Mello Donegá, C., Formation of nanoscale spatially indirect excitons: Evolution of the type-II optical character of CdTe/CdSe heteronanocrystals. *Physical Review B* **2010,** *81* (16), 165303.

306. Gur, I.; Fromer, N. A.; Geier, M. L.; Alivisatos, A. P., Air-Stable All-Inorganic Nanocrystal Solar Cells Processed from Solution. *Science* **2005,** *310* (5747), 462-465.

307. Simi, N. J.; Bernadsha, S. B.; Thomas, A.; Ison, V. V., Quantum dot sensitized solar cells using type-II CdSe-Cu2Se core-shell QDs. *Results in Optics* **2021,** *4*, 100088.

308. Li, X.; Tong, X.; Yue, S.; Liu, C.; Channa, A. I.; You, Y.; Wang, R.; Long, Z.; Zhang, Z.; Zhao, Z.; Liu, X.-F; Wang, Z. M., Rational design of colloidal AgGaS2/CdSeS core/shell quantum dots for solar energy conversion and light detection. *Nano Energy* **2021,** *89*, 106392.

309. Wang, Y.; Wang, Q.; Zhan, X.; Wang, F.; Safdar, M.; He, J., Visible light driven type II heterostructures and their enhanced photocatalysis properties: a review. *Nanoscale* **2013,** *5* (18), 8326-8339.

310. Zhou, Y.; Zhao, H.; Ma, D.; Rosei, F., Harnessing the properties of colloidal quantum dots in luminescent solar concentrators. *Chemical Society Reviews* **2018,** *47* (15), 5866-5890.

311. Klimov, V. I.; Ivanov, S. A.; Nanda, J.; Achermann, M.; Bezel, I.; McGuire, J. A.; Piryatinski, A., Single-exciton optical gain in semiconductor nanocrystals. *Nature* **2007,** *447* (7143), 441-446.

312. Liao, C.; Xu, R.; Xu, Y.; Zhang, C.; Xiao, M.; Zhang, L.; Lu, C.; Cui, Y.; Zhang, J., Ultralow-Threshold Single-Mode Lasing from Phase-Pure CdSe/CdS Core/Shell Quantum Dots. *The Journal of Physical Chemistry Letters* **2016,** *7* (24), 4968-4976.

1

313. Wu, K.; Song, N.; Liu, Z.; Zhu, H.; Rodríguez-Córdoba, W.; Lian, T., Interfacial Charge Separation and Recombination in InP and Quasi-Type II InP/CdS Core/Shell Quantum Dot-Molecular Acceptor Complexes. *The Journal of Physical Chemistry A* **2013,** *117* (32), 7561-7570.

314. Smith, C. T.; Leontiadou, M. A.; Clark, P. C. J.; Lydon, C.; Savjani, N.; Spencer, B. F.; Flavell, W. R.; O'Brien, P.; Binks, D. J., Multiple Exciton Generation and Dynamics in InP/CdS Colloidal Quantum Dots. *The Journal of Physical Chemistry C* **2017,** *121* (4), 2099-2107.

315. Karatum, O.; Jalali, H. B.; Sadeghi, S.; Melikov, R.; Srivastava, S. B.; Nizamoglu, S., Light-Emitting Devices Based on Type-II InP/ZnO Quantum Dots. *ACS Photonics* **2019,** *6* (4), 939-946.

316. Bahmani Jalali, H.; Mohammadi Aria, M.; Dikbas, U. M.; Sadeghi, S.; Ganesh Kumar, B.; Sahin, M.; Kavakli, I. H.; Ow-Yang, C. W.; Nizamoglu, S., Effective Neural Photostimulation Using Indium-Based Type-II Quantum Dots. *ACS Nano* **2018,** *12* (8), 8104-8114.

317. Karatum, O.; Eren, G. O.; Melikov, R.; Onal, A.; Ow-Yang, C. W.; Sahin, M.; Nizamoglu, S., Quantum dot and electron acceptor nano-heterojunction for photo-induced capacitive charge-transfer. *Scientific Reports* **2021,** *11* (1), 2460.

318. Shimizu, K. T.; Böhmer, M.; Estrada, D.; Gangwal, S.; Grabowski, S.; Bechtel, H.; Kang, E.; Vampola, K. J.; Chamberlin, D.; Shchekin, O. B., Toward commercial realization of quantum dot based white light-emitting diodes for general illumination. *Photonics Research* **2017,** *5* (2), A1-A6.

319. Toufanian, R.; Chern, M.; Kong, V. H.; Dennis, A. M., Engineering Brightness-Matched Indium Phosphide Quantum Dots. *Chemistry of Materials* **2021,** *33*, 1964-1975.

320. Dupont, D.; Tessier, M. D.; Smet, P. F.; Hens, Z., Indium Phosphide-Based Quantum Dots with Shell-Enhanced Absorption for Luminescent Down-Conversion. *Advanced Materials* **2017,** *29* (29), 1700686.

321. Karadza, B.; Van Avermaet, H.; Mingabudinova, L.; Hens, Z.; Meuret, Y., Efficient, high-CRI white LEDs by combining traditional phosphors with cadmium-free InP/ZnSe red quantum dots. *Photon. Res.* **2022,** *10* (1), 155-165.

322. Lee, S.-H.; Lee, K.-H.; Jo, J.-H.; Park, B.; Kwon, Y.; Jang, H. S.; Yang, H., Remote-type, high-color gamut white light-emitting diode based on InP quantum dot color converters. *Opt. Mater. Express* **2014,** *4* (7), 1297-1302.

323. Tian, W.; Dou, L.; Jin, Z.; Xiao, J.; Li, J., Full-color micro-LED displays with cadmium-free quantum dots patterned by photolithography technology. *Appl. Opt.* **2020,** *59* (35), 11112-11122.

324. Boivin, D. B.; Duffy, J. F.; Kronauer, R. E.; Czeisler, C. A., Dose-response relationships for resetting of human circadian clock by light. *Nature* **1996,** *379* (6565), 540-542.

325. Pauley, S. M., Lighting for the human circadian clock: recent research indicates that lighting has become a public health issue. *Medical Hypotheses* **2004,** *63* (4), 588-596.

326. Dong, K.; Goyarts, E. C.; Pelle, E.; Trivero, J.; Pernodet, N., Blue light disrupts the circadian rhythm and create damage in skin cells. *International Journal of Cosmetic Science* **2019,** *41* (6), 558-562.

327. Hye Oh, J.; Ji Yang, S.; Rag Do, Y., Healthy, natural, efficient and tunable lighting: four-package white LEDs for optimizing the circadian effect, color quality and vision performance. *Light: Science & Applications* **2014,** *3* (2), e141-e141.

328. Zhu, P.; Zhu, H.; Adhikari, G. C.; Thapa, S., Design of circadian white light-emitting diodes with tunable color temperature and nearly perfect color rendition. *OSA Continuum* **2019,** *2* (8), 2413-2427.

329. Lim, J.; Bae, W. K.; Lee, D.; Nam, M. K.; Jung, J.; Lee, C.; Char, K.; Lee, S., InP@ ZnSeS, core@ composition gradient shell quantum dots with enhanced stability. *Chemistry of Materials* **2011,** *23* (20), 4459-4463.

330. Lim, J.; Park, M.; Bae, W. K.; Lee, D.; Lee, S.; Lee, C.; Char, K., Highly efficient cadmium-free

quantum dot light-emitting diodes enabled by the direct formation of excitons within InP@ZnSeS quantum dots. *ACS nano* **2013,** *7* (10), 9019-9026.

331. Jo, J.-H.; Kim, J.-H.; Lee, K.-H.; Han, C.-Y.; Jang, E.-P.; Do, Y. R.; Yang, H., High-efficiency red electroluminescent device based on multishelled InP quantum dots. *Optics Letters* **2016,** *41* (17), 3984-3987.

332. Cao, F.; Wang, S.; Wang, F.; Wu, Q.; Zhao, D.; Yang, X., A Layer-by-Layer Growth Strategy for Large-Size InP/ZnSe/ZnS Core–Shell Quantum Dots Enabling High-Efficiency Light-Emitting Diodes. *Chemistry of Materials* **2018,** *30* (21), 8002-8007.

333. Zhang, H.; Hu, N.; Zeng, Z.; Lin, Q.; Zhang, F.; Tang, A.; Jia, Y.; Li, L. S.; Shen, H.; Teng, F., High-efficiency green InP quantum dot-based electroluminescent device comprising thick-shell quantum dots. *Advanced Optical Materials* **2019,** *7* (7), 1801602.

334. Iwasaki, Y.; Motomura, G.; Ogura, K.; Tsuzuki, T., Efficient green InP quantum dot light-emitting diodes using suitable organic electron-transporting materials. *Applied Physics Letters* **2020,** *117* (11), 111104.

335. Yang, J.; Choi, M. K.; Yang, U. J.; Kim, S. Y.; Kim, Y. S.; Kim, J. H.; Kim, D.-H.; Hyeon, T., Toward Full-Color Electroluminescent Quantum Dot Displays. *Nano Letters* **2020,** *21*, 26-33.

336. Han, C.-Y.; Yang, H., Development of Colloidal Quantum Dots for Electrically Driven Light-Emitting Devices. *J. Korean Ceram. Soc* **2017,** *54* (6), 449-469.

337. Chao, W.-C.; Chiang, T.-H.; Liu, Y.-C.; Huang, Z.-X.; Liao, C.-C.; Chu, C.-H.; Wang, C.-H.; Tseng, H.-W.; Hung, W.-Y.; Chou, P.-T., High efficiency green InP quantum dot light-emitting diodes by balancing electron and hole mobility. *Communications Materials* **2021,** *2* (1), 1-10.

338. Zhang, H.; Ma, X.; Lin, Q.; Zeng, Z.; Wang, H.; Li, L. S.; Shen, H.; Jia, Y.; Du, Z., High-Brightness Blue InP Quantum Dot-Based Electroluminescent Devices: The Role of Shell Thickness. *The Journal of Physical Chemistry Letters* **2020,** *11* (3), 960-967.

339. Mei, G.; Tan, Y.; Sun, J.; Wu, D.; Zhang, T.; Liu, H.; Liu, P.; Sun, X. W.; Choy, W. C. H.; Wang, K., Light extraction employing optical tunneling in blue InP quantum dot light-emitting diodes. *Applied Physics Letters* **2022,** *120* (9), 091101.

340. Thimsen, E.; Sadtler, B.; Berezin, M. Y., Shortwave-infrared (SWIR) emitters for biological imaging: a review of challenges and opportunities. *Nanophotonics* **2017,** *6* (5), 1043-1054.

341. Yun, S. H.; Kwok, S. J. J., Light in diagnosis, therapy and surgery. *Nature Biomedical Engineering* **2017,** *1* (1), 0008.

342. Yao, J.; Li, P.; Li, L.; Yang, M., Biochemistry and biomedicine of quantum dots: from biodetection to bioimaging, drug discovery, diagnostics, and therapy. *Acta Biomaterialia* **2018,** *74*, 36-55.

343. Zhao, P.; Xu, Q.; Tao, J.; Jin, Z.; Pan, Y.; Yu, C.; Yu, Z., Near infrared quantum dots in biomedical applications: current status and future perspective. *WIREs Nanomedicine and Nanobiotechnology* **2018,** *10* (3), e1483.

344. Lee, G.-H.; Moon, H.; Kim, H.; Lee, G. H.; Kwon, W.; Yoo, S.; Myung, D.; Yun, S. H.; Bao, Z.; Hahn, S. K., Multifunctional materials for implantable and wearable photonic healthcare devices. *Nature Reviews Materials* **2020,** *5* (2), 149-165.

345. Teutsch, M.; Sappa, A. D.; Hammoud, R. I., Computer Vision in the Infrared Spectrum: Challenges and Approaches. *Synthesis Lectures on Computer Vision* **2021,** *10* (2), 1-138.

346. Kahn, J. M.; Barry, J. R., Wireless infrared communications. *Proceedings of the IEEE* **1997,** *85* (2), 265-298.

347. Haffouz, S.; Zeuner, K. D.; Dalacu, D.; Poole, P. J.; Lapointe, J.; Poitras, D.; Mnaymneh, K.; Wu, X.; Couillard, M.; Korkusinski, M.; Schöll, E.; Jöns, K. D.; Zwiller, V.; Williams, R. L., Bright Single InAsP Quantum Dots at Telecom Wavelengths in Position-Controlled InP Nanowires: The Role of the Photonic Waveguide. *Nano Letters* **2018,** *18* (5), 3047-3052.

348. Lu, C.-Y.; Pan, J.-W., Quantum-dot single-photon sources for the quantum internet. *Nature Nanotechnology* **2021,** *16*, 1294–1296.

349. H. Sargent, E., Infrared Quantum Dots. *Advanced Materials* **2005,** *17* (5), 515-522.

350. Lu, H.; Carroll, G. M.; Neale, N. R.; Beard, M. C., Infrared Quantum Dots: Progress, Challenges, and Opportunities. *ACS Nano* **2019,** *13* (2), 939-953.
351. Jin, D.; Xi, P.; Wang, B.; Zhang, L.; Enderlein, J.; van Oijen, A. M., Nanoparticles for super-resolution microscopy and single-molecule tracking. *Nature Methods* **2018,** *15* (6), 415-423.
352. Chinnathambi, S.; Shirahata, N., Recent advances on fluorescent biomarkers of near-infrared quantum dots for in vitro and in vivo imaging. *Science and Technology of Advanced Materials* **2019,** *20* (1), 337-355.
353. Tong, X.; Wu, J.; Wang, Z. M., *Quantum Dot Photodetectors*. Springer: 2021.
354. Carey, G. H.; Abdelhady, A. L.; Ning, Z.; Thon, S. M.; Bakr, O. M.; Sargent, E. H., Colloidal Quantum Dot Solar Cells. *Chemical Reviews* **2015,** *115* (23), 12732-12763.
355. Zhang, L.; Yang, X.-Q.; An, J.; Zhao, S.-D.; Zhao, T.-Y.; Tan, F.; Cao, Y.-C.; Zhao, Y.-D., In vivo tumor active cancer targeting and CT-fluorescence dual-modal imaging with nanoprobe based on gold nanorods and InP/ZnS quantum dots. *Journal of Materials Chemistry B* **2018,** *6* (17), 2574-2583.
356. Zaban, A.; Mićić, O. I.; Gregg, B. A.; Nozik, A. J., Photosensitization of Nanoporous TiO2 Electrodes with InP Quantum Dots. *Langmuir* **1998,** *14* (12), 3153-3156.
357. Yang, S.; Zhao, P.; Zhao, X.; Qu, L.; Lai, X., InP and Sn:InP based quantum dot sensitized solar cells. *Journal of Materials Chemistry A* **2015,** *3* (43), 21922-21929.
358. Leemans, J.; Pejović, V.; Georgitzikis, E.; Minjauw, M.; Siddik, A. B.; Deng, Y.-H.; Kuang, Y.; Roelkens, G.; Detavernier, C.; Lieberman, I.; Malinowski, P. E.; Cheyns, D.; Hens, Z., Colloidal III–V Quantum Dot Photodiodes for Short-Wave Infrared Photodetection. *Advanced Science* **2022**, 2200844.
359. Lai, R.; Sang, Y.; Zhao, Y.; Wu, K., Triplet Sensitization and Photon Upconversion Using InP-Based Quantum Dots. *Journal of the American Chemical Society* **2020,** *142*, 19825-19829.
360. Klimov, V. I.; Mikhailovsky, A. A.; Xu, S.; Malko, A.; Hollingsworth, J. A.; Leatherdale, C. A.; Eisler, H. J.; Bawendi, M. G., Optical Gain and Stimulated Emission in Nanocrystal Quantum Dots. *Science* **2000,** *290* (5490), 314-317.
361. Geuchies, J. J.; Brynjarsson, B.; Grimaldi, G.; Gudjonsdottir, S.; van der Stam, W.; Evers, W. H.; Houtepen, A. J., Quantitative Electrochemical Control over Optical Gain in Quantum-Dot Solids. *ACS Nano* **2020,** *15*, 377–386.
362. Gao, S.; Zhang, C.; Liu, Y.; Su, H.; Wei, L.; Huang, T.; Dellas, N.; Shang, S.; Mohney, S. E.; Wang, J.; Xu, J., Lasing from colloidal InP/ZnS quantum dots. *Opt. Express* **2011,** *19* (6), 5528-5535.
363. Senellart, P.; Solomon, G.; White, A., High-performance semiconductor quantum-dot single-photon sources. *Nature Nanotechnology* **2017,** *12* (11), 1026-1039.
364. Michler, P., *Quantum Dots for Quantum Information Technologies*. 2017.
365. Benson, O.; Santori, C.; Pelton, M.; Yamamoto, Y., Regulated and Entangled Photons from a Single Quantum Dot. *Physical Review Letters* **2000,** *84* (11), 2513-2516.
366. Schimpf, C.; Reindl, M.; Basset, F. B.; Jöns, K. D.; Trotta, R.; Rastelli, A., Quantum dots as potential sources of strongly entangled photons: Perspectives and challenges for applications in quantum networks. *Applied Physics Letters* **2021,** *118* (10), 100502.
367. Trivedi, R.; Fischer, K. A.; Vučković, J.; Müller, K., Generation of Non-Classical Light Using Semiconductor Quantum Dots. *Advanced Quantum Technologies* **2020,** *3* (1), 1900007.
368. Akopian, N.; Lindner, N. H.; Poem, E.; Berlatzky, Y.; Avron, J.; Gershoni, D.; Gerardot, B. D.; Petroff, P. M., Entangled Photon Pairs from Semiconductor Quantum Dots. *Physical Review Letters* **2006,** *96* (13), 130501.
369. Lettner, T.; Gyger, S.; Zeuner, K. D.; Schweickert, L.; Steinhauer, S.; Reuterskiöld Hedlund, C.; Stroj, S.; Rastelli, A.; Hammar, M.; Trotta, R.; Jöns, K. D.; Zwiller, V., Strain-Controlled Quantum Dot Fine Structure for Entangled Photon Generation at 1550 nm. *Nano Letters* **2021,** *21*, 10501-10506.

370. Banin, U.; Cerullo, G.; Guzelian, A. A.; Bardeen, C. J.; Alivisatos, A. P.; Shank, C. V., Quantum confinement and ultrafast dephasing dynamics in InP nanocrystals. *Physical Review B* **1997,** *55* (11), 7059-7067.

371. Ellingson, R. J.; Blackburn, J. L.; Nedeljkovic, J.; Rumbles, G.; Jones, M.; Fu, H.; Nozik, A. J., Theoretical and experimental investigation of electronic structure and relaxation of colloidal nanocrystalline indium phosphide quantum dots. *Physical Review B* **2003,** *67* (7), 075308.

372. Narayanaswamy, A.; Feiner, L. F.; Meijerink, A.; van der Zaag, P. J., The Effect of Temperature and Dot Size on the Spectral Properties of Colloidal InP/ZnS Core–Shell Quantum Dots. *ACS Nano* **2009,** *3* (9), 2539-2546.

373. Huang, T.; Han, P.; Wang, X.; Feng, S.; Sun, W.; Ye, J.; Zhang, Y., Phonon induced pure dephasing process of excitonic state in colloidal semiconductor quantum dots. *Superlattices and Microstructures* **2016,** *92*, 52-59.

374. Brodu, A.; Ballottin, M. V.; Buhot, J.; Dupont, D.; Tessier, M.; Hens, Z.; Rabouw, F. T.; Christianen, P. C. M.; de Mello Donega, C.; Vanmaekelbergh, D., Exciton-phonon coupling in InP quantum dots with ZnS and (Zn, Cd) shells. *Physical Review B* **2020,** *101* (12), 125413.

375. Chandrasekaran, V.; Tessier, M. D.; Dupont, D.; Geiregat, P.; Hens, Z.; Brainis, E., Nearly Blinking-Free, High-Purity Single-Photon Emission by Colloidal InP/ZnSe Quantum Dots. *Nano Letters* **2017,** *17* (10), 6104-6109.

376. Rainò, G.; Becker, M. A.; Bodnarchuk, M. I.; Mahrt, R. F.; Kovalenko, M. V.; Stöferle, T., Superfluorescence from lead halide perovskite quantum dot superlattices. *Nature* **2018,** *563* (7733), 671-675.

377. Grim, J. Q.; Bracker, A. S.; Zalalutdinov, M.; Carter, S. G.; Kozen, A. C.; Kim, M.; Kim, C. S.; Mlack, J. T.; Yakes, M.; Lee, B.; Gammon, D., Scalable in operando strain tuning in nanophotonic waveguides enabling three-quantum-dot superradiance. *Nat Mater* **2019,** *18* (9), 963-969.

378. Kim, T.; Kim, Y.; Park, S.; Park, K.; Wang, Z.; Oh, S. H.; Jeong, S.; Kim, D., Shape-Tuned Multi-photon Emitting InP Nanotetrapod. *Advanced Materials* **2022,** *34*, 2110665.
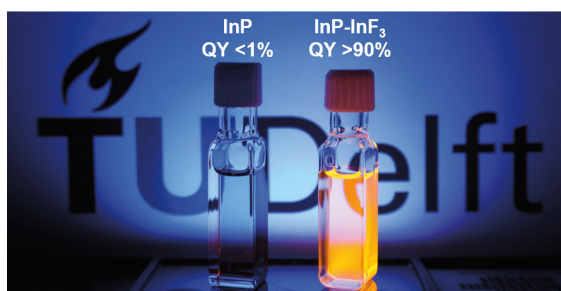
1

2

InF$_3$ charged with the task to fix the surface

A simple postsynthetic treatment to achieve near-unity photoluminescence quantum yield on InP core-only quantum dots

Indium phosphide (InP) quantum dots (QDs) are considered the most promising alternative for Cd and Pb-based QDs for lighting and display applications. However, while core-only QDs of CdSe and CdTe have been prepared with near-unity photoluminescence quantum yield (PLQY), this is not yet achieved for InP QDs. Treatments with HF have been used to boost the PLQY of InP core-only QDs up to 85%. However, HF etches the QDs, causing loss of material and broadening of the optical features. Here, we present a simple postsynthesis HF-free treatment that is based on passivating the surface of the InP QDs with InF$_3$. For optimized conditions, this results in a PLQY as high as 93% and nearly monoexponential photoluminescence decay. Etching of the particle surface is entirely avoided if the treatment is performed under stringent acid-free conditions. We show that this treatment is applicable to InP QDs with various sizes and InP QDs obtained *via* different synthesis routes. The optical properties of the resulting core-only InP QDs are on par with InP/ZnSe/ZnS core/shell/shell QDs, with significantly higher absorption coefficients in the blue, and with potential for faster charge transport. These are important advantages when considering InP QDs for use in micro-LEDs or photodetectors.

2

2.1 Introduction

Luminescent materials are of great importance in daily life applications such as displays and lighting. Colloidal quantum dots (QDs) are a unique class of luminescent materials with their high photoluminescence (PL) quantum yield (PLQY), narrow emission and size-dependent optical properties. These qualities make QDs promising candidates for application in, *e.g.*, light-emitting diodes, photodetectors, biomedical imaging, lasers, and photovoltaics.[1-13] In particular, InP-based QDs are of commercial interest since the material is free of toxic and RoHS-restricted elements such as Cd and Pb.[14, 15]

In general, as-synthesized InP QDs cores have a PLQY lower than 1% and show significant trap state emission.[16-20] It has been discussed that PL quenching is, to a significant amount, caused by surface oxides and undercoordinated P atoms on the surface.[18, 21, 22] Surface oxides are often removed with HF, either added directly or formed *in situ* in a postsynthesis treatment.[6, 18, 23, 24] Subsequent growth of wider band gap ZnSe and ZnS shells has resulted in InP/ZnSe/ZnS core/shell/shell QDs with near-unity PLQY.[6, 13, 18, 24-27]

Synthesizing high PLQY core-only QDs is relevant to fully understand and control how the surface of the QDs affects the optical properties. More practically, high PLQY core-only QDs offer several significant advantages. For example, the synthesis of core-only QDs is, compared to core/shell QDs, relatively simple and requires less material, reducing the production costs. Core-only InP QDs also have a larger absorption coefficient than core/shell QDs at photon energies below the band gap of the shell, implying that thinner layers suffice to absorb a predefined fraction of incoming light. This aspect becomes especially relevant when using QDs as down conversion phosphors in micro-LEDs. Furthermore, the absence of shells is advantageous for charge transport in QD LEDs and photodetectors.[18, 28]

The PLQY of core-only InP QDs has been promoted by treating the QDs with aqueous HF. In 1996, it was reported that treatment of InP QDs with HF or NH_4F resulted in a PLQY of 30%.[29] It was proposed that the F⁻ ion would fill surface P vacancies (*i.e.*, would bind to surface In) and replace oxygen atoms and therefore boost the PLQY. In further studies, PLQYs were reported up to 40% by treating InP QDs with aqueous HF solutions, sometimes in combination with photoirradiation to induce photoetching.[24, 30-33] Different mechanisms are proposed to describe the (photo)etching, including the removal of oxidized P atoms and fluoride passivation of the surface.[34] Moreover, HF treatment of InP QDs is often used before shell growth, yielding QDs with near-unity PLQY values.[6]

Recently, we reported a method to form HF *in situ*, allowing to work water-free and significantly reducing the hazards of working with HF.[18, 35, 36] This work showed that the *in situ* HF treatment on core-only InP QDs in the presence of excess ligands that coordinate to surface P anions (so-called Z-type ligands[37]) boosts the PLQY up to 85%.[18] Solid-state nuclear magnetic resonance (ssNMR) results demonstrated that this *in situ* HF treatment breaks up polyphosphates on the surface but does not remove all oxides. In addition, the HF treatment terminates the QD surface with fluoride ions.[18]

A significant downside of HF treatments is that they lead to etching of the surface, probably *via* the formation of PH_3 and InF_3. The same is observed for the *in situ* HF treatment described by Ubbink *et al.*[18] HF etching causes significant material losses and broadens

the optical features of InP QDs, significantly reducing their usefulness in light-emitting applications that rely on narrow emission. However, the understanding that emerged from these previous works is that a high PLQY of InP QDs does not necessarily require HF treatments. Rather, a high PLQY can be achieved if too severe surface oxidation, notably the occurrence of polyphosphates, is prevented, and undercoordinated surface atoms are coordinated with fluoride (for In atoms) and InF$_3$ for P atoms.[18] This is consistent with recent results reported by Reiss and coworkers who showed that the *in situ* HF treatment on oxide-free InP QDs works even at room temperature, which allowed them to achieve a PLQY of up to 79%, while minimizing the broadening of the optical features.[36]

For this reason, we sought a direct treatment that does not involve HF, but increases the ligand surface coverage of InP QDs that have only a minor degree of oxidation. Common ligands used to treat QDs are metal halides, metal carboxylates and metal phosphonates. In the case of Cd-chalcogenide QDs, such Z-type ligands lifted the PLQY above 90%.[38-41] For InP QDs, some Z-type ligand treatments have been explored, with a highest reported PLQY of 54% for QDs capped with Cd-oleate ligands.[16, 39, 42, 43] This comparably low PLQY raises the question whether there are other surface traps on InP QDs that limit the PLQY.

In this work, we developed a straightforward treatment of InP QDs with InF$_3$ as Z-type ligand leading to a PLQY up to 93%. We first screened several metal halide salts as suitable Z-type ligands. We found that InF$_3$ yields the highest PLQY under the selected reaction conditions, and we therefore selected this salt as the most promising candidate. Next, the treatment is optimized for surface passivation with InF$_3$. The passivation of the surface of the InP QDs requires the partial exchange of the surface capping ligand originating from the synthesis, with InF$_3$, which was found to be a thermally activated process. The optimization shows that exposing the InP QDs to InF$_3$ in hexadecane for 60 minutes at 180 °C results in a highest PLQY of 93% and nearly single exponent PL decay curve. We show that the presence of (trace amounts of) protons results in surface etching in addition to ligand exchange. However, this can be prevented completely by working under strict acid-free conditions, allowing to maintain the narrow full width at half-maximum (fwhm) of photoluminescence.

Finally, we show that applying the treatment to different sizes of InP QDs and to InP QDs made *via* different synthesis routes invariably improves the PLQY. Purposely oxidized InP QDs also show an increase in PLQY to ~40% but do not allow to reach near-unity values. We propose that severe surface oxidation impedes the complete coverage of the QD surface with Z-type ligands. The near-unity PLQY obtained for these core-only InP QDs shows that it is possible to completely heal the surface of InP with postsynthetic ligand treatments, a result suggesting that all nonradiative recombination before treatment occurs *via* surface states. The results further demonstrate that small amounts of surface oxidation are not deleterious for the PLQY, rather the presence of undercoordinated P atoms is. Coordinating these with small fluoride-based ligands, most notably InF$_3$, is key to achieving a near-unity PLQY.

The simple InF$_3$ treatment allows to reach near-unity PLQYs and results in narrow emission, making these InP core-only QDs interesting for applications in lighting, displays and photodetection.

2.2 Results and Discussion

2.2.1 Screening of metal halide ligands to enhance the PLQY of InP QDs

Since our previous work indicated that too severe surface oxidation should be avoided to achieve high PLQYs after HF treatment,[18] we selected a synthesis of InP QDs that minimizes oxidation. The InP QDs used in the first part of this study are made *via* a heat-up synthesis, based on the work of Li *et al.*, as detailed in the Experimental Section.[44] This method involves a shorter exposure of $In(PA)_3$ to high temperature than typical hot-injection synthesis methods (see Experimental Section for details), minimizing the formation of water in an *in situ* condensation reaction of the carboxylic acid ligands, which is known to cause surface oxidation for InP QDs.[45] The synthesis is performed under an atmosphere of Ar/H_2 to further minimize the oxidation of the surface of the InP QDs.[46, 47] We find that the degree of surface oxidation is indeed minimized by using this gas mixture and by using a heat-up synthesis *versus* a hot-injection synthesis. A one pulse ^{31}P ssNMR spectrum of the InP QDs after synthesis is shown in Figure 2.1A in black. The resonance belonging to P^{3-} in the InP QDs is present at around -200 ppm, as has been frequently reported.[45, 48] The resonances that are visible at -5 and 55 ppm have been assigned to PO_4^{3-} and trioctylphosphine oxide (TOPO), respectively.[18, 49] TOPO is formed during the synthesis by oxidation of trioctylphosphine (TOP) and coordinates to the surface of the QDs. By integration, we find that ~5% of the phosphorous atoms of the InP QDs are in the oxidized PO_4^{3-} state.
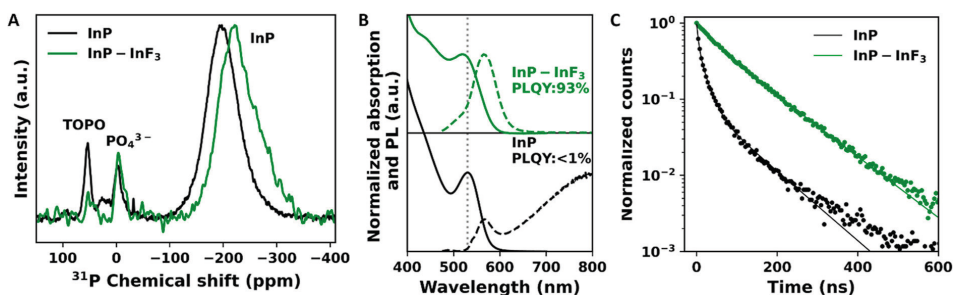

Figure 2.1: (A) ^{31}P ssNMR spectra of InP (black) and InP-InF$_3$ (green). (B) Absorption and PL spectra of InP (black) and InP-InF$_3$ (green) QDs. The dashed gray line indicates the 1S absorption peak of the InP QDs before treatment. (C) Time-resolved PL lifetime measurements of InP (black) and InP-InF$_3$ (green). The solid lines show multi-exponential fits to the experimental data (see the text).

The steady-state absorption and PL spectra of as-synthesized QDs are shown in Figure 2.1B using solid and dashed black lines, respectively. These as-synthesized QDs have a PLQY of <1%, on par with reported values in literature.[16-19] These QDs exhibit multiexponential PL decay as shown in Figure 2.1C (the black solid line is a triexponential fit to the data), with an intensity averaged lifetime of 53 ns. We attempted to increase the PLQY of these QDs using various metal halides as ligands with the procedure that is illustrated in Scheme 1.1. Briefly, a solid metal halide salt is dispersed in hexadecane together with solid $In(PA)_3$ in a vial. $In(PA)_3$ is added to maintain colloidal stability, as discussed further below. Then, InP QDs, dispersed in hexadecane, are added, and the mixture is heated to a temperature

between 120 and 180 °C for 1 to 150 minutes. The green spectra in Figure 2.1B, the green PL transient in Figure 2.1C and the green ^{31}P ssNMR spectrum in Figure 2.1A, are recorded for InP QDs that have been treated with InF$_3$ for 60 minutes at 180 °C which we found most effective in increasing the PLQY. We will return to these results below, after we have discussed the screening of various ligand treatments and the optimization of the experimental conditions during the treatment.

2
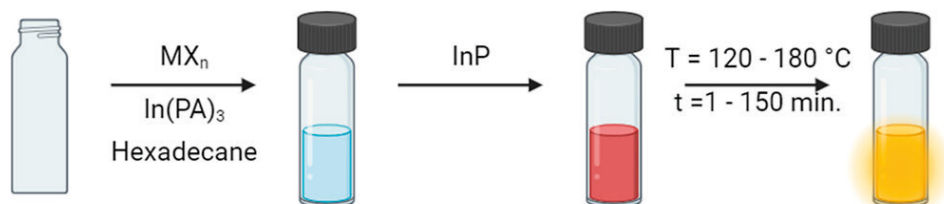
Scheme 1.1: Schematic description of the InF$_3$ treatment. To a vial, hexadecane, In(PA)$_3$ and MX$_n$ are added (with M = Mg, Al, Cd, Zn and In and X = F, Cl, Br and I). An InP QD dispersion is added to the solution, and the mixture is heated to the desired temperature for the desired time.

A series of metal salts were tested as Z-type ligands to select the ligand that results in InP QDs with the optimal PLQY and fwhm. Based on previous studies on the addition of Z-type ligands to boost the PLQY of QDs, we chose to test metal halides as ligands.[39, 42] Metal halides are relatively small compared to metal carboxylates and should therefore reduce steric hinderance and enable a high surface coverage of Z-type ligands.[39] The metal halides tested for this study are InCl$_3$, ZnCl$_2$, ZnF$_2$, ZnBr$_2$, ZnI$_2$, AlF$_3$, AlCl$_3$, CdCl$_2$, MgF$_2$ and InF$_3$; the QDs are exposed to these metal halides for 30 minutes at 150 °C.

Typical ligand treatments with metal halides use primary amines (usually oleylamine), that act as L-type ligands and solubilize both the metal halide salt as well as the QDs after ligand treatment.[39-41] Motivated by the high PLQY obtained after the *in situ* HF treatment reported in the work of Ubbink *et al.*, which did not include any amines, we chose here to work with the pure metal halide salts.[18] However, metal halides are small and polar compared to long carboxylic acid chains. Therefore, a complete coverage of the InP QD surface with metal halides after the treatment leads to an unstable dispersion of the QDs in hexadecane. To prevent precipitation, In(PA)$_3$ is added to the treatment. For QDs to have a high PLQY and to be stable in dispersion, the QDs should contain In(PA)$_3$ and metal halide ligands in an optimal ratio such that all surface atoms are covered, yet the QDs are still stable in dispersion.

The InP QDs treated with InCl$_3$, ZnCl$_2$, ZnBr$_2$, ZnI$_2$, AlCl$_3$ and CdCl$_2$ all precipitated. Efforts to redisperse these QDs in more polar solvents were unsuccessful. Treatments using ZnF$_2$, AlF$_3$, MgF$_2$ and InF$_3$ on the other hand resulted in QDs that from stable dispersions in hexadecane. This shows that, under these circumstances, only QDs treated with metal fluoride salts are colloidally stable in hexadecane.

2

The surface treatment with metal halide salts (MX_n) can be seen as the following, simplified reaction, wherein MX_n competes with $In(PA)_3$ for surface sites:

$$InP[In(PA)_3]_x + yMX_n \rightleftarrows InP[MX_n]_y + xIn(PA)_3 \tag{1}$$
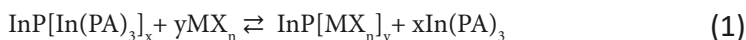
The fact that the treatment with the nonfluoride metal halides results in a loss of colloidal stability can be explained based on the solubility of the ligands. The water solubility values of the metal halides used in this study are shown in Table A2.1. The solubility of the fluoride salts is, in general, a factor 10-100 lower than nonfluoride salts. This is largely caused by the larger lattice free energy of fluoride salts which in turn is the result of the small ionic radius of the fluoride ion. So, while the reported solubilities relate to water as a solvent, a similar trend is expected in other solvents. A higher solubility of the salts results in a higher concentration of the metal halides during the treatment. This higher concentration will shift the equilibrium in Reaction 1 to the right, resulting in an almost complete coverage of the surface with metal halides. The fact that the outcome of the treatment depends on the equilibrium between the $In(PA)_3$ and metal halide ligands on the surface indicates that the other metal halides could be successful at passivating the surface of the QD, provided that the right ratio of metal halide to $In(PA)_3$ is found, or if amines are added to act as L-type ligands on the InP QD surface. In this work, however, we will focus on the fluoride metal halides.

Figure 2.2 displays the absorption (solid) and PL spectra (dashed) of InP QDs before and after treatment with various metal fluorides at 150 °C for 30 minutes. The 1S transition in absorption and PL of the untreated QDs are, respectively, observed at 540 nm and 575 nm and are indicated with dashed gray lines. The spectra of a control treatment with $In(PA)_3$ but without a metal fluoride at 150 °C for 30 minutes show a widening of the 1S peak indicative of size broadening. The PLQY remained <1%, indicating that the $In(PA)_3$ treatment does not effectively passivates surface defects.

The red, turquoise, orange, and purple spectra show the absorption and PL after exposing the QDs to MgF_2, AlF_3, ZnF_2 and InF_3, respectively. The treatment with MgF_2 raised the PLQY to 2% and AlF_3 improved the PLQY to 11%. The AlF_3 treatment led to a blue-shift of the absorption and PL spectra, indicating a decrease in effective size of the InP QDs. The decrease in size could be the consequence of replacement of outer In^{3+} ions with Al^{3+} atoms, effectively reducing the size of the InP core and suggesting an exchange of $In(PA)_3$ with AlF_3, as indicated in Reaction 1. The treatment with ZnF_2 resulted in a PLQY of 46%, and both the absorption and PL peaks are slightly shifted to shorter wavelengths, again indicating a decrease in size of the QDs. The highest PLQY, 70%, is obtained by treatment of the InP QDs with InF_3. In this case, a small red-shift is observed in the absorption and PL spectra, suggesting that the addition of InF_3 results in a net size increase, hence more In on the surface. Thus, in addition to replacing $In(PA)_3$ with InF_3, the surface coverage of Z-type InF_3 ligands has increased, implying that y > x in Reaction 1. The use of InF_3 to passivate the surface of InP QDs is similar to what was reported previously by Ubbink *et al.* but an important difference is the addition of $In(PA)_3$.[18] As mentioned earlier, $In(PA)_3$ ensures that InP QDs with a high coverage number remain stable in dispersion.
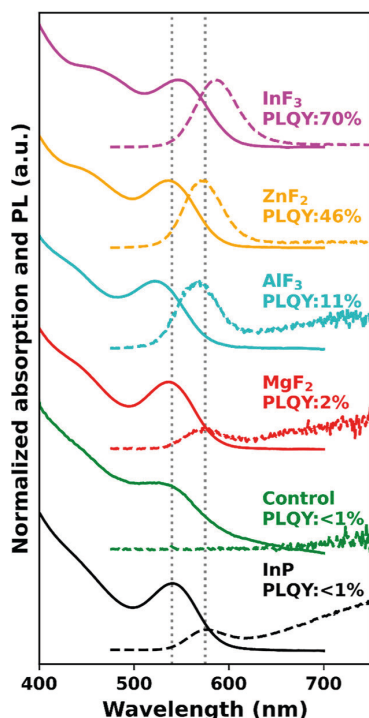
Figure 2.2: Absorption (solid) and PL (dashed) spectra of InP before (black) and after treatment at 150 °C for 30 minutes with various metal halide salts: MgF$_2$ (red), AlF$_3$ (turquoise), ZnF$_2$ (orange), and InF$_3$ (purple). The PLQY before and after the treatment is shown in the figure. The gray dashed lines indicate the wavelength of the 1S absorption and emission peaks before treatment.

A slight broadening of the absorption and PL line widths, indicative of etching, is observed but this broadening is rather small compared to HF-based treatments reported in the literature.[18, 20, 34] We will come back to this issue of etching below. InF$_3$ is thus selected as the most promising Z-type ligand for surface passivation of InP QDs. As we will show next, the procedure can be significantly improved by a further optimization of the reaction conditions.

2.2.2 Optimization of the InF3 treatment
The treatment of InP QDs with InF$_3$ was optimized by measuring the optical properties of the InP-InF3 QDs after treatment at 120, 150, or 180 °C at different time intervals. Figure 2.3A shows the PLQY as a function of the treatment time for these three temperatures. For all three temperatures, three phases are observed during the treatment. In the first 30 minutes, a fast increase in PLQY is observed. In this initial phase, the PLQY increases from <1 to 24% at 120 °C, to 55% at 150 °C, and to 85% at 180 °C. From these results, it is clear that the chemical reaction that is happening in this first phase is thermally activated.

In the second phase, in the subsequent 30 minutes, a further but slower increase in PLQY is observed for all three temperatures. After 60 minutes, the third phase occurs where a

51

plateau in the PLQY is reached for the treatment at 120 and 150 °C, and a slight decrease is observed for the treatment at 180 °C. The highest PLQYs obtained are 44, 74, and 93% for the treatments at 120, 150, and 180 °C, respectively. For the treatment at 120 and 150 °C, the maximal PLQY is reached after 150 minutes; at 180 °C, the maximum PLQY is obtained after 60 minutes. These results show that both the rate of PLQY increase and the final PLQY depend on temperature, suggesting that the exchange Reaction 1 is thermally activated, and perhaps is endothermic, such that the equilibrium shifts to the right with increasing temperature.

2
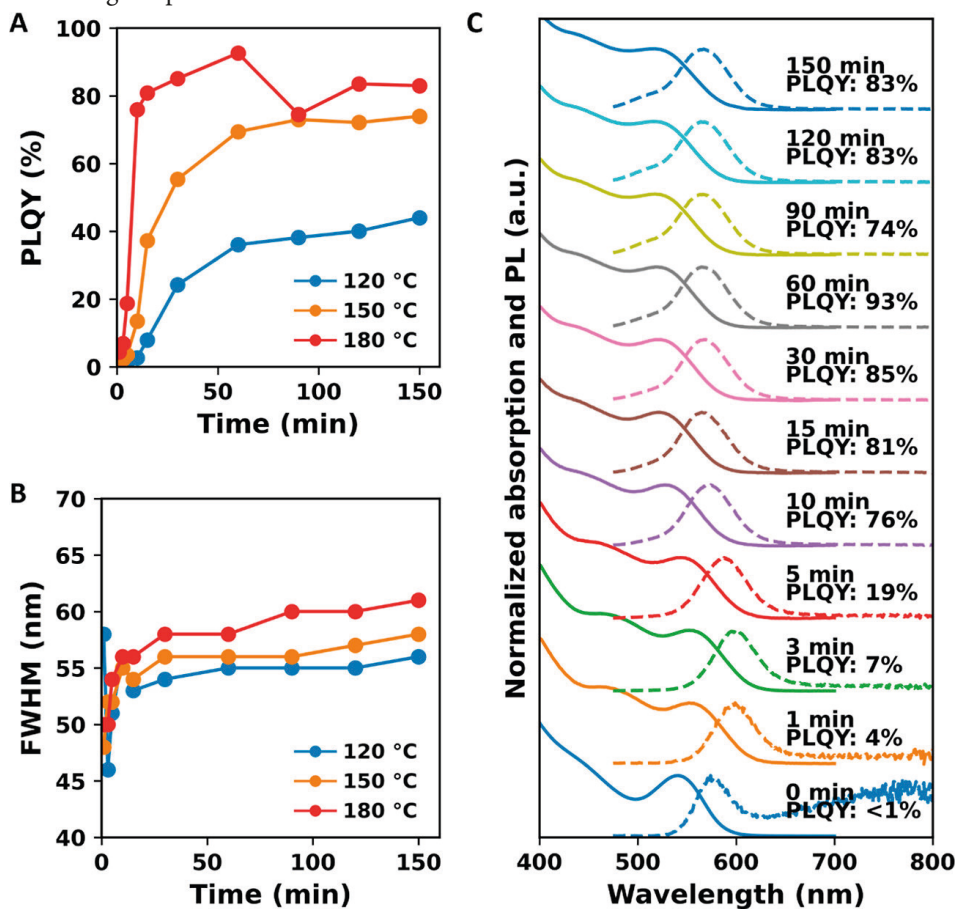
Figure 2.3: Optimization of the InF$_3$ treatment. A) The PLQY and B) fwhm of InP QDs as a function of the treatment time and temperature C) The absorption and PL spectra of aliquots collected during the treatment at 180 °C. Time and PLQY are shown on top of each plot.

Figure 2.3B shows the fwhm of the PL peak as a function of the treatment time for the three treatment temperatures. Regardless of the temperature, we observe an initial rise in fwhm in the first 10 minutes, followed by a much slower and smaller increase. The fwhm increase is smallest for the treatment at 120 °C and largest at 180 °C, demonstrating that

the fwhm increase is related to temperature. The broadening of the optical features is also visible in the control experiment, as shown in Figure 2.2, where InP QDs are heated in the presence of In(PA)$_3$ without a metal halide present. This suggests that the process is simply induced by the prolonged exposure to elevated temperatures, and not to the InF$_3$ treatment, for example due to Ostwald ripening.

From the development of the PLQY with reaction time, it is clear that the highest PLQY can be obtained with the treatment at 180 °C, at the expense of a limited increase in the fwhm of the PL. Considering both criteria, the treatment at 180 °C for 60 minutes provides the best balance between a PLQY increase and a limited increase in fwhm, prompting a PLQY increase up to 93% and a fwhm of 58 nm. To the best of our knowledge, this is the highest PLQY reported for core-only InP QDs.

To study the reproducibility of the treatment and the error on our PLQY measurement, we treated five InP QD samples using the optical conditions identified above. Table A2.2 displays the PLQY of these five samples measured two times with a calibrated integrating sphere and two times with a reference dye. On average, a PLQY of 91.6 ± 3.2% was measured using the reference dye, and a PLQY of 89.9 ± 3.5% was obtained with the integrating sphere.

2.2.3 Analysis of optical and structural changes during the InF3 treatment

The absorption and PL spectra of InF$_3$-treated InP QDs (green lines) are compared to the as-synthesized InP QDs (black lines) in Figure 2.1B. After the InF$_3$ treatment, the PL decay, as shown in Figure 2.1C, is fitted with a biexponential function [0.30 exp($-$t/42 ns) + 0.70 exp($-$t/108 ns)] corresponding to an average PL lifetime of 99 ns. This lifetime is significantly longer than that observed for CdSe and CdTe QDs with near-unity PLQY[39, 41] but is similar to the PL lifetime of high PLQY InP prepared *via* the *in situ* HF treatment we reported previously.[18, 46]

We also investigated the presence of oxides on the surface of the InP QDs with ssNMR. In Figure 2.1A, the one pulse ^{31}P NMR spectrum is shown in green for the InP-InF3 QDs. The nature of the surface oxides, PO$_4^{3-}$, did not change during the treatment; however, the amount of oxides slightly increased (6% after InF$_3$ vs 5% before). These results are in agreement with the work of Ubbink *et al*. which showed that mainly polyphosphates result in trap states for InP QDs, and that phosphate does not introduce trap states in the band gap.[18]

The ssNMR spectrum also shows that the amount of TOPO decreases compared to untreated particles, indicating that TOPO is replaced by InF$_3$ and In(PA)$_3$ during the treatment. Additionally, the phosphide resonance at ~200 ppm moves to a more negative chemical shift after treatment. Tomaselli *et al*. showed that a reduction in size can cause such a shift for InP QDs.[48] However, the resonance shift is much larger than what would be reasonably expected for a change in QD size. We therefore speculate that the nearby presence of fluoride influences the chemical shift of the P^{3-} resonance.

The presence of In(PA)$_3$ after InF$_3$ treatment is determined by comparing the ^{1}H NMR spectra of the QDs with a ^{1}H NMR spectrum of In(PA)$_3$. The spectra in Figure A2.1A,B

2

show resonances at 0.88, 1.25, 1.55, and 2.32 ppm for both the $In(PA)_3$ and the QDs. This confirms that $In(PA)_3$ is present in the QD sample. The broadening of the resonances at 1.55 and 2.32 ppm indicates that the majority of the $In(PA)_3$ is coordinated to the QDs, though a small amount of free palmitate is observed. The XPS spectrum in Figure A2.2A displays that after InF_3 treatment F is present in the QD sample, while none is detected before. After treatment, we observe that the In/P ratio increases from 1.3 to 2.0 (see Table A2.3). This suggests that the surface coverage of In has increased, although the ratio of 2.0 seems unrealistically high, even for the small InP QDs investigated. We consider that some of the additional In is present as excess $In(PA)_3$, in line with the relative increase in C and O content. If we assume that all additional In resides on the surface and that the core has an In/P ratio of 1:1, we estimate from the atomic composition a surface InF_3/$In(PA)_3$ ratio of 1:5.5. If we assume all measured carbon is part of $In(PA)_3$, we estimate an InF_3/$In(PA)_3$ ratio of 1:4. These numbers set a lower and upper bound to the real InF_3/$In(PA)_3$ ratio on the QD surface.

Additionally, ^{19}F NMR spectra are recorded for InF_3 and InP-InF_3 QDs and are shown in Figure A2.3. The solubility of InF_3 is low in any solvent, but it is found that DMSO-d_6 dissolves a measurable amount of InF3. The ^{19}F NMR spectrum for InF_3 shows a doublet around −166 ppm. However, in the ^{19}F NMR spectrum for InP-InF_3, recorded in $CDCl_3$ (since the QDs are insoluble in DMSO), no signal is observed. It is common for NMR signals from ligands to broaden when the ligand is coordinated to the QD surface due to the slower molecular tumbling compared to the free molecules in solution.[50, 51] Since it is clear from the XPS measurements that F is present in the InP-InF3 samples, this suggest that all F resides on the QD surface and that ^{19}F NMR spectrum of the InP-InF3 QDs has broadened so much that it becomes impossible to distinguish it from the measured noise. It is concluded from the ssNMR, ^{1}H NMR, ^{19}F NMR, and the XPS that the InF_3 treatment leads to the introduction of InF_3 as Z-type ligand on the QD surface without the complete exchange of $In(PA)_3$. Both InF_3 and $In(PA)_3$ reside on the surface. The $In(PA)_3$ is responsible for the colloidal stability in nonpolar solvents, while the small InF_3 increases the surface coverage of Z-type ligands and results in full passivation of P dangling bonds.

2.2.4 Preventing etching during InF3 treatment
Figure 2.3C shows the absorption and PL spectra for each data point during the treatment performed at 180 °C. After an initial red-shift, indicating addition of InF_3 to the surface, a blue-shift is observed for the 1S peak for longer treatment times, both in absorption and PL. Additionally, a shoulder appears on the blue side of the PL spectrum and becomes more pronounced at prolonged treatment times. The absorption and PL spectra of QDs treated at 120 and 150 °C are shown in Figure A2.4A,B and display similar blue-shifts and the rising of a PL shoulder at shorter wavelengths during the treatment. The shoulder at the blue sides of the PL spectra contributes to the increase in fwhm observed during the treatment. We found that this blue-shift is the result of the presence of trace amounts of free Brønsted acids which etch the QDs.

To test the effect of free Brønsted acid during the InF_3 treatment, an InF_3 treatment was performed both under strict acid-free conditions and in the presence of excess palmitic acid. The resulting absorption and PL spectra are shown in Figure 2.4 together with
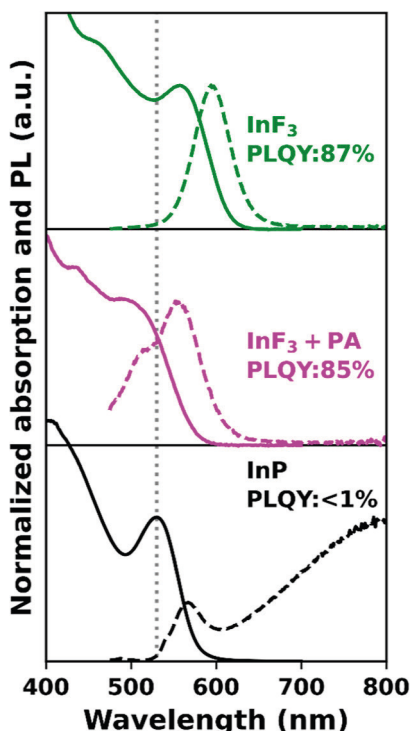
Figure 2.4: Absorption (solid) and PL (dashed) spectra for InP QDs before (black) and after InF$_3$ treatment at 180 °C for 60 minutes under excess acid (purple) and acid-free (green) conditions. The dashed grey line indicates the 1S absorption peak for the InP QDs before treatment.

the spectra for the InP QDs before treatment in green, purple, and black, respectively. For the InF$_3$ treatment in the presence of excess acid, the absorption blue-shifts and broadens, while a red-shift is observed after an acid-free treatment. The red-shift is in agreement with the increased size observed in TEM images, 2.9 nm before and 3.3 nm after treatment, as shown in Figure A2.5. Additionally, a clear blue-shifted shoulder is observed in the PL spectrum for the treatment with excess acid, and the fwhm of the PL increases to 87 nm, vs 50 nm for the acid-free treatment. The PLQYs obtained for the treatment with and without acid are 85 and 87%, respectively, showing that the presence of acid does not significantly affect the PLQY. Overall, this suggests that a small amount of Brønsted acid does not result in a different surface composition, but that it does cause deleterious etching of the InP QDs, similar to what was observed for HF treatments.[18, 29, 31, 32] We attribute the blue-shifted shoulder in the PL spectrum to a fraction of smaller QDs generated *via* acid etching.

We note that avoiding this etching requires stringent acid-free conditions. In our case, this included the use of clean, anhydrous solvents, pure In(PA)$_3$ without any free palmitic acid and, surprisingly, the use of clean and new stir bars. The acid-free nature of the In(PA)$_3$ was confirmed by ^{1}H NMR where an acid proton, at 10.88 ppm, as observed for PA is absent, see Figure A2.6. Proposedly, the PTFE coating of stir bars gets damaged at high

temperatures and is prone to absorbing and releasing contaminants, an observation that has been reported before.[52]

2.2.5 Generality of the method

We tested the generality of the method by performing the InF$_3$ treatment on InP QDs of different sizes and on InP QDs and made *via* different synthesis routes. We note that the treatment was not optimized for each case. The InF$_3$ treatment is applied to five different sizes of InP QDs with the exciton absorption, ranging from 490 to 630 nm. The QDs with the exciton absorption at 490, 540, and 560 nm were synthesized *via* a heat-up method, and those with an exciton absorption at 500 and 630 nm *via* a hot-injection synthesis. The absorption and PL spectra for these five InP QDs sizes after InF$_3$ treatment are shown in Figure 2.5A together with their PLQY.
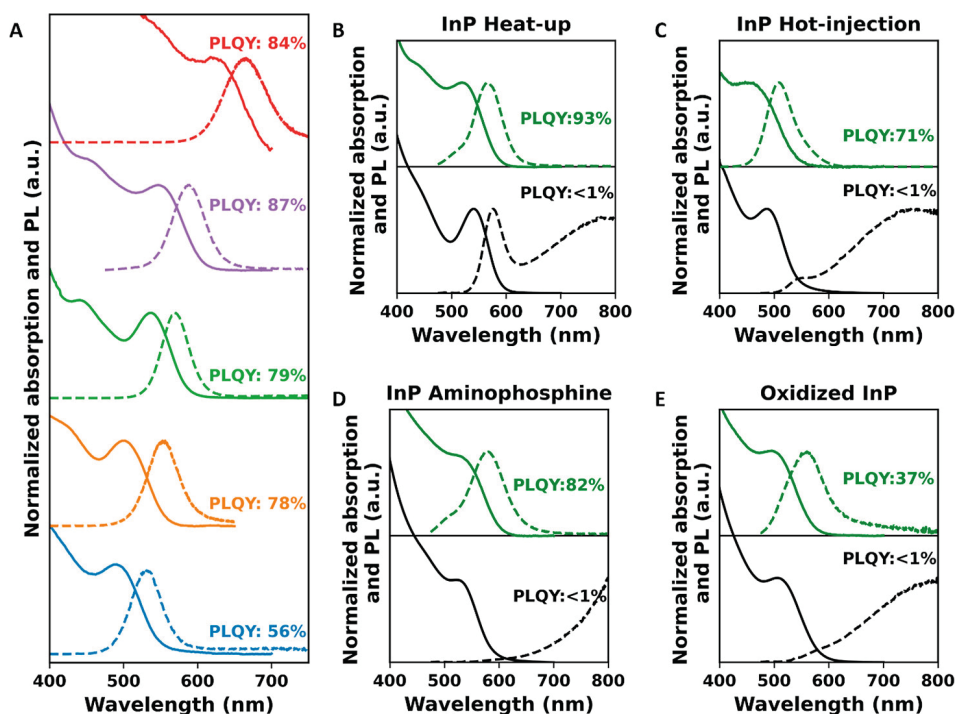
Figure 2.5: (A) Absorption (solid) and PL (dashed) spectra after InF$_3$ treatment at 180 °C for 60 minutes for five sizes of InP QDs. (B-E) Absorption (solid) and PL (dashed) spectra before (black) and after (green) InF$_3$ treatment at 180 °C for 60 minutes for InP QDs made *via* the heat-up synthesis method, InP QDs made *via* the hot-injection method, InP QDs made with the aminophosphine precursors and that are oxidized, respectively.

The PLQY increased from <1% to over 55% for the smallest InP QDs and peaks above 75% for the three other sizes of QDs. The PLQY has not been optimized independently for each QD size, which probably explains why the PLQY is not as high as that shown in Figure 2.2, but it is evident that the treatment is effective on all sizes.

Finally, we tested whether the effectiveness of the InF$_3$ treatment depends on the synthesis method and consequently the surface composition. In the literature, two types of phosphorus precursors are commonly used in the synthesis of InP QDs: tris(trimethylsilyl) phosphine (TMSP) or amino-phosphines such as tris(dimethylamino)phosphine and tris-(diethylamino)phosphine.[15, 26] In general, the synthesis with TMSP is performed at higher temperatures and involves long chain carboxylic acid ligands.[6, 15, 44, 46] The synthesis with aminophosphines, on the other hand, is performed at lower temperatures and is often combined with halide salts and fatty amine ligands.[26, 53] One of the main differences between InP QDs made *via* these two methods is therefore the ligands that are passivating the surface of the QDs. In the case of the synthesis with aminophosphines, this results in a surface copassivated by halides and amines, whereas a synthesis with TMSP generally leads to surface passivated with long carboxylic acids.[6, 25, 54] Within the TMSP synthesis method, two different methods can be distinguished: the hot-injection synthesis and the heat-up synthesis method. The difference between these synthesis methods is the temperature when the phosphorus precursor is injected, which as mentioned earlier, results in changes in the degree of surface oxidation.[18]

InP QDs made *via* the heat-up synthesis, the hot-injection method and with the aminophosphine precursor are synthesized, as described in the Experimental Section. Furthermore, to test whether the InF$_3$ treatment is also suitable for boosting the PLQY of InP QDs with a high degree of surface oxidation, InP QDs were deliberately oxidized after synthesis. The oxidation is performed by exposing the InP QDs made *via* the heat-up synthesis to an atmosphere of 20% O$_2$ and 80% N$_2$ gas at 120 °C for 30 minutes.

The InF$_3$ treatment was performed on the four types of InP QDs. The absorption and PL spectra are shown as the green lines in Figure 2.5B-E, and the PLQY is indicated in the figures. For all QDs, there is a clear increase in PLQY, but the final PLQY differs. The InP QDs made *via* the heat-up synthesis reach 93% PLQY, while those made *via* the hot-injection method reach 71%. The InP QDs synthesized with amino-phosphine precursors reach a PLQY of 82%. This PLQY is similar to the results obtained by Reiss and co-workers after performing an *in situ* HF treatment on InP QDs made with aminophosphine precursors.[36] An important difference, however, is that their result is obtained at room temperature, whereas the InF$_3$ in this work is performed at 180 °C. We remark again that the full optimization of the InF$_3$ treatment was performed only for the QDs made with the heat-up synthesis, and these conditions were applied to all samples. Hence, it is possible that higher PLQY values can be achieved for the other synthesis methods if the conditions are optimized. We interpret these results to mean that the InF$_3$ treatment is applicable to InP QDs regardless of their synthesis method or the surface composition.

In contrast, the maximum achieved PLQY for the InP QDs that were oxidized on purpose was only 36%. This suggests that the degree of oxidation of the InP QD surface is crucial for the success of this treatment, even if it is clear from DFT calculations[18] and the presence of PO$_4^{3-}$ in near-unity PLQY InP QD samples that surface phosphate does not introduce in-gap trap states. Rather, we speculate that too severe oxidation of the surface prevents the complete coverage of the QD surface with Z-type ligands.

The results of this study are promising for implementation of this treatment in industrial

2

processes, necessitating the scaling up of the treatment method. Critical aspects include ensuring uniform heating of the reaction mixture, efficient mixing of reactants, and effective separation of products. These factors must be addressed before implementing the InF_3 treatment for enhancing the PLQY of InP QDs industrially. Additionally, optimizing the treatment based on the surface chemistry of synthesized InP QDs is essential. Besides the challenges of scaling up this reaction, the environmental impact of this treatment must also be considered. InF_3 as a chemical is considered relatively safe but the synthesis, usage, and disposal pose the largest environmental concerns. Production of InF_3 can release fluorine byproducts, potentially harming ecosystems, and disposal may lead to the persistence of indium and fluorine, impacting soil and water quality.

2.3 Conclusions

In conclusion, this work describes a simple but effective postsynthesis treatment that consist of covering the surface of InP QDs with InF_3. Under optimized conditions, InP core-only QDs are obtained with a near-unity PLQY and single exponential photoluminescence decay curves. We further show that etching of the InP QDs can be fully prevented by working under acid-free conditions allowing for a near-unity PLQY without significant spectral broadening. Furthermore, it is shown that this method is effective on InP QDs of a wide range of sizes and made *via* different synthesis methods. Only severe oxidation of the surface of InP QDs limits the effectiveness of the InF_3 treatment.

2.4 Methods/experimental

Materials

The following materials were purchased from Merck Sigma and used as received: indium acetate [$In(OAc)_3$, 99.99%], myristic acid (MA, >99%), anhydrous hexadecane (99%), trioctyl-phosphide (TOP, 97%), anhydrous acetone (99.8%), palmitic acid (PA, 99%), fluorescein, $InCl_3$ (99.999%), $ZnCl_2$ (>98%), $ZnBr^2$ (99.999%), ZnI^2 (98%), AlF^3 (99%), $AlCl^3$ (99.99%), $CdCl^2$(99.99%), MgF_2 (99.99), and tris(diethylamino)phosphine (97%). Octadecene (ODE, 90%, Merck Sigma) is degassed in vacuo at 100 °C before being stored in the glovebox. Ar (6 N), Ar/H_2 (98:2, 6 N), and N_2/O_2 (80:20, 6 N) were purchased from Linde. InF_3 (99.95%) and anhydrous toluene (99.8) were purchased from Alfa Aesar. NaOH pellets (98.5%) and oleylamine (80–90%) were bought from Acros. Tris(trimethylsilyl)phosphine (TMSP, 98%) was obtained from Strem. ZnF_2 (99%), heptane (99%), chloroform, and ethanol were purchased from VWR.

Heat-up TMSP based synthesis of InP QDs

The synthesis is adapted from method described in the work of Li, *et al.*[44] In a typical synthesis, $In(OAc)_3$ (200 mg, 0.685 mmol), MA (469.6 mg, 2.06 mmol) and anhydrous hexadecane (24.6 mL) were added to a three-neck round-bottom flask. The mixture was degassed at a Schlenk line under vacuum at room temperature for 30 minutes. Ar/H_2 (98:2) was then bubbled through the solution at a rate of 0.3 L/min and the mixture was heated to 150 °C for 30 minutes. TOP (3000 mg, 8.09 mmol) was injected into the mixture and the mixture was reheated to 150 °C. At this temperature, a solution of TMSP (82.70 mg, 0.33 mmol) in anhydrous hexadecane (5.09 mL) was swiftly injected in the reaction mixture and the temperature was ramped to 270 °C in ten minutes. The mixture was

cooled to room temperature with an air gun after the reaction had run for 7 minutes. The QDs were purified by precipitation with 5 volume equivalents of anhydrous acetone, followed by centrifugation at 5000 rpm for 10 minutes. The supernatant was discarded and the solid residue was redispersed in anhydrous toluene. This purification step was repeated once and afterwards the QDs were dispersed in anhydrous hexadecane.

Hot-injection TMSP based synthesis of InP QDs

The synthesis method is based on the works reported by Won, et al and Ubbink, *et al.*[6, 18] In a three-neck round-bottom flask, In(OAc)$_3$ (585 mg, 2.00 mmol), PA (1535 mg, 6.00 mmol) and ODE (50 mL) are loaded. The flask is connected to a Schlenk line and the mixture is degassed at 120 °C under vacuum for 60 minutes. The atmosphere is then changed to N$_2$ gas and N$_2$ gas is blown over the surface of the reaction mixture with a rate of 0.4 L/min. The temperature is raised to 280 °C and a solution of TMSP (375.81 mg) in TOP (5 mL) is swiftly injected, prompting a decrease in reaction temperature. The temperature is set to 260 °C and the reaction proceeded for 12 minutes. The reaction mixture is cooled to room temperature with an air gun. The purification was performed in the same way as stated above for the heat-up synthesis method.

Oxidation of InP QDs

In a typical synthesis, anhydrous hexadecane (5 mL) is loaded in a three-neck round-bottom flask and degassed at a Schlenk line under vacuum at room temperature for 30 minutes. The flask is then placed under Ar atmosphere and InP QDs (60 nmol, in anhydrous toluene) are injected. The solution is then degassed under vacuum for 30 minutes. The reaction flask is then disconnected from the Schlenk line, keeping the reaction mixture under reduced pressure. A gaseous O$_2$/N$_2$ mixture (80:20) is bubbled through the solution until atmospheric pressure is obtained. The reaction mixture is heated to 150 °C for 30 minutes and then cooled to room temperature with an air gun. The purification was performed in the same way as stated above for the heat-up synthesis method.

Aminophosphine-based synthesis of InP QDs

The procedure is based on the method previously published by Tessier et al.[53] 100 mg (0.45 mmol) of indium(III) chloride and 300 mg (2.20 mmol) of zinc(II) chloride were mixed in 3 mL (9.10 mmol) of anhydrous oleylamine in a 25 mL flask. The mixture was stirred and degassed at 120°C for an hour and then heated to 180°C under inert atmosphere. Upon reaching 180°C, 0.50 mL (1.83 mmol) of tris(diethylamino)phosphine, transaminated with 2 mL (6.07 mmol) of anhydrous oleylamine, was quickly injected in the reaction mixture described above and the InP nanocrystal synthesis proceeded for 30 min. The synthetized InP QDs were purified using anhydrous ethanol.

Preparation of the In(PA)3 precursor

The procedure is based on the method previously published in the work of Angele, *et al.*[55] PA (5.1 g, 13.2 mmol) and In(OAc)$_3$ (0.6 g, 1.36 mmol) are loaded in a 25 mL 3-neck round-bottom flask. The reaction mixture is stirred under reduced atmosphere at 120 °C for 6 hours. The reaction mixture is then filtered over a glass filter and the solid is washed with ethanol (5 × 20 mL), heptane (5 × 20 mL) and chloroform (1 × 20 mL). The solid is then dried *in vacuo* and subsequently stored in the glovebox.

Metal halide treatment of InP QDs

In a typical metal halide treatment, the metal halide (0.73 mmol), $In(PA)_3$ (44 mg, 0.05 mmol) and InP QDs (1.0 mL in anhydrous hexadecane, 50 μM) are mixed in a glass vial. The mixture is heated to a temperature between 120 and 180 °C and stirred for 1-150 minutes. The reaction mixture is cooled to room temperature and centrifuged at 5000 rpm for 10 minutes to separate the remaining solid metal halide from the QDs in dispersion. The supernatant containing the InP QDs was then diluted with anhydrous acetone and centrifuged at 5000 rpm for 10 minutes. The supernatant was discarded and the treated InP QDs were redispersed in anhydrous toluene.

In a typical InF_3 treatment performed at the optimal parameters, InF_3 (125 mg, 0.73 mmol), $In(PA)_3$ (44 mg, 0.05 mmol) and InP QDs (1.25 mL in anhydrous hexadecane, 50 μM) are mixed in a glass vial. We note that InF_3 is poorly soluble in hexadecane so that a saturated solution with noticeable white precipitate results. The mixture is heated to 180 °C and stirred for 60 minutes. The separation and redispersion in anhydrous toluene are performed in the same manner as described for the general metal halide treatment.

Optical characterization

A PerkinElmer Lambda 365 spectrometer was used for recording the UV-vis absorption spectra. An Edinburgh Instruments FLS980 spectrofluorometer with double grating monochromators for both excitation and emission paths and a 450 W Xenon lamp as an excitation source. PLQY values were obtained with respect to the Fluorescein reference dye in 0.1 M NaOH in water at room temperature. The PLQY was calculated using the following equation;

$$PLQY = PLQY_{fluorescein} \times \frac{I^{PL}_{QD\ solution} \times f_{fluorescein}}{I^{PL}_{fluorescein} \times f_{QD\ solution}} \times \left(\frac{n_{toluene}}{n_{water}}\right)^2$$

Where $PLQY_{Fluorescein}$ is set to be 92% for an excitation wavelength of 465 nm,[56] I^{PL} is the intensity of the PL signal of either the Fluorescein solution or the QD solution, n is the refractive index of toluene or water at 465 nm (1.4969 and 1.333) and f is the fraction of absorbed light for the Fluorescein or toluene solution, calculated as $f = 10^{-OD}$ with the OD being the optical density of the Fluorescein or QD solution at 465 nm. PLQYs obtained *via* this method were found to be reproducible, with an measurement error of <3% on the PLQY values based on replication of the PLQY measurement on various samples that we prepared in identical fashion.

Additionally, the PLQY was measured using an Edinburgh Instruments FLS980 spectrometer with a calibrated integrating sphere. The emission was recorded between 475 and 800 nm and the samples were excited at 465 nm.

An Edinburgh Instruments Lifespec TCSPC with a 400 nm pulsed laser was used for recording the PL decay traces. The PL decay traces are fitted with a biexponential or triexponential fitting function and the intensity-weighted average lifetimes are calculated with the equation $\tau_{ave} = (A_1\tau_1^2 + A_2\tau_2^2)/(A_1\tau_1 + A_2\tau_2)$ and $\tau_{ave} = (A_1\tau_1^2 + A_2\tau_2^2 + A_3\tau_3^2)/(A_1\tau_1 + A_2\tau_2 + A_3\tau_3)$ with A_n and τ_n the amplitude and lifetime of the first and second exponent.

2

ssNMR characterization

For solid state NMR analysis, samples dispersed in anhydrous toluene were dried by evaporating the solvent *in vacuo*, then the dried QDs were mixed with activated alumina and loaded into a 4 mm Zirconia rotor. Measurements were performed with a Bruker Ascend 500 magnet (11.7 T) equipped with a NEO console operating at a ^{31}P resonance frequency of 202.45 MHz, using a three channel DVY MAS probe from Bruker. ^{31}P spectra were referenced to external H$_3$PO$_4$ (= 0 ppm). Single pulse ^{31}P spectra were collected with a MAS frequency of 8 kHz, a recycle delay (d1) of 50 s and a 4.8 µs pulse width. Proton decoupling was performed during acquisition using the Spinal-64 decoupling sequence.

Solution Nuclear Magnetic Resonance (NMR)

An Agilent 400-MR DD2 which is equipped with a 5 mm ONE NMR Probe was used to record solution NMR spectra. ^{1}H-NMR (399.7 MHz) spectra were obtained with a recycle delay of 1 s in deuterated chloroform. Signals are referenced with residual chloroform peaks (7.26 ppm). ^{19}F-NMR (399.7 MHz) spectra were obtained with a recycle delay of 1 s in deuterated chloroform or DMSO.

X-ray Photoelectron Spectroscopy (XPS)

Samples are dropcasted on thin conductive substrates. XPS measurements were performed in ultra high vacuum with a ThermoFisher K-Alpha equipped with an Al Kα source which radiates with an energy of 1486 eV. An Ar flood gun was used during the measurements to prevent charging.

Transmission Electron Microscopy (TEM)

Samples are dropcasted on grids and TEM images were acquired with a JEOL JEM1400 transmission electron microscope which operates at 120 kV.

References

1.   Wu, Z.; Liu, P.; Zhang, W.; Wang, K.; Sun, X. W., Development of InP Quantum Dot-Based Light-Emitting Diodes. *ACS Energy Letters* **2020,** *5* (4), 1095-1106.
2.   Geuchies, J. J.; Brynjarsson, B.; Grimaldi, G.; Gudjonsdottir, S.; van der Stam, W.; Evers, W. H.; Houtepen, A. J., Quantitative Electrochemical Control over Optical Gain in Quantum-Dot Solids. *ACS Nano* **2020**.
3.   Coe-Sullivan, S.; Liu, W.; Allen, P.; Steckel, J. S., Quantum Dots for LED Downconversion in Display Applications. *ECS Journal of Solid State Science and Technology* **2013,** *2* (2), R3026.
4.   Park, Y.-S.; Roh, J.; Diroll, B. T.; Schaller, R. D.; Klimov, V. I., Colloidal quantum dot lasers. *Nature Reviews Materials* **2021,** *6* (5), 382-401.
5.   Talapin, D. V.; Steckel, J., Quantum dot light-emitting devices. *MRS Bulletin* **2013,** *38* (9), 685-691.
6.   Won, Y.-H.; Cho, O.; Kim, T.; Chung, D.-Y.; Kim, T.; Chung, H.; Jang, H.; Lee, J.; Kim, D.; Jang, E., Highly efficient and stable InP/ZnSe/ZnS quantum dot light-emitting diodes. *Nature* **2019,** *575* (7784), 634-638.
7.   Carey, G. H.; Abdelhady, A. L.; Ning, Z.; Thon, S. M.; Bakr, O. M.; Sargent, E. H., Colloidal Quantum Dot Solar Cells. *Chemical Reviews* **2015,** *115* (23), 12732-12763.
8.   Ganesan, A. A.; Houtepen, A. J.; Crisp, R. W. Quantum Dot Solar Cells: Small Beginnings Have Large Impacts *Applied Sciences* [Online], 2018.
9.   Geiregat, P.; Houtepen, A. J.; Sagar, L. K.; Infante, I.; Zapata, F.; Grigel, V.; Allan, G.; Delerue, C.; Van Thourhout, D.; Hens, Z., Continuous-wave infrared optical gain and amplified

spontaneous emission at ultralow threshold by colloidal HgTe quantum dots. *Nature Materials* **2018,** *17* (1), 35-42.

10. Lim, J.; Park, Y.-S.; Klimov, V. I., Optical gain in colloidal quantum dots achieved with direct-current electrical pumping. *Nature Materials* **2018,** *17* (1), 42-49.

11. Karadza, B.; Van Avermaet, H.; Mingabudinova, L.; Hens, Z.; Meuret, Y., Efficient, high-CRI white LEDs by combining traditional phosphors with cadmium-free InP/ZnSe red quantum dots. *Photon. Res.* **2022,** *10* (1), 155-165.

12. Kwak, D.-H.; Ramasamy, P.; Lee, Y.-S.; Jeong, M.-H.; Lee, J.-S., High-Performance Hybrid InP QDs/Black Phosphorus Photodetector. *ACS Applied Materials & Interfaces* **2019,** *11* (32), 29041-29046.

13. Zhang, Y.; Lv, Y.; Li, L.-S.; Zhao, X.-J.; Zhao, M.-X.; Shen, H., Aminophosphate precursors for the synthesis of near-unity emitting InP quantum dots and their application in liver cancer diagnosis. *Exploration* **2022,** *2* (4), 20220082.

14. Karadza, B.; Schiettecatte, P.; Van Avermaet, H.; Mingabudinova, L.; Giordano, L.; Respekta, D.; Deng, Y.-H.; Nakonechnyi, I.; De Nolf, K.; Walravens, W.; Meuret, Y.; Hens, Z., Bridging the Green Gap: Monochromatic InP-Based Quantum-Dot-on-Chip LEDs with over 50% Color Conversion Efficiency. *Nano Letters* **2023,** *23* (12), 5490-5496.

15. Almeida, G.; Ubbink, R. F.; Stam, M.; du Fossé, I.; Houtepen, A. J., InP colloidal quantum dots for visible and near-infrared photonics. *Nature Reviews Materials* **2023,** *8* (11), 742-758.

16. Hughes, K. E.; Stein, J. L.; Friedfeld, M. R.; Cossairt, B. M.; Gamelin, D. R., Effects of Surface Chemistry on the Photophysics of Colloidal InP Nanocrystals. *ACS Nano* **2019,** *13* (12), 14198-14207.

17. Gary, D. C.; Terban, M. W.; Billinge, S. J. L.; Cossairt, B. M., Two-Step Nucleation and Growth of InP Quantum Dots via Magic-Sized Cluster Intermediates. *Chemistry of Materials* **2015,** *27* (4), 1432-1441.

18. Ubbink, R. F.; Almeida, G.; Iziyi, H.; du Fossé, I.; Verkleij, R.; Ganapathy, S.; van Eck, E. R. H.; Houtepen, A. J., A Water-Free In Situ HF Treatment for Ultrabright InP Quantum Dots. *Chemistry of Materials* **2022,** *34* (22), 10093-10103.

19. Achorn, O. B.; Franke, D.; Bawendi, M. G., Seedless Continuous Injection Synthesis of Indium Phosphide Quantum Dots as a Route to Large Size and Low Size Dispersity. *Chemistry of Materials* **2020,** *32* (15), 6532-6539.

20. Janke, E. M.; Williams, N. E.; She, C.; Zherebetskyy, D.; Hudson, M. H.; Wang, L.; Gosztola, D. J.; Schaller, R. D.; Lee, B.; Sun, C.; Engel, G. S.; Talapin, D. V., Origin of Broad Emission Spectra in InP Quantum Dots: Contributions from Structural and Electronic Disorder. *Journal of the American Chemical Society* **2018,** *140* (46), 15791-15803.

21. Tessier, M. D.; Baquero, E. A.; Dupont, D.; Grigel, V.; Bladt, E.; Bals, S.; Coppel, Y.; Hens, Z.; Nayral, C.; Delpech, F., Interfacial Oxidation and Photoluminescence of InP-Based Core/Shell Quantum Dots. *Chemistry of Materials* **2018,** *30* (19), 6877-6883.

22. Cho, E.; Kim, T.; Choi, S.-m.; Jang, H.; Min, K.; Jang, E., Optical Characteristics of the Surface Defects in InP Colloidal Quantum Dots for Highly Efficient Light-Emitting Applications. *ACS Applied Nano Materials* **2018,** *1* (12), 7106-7114.

23. Yang, W.; Yang, Y.; Kaledin, A. L.; He, S.; Jin, T.; McBride, J. R.; Lian, T., Surface passivation extends single and biexciton lifetimes of InP quantum dots. *Chemical Science* **2020,** *11* (22), 5779-5789.

24. Kim, T.-G.; Zherebetskyy, D.; Bekenstein, Y.; Oh, M. H.; Wang, L.-W.; Jang, E.; Alivisatos, A. P., Trap Passivation in Indium-Based Quantum Dots through Surface Fluorination: Mechanism and Applications. *ACS Nano* **2018,** *12* (11), 11529-11540.

25. Dümbgen, K. C.; Leemans, J.; De Roo, V.; Minjauw, M.; Detavernier, C.; Hens, Z., Surface Chemistry of InP Quantum Dots, Amine–Halide Co-Passivation, and Binding of Z-Type Ligands. *Chemistry of Materials* **2023,** *35* (3), 1037-1046.

26. Van Avermaet, H.; Schiettecatte, P.; Hinz, S.; Giordano, L.; Ferrari, F.; Nayral, C.; Delpech, F.;

Maultzsch, J.; Lange, H.; Hens, Z., Full-Spectrum InP-Based Quantum Dots with Near-Unity Photoluminescence Quantum Efficiency. *ACS Nano* **2022**.

27. Kim, Y.; Ham, S.; Jang, H.; Min, J. H.; Chung, H.; Lee, J.; Kim, D.; Jang, E., Bright and Uniform Green Light Emitting InP/ZnSe/ZnS Quantum Dots for Wide Color Gamut Displays. *ACS Applied Nano Materials* **2019**, *2* (3), 1496-1504.

28. Zhao, T.; Zhao, Q.; Lee, J.; Yang, S.; Wang, H.; Chuang, M.-Y.; He, Y.; Thompson, S. M.; Liu, G.; Oh, N.; Murray, C. B.; Kagan, C. R., Engineering the Surface Chemistry of Colloidal InP Quantum Dots for Charge Transport. *Chemistry of Materials* **2022**, *34* (18), 8306-8315.

29. Mićić, O. I.; Sprague, J.; Lu, Z.; Nozik, A. J., Highly efficient band-edge emission from InP quantum dots. *Applied Physics Letters* **1996**, *68* (22), 3150-3152.

30. Trung, H. M.; Thien, N. D.; Van Vu, L.; Long, N. N.; Hieu, T. K., Synthesis of indium phosphide nanocrystals by sonochemical method and survey of optical properties*. *Eur. Phys. J. Appl. Phys.* **2013**, *64* (1), 10402.

31. Adam, S.; Talapin, D. V.; Borchert, H.; Lobo, A.; McGinley, C.; de Castro, A. R. B.; Haase, M.; Weller, H.; Möller, T., The effect of nanocrystal surface structure on the luminescence properties: Photoemission study of HF-etched InP nanocrystals. *The Journal of Chemical Physics* **2005**, *123* (8), 084706.

32. Talapin, D. V.; Gaponik, N.; Borchert, H.; Rogach, A. L.; Haase, M.; Weller, H., Etching of Colloidal InP Nanocrystals with Fluorides: Photochemical Nature of the Process Resulting in High Photoluminescence Efficiency. *The Journal of Physical Chemistry B* **2002**, *106* (49), 12659-12663.

33. Mićić, O. I.; Jones, K. M.; Cahill, A.; Nozik, A. J., Optical, Electronic, and Structural Properties of Uncoupled and Close-Packed Arrays of InP Quantum Dots. *The Journal of Physical Chemistry B* **1998**, *102* (49), 9791-9796.

34. Click, S. M.; Rosenthal, S. J., Synthesis, Surface Chemistry, and Fluorescent Properties of InP Quantum Dots. *Chemistry of Materials* **2023**, *35* (3), 822-836.

35. Li, H.; Zhang, W.; Bian, Y.; Ahn, T. K.; Shen, H.; Ji, B., ZnF2-Assisted Synthesis of Highly Luminescent InP/ZnSe/ZnS Quantum Dots for Efficient and Stable Electroluminescence. *Nano Letters* **2022**, *22* (10), 4067-4073.

36. Yadav, R.; Kwon, Y.; Rivaux, C.; Saint-Pierre, C.; Ling, W. L.; Reiss, P., Narrow Near-Infrared Emission from InP QDs Synthesized with Indium(I) Halides and Aminophosphine. *Journal of the American Chemical Society* **2023**, *145* (10), 5970-5981.

37. Green, M. L. H., A new approach to the formal classification of covalent compounds of the elements. *Journal of Organometallic Chemistry* **1995**, *500* (1), 127-148.

38. Bullen, C.; Mulvaney, P., The Effects of Chemisorption on the Luminescence of CdSe Quantum Dots. *Langmuir* **2006**, *22* (7), 3007-3013.

39. Kirkwood, N.; Monchen, J. O. V.; Crisp, R. W.; Grimaldi, G.; Bergstein, H. A. C.; du Fossé, I.; van der Stam, W.; Infante, I.; Houtepen, A. J., Finding and Fixing Traps in II–VI and III–V Colloidal Quantum Dots: The Importance of Z-Type Ligand Passivation. *Journal of the American Chemical Society* **2018**, *140* (46), 15712-15723.

40. Page, R. C.; Espinobarro-Velazquez, D.; Leontiadou, M. A.; Smith, C.; Lewis, E. A.; Haigh, S. J.; Li, C.; Radtke, H.; Pengpad, A.; Bondino, F.; Magnano, E.; Pis, I.; Flavell, W. R.; O'Brien, P.; Binks, D. J., Near-Unity Quantum Yields from Chloride Treated CdTe Colloidal Quantum Dots. *Small* **2015**, *11* (13), 1548-1554.

41. Gao, Y.; Peng, X., Photogenerated Excitons in Plain Core CdSe Nanocrystals with Unity Radiative Decay in Single Channel: The Effects of Surface and Ligands. *Journal of the American Chemical Society* **2015**, *137* (12), 4230-4235.

42. Calvin, J. J.; Swabeck, J. K.; Sedlak, A. B.; Kim, Y.; Jang, E.; Alivisatos, A. P., Thermodynamic Investigation of Increased Luminescence in Indium Phosphide Quantum Dots by Treatment with Metal Halide Salts. *Journal of the American Chemical Society* **2020**, *142* (44), 18897-18906.

43. Stein, J. L.; Mader, E. A.; Cossairt, B. M., Luminescent InP Quantum Dots with Tunable

2

Emission by Post-Synthetic Modification with Lewis Acids. *The Journal of Physical Chemistry Letters* **2016,** *7* (7), 1315-1320.

44. Li, Y.; Hou, X.; Dai, X.; Yao, Z.; Lv, L.; Jin, Y.; Peng, X., Stoichiometry-Controlled InP-Based Quantum Dots: Synthesis, Photoluminescence, and Electroluminescence. *Journal of the American Chemical Society* **2019,** *141* (16), 6448-6452.

45. Cros-Gagneux, A.; Delpech, F.; Nayral, C.; Cornejo, A.; Coppel, Y.; Chaudret, B., Surface Chemistry of InP Quantum Dots: A Comprehensive Study. *Journal of the American Chemical Society* **2010,** *132* (51), 18147-18157.

46. Almeida, G.; van der Poll, L.; Evers, W. H.; Szoboszlai, E.; Vonk, S. J. W.; Rabouw, F. T.; Houtepen, A. J., Size-Dependent Optical Properties of InP Colloidal Quantum Dots. *Nano Letters* **2023,** *23* (18), 8697-8703.

47. Baquero, E. A.; Virieux, H.; Swain, R. A.; Gillet, A.; Cros-Gagneux, A.; Coppel, Y.; Chaudret, B.; Nayral, C.; Delpech, F., Synthesis of Oxide-Free InP Quantum Dots: Surface Control and H2-Assisted Growth. *Chemistry of Materials* **2017,** *29* (22), 9623-9627.

48. Tomaselli, M.; Yarger, J. L.; Bruchez, M., Jr.; Havlin, R. H.; deGraw, D.; Pines, A.; Alivisatos, A. P., NMR study of InP quantum dots: Surface structure and size effects. *The Journal of Chemical Physics* **1999,** *110* (18), 8861-8864.

49. Stein, J. L.; Holden, W. M.; Venkatesh, A.; Mundy, M. E.; Rossini, A. J.; Seidler, G. T.; Cossairt, B. M., Probing Surface Defects of InP Quantum Dots Using Phosphorus Kα and Kβ X-ray Emission Spectroscopy. *Chemistry of Materials* **2018,** *30* (18), 6377-6388.

50. Hens, Z.; Martins, J. C., A Solution NMR Toolbox for Characterizing the Surface Chemistry of Colloidal Nanocrystals. *Chemistry of Materials* **2013,** *25* (8), 1211-1221.

51. Vogel, Y. B.; Stam, M.; Mulder, J. T.; Houtepen, A. J., Long-Range Charge Transport via Redox Ligands in Quantum Dot Assemblies. *ACS Nano* **2022,** *16* (12), 21216-21224.

52. Pentsak, E. O.; Eremin, D. B.; Gordeev, E. G.; Ananikov, V. P., Phantom Reactivity in Organic and Catalytic Reactions as a Consequence of Microscale Destruction and Contamination-Trapping Effects of Magnetic Stir Bars. *ACS Catalysis* **2019,** *9* (4), 3070-3081.

53. Tessier, M. D.; Dupont, D.; De Nolf, K.; De Roo, J.; Hens, Z., Economic and Size-Tunable Synthesis of InP/ZnE (E = S, Se) Colloidal Quantum Dots. *Chemistry of Materials* **2015,** *27* (13), 4893-4898.

54. Kim, K.; Yoo, D.; Choi, H.; Tamang, S.; Ko, J.-H.; Kim, S.; Kim, Y.-H.; Jeong, S., Halide–Amine Co-Passivated Indium Phosphide Colloidal Quantum Dots in Tetrahedral Shape. *Angewandte Chemie International Edition* **2016,** *55* (11), 3714-3718.

55. Angelé, L.; Dreyfuss, S.; Dubertret, B.; Mézailles, N., Synthesis of Monodisperse InP Quantum Dots: Use of an Acid-Free Indium Carboxylate Precursor. *Inorganic Chemistry* **2021,** *60* (4), 2271-2278.

56. Magde, D.; Wong, R.; Seybold, P. G., Fluorescence Quantum Yields and Their Relation to Lifetimes of Rhodamine 6G and Fluorescein in Nine Solvents: Improved Absolute Standards for Quantum Yields. *Photochemistry and Photobiology* **2002,** *75* (4), 327-334.

57. https://www.chemspider.com/, accessed on March 1st 2024.

58. https://www.chemeurope.com/en/encyclopedia/Solubility_table.html, accessed on March 1st 2024.

Appendix

Table A2.1: Solubility of several metal halide salts in water at 20 °C in g/100 cm^3.[57, 58]

Compound	Formula	Solubility g/100 cm^3 in water (20 °C)
Indium(III) Fluoride	InF$_3$	11.2
Indium(III) Chloride	InCl$_3$	212
Zinc(II) Chloride	ZnCl$_2$	395
Zinc(II) Fluoride	ZnF$_2$	1.6
Zinc(II) Bromide	ZnBr$_2$	446
Zinc(II) Iodide	ZnI$_2$	432
Aluminum(III) Fluoride	AlF$_3$	0.67
Aluminum(III) Chloride	AlCl$_3$	45.8
Cadmium(II) Chloride	CdCl$_2$	135
Magnesium(II) Fluoride	MgF$_2$	0.007325
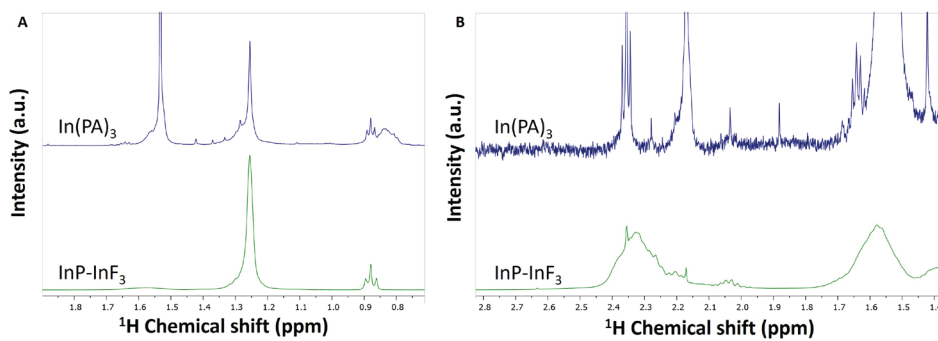
Figure A2.1: ^{1}H NMR of In(PA)$_3$ and InP-InF$_3$ QDs in CDCl$_3$.

Table A2.2: PLQY measured for five InP QD samples treated at the optimal conditions (180 °C for 60 minutes) with respect to a reference dye and in an integrating sphere. The symbols μ and σ indicate the PLQY average and standard deviation (in absolute percentages), respectively.

| #	PLQY dye (%)	PLQY dye (next day) (%)	PLQY sphere (%)	PLQY sphere (next day) (%)	μ dye (%)	σ dye (%)	μ sphere (%)	σ sphere (%)	μ all (%)	σ all (%)
1	91.6	89.6	83.9	88.9	90.6	1.0	86.4	2.5	88.5	2.8
2	98.5	90.3	91.6	89	94.4	4.1	90.3	1.3	92.4	3.7
3	90.6	88.4	85.4	90.2	89.5	1.1	87.8	2.4	88.7	2.1
4	94.8	87.5	87.4	93.7	91.2	3.7	90.6	3.2	90.9	3.4
5	94.9	90.1	94.2	94.4	92.5	2.4	94.3	0.1	93.4	1.9
μ	94.1	89.2	88.5	91.2	91.6		89.9		90.8	
σ	2.8	1.1	3.8	2.3	3.2		3.5		3.5	
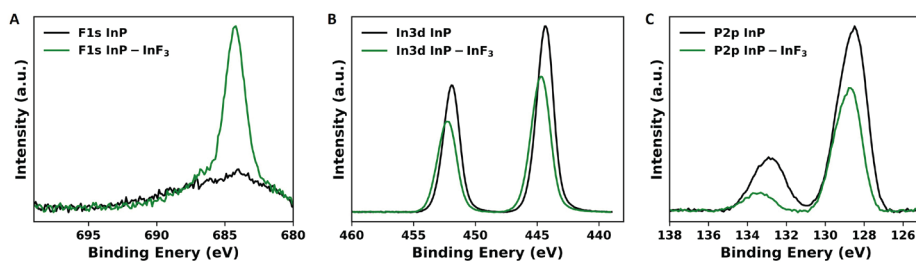
Figure A2.2: XPS spectrum of the F1s (A), In3d (B) and P2p (C) photoemission line for InP (black) and InP-InF$_3$ (green).

Table A2.3: Elemental composition of InP QD samples before and after InF$_3$ treatment, as determined by XPS.

	Surface scan		After ion beam etching	
Element	As synthesized	InF3 treated	As synthesized	InF3 treated
C(%)	75.86	74.67	72.59	82.09
In(%)	5.62	4.53	12.77	7.27
O(%)	14.33	17.51	6.58	5.76
P(%)	4.19	2.22	8.06	3.3
F(%)		1.07		1.57
In:P	1.34	2.04	1.58	2.20
In:F		4.23		4.63
P:F		2.07		2.10
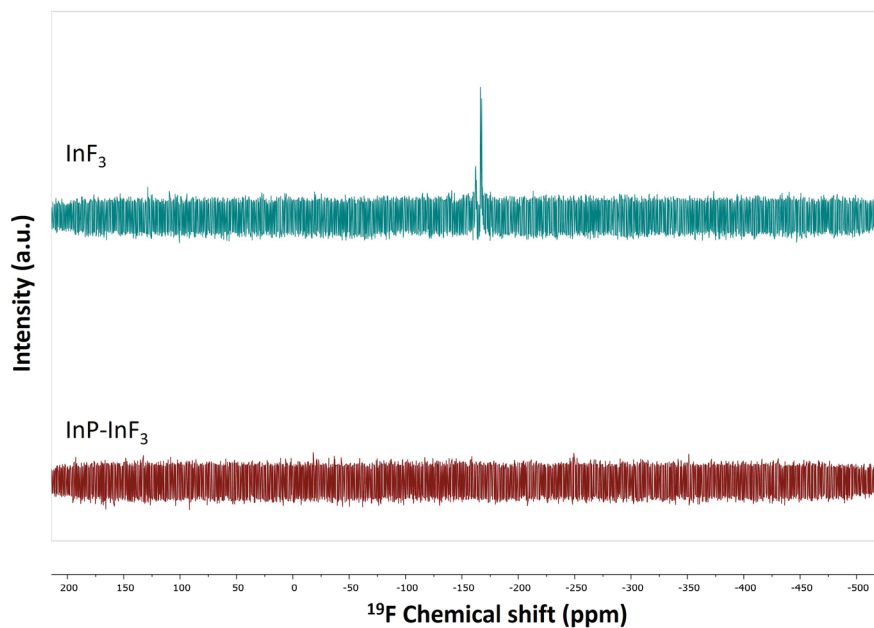
Figure A2.3: ^{19}F NMR of InF$_3$ (TOP) and InP-InF$_3$ (bottom) in DMSO-d$_6$ and CDCl$_3$, respectively.

2
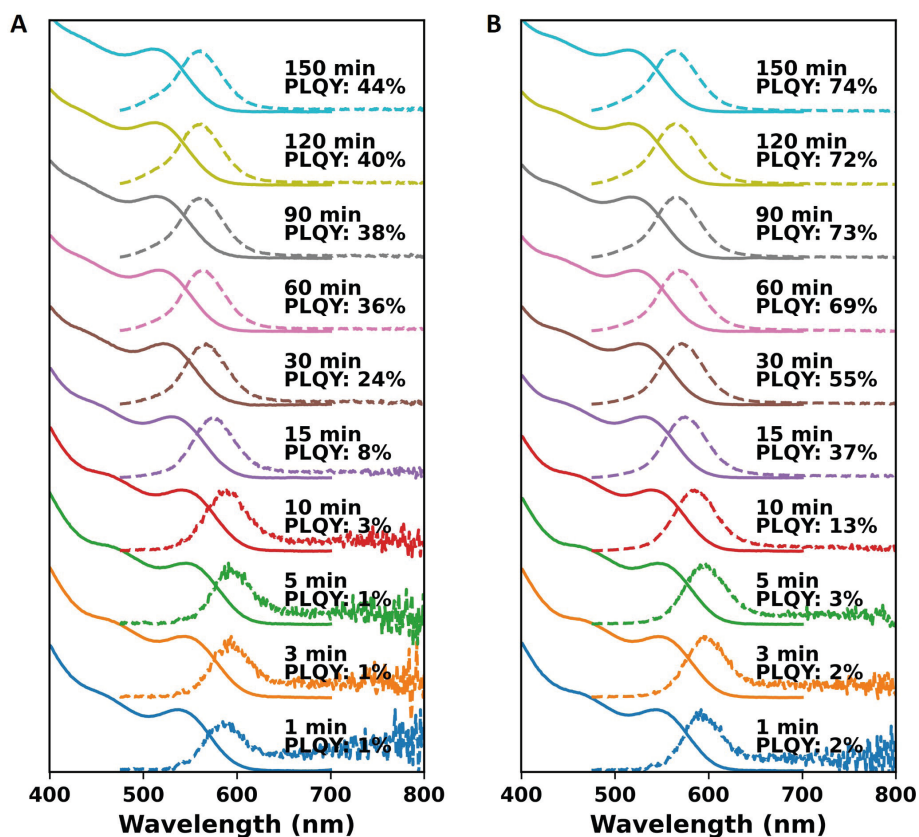
Figure A2.4: The absorption and PL spectra of aliquots collected during the treatment at 120 °C A) and 150 °C B). Time and PLQY are shown on top of each plot.
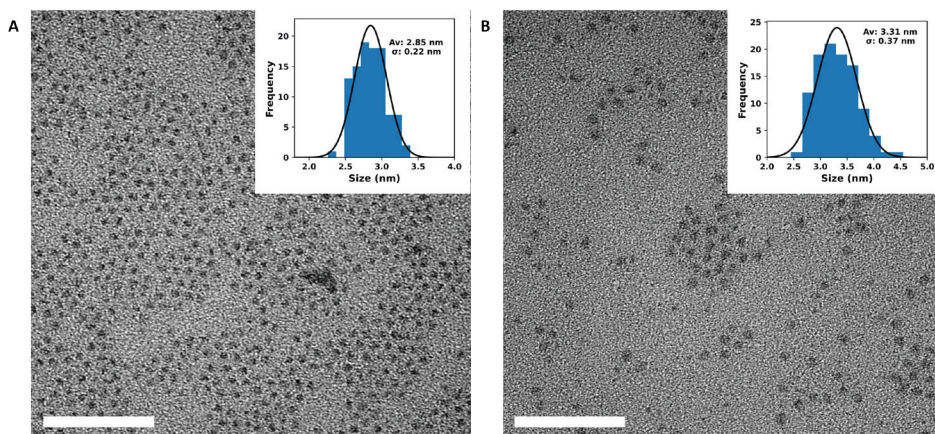
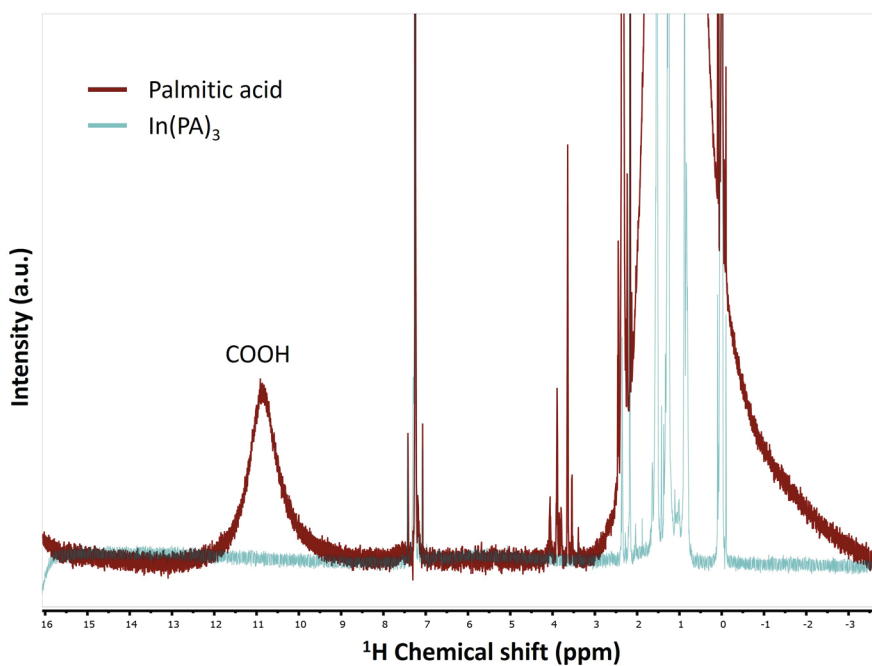**Figure A2.5**: TEM images of A) InP and B) InP-InF$_3$ QDs.

Figure A2.6: ^{1}H NMR of palmitic acid (red) and In(PA)$_3$ (blue) in CDCl$_3$.
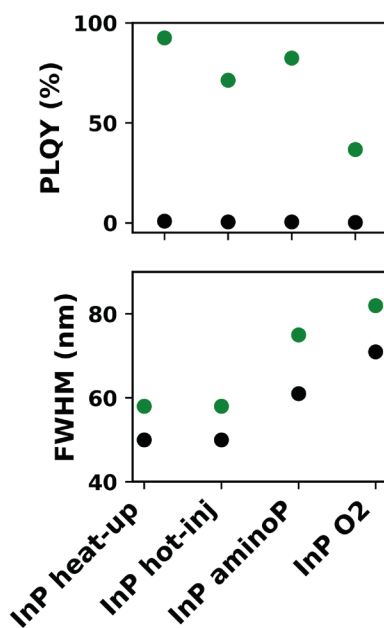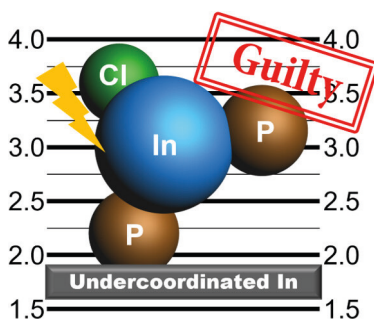

Figure A2.7: PLQY and FWHM for four types of InP QDs before (black) and after (green) InF$_3$ treatment.

3

Guilty as Charged

The Role of Undercoordinated Indium in Electron-Charged Indium Phosphide Quantum Dots

Quantum dots (QDs) are known for their size-dependent optical properties, narrow emission bands, and high photoluminescence quantum yield (PLQY), which make them interesting candidates for optoelectronic applications. In particular, InP QDs are receiving a lot of attention since they are less toxic than other QD materials and are hence suitable for consumer applications. Most of these applications, such as LEDs, photovoltaics, and lasing, involve charging QDs with electrons and/or holes. However, charging of QDs is not easy nor innocent, and the effect of charging on the composition and properties of InP QDs is not yet well understood. This work provides theoretical insight into electron charging of the InP core and InP/ZnSe QDs. Density functional theory calculations are used to show that charging of InP-based QDs with electrons leads to the formation of trap states if the QD contains In atoms that are undercoordinated and thus have less than four bonds to neighboring atoms. InP core-only QDs have such atoms at the surface, which are responsible for the formation of trap states upon charging with electrons. We show that InP/ZnSe core–shell models with all In atoms fully coordinated can be charged with electrons without the formation of trap states. These results show that undercoordinated In atoms should be avoided at all times for QDs to be stably charged with electrons.

3

3.1 Introduction

Quantum dots (QDs) have size-dependent optical properties, narrow emission bands, and high photoluminescence quantum yields (PLQYs). These properties make QDs interesting candidates for optoelectronic applications, including photovoltaics, light-emitting diodes, and lasers.[1–10] In particular, InP QDs are of commercial interest since the material is considered less toxic than Cd chalcogenide and Pb halide perovskite QD materials, making it more suitable for consumer applications.

InP-based QDs with high PLQY and narrow full width at half-maximum (fwhm) are nowadays synthesized and used in electronic devices.[6,11–14] A common element in these devices is that charging of the materials with electrons and holes is required, through either electrical charge injection, intentional electronic doping, or photoexcitation.[2,15–27] The simplest picture is that this results in the addition of charges to the conduction band (CB) or valence band (VB) states. Possibly present trap states in the bandgap would also simply be filled or emptied upon doping. However, it is well known that charging of semiconductors can result in the formation of charge-compensating defects.[28] For semiconductor nanocrystals such defects most likely appear on the surface in the form of local reduction/oxidation of surface atoms or the formation of dimers.[29] For example, Du Fossé et al. showed in a computational study that Cd-based QDs without dangling bonds are stable up to a charge of one electron but form trap states after injection of more electrons.[29,30] Additionally it was shown that the local geometry of Cd atoms determines whether the reduction of a Cd atom is energetically favorable or not: absence of ligands results in reduction, and the presence of L-type ligands prevents reduction.[29,30] Localized energy states in the bandgap are also observed for PbS QDs after the injection of three or four electrons, originating from undercoordinated Pb atoms leading to dimers on the surface.[31,32] However, to the best of our knowledge, there is no atomistic understanding of the effects of charging InP QDs.

This work provides theoretical insight into electron charging of InP core-only and InP/ZnSe core/shell QDs. The influence of additional electrons on the structure and the electronic states of the QDs is studied. In line with the current understanding of the surface of InP QDs the QD models used in this study are all cation rich and contain negatively charged surface ligands, which compensate the positive charge from the excess cations on the surface.[33–38] The structure and density of states (DOS) are first determined by density functional theory (DFT) calculations for the neutral QD, and consecutively the QD is subjected to electron charging. The method for simulating electron charging is adapted from the work of Du Fossé et al. and consists of the placement of one or more neutral K atoms on the surface of the QD.[29] Per K atom, one electron is donated to the QD, resulting in a negatively charged QD and a positively charged K atom, while the overall system is charge neutral. DFT calculations are then performed to determine the effect of the additional electron in the QD.

Initially, DFT calculations, simulating electrochemical electron charging, are performed on InP core-only QDs with either a spherical or tetrahedral shape. The introduction of an electron into the QDs results in the formation of a trap state for both shapes. This trap is associated with a single undercoordinated surface In atom, which gets reduced upon

electron addition, for both spherical and tetrahedral InP QDs.

A well-known solution to passivate the surface of QDs and thus creating fully coordinated atoms at the surface is the growth of an epitaxial shell on the QD core.[20,39] To study the role of undercoordinated In atoms, two types of core/shell InP/ZnSe QDs are simulated in this study. One type contains undercoordinated In atoms, and in the other type, all In atoms are in a 4-fold coordination. Only the core/shell QDs with all In atoms in a 4-fold coordination have a trap state free bandgap after electron charging, even up to the addition of six electrons. Thus, the presence of undercoordinated In invariably leads to trap states when additional electrons are introduced in the QD. This shows that undercoordinated In atoms are not innocent but guilty as charged and responsible for charge compensation and trap state formation upon electron addition.

3.2 Results and discussion

3.2.1 InP Core-Only Spherical QDs

InP QDs are reported with various shapes, but spherical and tetrahedral QDs are most commonly observed. The work of Dümbgen et al. predicts that both shapes are possible for small InP QDs but that at larger sizes only tetrahedral-shaped InP QDs allow for complete surface passivation.[35] The requirement of charge balance requires three negatively charged ligands per excess In atom, and steric hindrance prevents this in large spherical QDs. In this work, both relatively small spherical and tetrahedral InP QDs are modeled and charged with electrons to determine and compare their stability upon electron charging. This section describes the results of electron charging InP core-only spherical QDs. Figure 3.1A-i shows the uncharged spherical InP QD, which is a zincblende $In_{68}P_{55}Cl_{39}$ nanocrystal with a diameter of 1.9 nm. Figure 3.1B-i shows the DOS for this QD. It exhibits a bandgap that is free of electronic states and with all VB levels filled with electrons, which are below the dashed black line, and all CB levels empty, which are above the dashed black line. Contour plots of the lowest unoccupied molecular orbital (LUMO) and the highest occupied molecular orbital (HOMO) are shown in Figure 3.1C-i and D-i, respectively. Both the LUMO and HOMO are delocalized molecular orbitals (MOs), indicating that the VB and CB edges are not localized trap states. This shows that this QD model results in a trap-free bandgap, in line with similar results on Cd-based QDs and recent results on InP QDs.[29,33,35]

After establishing that the spherical InP QD model corresponds to a trap-free system, we investigated what happens upon electron charging. Figure 3.1A-ii shows the InP QD with an additional K atom, which results in the injection of one electron in the QD. It is observed that one In atom is ejected from the lattice at the surface of the InP model, shown in orange, indicating a structural change in the model. A close-up of this In atom in both the neutral QD and the electron charged QD is shown in Figure A3.1. Figure 3.1B-ii shows the DOS for this QD separated into the DOS for the spin-up (α) MOs and spin-down (β) MOs, as a result of the unrestricted calculation used for an odd number of electrons.[29] The DOS in Figure 3.1B-ii shows trap states in the bandgap at −5.63 and −5.12 eV for the α and β MOs, respectively. The contribution of the ejected In atom to this trap state is 42% and 38% for the α and β MOs, respectively, indicating that this In atom is

3
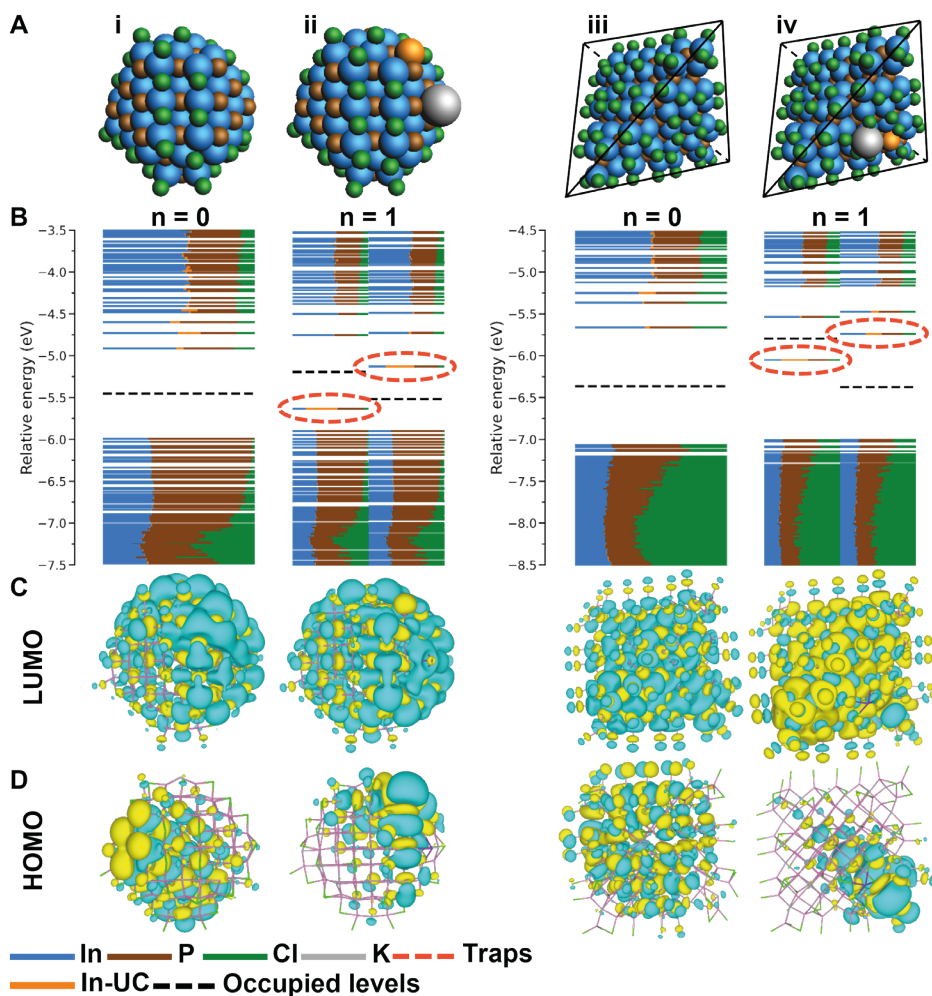
Figure 3.1. Charging of spherical and tetrahedral InP QDs. (A) Structures of the QD models where *n* indicates the number of injected electrons in the system. The black lines indicate a perfect tetrahedral shape. (B) The DOS for each of the QD models. Each horizontal line depicts an MO where the color indicates the fractional contribution to the MO of the corresponding element. The dashed black line indicates to which energy the MOs are filled with electrons. In the case of an odd number of electrons in the system (*n* = 1), the unrestricted calculation results in separated spin-up (α) and spin-down (β) orbitals, which are shown separately in the graph. Trap states are indicated by a dashed red circle. (C) Contour plots of the LUMO of the QDs or the LUMO of the α MOs for QDs with *n* = 1. (D) Contour plots of the HOMO of the QDs or the HOMO of the α MOs for QDs with *n* = 1.

mainly responsible for the formation of the trap state. The energy distribution of the DOS for the spherical InP QD for n = 0 and n = 1 is shown in Figure A3.2. The contour plots

of the MO of the trap state, the HOMO of the α MOs, and the LUMO of the β MOs are shown in Figure 3.1C-ii and in Figure A3.3, respectively. These contour plots indicate the localization of the trap state MO on the ejected In atom. The LUMO of the α MOs remains delocalized, as shown in Figure 3.1D-ii, showing that the CB edge has not changed. From these results, it is concluded that the ejected atom is responsible for the formation of the trap state.

To understand why this particular In atom forms a trap state after electron addition, the coordination number of the In atoms in the QD is calculated. The geometry optimized model of the InP spherical QD has In–P and In–Cl bond lengths of 2.53 to 2.65 Å and 2.34 to 2.73 Å, respectively. The coordination number for every atom is therefore calculated by determining the number of atoms within a radius of 2.75 Å. Following this definition, it was found that the QD has 16 In atoms with a 3-fold coordination, whereas the preferred coordination number for InP in the zinc-blende lattice is four. These undercoordinated atoms are all located on the surface of the QD, as can be seen in Figure A3.4 with the undercoordinated atoms in red. In accordance with literature, no trap states are formed by these 3-fold-coordinated atoms before the addition of extra electrons, as has already been shown in the DOS in Figure 3.1B-i.[33,35] However, the atom that is ejected from the QD lattice after electron addition, as described above, is one of the undercoordinated In atoms. The fact that the trap state is localized on the undercoordinated In atom leads to the hypothesis that undercoordinated In atoms are responsible for trap formation when additional electrons are provided. Further charging of the QD with n = 2 does not lead to the creation of more trap states but to filling of the energy level of the trap state with two electrons, indicating that the same surface In atom gets further reduced. However, charging the QD with n = 3 results in an additional trap state in the bandgap, as displayed in Figure A3.5. The additional trap state for the QD with n = 3 is localized on another undercoordinated In atom. Charging with n = 4 again does not lead to the formation of an additional trap state but rather to the filling of the second trap state with a second electron.

3.2.2 InP Core-Only Tetrahedral QDs
To determine whether the formation of a trap state after the addition of an electron depends on the shape of the InP QD, tetrahedral QDs were also investigated. Figure 3.1A-iii shows a tetrahedral $In_{84}P_{56}Cl_{84}$ QD with an edge diameter of 2.6 nm. The calculated DOS is shown in Figure 3.1B-iii and shows a bandgap that is free of trap states, and the contour plots shown in Figure 3.1C-iii and D-iii indicate delocalization of the LUMO and HOMO orbitals. Hence, similar to the spherical QD in Figure 3.1A-i, the tetrahedral QD model results in a trap-free bandgap.

To simulate the electron charging for the tetrahedral QD, one potassium atom is placed on the surface of the model, as shown in Figure 3.1A-iv. The resulting DOS is shown in Figure 3.1B-iv, and trap states within the bandgap are observed at energies of −6.04 and −5.73 eV for the α and β orbitals, respectively. A contour plot of the α trap level is shown in Figure 3.1D-iv and shows a localization of the wave function in one of the corners of the QD. The largest contribution, 35%, to this trap state comes from one In atom, and it is therefore concluded that this In atom is responsible for the formation of the trap state. The coordination number of this particular In atom is three, again indicating

3

that undercoordinated In atoms are responsible for trap state formation upon electron charging.

Thus, for both the spherical- and tetrahedral-shaped InP QD models, it is an undercoordinated In atom that has a large contribution to the formation of a trap state after the injection of one electron. Interestingly, reduction of Cd in CdSe QDs only occurs after the addition of two electrons.[30] The more facile reduction of In can be explained by its higher Pauling electronegativity of 1.78 compared to cadmium with an electronegativity of 1.69 and is in line with the more positive standard reduction potential for In3+ reduction (In3+ + 3e– → In; E0 = −0.34 V vs NHE) than for Cd2+ reduction (Cd2+ + 2e– → Cd; E0 = −0.40 V vs NHE),[40–42] although it should be noted that these reduction potentials depend on the solvation energy of the ions in water and represent the reduction of free metal ions not the semiconductor. The formation of a trap state after injection of one electron suggests that in the presence of excess electrons trap states form due to undercoordinated atoms independent of the shape of the InP QD, suggesting that it is mostly the local coordination that determines the stability of In atoms against reduction. The role of undercoordinated In also suggests that trap state formation can be prevented by ensuring full coordination of every atom.

Such full coordination can be achieved by growing an epitaxial shell around the core with a different material that has the same crystal structure and a matching lattice constant. Currently, the best InP-based QDs that are reported in literature are InP/ZnSe/ZnS core/shell/shell particles with PLQYs reaching unity.[6,12,14,43,44] The result of shelling with ZnSe or ZnS is that the QDs are terminated with Zn atoms instead of In atoms. The Pauling electronegativity of Zn is 1.65, which is lower than both In (1.78) and Cd (1.69). In line with this, the standard reduction potential of Zn2+ is much more negative (E0 = −0.76 V vs NHE), so it is expected that Zn ions are more stable under reductive conditions. In both experimental and computational studies it is indeed found that Zn-terminated particles have higher electrochemical stability for both CdSe/CdS/ZnS and InP/ZnSe/ZnS QDs.[20,23,29] With both the complete coverage of the core In atoms and the increased stability in mind, InP/ZnSe core/shell QD models are developed for this study.
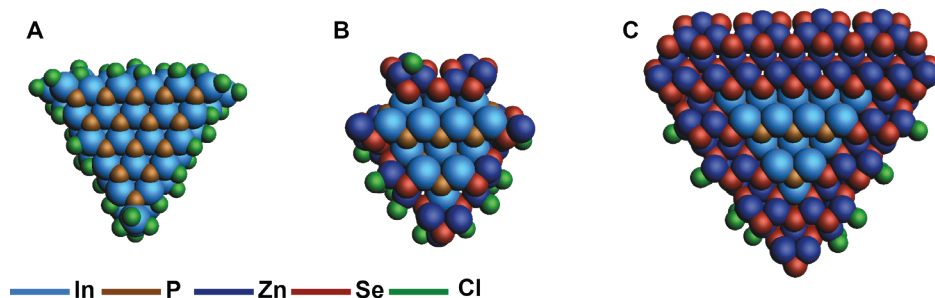
3.2.3 InP/ZnSe Core/Shell QDs
The effect of passivating surface In with the ZnSe shell is tested by first constructing a QD with an incomplete monolayer, leaving some surface In exposed and undercoordinated. Such QDs with thin/incomplete shells have recently also been described in experimental literature.[45] Next we added an additional complete ZnSe monolayer to fully coordinate all In atoms and to simulate QDs with a thicker shell.

The exact composition of the incomplete shell is not chosen randomly, but corresponds to the introduction of specific surface vacancies which are known to occur on bulk III–V and II–VI semiconductor surfaces and prevent the formation of surface bands.[46] We are currently preparing a manuscript on this topic. Here the surface reconstruction that we introduce is the removal of 25% of the surface Zn atoms from the (111) facets. Figure A3.6 shows a schematic example of the surface reconstruction. Charge balance of the model is achieved by adapting the number of surface Cl atoms. Such cation vacancies have earlier been shown to lead to delocalized HOMO and LUMO levels for CdSe QDs by Vozzny and

Sargent.[47]

The two InP/ZnSe core/shell QDs developed for this study both include surface reconstructions and are based on tetrahedral shapes. The tetrahedral-shaped QDs are chosen because the work of Dümbgen et al. shows that larger InP QDs prefer a tetrahedral shape to produce sufficient surface area for all required ligands.[35] Cross-sections of the InP core-only and InP/ZnSe core–shell QDs are shown in Figure 3.2. Figure 3.2B shows an In31P20Zn72Se72Cl33 QD which has one monolayer of the ZnSe shell, including surface reconstructions, and is called InP/ZnSe(1 ML) for simplicity. Note that for this QD the four corner In atoms of the core are removed, which is because they were found to be unstable during the geometry optimization calculations. The surface reconstructions lead to an incomplete ZnSe shell, allowing to test our hypothesis that the presence of undercoordinated In atoms will lead to the formation upon charging of the QD with electrons. Figure 3.2C shows the $In_{35}P_{20}Zn_{322}Se_{328}Cl_{33}$ QD with two monolayers of ZnSe shell named InP/ZnSe(2 ML) and has the surface reconstructions on the outermost ZnSe layer. Due to the second layer of ZnSe, all In atoms have a 4-fold coordination, which should lead to a trap-free system upon charging with electrons, according to our hypothesis. The results of the addition of electrons to these QDs are discussed in the following sections.

In —— **P** —— **Zn** —— **Se** —— **Cl**

Figure 3.2. Two-dimensional cross-sections of the tetrahedral core and core/shell QD models. (A) InP core, (B) InP/ZnSe(1 ML) and (C) InP/ZnSe(2 ML).

The InP/ZnSe(1 ML) QD is shown in Figure 3.3A-i, and the cross-section of this model is shown in Figure 3.2B. The model is created by taking an InP core QD and adding one epitaxial layer of ZnSe. Subsequently, surface reconstructions are performed on the ZnSe layer, meaning that 25% of the surface Zn atoms are removed to create vacancies in the pattern as shown in Figure A3.6. However, the result of the surface reconstruction is that not all In atoms have a 4-fold coordination.

The DOS for the InP/ZnSe(1 ML) QD is shown in Figure 3.3B-i. It features a bandgap of 1.36 eV, clear of localized states, and evident contribution of Zn and Se to all MOs is observed. The LUMO, displayed in Figure 3.3C-i, is delocalized over both the core and the shell atoms. In Figure 3.3D-i, the HOMO of the core/shell QD is shown, and the MO is mostly delocalized over the shell atoms, which is in agreement with the relatively large contribution of Zn and Se observed in the DOS. A true type-I offset is not observed. This can be the result of the small size of the InP core but is likely also the result of electric fields arising at the core–shell interface.[48] Therefore, it is difficult to draw conclusions about the
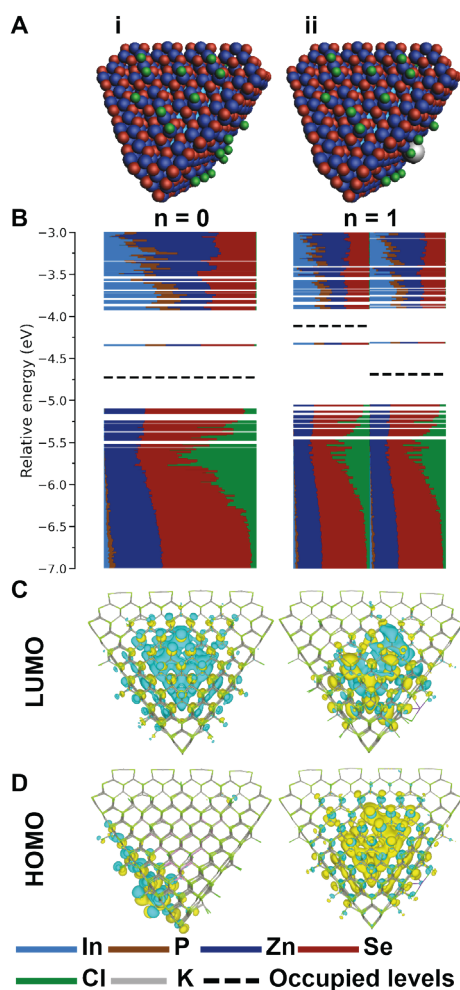
3
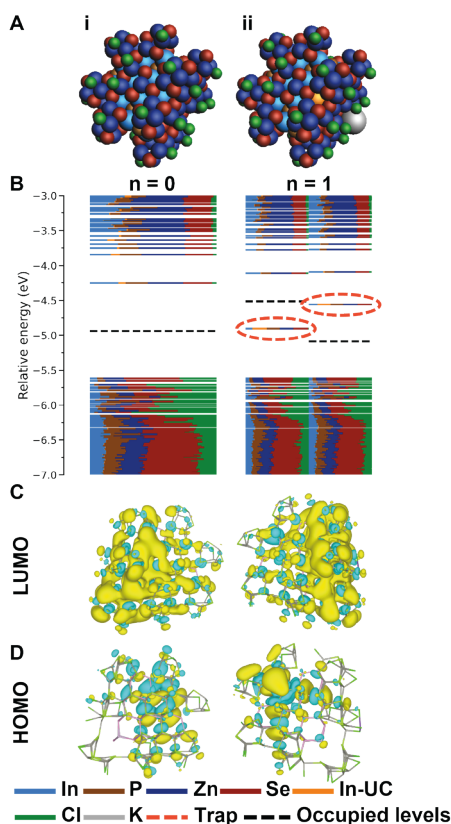
Figure 3.3. Charging of the InP/ZnSe(1 ML) QD. (A) Structures of the QDs where *n* indicates the number of injected electrons in the system. (B) The DOS for both QDs. The trap states are indicated with a dashed red circle. (C) Contour plot of the LUMO of the QD for *n* = 0 and the LUMO of the α MOs for *n* = 1. (D) Contour plot of the HOMO of the QD for *n* = 0 and the HOMO of the α MOs for *n* = 1.

energy offset between the core and the shell. The coordination number for all In atoms is determined for this model, and it is found that four In atoms are undercoordinated. Similar to the InP core, these undercoordinated In atoms do not result in trap states for the QD without excess electrons.

The addition of electrons is again simulated by placing a potassium atom on the surface of the InP/ZnSe(1 ML) QD. Figure 3.3A-ii shows the structure of the InP/ZnSe(1 ML) QD core/shell QD charged with a single electron (and a single potassium cation for charge compensation). The corresponding DOS, shown in Figure 3.3B-ii, contains in-gap trap states at −4.91 and −4.56 eV for the α and β orbitals, respectively. A contour plot of the in-gap trap state of the α orbitals is shown in Figure 3.3D-ii. The MO is significantly localized on one of the In atoms of the InP core and is colored orange in Figure 3.3A-ii. The contribution of this particular In atom to the MO is 23%, shown in orange in the DOS, indicating that the state is significantly localized on this In atom. The In atom

Figure 3.4. Charging the InP/ZnSe(2 ML) QD. (A) Structures of the QDs where *n* indicates the number of injected electrons in the system. (B) The DOS for both QDs. (C) Contour plot of the LUMO of the QD for *n* = 0 and the LUMO of the α MOs for *n* = 1. (D) Contour plot of the HOMO of the QD for *n* = 0 and the HOMO of the α MOs for *n* = 1.

responsible for the trap state has a 3-fold coordination. These results show that the presence of an incomplete ZnSe shell is not sufficient to prevent trap state formation after electron addition if undercoordinated In atoms are present.

To prevent undercoordinated In atoms, a second layer of ZnSe is added to the QD model, resulting in InP/ZnSe(2 ML). The cross-section in Figure 3.2C and the full QD in Figure 3.4A-i display that all In atoms of the InP core are covered by the ZnSe shell layers. The DOS calculated for this QD is shown in Figure 3.4B-i, and a bandgap of 0.77 eV is observed. Although the LUMO has a relatively large energy difference with the other MOs in the CB, the energy state is clearly delocalized over the entire QD, as shown in Figure 3.4C-i. The

3

HOMO is delocalized over several shell atoms, indicating that it is not a trap state level, as shown in Figure 3.4D-i. Moreover, all In atoms are 4-fold coordinated, meaning that there are no undercoordinated In atoms present.

With all In atoms 4-fold coordinated, the InP/ZnSe (2 ML) QD is subjected to the addition of an extra electron. The QD with the extra potassium atom on the surface is visible in Figure 3.4A-ii, and the corresponding DOS is plotted in Figure 3.4B-ii. The DOS shows a bandgap of 0.74 eV, which is clear from gap trap states. The HOMO of the α set of the orbitals is shown in Figure 3.4D-ii and displays delocalization of the energy state over the entire QD, indicating that the filled orbital is not a trap state but that the electron is injected into the CB. To study the stability of the InP/ZnSe(2 ML), the QD was charged with up to six electrons and no trap states were formed; see Figure A3.7. These results confirm that a 4-fold coordination due to two layers of a ZnSe shell prevents formation of trap states when electrons are added to the QD. The work of Park et al. shows that electrochemical charging of InP-based QDs is based on QDs with complete coverage of ZnSe/ZnS shells.[23] However, there is no discussion on In reduction on the surface of InP core-only QDs after electron charging. Passivation of the undercoordinated In atoms is here achieved by a complete ZnSe shell, but this might also be achieved by coordination to ligands. The exact effects of coordination of undercoordinated In atoms is outside the scope of this work, but the work of Du Fossé et al. shows that L-type ligands stabilize QDs against surface reduction, and it is likely that these results also hold for InP QDs.[30]

It is concluded from the results in this work that trap state formation after electron charging a QD can only be prevented by ensuring 4-fold passivation of all the In atoms in the QD. Implementation of InP-based QDs in electronic devices depending on electron charging of these QDs therefore requires attention to surface and interface coordination of the In atoms.

3.3 Conclusion
In conclusion, this work describes the effect of adding electrons to InP core-only and InP/ZnSe core–shell QDs by DFT calculations. The results show that charging of InP QDs with electrons always results in the reduction of a surface or interface ion if undercoordinated In atoms are present. Only the formation of a complete ZnSe shell prevents this reduction. InP is thus intrinsically less stable against reduction than Cd-based QDs, but it can be stabilized with Zn chalcogenide shells, provided that all In atoms become fully coordinated.

3.4 Experimental
In agreement with previous work and the current understanding of the surface composition of InP QDs, the QD models in this work are cation-rich and have chloride anions on the surface to preserve charge balance.[33–38] The chloride anions are electronically similar to the carboxylic acid ligands used in experiments but are computationally less expensive.[29,35,49] To calculate the required number of chloride atoms and the number of excess electrons after charging, the charge-orbital model of Voznyy *et al.* is used, which is defined as

$$n = \sum_i N_i \times q_i$$

with *n* representing the number of excess electrons, N_i the number of atoms of type *i*, and q_i the most common oxidation state of atom type *i*.[50] For *n* > 0, excess electrons are present in the QD and the QD is therefore negatively charged; for *n* < 0 the QD becomes positively charged. The oxidation states of the atom types used in the QD models of this work are assumed to be 3+, 2+, 1+, 3–, 2–, and 1– for In, Zn, K, P, Se, and Cl, respectively.

Calculations for structural relaxations, DOS, and MOs are all performed at the DFT level using the CP2K quantum chemistry software package.[51,52] A Perdew–Burke–Ernzerhof (PBE) exchange–correlation functional and a double-ζ valence polarization basis set are used for all atoms.[53,54] Effective core potentials from the GTH pseudopotentials account for scalar relativistic effects. Simulations were all performed at 0 K in the gas phase. For QD systems with an odd number of electrons, unrestricted spin calculations were performed. In unrestricted calculations, the spin-up (α) and spin-down (β) electrons are calculated independently from each other, resulting in separate densities of states and MOs. For all contour plots of MOs a value of 0.005 e/bohr³ was used.

It should be noted that the use of the PBE exchange–correlation leads to underestimation of the bandgap.[55] The absolute energies of the MOs may therefore differ from the experimentally obtained values. The energy levels cannot directly be related to experiments, but the trends described in this work are expected to be valid.[29]

References

1.   Wu, Z.; Liu, P.; Zhang, W.; Wang, K.; Sun, X. W., Development of InP Quantum Dot-Based Light-Emitting Diodes. *ACS Energy Letters* **2020,** *5* (4), 1095-1106.
2.   Geuchies, J. J.; Brynjarsson, B.; Grimaldi, G.; Gudjonsdottir, S.; van der Stam, W.; Evers, W. H.; Houtepen, A. J., Quantitative Electrochemical Control over Optical Gain in Quantum-Dot Solids. *ACS Nano* **2020**.
3.   Coe-Sullivan, S.; Liu, W.; Allen, P.; Steckel, J. S., Quantum Dots for LED Downconversion in Display Applications. *ECS Journal of Solid State Science and Technology* **2013,** *2* (2), R3026.
4.   Park, Y.-S.; Roh, J.; Diroll, B. T.; Schaller, R. D.; Klimov, V. I., Colloidal quantum dot lasers. *Nature Reviews Materials* **2021,** *6* (5), 382-401.
5.   5. Talapin, D. V.; Steckel, J., Quantum dot light-emitting devices. *MRS Bulletin* **2013,** *38* (9), 685-691.
6.   Won, Y.-H.; Cho, O.; Kim, T.; Chung, D.-Y.; Kim, T.; Chung, H.; Jang, H.; Lee, J.; Kim, D.; Jang, E., Highly efficient and stable InP/ZnSe/ZnS quantum dot light-emitting diodes. *Nature* **2019,** *575* (7784), 634-638.
7.   Carey, G. H.; Abdelhady, A. L.; Ning, Z.; Thon, S. M.; Bakr, O. M.; Sargent, E. H., Colloidal Quantum Dot Solar Cells. *Chemical Reviews* **2015,** *115* (23), 12732-12763.
8.   Ganesan, A. A.; Houtepen, A. J.; Crisp, R. W. Quantum Dot Solar Cells: Small Beginnings Have Large Impacts *Applied Sciences* [Online], 2018.
9.   Geiregat, P.; Houtepen, A. J.; Sagar, L. K.; Infante, I.; Zapata, F.; Grigel, V.; Allan, G.; Delerue, C.; Van Thourhout, D.; Hens, Z., Continuous-wave infrared optical gain and amplified spontaneous emission at ultralow threshold by colloidal HgTe quantum dots. *Nature Materials* **2018,** *17* (1), 35-42.
10.   Lim, J.; Park, Y.-S.; Klimov, V. I., Optical gain in colloidal quantum dots achieved with direct-current electrical pumping. *Nature Materials* **2018,** *17* (1), 42-49.
11.   Ubbink, R. F.; Almeida, G.; Iziyi, H.; du Fossé, I.; Verkleij, R.; Ganapathy, S.; van Eck, E. R.

3

H.; Houtepen, A. J., A Water-Free In Situ HF Treatment for Ultrabright InP Quantum Dots. *Chemistry of Materials* **2022,** *34* (22), 10093-10103.

12. Van Avermaet, H.; Schiettecatte, P.; Hinz, S.; Giordano, L.; Ferrari, F.; Nayral, C.; Delpech, F.; Maultzsch, J.; Lange, H.; Hens, Z., Full-Spectrum InP-Based Quantum Dots with Near-Unity Photoluminescence Quantum Efficiency. *ACS Nano* **2022.**

13. Zhang, Y.; Lv, Y.; Li, L.-S.; Zhao, X.-J.; Zhao, M.-X.; Shen, H., Aminophosphate precursors for the synthesis of near-unity emitting InP quantum dots and their application in liver cancer diagnosis. *Exploration* **2022,** *2* (4), 20220082.

14. Kim, Y.; Ham, S.; Jang, H.; Min, J. H.; Chung, H.; Lee, J.; Kim, D.; Jang, E., Bright and Uniform Green Light Emitting InP/ZnSe/ZnS Quantum Dots for Wide Color Gamut Displays. *ACS Applied Nano Materials* **2019,** *2* (3), 1496-1504.

15. Sahu, A.; Russ, B.; Liu, M.; Yang, F.; Zaia, E. W.; Gordon, M. P.; Forster, J. D.; Zhang, Y.-Q.; Scott, M. C.; Persson, K. A.; Coates, N. E.; Segalman, R. A.; Urban, J. J., In-situ resonant band engineering of solution-processed semiconductors generates high performance n-type thermoelectric nano-inks. *Nature Communications* **2020,** *11* (1), 2069.

16. Koh, W.-k.; Koposov, A. Y.; Stewart, J. T.; Pal, B. N.; Robel, I.; Pietryga, J. M.; Klimov, V. I., Heavily doped n-type PbSe and PbS nanocrystals using ground-state charge transfer from cobaltocene. *Scientific Reports* **2013,** *3* (1), 2004.

17. Shim, M.; Guyot-Sionnest, P., n-type colloidal semiconductor nanocrystals. *Nature* **2000,** *407* (6807), 981-983.

18. Meng, L.; Xu, Q.; Thakur, U. K.; Gong, L.; Zeng, H.; Shankar, K.; Wang, X., Unusual Surface Ligand Doping-Induced p-Type Quantum Dot Solids and Their Application in Solar Cells. *ACS Applied Materials & Interfaces* **2020,** *12* (48), 53942-53949.

19. van der Stam, W.; du Fossé, I.; Grimaldi, G.; Monchen, J. O. V.; Kirkwood, N.; Houtepen, A. J., Spectroelectrochemical Signatures of Surface Trap Passivation on CdTe Nanocrystals. *Chemistry of Materials* **2018,** *30* (21), 8052-8061.

20. van der Stam, W.; Grimaldi, G.; Geuchies, J. J.; Gudjonsdottir, S.; van Uffelen, P. T.; van Overeem, M.; Brynjarsson, B.; Kirkwood, N.; Houtepen, A. J., Electrochemical Modulation of the Photophysics of Surface-Localized Trap States in Core/Shell/(Shell) Quantum Dot Films. *Chemistry of Materials* **2019,** *31* (20), 8484-8493.

21. Vogel, Y. B.; Stam, M.; Mulder, J. T.; Houtepen, A. J., Long-Range Charge Transport via Redox Ligands in Quantum Dot Assemblies. *ACS Nano* **2022,** *16* (12), 21216-21224.

22. Gudjonsdottir, S.; Koopman, C.; Houtepen, A. J., Enhancing the stability of the electron density in electrochemically doped ZnO quantum dots. *The Journal of Chemical Physics* **2019,** *151* (14), 144708.

23. Park, J.; Won, Y.-H.; Kim, T.; Jang, E.; Kim, D., Electrochemical Charging Effect on the Optical Properties of InP/ZnSe/ZnS Quantum Dots. *Small* **2020,** *16* (41), 2003542.

24. Ganguly, S.; Tang, X.; Yoo, S.-S.; Guyot-Sionnest, P.; Ghosh, A. W., Extrinsic voltage control of effective carrier lifetime in polycrystalline PbSe mid-wave IR photodetectors for increased detectivity. *AIP Advances* **2020,** *10* (9), 095117.

25. Rinehart, J. D.; Schimpf, A. M.; Weaver, A. L.; Cohn, A. W.; Gamelin, D. R., Photochemical Electronic Doping of Colloidal CdSe Nanocrystals. *Journal of the American Chemical Society* **2013,** *135* (50), 18782-18785.

26. Tsui, E. Y.; Carroll, G. M.; Miller, B.; Marchioro, A.; Gamelin, D. R., Extremely Slow Spontaneous Electron Trapping in Photodoped n-Type CdSe Nanocrystals. *Chemistry of Materials* **2017,** *29* (8), 3754-3762.

27. Hou, X.; Kang, J.; Qin, H.; Chen, X.; Ma, J.; Zhou, J.; Chen, L.; Wang, L.; Wang, L.-W.; Peng, X., Engineering Auger recombination in colloidal quantum dots via dielectric screening. *Nature Communications* **2019,** *10* (1), 1750.

28. Walukiewicz, W., Defects and Self-Compensation in Semiconductors. In *Wide-Gap Chalcopyrites*, Siebentritt, S.; Rau, U., Eds. Springer Berlin Heidelberg: Berlin, Heidelberg,

2006; pp 35-54.

29. du Fossé, I.; ten Brinck, S.; Infante, I.; Houtepen, A. J., Role of Surface Reduction in the Formation of Traps in n-Doped II–VI Semiconductor Nanocrystals: How to Charge without Reducing the Surface. *Chemistry of Materials* **2019**, *31* (12), 4575-4583.

30. du Fossé, I.; Lal, S.; Hossaini, A. N.; Infante, I.; Houtepen, A. J., Effect of Ligands and Solvents on the Stability of Electron Charged CdSe Colloidal Quantum Dots. *The Journal of Physical Chemistry C* **2021**, *125* (43), 23968-23975.

31. Voznyy, O.; Thon, S. M.; Ip, A. H.; Sargent, E. H., Dynamic Trap Formation and Elimination in Colloidal Quantum Dots. *The Journal of Physical Chemistry Letters* **2013**, *4* (6), 987-992.

32. Giansante, C.; Infante, I., Surface Traps in Colloidal Quantum Dots: A Combined Experimental and Theoretical Perspective. *The Journal of Physical Chemistry Letters* **2017**, *8* (20), 5209-5215.

33. Houtepen, A. J.; Hens, Z.; Owen, J. S.; Infante, I., On the Origin of Surface Traps in Colloidal II–VI Semiconductor Nanocrystals. *Chemistry of Materials* **2017**, *29* (2), 752-761.

34. 3Dümbgen, K. C.; Pascazio, R.; van Beek, B.; Hens, Z.; Infante, I., Classical Force Field Parameters for InP and InAs Quantum Dots with Various Surface Passivations. *The Journal of Physical Chemistry A* **2023**, *127* (15), 3427-3436.

35. Dümbgen, K. C.; Zito, J.; Infante, I.; Hens, Z., Shape, Electronic Structure, and Trap States in Indium Phosphide Quantum Dots. *Chemistry of Materials* **2021**, *33* (17), 6885-6896.

36. Janke, E. M.; Williams, N. E.; She, C.; Zherebetskyy, D.; Hudson, M. H.; Wang, L.; Gosztola, D. J.; Schaller, R. D.; Lee, B.; Sun, C.; Engel, G. S.; Talapin, D. V., Origin of Broad Emission Spectra in InP Quantum Dots: Contributions from Structural and Electronic Disorder. *Journal of the American Chemical Society* **2018**, *140* (46), 15791-15803.

37. Kim, K.; Yoo, D.; Choi, H.; Tamang, S.; Ko, J.-H.; Kim, S.; Kim, Y.-H.; Jeong, S., Halide–Amine Co-Passivated Indium Phosphide Colloidal Quantum Dots in Tetrahedral Shape. *Angewandte Chemie International Edition* **2016**, *55* (11), 3714-3718.

38. Kim, T.-G.; Zherebetskyy, D.; Bekenstein, Y.; Oh, M. H.; Wang, L.-W.; Jang, E.; Alivisatos, A. P., Trap Passivation in Indium-Based Quantum Dots through Surface Fluorination: Mechanism and Applications. *ACS Nano* **2018**, *12* (11), 11529-11540.

39. Reiss, P.; Protière, M.; Li, L., Core/Shell Semiconductor Nanocrystals. *Small* **2009**, *5* (2), 154-168.

40. Allred, A. L., Electronegativity values from thermochemical data. *Journal of Inorganic and Nuclear Chemistry* **1961**, *17* (3), 215-221.

41. Bard, A. J.; Faulkner, L. R., *Electrochemical Methods: Fundamentals and Applications, 2nd Edition*. Wiley Textbooks: 2001.

42. Haynes, W. M., CRC Handbook of Chemistry and Physics, 95th Edition. 95th ed ed.; CRC Press: Hoboken, 2014.

43. Shim, H. S.; Ko, M.; Nam, S.; Oh, J. H.; Jeong, S.; Yang, Y.; Park, S. M.; Do, Y. R.; Song, J. K., InP/ZnSeS/ZnS Quantum Dots with High Quantum Yield and Color Purity for Display Devices. *ACS Applied Nano Materials* **2023**, *6* (2), 1285-1294.

44. Cavanaugh, P.; Sun, H.; Jen-La Plante, I.; Bautista, M. J.; Ippen, C.; Ma, R.; Kelley, A. M.; Kelley, D. F., Radiative dynamics and delayed emission in pure and doped InP/ZnSe/ZnS quantum dots. *The Journal of Chemical Physics* **2021**, *155* (24).

45. Li, Y.; Hou, X.; Dai, X.; Yao, Z.; Lv, L.; Jin, Y.; Peng, X., Stoichiometry-Controlled InP-Based Quantum Dots: Synthesis, Photoluminescence, and Electroluminescence. *Journal of the American Chemical Society* **2019**, *141* (16), 6448-6452.

46. Duke, C. B., Semiconductor Surface Reconstruction: The Structural Chemistry of Two-Dimensional Surface Compounds. *Chemical Reviews* **1996**, *96* (4), 1237-1260.

47. Voznyy, O.; Sargent, E. H., Atomistic Model of Fluorescence Intermittency of Colloidal Quantum Dots. *Physical Review Letters* **2014**, *112* (15), 157401.

48. Zhu, D.; Bahmani Jalali, H.; Saleh, G.; Di Stasio, F.; Prato, M.; Polykarpou, N.; Othonos, A.;

3

3

Christodoulou, S.; Ivanov, Y. P.; Divitini, G.; Infante, I.; De Trizio, L.; Manna, L., Boosting the Photoluminescence Efficiency of InAs Nanocrystals Synthesized with Aminoarsine via a ZnSe Thick-Shell Overgrowth. *Advanced Materials n/a* (n/a), 2303621.

49. Drijvers, E.; De Roo, J.; Martins, J. C.; Infante, I.; Hens, Z., Ligand Displacement Exposes Binding Site Heterogeneity on CdSe Nanocrystal Surfaces. *Chemistry of Materials* **2018,** *30* (3), 1178-1186.

50. Voznyy, O.; Zhitomirsky, D.; Stadler, P.; Ning, Z.; Hoogland, S.; Sargent, E. H., A Charge-Orbital Balance Picture of Doping in Colloidal Quantum Dot Solids. *ACS Nano* **2012,** *6* (9), 8448-8455.

51. Hutter, J.; Iannuzzi, M.; Schiffmann, F.; VandeVondele, J., cp2k: atomistic simulations of condensed matter systems. *WIREs Computational Molecular Science* **2014,** *4* (1), 15-25.

52. Kühne, T. D.; Iannuzzi, M.; Del Ben, M.; Rybkin, V. V.; Seewald, P.; Stein, F.; Laino, T.; Khaliullin, R. Z.; Schütt, O.; Schiffmann, F.; Golze, D.; Wilhelm, J.; Chulkov, S.; Bani-Hashemian, M. H.; Weber, V.; Borštnik, U.; Taillefumier, M.; Jakobovits, A. S.; Lazzaro, A.; Pabst, H.; Müller, T.; Schade, R.; Guidon, M.; Andermatt, S.; Holmberg, N.; Schenter, G. K.; Hehn, A.; Bussy, A.; Belleflamme, F.; Tabacchi, G.; Glöß, A.; Lass, M.; Bethune, I.; Mundy, C. J.; Plessl, C.; Watkins, M.; VandeVondele, J.; Krack, M.; Hutter, J., CP2K: An electronic structure and molecular dynamics software package - Quickstep: Efficient and accurate electronic structure calculations. *The Journal of Chemical Physics* **2020,** *152* (19), 194103.

53. Perdew, J. P.; Burke, K.; Ernzerhof, M., Generalized Gradient Approximation Made Simple. *Physical Review Letters* **1996,** *77* (18), 3865-3868.

54. VandeVondele, J.; Hutter, J., Gaussian basis sets for accurate calculations on molecular systems in gas and condensed phases. *The Journal of Chemical Physics* **2007,** *127* (11), 114105.

55. Azpiroz, J. M.; Ugalde, J. M.; Infante, I., Benchmark Assessment of Density Functional Methods on Group II–VI MX (M = Zn, Cd; X = S, Se, Te) Quantum Dots. *Journal of Chemical Theory and Computation* **2014,** *10* (1), 76-89.

Appendix
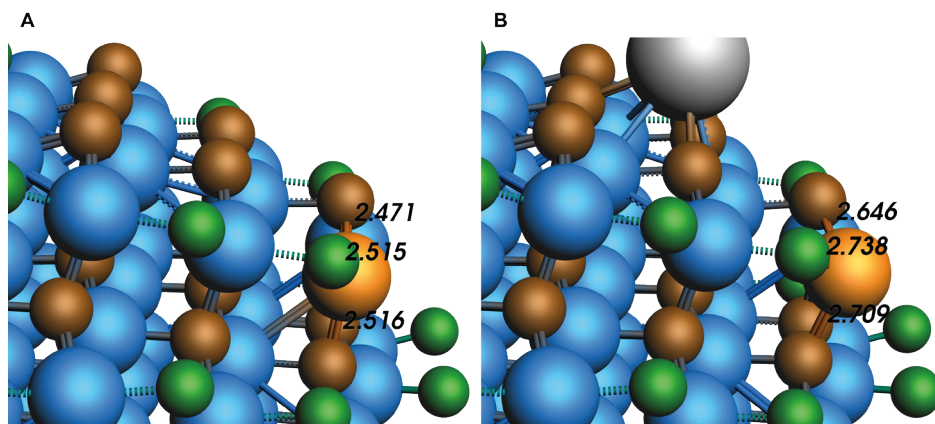
Figure A3.1. Close-up of the undercoordinated In atom in the spherical core-only InP QD that is responsible for the formation of the trap state after electron charging for the neutral QD in A) and for n = 1 in B). The undercoordinated In atom is colored in orange and the distance between the coordinating atoms in given in Å.
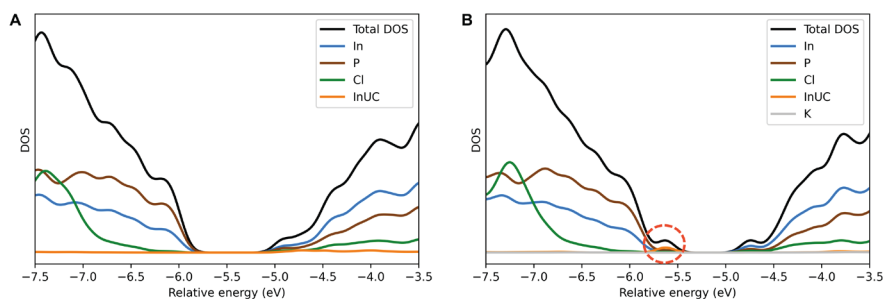

Figure A3.2. DOS for the spherical core-olny QD for n = 0 in A) and for n = 1 in B). The trap state is indicated by a red dashed circle.

Table A3.1. Relative energy levels for each used QD model of the valence and conduction band, the relative energy of the trap states and the bandgap energy.

|	VB (eV)	Trap (eV)	CB (eV)	BG (eV)
Spherical InP n = 0	-5.999	N/A	-4.920	1.078
Spherical InP n = 1	-5.893	-5.627	-4.747	1.146
Tetrahedral InP n = 0	-7.061	N/A	-5.656	1.405
Tetrahedral InP n = 1	-7.003	-6.045	-5.530	1.473
InP/ZnSe(1ML) n = 0	-5.623	N/A	-4.258	1.365
InP/ZnSe(1ML) n = 1	-5.624	-4.911	-4.121	1.502
InP/ZnSe(2ML) n = 0	-5.115	N/A	-4.348	0.767
InP/ZnSe(2ML) n = 1	-5.060	N/A	-4.325	0.735

3
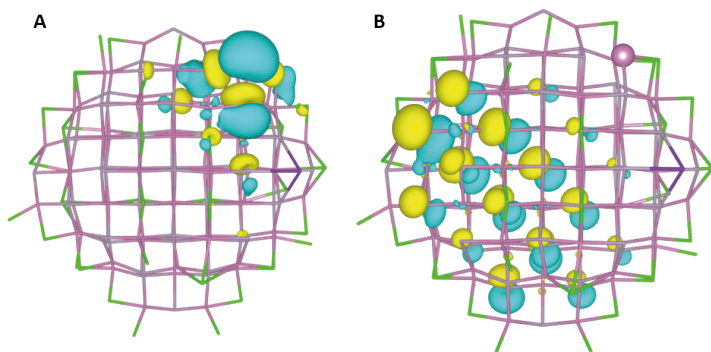
Figure A3.3. A) Contour plot of the LUMO of the β MOs of the spherical core-only InP QD for n = 1 using a contour plot value of 0.005 e/bohr³. B) Contour plot of the HOMO of the β MOs of the spherical core-only InP QD.
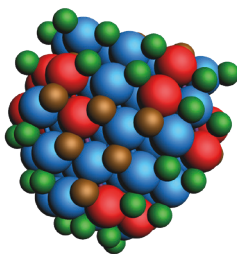
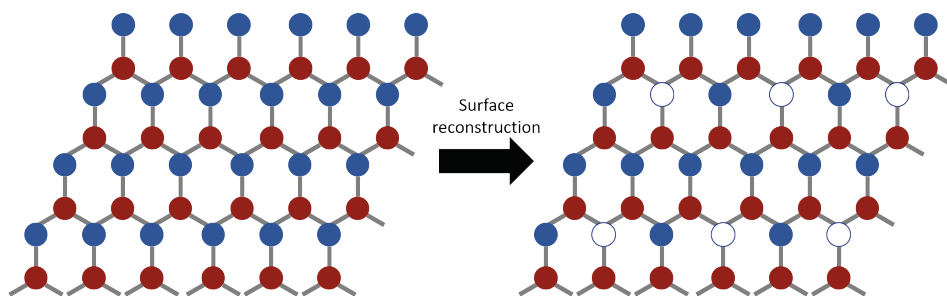

**Figure A3.4.** Structure of the spherical core-only QD with the undercoordinated In atoms in red.
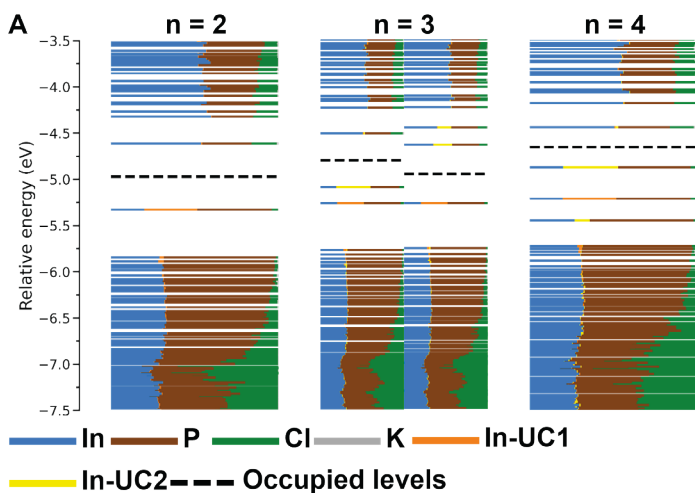
Figure A3.5. Charging of InP QDs with n = 2, 3 and 4. The second In atom that is reduced due to charging is indicated with a yellow color.

Figure A3.6. Schematic drawing of the surface reconstruction where cation vacancies are systematically introduced. The cations are depicted as blue spheres, the anions as red spheres and the introduced vacancies as white spheres with a blue outline.
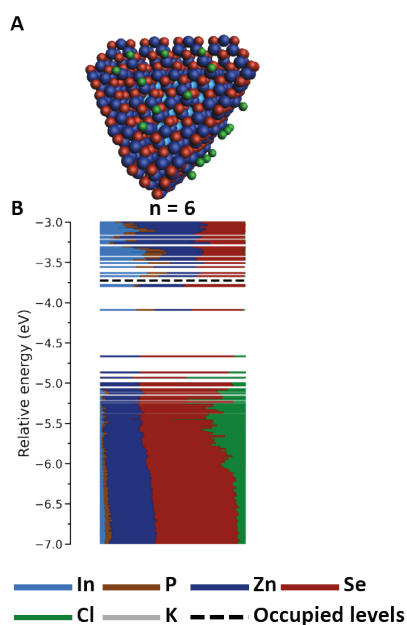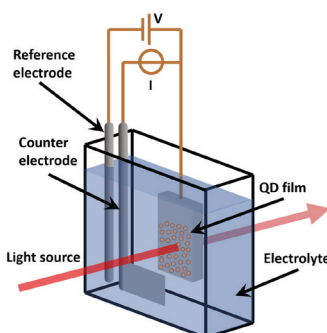

Figure A3.7. Charging of the InP/ZnSe(2ML) QD with n = 6. A) The structure of the QD with six potassium atoms on the surface. B) The DOS for the InP/ZnSe(2ML) with n = 6.

4

Who is in charge?

A spectroelectrochemical study on InP-based QD films

InP-based quantum dots (QDs) are emerging as a viable alternative to Cd chalcogenide and Pb halide perovskite QD materials for optoelectronic applications. Most of these applications require the injection of electrons and holes, which can lead to reduction or oxidation reactions. Here we explore the stability and charge dynamics of InP core-only and InP/ZnSe/ZnS QD films using spectroelectrochemical methods. For InP core-only QD films, the absorbance spectrum remains unchanged, indicating that injected charges do not remain in the conduction band, and reduction reactions are related to the surface ligands. InP/ZnSe/ZnS QD films with a mixture of chloride and oleylamine as ligands exhibit reversible photoluminescence (PL) quenching at negative potentials but not at positive potentials, while in ligand exchanged QD films with ethylenediamine (2DA) and sodium sulfide (Na_2S) reversible PL quenching at both positive and negative potentials is observed. Despite the PL quenching, no change in absorbance is measured during the spectroelectrochemical measurements, suggesting that charges do not remain in the conduction or valence band. We propose that trap states within the band gap are populated by injected charges, or injected charges induce electrochemical reactions after the films become conductive, creating trap states that lead to quenching of the PL in InP/ZnSe/ZnS QD films.

4.1 Introduction

Quantum dots (QDs) are luminescent materials with size-dependent optical properties, high photoluminescence (PL) quantum yield (PLQY) and narrow emission bands. These properties make QDs appealing for numerous optoelectronic applications such as photodetectors, LEDs and lasers.[1-7] The toxic nature of Cd chalcogenide and Pb halide perovskite QD materials has directed research towards InP-based QDs which are compliant with the Restriction of Hazardous Substances (RoHS) directive (Directive 2011/65/EU of the European Parliament).

Currently, InP-based QDs can be synthesized with near-unity PLQY[8-10] and narrow emission bands,[11, 12] and LED devices have been fabricated with these QDs.[8, 12-14] Most applications, like LEDs, photodetectors or phosphors, require charging of the QD materials with electrons and holes, either optically, electrically or chemically. It is often assumed that charge carriers are innocently injected in the conduction band (CB) and valence band (VB) and that present trap states are filled or emptied upon (de)charging. However, it has been proven that the injection of charge carriers can lead to charge-compensating defects for bulk semiconductors.[15-17] Electrochemical measurements offer a promising approach to probe the stability of InP-based QDs during charge injection, as charges are continuously supplied throughout the measurement. This continuous charge injection accentuates the effects, increasing the likelihood of detecting stability changes compared to methods such as photoexcitation, where charge carriers are transient.

The effects of charge injection into QDs have been studied both computationally and experimentally. Theoretical studies on Cd-based QDs show that injection of more than one electron can lead to the formation of trap states, even in completely passivated QDs, and that the absence of ligands can facilitate the reduction of Cd atoms on the surface.[18, 19] In experimental work, charge injection into the CB for CdSe/CdS/ZnS QD films is reported,[20, 21] but the protective ZnS shell is necessary to remove shallow trap states that are suspected to give rise to enhanced hole trapping once these traps are filled with electrons electrochemically.[22] Moreover, using electrochemically stable ligands, such as amines instead of cadmium carboxylates, proved essential to maintain high electroluminescence in Cd-based QD-LEDs.[23]

On ZnO and PbS QD films, it is possible to reversibly inject and extract electrons into/from the CB without degrading the QD films.[24-29] On InP-based QDs, a theoretical study reports that undercoordinated In atoms at the surface of core-only InP QDs are responsible for trap state formation when negative charges are injected, which can be prevented by growing a protective ZnSe layer around these cores.[30] These findings seem to line up with experimental work on bulk (100)-oriented InP electrodes where metallic In is formed during charging[31] and with the reported work on InP-based QDs in dispersion where charging of InP/ZnSe/ZnS is observed.[32, 33] However, knowledge on InP-based QD films, which resemble more closely QDs in devices, is lacking.

In this work InP core-only and InP/ZnSe/ZnS core/shell/shell QDs films are studied through spectroelectrochemical experiments. In these experiments, a potential is applied on the QD film and both the electrochemical current and the optical response are monitored. During the cyclic voltammograms (CVs) recorded on these films, a negative

current is measured for negative potentials but no significant changes in the absorbance and X-ray photoelectron spectroscopy (XPS) spectra are observed on the QD films. The PL of the InP/ZnSe/ZnS QD films with the original ligands decreases when a negative potential is applied and only recovers fully when the potential is scanned to positive values. A solid-state ligand exchange is performed on the core/shell/shell QD films to improve charge carrier mobilities using either 1,2-ethanedithiol (2DT), ethylenediamine (2DA), or sodium sulfide (Na_2S).[34] For the films with 2DA and Na_2S ligands, a drop in the PL intensity is also observed for positive potentials. This suggests that the absolute energy of the electronic states in the QDs is shifted or that the ligand exchange induces trap states. However, the absorbance for all InP/ZnSe/ZnS QD films shows no changes during the measurements, indicating that the charges are not maintained in the CB or VB. We propose two explanations for the decrease in PL without the presence of charges carriers in the CB or VB. The first is that injected charges are trapped in already existing trap states in the band gap where the filled traps result in quenching of the PL. The second is that injected charges react with species on or near the surface, ligands or impurities, which then create trap states on the surface that recover on the scan to positive potentials.

4.2 Results/Discussion

4.2.1 Core-only InP QD films
Core-only InP QDs are synthesized *via* an aminophosphine-based synthesis as described in the methods/experimental section.[35] These QDs have a 1S absorbance peak at approximately 530 nm and the PL spectrum is dominated by trap state emission (see Figure A4.1), which is common for as-synthesized InP QDs.[10, 36-40] Core-only QD thin films are fabricated by dropcasting a concentrated QD dispersion onto an Fluorine-doped Tin Oxide (FTO) substrate. The QD films are either directly used for further experiments, or a solid-state ligand exchange is performed to replace the original capping ligands, *i.e.* chloride and oleylamine, with 1,2-ethanedithiol (EDT) as cross-linking ligand.[41] The films are loaded in a spectroelectrochemistry setup which allows to probe both the absorbance and the PL of the QD films as a function of an applied potential while simultaneously measuring the current. The potentials reported are measured with respect to a Ag pseudoreference electrode which is calibrated with the ferrocene/ferrocenium (Fc/Fc+) redox couple at -0.39 V *vs*. Fc/Fc+ which corresponds to -4.69 V *vs*. vacuum (see Figure A4.2).[42, 43] Further details on the film fabrication, the ligand exchange and the spectroelectrochemistry setup are provided in the methods/experimental section.

In a typical measurement on a core-only QD film, the potential is cycled three times between the open circuit potential (OCP) and a negative vertex potential with a scan rate of 50 mV/s in a 0.1 M TBAPF$_6$ solution as electrolyte. Figure 4.1A shows the CVs recorded on one core-only QD film with original ligands with negative vertex potentials at -1.6, -1.8, -2.0 and -2.2 V. The increasingly negative potential is applied to determine either the potential at which charges are injected into the CB of the QDs or the potential at which cathodic decomposition of the QDs starts. In each CV, a cathodic current flows when the potential is scanned to values more negative than -1.3 V. These currents are however, comparable to the cathodic current measured on a bare FTO substrate (see Figure A4.3) indicating that the QD films are not very conductive. The cathodic current increases with

91

4

more negative potentials, with the first scan showing higher currents than successive scans.

In the reverse scan in the CVs with cathodic vertex at -1.6 and -1.8 V there is no positive current, demonstrating that the electrons injected in the forward scan are not extracted, *i.e.* the charge injection is irreversible and that no oxidative reactions occur. However, CVs to -2.0 and -2.2 V, contain an oxidative peak around -1.1 V on the backward scan, linked to a reduction reaction occurring at potentials more negative than -1.8 V.

A solid-state ligand exchange is performed with the bidentate ligand 2DT to reduce the distance between the InP QDs, increasing the charge carrier mobility in the film.[34] The CVs recorded on these QD films are depicted in Figure 4.1B for the same potential ranges as in Figure 4.1A. Larger currents are recorded for the 2DT-passivated QD film compared to the CVs in Figure 4.1A. The highest current appeared in the first scan of the CV to -1.6 V, with subsequent scans exhibiting smaller cathodic current which is equal to the first scan of the CV to -1.8 V. This pattern repeats for each CV, indicating that an irreversible cathodic reaction occurs during the first scan, which is not repeated during the consecutive scans. The exact nature of this cathodic reaction is unknown, but it is associated with the 2DT ligands, as it does appear for the film with the original ligands. The anodic peak in the backward scan, observed in Figure 4.1A, is not detected for the film with 2DT ligands. The absence of this peak indicates that this anodic reaction is related to the original ligands on the core-only QDs.

Further insight about the charge injection in the core-only QD films can be obtained from the absorbance changes during the CVs. Electrons injection in the CB decreases absorbance at the 1S peak, as the excitation of electrons from the VB edge to the CB edge is blocked by the injected electrons.[21, 22, 24, 25, 28] In Figure 4.1C and E, steady-state and differential absorbance spectra for the core-only QD film with the original ligands are plotted at the OCP and at the most negative potentials for the CVs to -1.6 and -2.2 V, respectively. For the CV to -1.6 V, the absorbance around the 1S peak, at approximately 530 nm, shows a minimal increase of up to 1 mOD. This value is close to the detection limit of our setup and, in relation to the steady-state absorbance of approximately 400 mOD at the 1S peak, indicates negligible change in the film. For the CVs to -2.2 V, a larger change in absorbance is witnessed after repeatedly reaching the negative vertex. The absorbance increases around 560 nm and decreases around the 1S peak, indicating a red-shift of the 1S peak, rather than a bleach of the 1S absorbance, as would be expected when electrons occupy the CB. Such red-shifts can occur due to charges that are present near the QDs, for instance on the QD surface, as has been reported for electrochemically charged CdSe and CdTe QD films.[22, 44-46] In addition, an increase of absorbance over the full wavelength range is observed, reminiscent of enhanced light scattering. This scattering could be due to expansion of the film, or due to an increase in dielectric constant for instance caused by the electrodeposition of metal domains.[47] However, the absorbance change is at its maximum approximately 8 mOD, representing a change of up to 2% of the absorbance. Similar minimal changes in absorbance are seen in CVs to -1.8 and -2.0 V (see Figure A4.4). The differential absorbance data indicate that, despite the oxidative peak during the reverse scan, the changes are not reversible.
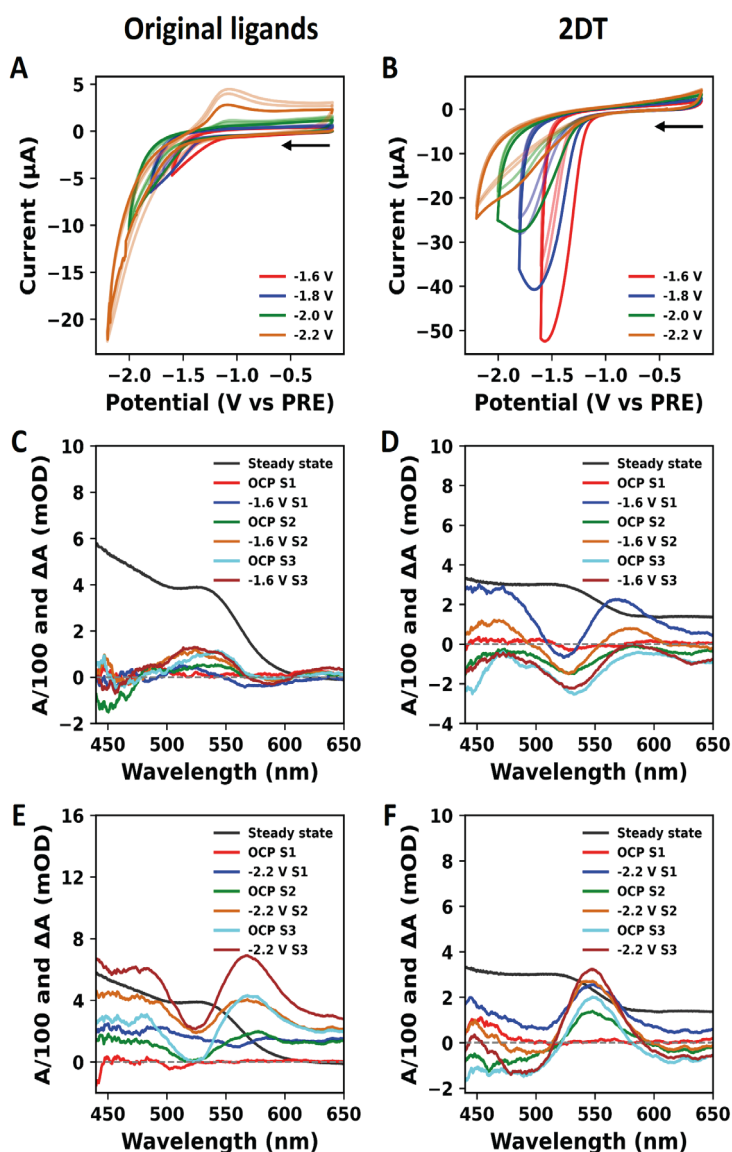
Figure 4.1: CVs starting at OCP at -0.11 V to different negative potentials for InP core-only QD films with a mixture of chloride and oleylamine ligands called original ligands (A) and 2DT as ligands (B) recorded at a scan rate of 50 mV/s in 0.1 M TBA PF$_6$ in ACN as electrolyte. Each CV contains three scans where the first scan is indicated in a dark shade and the second and third scan in a lighter shade of the same color. The scan direction for each CV is indicated by the black arrow. The absorbance and differential absorbance for QD films at OCP and the most negative potential for three consecutive scans are displayed in (C) and (E) for films with the original ligands and in (D) and (F) for films with the 2DT ligands.

93

XPS is performed on the core-only QD film to study the oxidation state of the In atoms. Figure A4.5 displays the XPS spectrum before and after a spectroelectrochemical measurement. In the case of reduction of In^{3+} ions to metallic In, peak broadening at higher binding energies and the raise of a signal around 456 eV would be expected. Both features are not visible in the XPS spectrum after electrochemical measurements, suggesting that there is no reduction of In^{3+} in the QD film.

Figure 4.1D displays the steady-state absorbance and the differential absorbance during the CV to -1.6 V of the 2DT film. A decrease at the 1S peak at 530 nm and an increase at 560 nm suggest a small red-shift of the 1S peak, similar to the red-shift for the QD film with the original ligand in Figure 4.1E. In the steady-state and differential absorbance measured during the CV to -2.2 V, displayed in Figure 4.1F, an increase in intensity around 550 nm is observed. This increase can be explained by the forementioned red-shift caused by nearby charges in combination with a change in light scattering by the film. The steady-state absorbance and the differential absorbance measured during the CVs to -1.8 and -2.0 V are plotted in Figure A4.4B and D respectively and show similar changes in the absorbance during the CVs. However, in all cases the change in the absorbance is only a few mOD, indicating that the absorbance changes 2% at most.

For both types of QD films, cathodic currents are recorded during CV measurements without detectable electron presence in the CB, as no reversible absorbance bleach is observed. Injected charges are not recovered, except for an oxidative peak in the original ligand film at potentials more negative than -1.8 V. Thus, two processes occur in the original ligand film: charge injection without electron retention in the CB, and a reduction reaction linked to the oxidation peak at -1.1 V, only for potentials more negative than -1.8 V. This second process is absent in the film with 2DT ligands, where only non-recovered current flow is detected, indicating that the reduction reaction is coupled to the original ligands.

We propose two processes that could explain this injection of charges without filling the CB. In either case it is assumed that the film becomes conductive once the potential reaches the potential of the CB. In the first explanation, shown in Scheme 4.1A, the injected charges are captured in existing trap states. In the trap states, the charges do not contribute to a decrease in absorption. When the film reaches the potential where the traps would be emptied, the potential is already below the CB, preventing conduction and stopping the charges from flowing back to the electrode. We refer to this explanation as the electrochemical filling of existent trap states. In the second explanation, depicted in Scheme 4.1B, the injected charges induce an electrochemical reaction. This could involve surface species such as ligands or contaminants in the electrolyte, for example molecular oxygen, but also the formation of metal dimers on the surface. In these scenarios a trap state is formed only after an additional charge carrier is supplied and reacts. To this explanation we refer as electrochemical formation of trap states. In both scenarios the reverse process is kinetically slowed down, making it appear irreversible in the CVs, as it occurs when the applied potential is in the band gap and transport of electrons through the CV levels is slow.
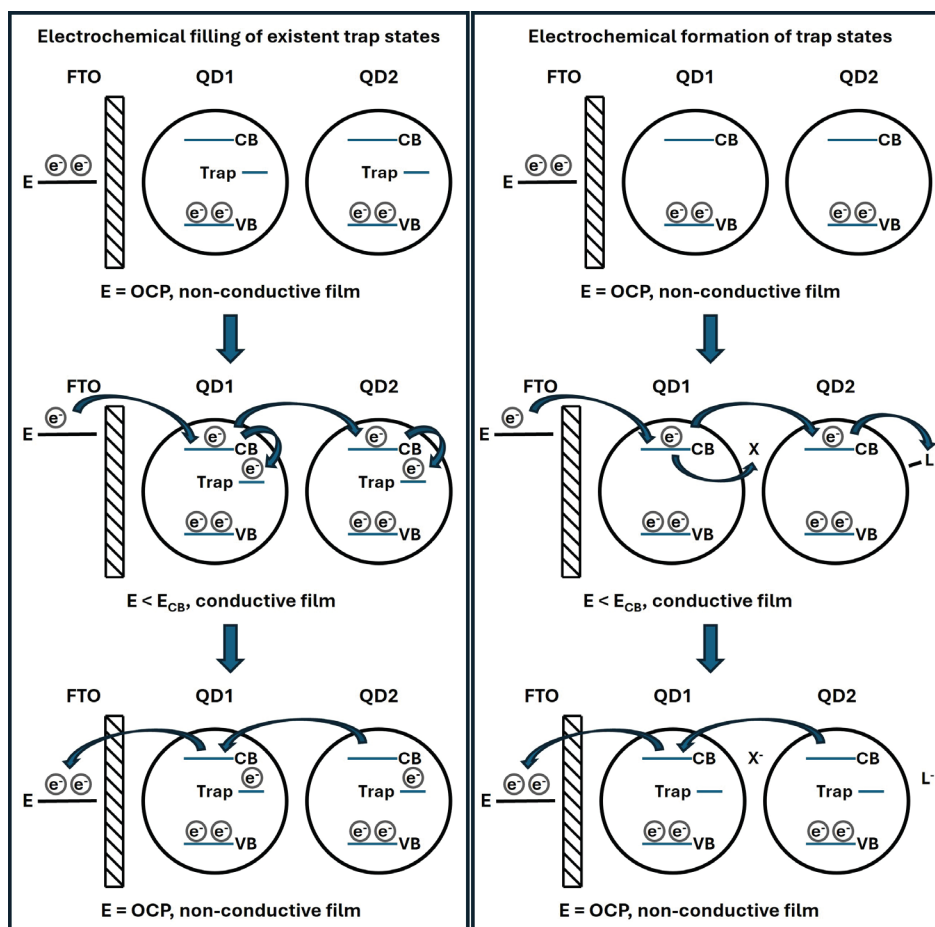
Scheme 4.1: (A) Electrochemical filling of existent trap states with negative charges upon applying a potential more negative than the CB. The charges are not extracted from the trap states when the potential is back to OCP. (B) Electrochemical formation of trap states by reactions with species in solution (X) or on the surface (L). The trap states trap the charges from the CB.

Based on our data, it cannot be distinguished whether scenario A, B, or both in Scheme 4.1, is responsible for the observed CVs. The potential at which the reductive current begins to flow is consistent with the work of Park *et al.*, where QDs in dispersion are charged.[33] Here, too, it is found that the injected charge carriers are not recovered.

4.2.2 Core/shell/shell InP/ZnSe/ZnS QD films
Next, we performed similar experiments on InP/ZnSe/ZnS QD films. The increased luminescence of InP/ZnSe/ZnS QD allows to simultaneously probe the PL during the spectroelectrochemical measurement. Additionally, it is expected that InP/ZnSe/ZnS QDs are electrochemically more stable than core-only QDs as Zn^{2+} should be harder to reduce than In^{3+}; the standard reduction potential for In^{3+}, -0.34 V *vs.* NHE, is more positive than

4

for Zn^{2+}, -0.76 V *vs.* NHE.[48-50] The protective role of Zn on the outer layer of InP/ZnSe QDs is also described in the computational work of Stam, *et al.*[30] and on CdSe/CdS/ZnS QDs in the work of Van der Stam, *et al.*[22] The synthesis of the InP/ZnSe/ZnS QDs is described in the methods/experimental section. The final QD dispersion has a 1S absorbance and emission at 580 nm and 611 nm, respectively and a PLQY of 63% (see Figure A4.6). The InP/ZnSe/ZnS QDs have a mixture of oleylamine, zinc oleate and zinc acetate as capping ligands on their surface.[51] Films of the QDs were prepared in the same manner as the core-only QD films, *i.e.* by dropcasting a concentrated InP/ZnSe/ZnS QD dispersion onto an FTO substrate.

Figure 4.2A shows the CV recorded between the OCP and -1.8 V on an InP/ZnSe/ZnS film without ligand exchange, together with the evolution of the PL at 615 nm during the CV. The 2D plot of the PL corresponding to this CV is depicted in Figure 4.2B. Similar to the CV on the core-only QD film, a cathodic current starts to flow when a potential more negative than -1.0 V is applied. The PL starts decreasing around the same potential and continues to decrease until the scan direction is reversed. The CV on this film also shows that the injected charge carriers are not recovered from the film. PL recovery on the reverse scan is much slower than the PL quenching on the forward scan as demonstrated in Figure 4.2A and Figure 4.2B. In the second and third scan, less current flows through the film at the most negative potentials. Figure 4.2B also demonstrates that in subsequent scans, the PL decreases again when scanned towards negative potentials and only partially recovers when scanning back to the OCP.

A CV between the OCP and +1.0 V on an InP/ZnSe/ZnS QD film is displayed in Figure 4.2C, together with the evolution of the PL during this measurement in Figure 4.2D. A small positive current flows during this measurement and the PL decreases minimally but returns to the same level at the end of the measurement as at the beginning. The CVs between OCP and -1.8 V and between OCP and +1.0 V reveal that in this potential range more electrons are injected at negative potentials than that holes are injected at the positive potentials.

Figure 4.2E shows a measurement over the full potential range, between -1.8 V and +1.0 V, starting and ending at the OCP, and scanning first in the cathodic direction. Again, a cathodic current is measured when a potential is applied that is more negative than -1.0 V, similar to the CV in Figure 4.2A. The PL, in Figure 4.2E and Figure 4.2F, decreases around the same negative potential. Reversing the scan direction leads again to a relatively slow recovery of the PL and the PL further increases when the most positive potential of +1.0 V is reached. Ultimately, the PL returns to the starting level, which contrasts with the scan that only goes negative in Figure 4.2A. The observed PL decrease at negative potentials is thus connected with the PL increase at positive potentials. This can be explained by the concept that electrons move in the CB at negative potentials once the film is conductive and immediately fill trap states at energies within the band gap. While scanning back and reaching energies within the band gap, the electrons remain in the trap states as the QD film is no longer conductive. Only upon reaching the VB the film becomes conductive again allowing for the extraction of electrons from the trap states. This explanation aligns with the CV in the reversed direction in Figure A4.7A and B, where the anodic current
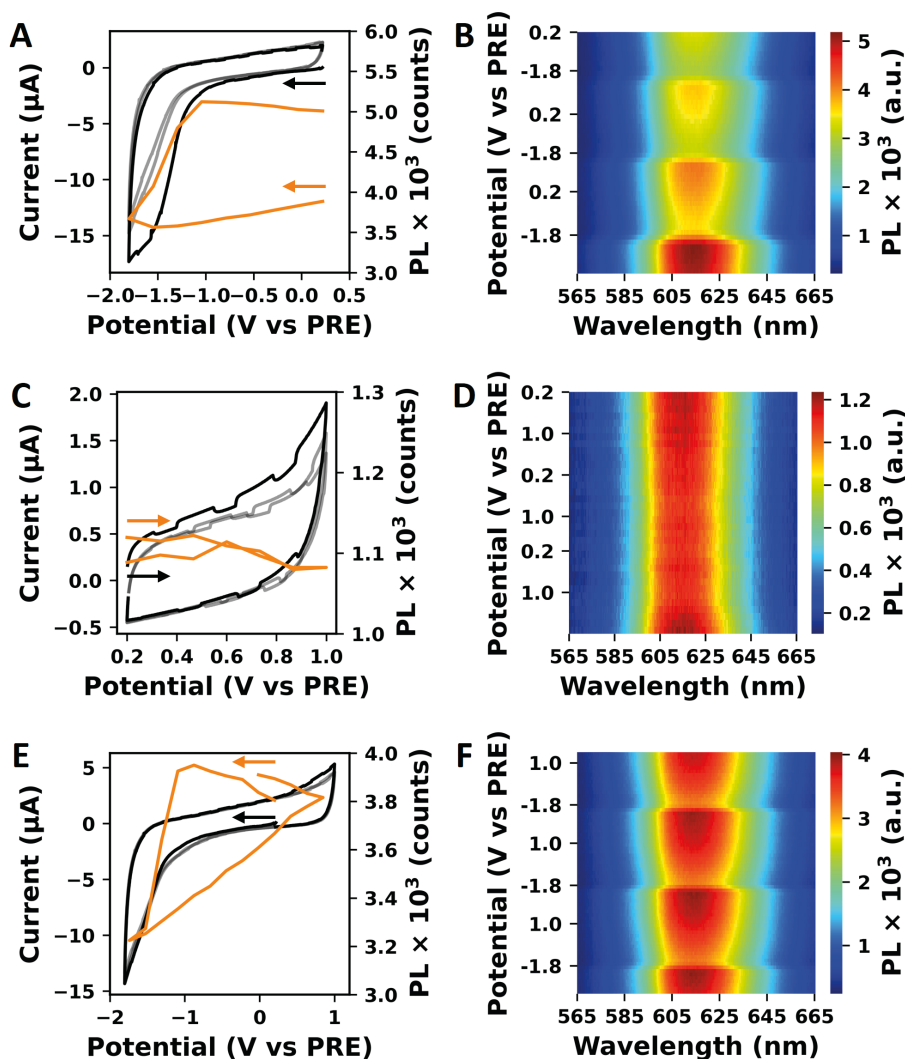
Figure 4.2: Spectroelectrochemical measurements on an InP/ZnSe/ZnS QD film. CVs (black) between OCP and -1.8 V (A), OCP and +1.0 V (C) and -1.8 and 1.0 V (E) recorded at a scan rate of 100 mV/s starting at 0.2 V in 0.1 M TBA PF$_6$ in ACN as electrolyte, the second and third scan are indicated in grey. The black arrow indicates the starting point and the direction of the CV and the orange arrow indicates the starting point and the direction the PL development during the CV. The PL intensity over one scan is shown in orange. (B), (D) and (F) are the corresponding 2D plots over the entire CVs.

increases after the first time that negative potentials are applied. Removing electrons from the trap states seems to occur spontaneously as well as the PL recovers slowly during the potentials in the band gap, which we ascribe to reactions with impurities such as residual O$_2$.

97

4

The PL changes witnessed during the CVs indicate that applying a potential affects the optical properties of the QD film. However, the absence of a bleach in the absorbance at the 1S peak (see Figure A4.8) for all three CVs in Figure 4.2, illustrates that charge carriers are not stably injected in the CB and VB of the QDs. The change in PL at negative potentials can thus not be explained by stable filling of CB energy levels which brings us back to the explanations drawn in Scheme 4.1A and 1B. The injected charges are captured in existing trap states where they act as efficient hole traps as suggested in earlier works,[22] or charges entering the CB react with a reactive species such as oxygen or ligands to form trap states which reduces the PL intensity.

The effect of ligand exchange on the charging of InP/ZnSe/ZnS QD films is also investigated. The measured CVs and the PL change during these CVs are displayed for films with the original ligands, 2DT, 2DA and Na$_2$S in Figure 4.3. It was demonstrated before that the charge carrier mobility of InZnP QD films increased for these ligands with respect to the original ligands with the Na$_2$S ligand resulting in the largest increase.[34] Figure 4.3A shows the CV between -1.8 V and +1.0 V recorded with a scan rate of 30 mV/s for an InP/ZnSe/ZnS QD film with the original ligands. The PL evolution is displayed in Figure 4.3A for one scan and in Figure 4.3B for the complete CV. In the CV and PL evolution, it is visible that when scanning to a negative potential, a cathodic current flows, and the PL decreases. When subsequently scanning in the positive direction, the PL recovers to its original value, which is similar to the behavior in Figure 4.2E.

The CV for the InP/ZnSe/ZnS QD film with 2DT ligands, in Figure 4.3C, is comparable to the CV for the film with the original ligands in Figure 4.3A. Similarly, the PL decreases when a negative potential is applied and recovers when scanning positively. Unlike what is observed for core-only InP QD films with 2DT, the electrochemical current is not increased with respect to the films with original ligands, suggesting that the 2DT ligand exchange is not as effective on the core-shell QDs as on the core-only QDs.

Figure 4.3E depicts the CV and PL evolution over one scan for an InP/ZnSe/ZnS QD film with 2DA ligands. A strong cathodic current is measured when scanning to negative potentials. At the start of the CV, the PL first increases when a negative potential is applied, but when a negative potential of approximately -1.2 V is reached, the PL starts to decrease rapidly. At the most negative potential, the PL decreases to nearly zero, as also seen in Figure A4.9. When the potential is scanned back in the positive direction, the PL initially returns to approximately the starting value at a potential of +0.5 V. Subsequently, the PL partially decreases again when a larger positive potential is applied. Figure 4.3F shows that this process repeats throughout the subsequent CV scans.

Figures 3G and 3H plot the CV and PL evolution recorded on the film with Na$_2$S ligands. Both the CV and the PL are comparable to the measurement on the film with 2DA ligands. The PL decreases both at the most negative and the most positive potential and recovers when the potential is between the two extremes. However, the PL modulations are less pronounced compared to the film with 2DA ligands (see Figure A4.9 for a direct comparison of the PL changes in the films).

Changing the surface ligands on the InP/ZnSe/ZnS QD films thus affects the magnitude of
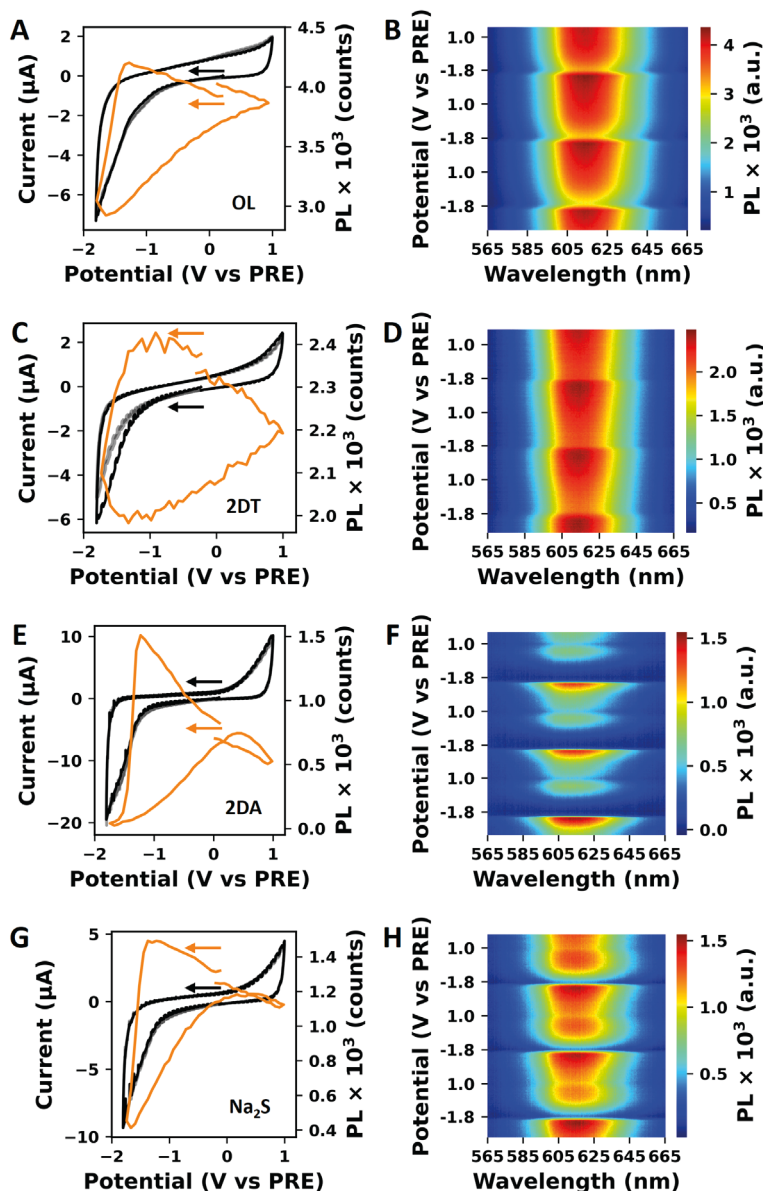
Figure 4.3: CVs and PL intensity over one scan of InP/ZnSe/ZnS QD films with the original (A), 2DT (C), 2DA (E) and Na$_2$S (G) ligands recorded at a scan rate of 30 mV/s in 0.1 M TBA PF$_6$ in ACN as electrolyte. The first scan is indicated in black, the second and third scan are shown in grey. The CVs in (A), (C), (E) and (G) start at the OCP of the corresponding film which is at 0.2 V, -0.23 V, 0.1 V and -0.12 V, respectively. The black arrow indicates the starting point and the direction of the CV and the orange arrow indicates the starting point and the direction the PL development during the CV. The corresponding 2D plots of the PL for each ligand are plotted in (B), (D), (F) and (H).

the current that flows, the extent of PL quenching, the PL quenching onset potential and whether quenching at positive potentials is observed. However, what is not affected is the absorbance during the CV, as none of the QD films display a bleach of the 1S absorbance, see Figure A4.10.

Surface ligands determine the absolute energy of the energy levels of a semiconductor.[52, 53] Changing the surface ligands will thus lead to a shift in the absolute energies where the intrinsic dipole of the ligand and the interface dipole play an important role in the size of the shift. It has been shown for 2DT and 2DA that the energy levels are shifted to more negative potentials compared to halides.[52-54] The higher surface coverage of these smaller ligands compared to the original ligands is expected to shift the energy levels within the QDs to a more negative potential. However, the increased charge carrier mobility will reduce the overpotential required to reach the energy levels, probably countering this shift to more negative potentials to a certain extent. Table A4.1 lists the potentials at which the PL begins to decrease during the CVs in Figure 4.3. The negative potential at which the PL starts to decrease is approximately the same for the films with the original, 2DT, and Na_2S ligands, ranging between -1.3 and -1.4 V. The film with 2DA ligands leads to PL quenching at a less negative potential of -1.23 V. Only the QD films with 2DA and Na_2S ligands show a decrease in PL during the positive scan, both at a potential of +0.47 V. These potentials indicate that there is at most a small ligand-induced shift in the injection potentials. The energy difference between the two points at which the PL decreases for the films with 2DA and Na2S ligands are 1.70 V and 1.84 V, respectively, both of which are less than the optical band gap of the QDs in the film (2.1 eV). We conclude that the onset of PL quenching lies below the CB and VB, and is hence most likely related to populating existing trap states in the band gap (scenario A in Scheme 4.1), or inducing electrochemical reactions at potentials inside the band gap to form trap states (scenario B in Scheme 4.1). Although the difference between the scenarios is whether the trap states are already present or formed, both scenarios involve the transfer of a charge carrier, followed by some reorganization. The degree of reorganization is likely different but what really matters is the timescale of the charge transfer event. If the charge transfer rate is larger than rate of recombination of excitons, it results in PL quenching, what is usually referred to as trapping. From our experiments it is clear that implementation of InP-based QDs in applications involving charging is not straightforward. Applications would require the stable injection of charge carriers into the QDs and to achieve this the presence or creation of trap states must be prevented.

4.3 Conclusions
Core-only InP QD films with chloride and oleylamine ligands exhibit a reduction reaction coupled to an oxidation reaction when scanned to potentials more negative than -1.8 V. Core-only InP QDs with 2DT ligands show a different irreversible reduction reaction at potentials of -1.6 V. For both films, absorbance changes are negligible, indicating charges do not remain in the CB of the QDs, and the reduction reactions are related to surface ligands. We propose that electrons either populate trap states that already exist in the band gap or induce electrochemical reactions after the films become conductive by reaching the CB or VB to form trap states. InP/ZnSe/ZnS QD films with original and 2DT ligands demonstrate PL quenching only at negative potentials, while films with 2DA and Na_2S

ligands show PL quenching at both negative and positive potentials. For all InP/ZnSe/ZnS QD films, negligible absorbance changes indicate charges do not remain in the CB or VB. Our explanations also apply to the InP/ZnSe/ZnS QD films where it is found that trap states are formed at positive potentials for films with 2DA and Na_2S ligands.

4.4 Methods/Experimental

Materials

The following materials were purchased from Merck Sigma: Fluorescein, $InCl_3$ (99.999%), $ZnCl_2$ (>98%), tris(diethylamino)phosphine (97%), triethylamine (≥99%), zinc oxide (99.999%), 1,2-ethanedithiol (≥98.0%), ethylenediamine (≥99%), sodium sulfide, and tetrabutylammonium hexafluorophosphate for the electrolyte ($TBAPF_6$) (≥99.0%). Anhydrous toluene (99.8%), selenium powder 200 mesh (99.999%), oleic acid (technical 90%), trifluoroacetic acid (99%), trifluoroacetic anhydride (> 99%) and 1-octadecene (technical 90%) were acquired from Alfa Aesar. Tri-n-octylphosphine (> 97%) and sulfur powder (99.999%) were collected from Strem Chemicals. NaOH pellets (98.5%), oleylamine (80-90%), calcium(II)hydride (93%) and zinc acetate (99%) were bought from Acros Organics. Anhydrous ethanol (>99.5%) tetrabutylammonium hexafluorophosphate for synthesis (98%) and anhydrous acetonitrile (≥99.95%) were purchased from VWR. Methanol was obtained from Fisher Chemicals. 2-propanol (99.7%) was purchased from Chem-Lab Analytical. Ar (6 N) was purchased from Linde. Fluorine-doped tin oxide (FTO) on glass slides (1.1 mm thick, 12-15 Ohm/sq) was purchased from MSE supplies. Oleylamine and 1-octadecene were dried over calcium(II)hydride, degassed via a vacuum distillation and stored over molecular sieves in a nitrogen-filled glovebox prior to use. All other chemicals were used without further purification.

Transamination of tris(diethylamino)phosphine

Transamination of tris(diethylamino)-phosphine occurs in the presence of three equivalents of oleylamine at 120-140 °C until the solution turns pale yellow in a nitrogen-filled glovebox. Typically, 0.25 mL (0.91 mmol) of tris(diethylamino)-phosphine is added to 1 mL (3.03 mmol) of oleylamine. Afterwards, while stirring, the temperature is raised to 120-140 °C. The evaporated diethylamine gas is removed via a continuous flushing of the glovebox.

Zinc(II)Oleate Synthesis

We used a procedure based on the synthesis of lead(II)oleate by Hendricks et al. that was adapted by Dhaene et al. for the production of zinc oleate.[55, 56] More specifically, 14.64 g (180 mmol) of zinc oxide was mixed in 80 mL (1.532 mol) of acetonitrile and, while cooled, 25.44 mL (180 mmol) of trifluoroacetic anhydride and 2.76 mL (36 mmol) of trifluoroacetic acid were added. The solution is stirred overnight and a clear and colourless solution was obtained upon reaching room temperature. This zinc trifluoroacetate solution was added to a mixture of 102.2 g (361.8 mmol) of oleic acid, 41.16 g (406.8 mmol) of triethylamine and 720 mL (2.351 mol) of 2-propanol resulting in the formation of a white precipitate. The resulted mixture was stirred and dissolution of the product occurred at reflux temperature. The flask is cooled down to room temperature over a period of 2 hours, followed by freezing to -20 °C overnight. The resulting white crystals were filtered off and washed with cold methanol. The synthesized powder was dried under vacuum and

a chemical yield of 95 ± 2% is obtained.

Tri-n-octylphosphine Selenide
A 2.24 M TOP-Se solution was prepared by dissolving 6.196 g (78.5 mmol) of selenium powder into 35 mL (78.5 mmol) of TOP at 90 °C for one hour in a nitrogen-filled glovebox. Afterwards, the mixture was kept for 30 minutes at 110 °C - upon which the mixture turned yellow. This TOP-Se solution was pushed through a 0.2 μm PTFE filter (VWR) and extra drops of TOP were added at 90 °C using a Pasteur pipette until the yellow colour disappeared.

Tri-n-octylphospine Sulfide
A 2.24 M TOP-S solution was prepared by dissolving 2.517 g (78.5 mmol) of sulphur powder into 35 mL (78.5 mmol) of TOP at 90 °C for one hour in a nitrogen-filled glovebox. Afterwards, the hot solution was pushed through a 0.2 μm PTFE filter (VWR).

Synthesis of core-only InP QDs
The procedure is based on the method previously published by Tessier et al.[35] 100 mg (0.45 mmol) of indium(III) chloride and 300 mg (2.20 mmol) of zinc(II) chloride were mixed in 3 mL (9.10 mmol) of anhydrous oleylamine in a 25 mL flask. The mixture was stirred and degassed at 120°C for an hour and then heated to 180°C under inert atmosphere. Upon reaching 180°C, 0.50 mL (1.83 mmol) of tris(diethylamino)phosphine, transaminated with 2 mL (6.07 mmol) of anhydrous oleylamine, was quickly injected in the reaction mixture described above and the InP nanocrystal synthesis proceeded for 30 min. The synthetized InP QDs were purified using anhydrous ethanol.

Synthesis of core/shell/shell InP/ZnSe/ZnS QDs
In a 25 mL three neck flask, 100 mg (0.45 mmol) of indium(III) chloride as indium raw material and 300 mg (2.20 mmol) of zinc(II) chloride as zinc raw material were mixed in 3 mL (9.10 mmol) of anhydrous oleylamine. The mixture was stirred and degassed at 120 °C for an hour and then heated to 180 °C under inert atmosphere. Upon reaching 180 °C, 0.50 mL (1.83 mmol) of tris(diethylamino)phosphine, transaminated with 2 mL (6.07 mmol) of anhydrous oleylamine, was quickly injected in the reaction mixture described above and the InP nanocrystal synthesis proceeded. After 30 min, the dispersion was cooled to 120 °C, and 120 mg (0.31 mmol) of tetrabutylammonium hexafluorophosphate, 0.3 mL (16.65 mmol) of water, and 2 g (3.18 mmol) of zinc(II) oleate mixed in 2 mL (6.07 mmol) of oleylamine and 4 mL (12.50 mmol) of 1-octadecene were added as a surface treatment prior to ZnSe shell growth. Subsequently, the mixture was stirred and degassed for an hour. Afterward, 1.6 mL of a stoichiometric TOP-Se (2.24 M) solution was injected, and the temperature was raised to 330 °C. At this temperature, the shell growth went on for 45 min. Subsequent to the ZnSe shell growth, the reaction mixture was cooled down to 120 °C, after which 400 mg (2.21 mmol) of zinc(II) acetate was added and the mixture was stirred and degassed for 1 h. Consecutively, 1 mL of a stoichiometric TOP-S (2.24 M) solution was injected, and the temperature was raised to 300 °C. After 1 h of ZnS shell growth, the reaction was stopped by cooling down the mixture to room temperature. InP/ZnSe/ZnS QDs were then precipitated once using ethanol, redispersed in toluene, and stored in a N_2-filled glovebox.

QD film preparation and ligand exchange

The QD film were prepared by drop-casting the QD dispersion (30 µL) on the FTO substrate and letting the solvent evaporate at room temperature. For the ligand exchange, the dry films were submerged in a 0.1 M solution of the preferred ligand (2DT, 2DA or Na_2S) in anhydrous acetonitrile for 30 seconds and afterwards rinsed anhydrous acetonitrile.

Spectroelectrochemical measurements

An Autolab PGSTAT128N potentiostat operated with NOVA 2.1 software is used for the spectroelectrochemical measurement. The electrochemical cell is composed in a three-electrode setup with a platinum sheet as counter electrode, a silver wire as pseudoreference electrode and the QD film on FTO as working electrode. All experiments were performed inside a N_2 filled glovebox. A 0.1 M solution of $TBAPF_6$ in anhydrous acetonitrile was purged with argon gas (99.999%) for 15 minutes and used as electrolyte. The optical spectra were recorded with a fiber coupled spectrophotometer (Ocean Optics USB2000) and the white light for absorbance and blue light for photoluminescence measurements were generated by an Ocean Optics deuterium DH-2000 lamp and a 4.5 mW collimated laser diode from Thorlabs at a wavelength of 405 nm, respectively.

Optical characterization

A PerkinElmer Lambda 365 spectrometer was used for recording the UV-vis absorbance spectra. An Edinburgh Instruments FLS980 spectrofluorometer with double grating monochromators for both excitation and emission paths and a 450 W Xenon lamp as an excitation source. PLQY values were obtained with respect to the Fluorescein reference dye in 0.1 M NaOH in water at room temperature. The PLQY was calculated using the following equation;

$$PLQY = PLQY_{Fluorescein} \times \frac{I^{PL}_{QD\ disperion} \times f_{Fluorescein}}{I^{PL}_{Fluorescein} \times f_{QD\ dispersion}} \times \left(\frac{n_{toluene}}{n_{water}}\right)^2$$

Where $PLQY_{Fluorescein}$ is set to be 92% for an excitation wavelength of 465 nm,[57] I^{PL} is the intensity of the PL signal of either the Fluorescein solution or the QD dispersion, n is the refractive index of toluene or water at 465 nm (1.497 and 1.333) and f is the fraction of absorbed light for the Fluorescein or toluene solution, calculated as $f = 10^{-OD}$ with the OD being the optical density of the Fluorescein or QD dispersion at 465 nm.

X-ray Photoelectron Spectroscopy (XPS)

Samples are dropcasted on thin conductive substrates. XPS measurements were performed in ultra-high vacuum with a ThermoFisher K-Alpha equipped with an Al Kα source which radiates with an energy of 1486 eV. An Ar flood gun was used during the measurements to prevent charging of the films.

References

1. Almeida, G.; Ubbink, R. F.; Stam, M.; du Fossé, I.; Houtepen, A. J., InP colloidal quantum dots for visible and near-infrared photonics. *Nature Reviews Materials* **2023,** *8* (11), 742-758.
2. Wu, Z.; Liu, P.; Zhang, W.; Wang, K.; Sun, X. W., Development of InP Quantum Dot-Based Light-Emitting Diodes. *ACS Energy Letters* **2020,** *5* (4), 1095-1106.
3. Park, Y.-S.; Roh, J.; Diroll, B. T.; Schaller, R. D.; Klimov, V. I., Colloidal quantum dot lasers. *Nature Reviews Materials* **2021,** *6* (5), 382-401.
4. Coe-Sullivan, S.; Liu, W.; Allen, P.; Steckel, J. S., Quantum Dots for LED Downconversion in Display Applications. *ECS Journal of Solid State Science and Technology* **2013,** *2* (2), R3026.
5. Talapin, D. V.; Steckel, J., Quantum dot light-emitting devices. *MRS Bulletin* **2013,** *38* (9), 685-691.
6. Geiregat, P.; Houtepen, A. J.; Sagar, L. K.; Infante, I.; Zapata, F.; Grigel, V.; Allan, G.; Delerue, C.; Van Thourhout, D.; Hens, Z., Continuous-wave infrared optical gain and amplified spontaneous emission at ultralow threshold by colloidal HgTe quantum dots. *Nature Materials* **2018,** *17* (1), 35-42.
7. Geuchies, J. J.; Brynjarsson, B.; Grimaldi, G.; Gudjonsdottir, S.; van der Stam, W.; Evers, W. H.; Houtepen, A. J., Quantitative Electrochemical Control over Optical Gain in Quantum-Dot Solids. *ACS Nano* **2020,** *15* (1), 377-386.
8. Won, Y.-H.; Cho, O.; Kim, T.; Chung, D.-Y.; Kim, T.; Chung, H.; Jang, H.; Lee, J.; Kim, D.; Jang, E., Highly efficient and stable InP/ZnSe/ZnS quantum dot light-emitting diodes. *Nature* **2019,** *575* (7784), 634-638.
9. Van Avermaet, H.; Schiettecatte, P.; Hinz, S.; Giordano, L.; Ferrari, F.; Nayral, C.; Delpech, F.; Maultzsch, J.; Lange, H.; Hens, Z., Full-Spectrum InP-Based Quantum Dots with Near-Unity Photoluminescence Quantum Efficiency. *ACS Nano* **2022,** *16* (6), 9701-9712.
10. Stam, M.; Almeida, G.; Ubbink, R. F.; van der Poll, L. M.; Vogel, Y. B.; Chen, H.; Giordano, L.; Schiettecatte, P.; Hens, Z.; Houtepen, A. J., Near-Unity Photoluminescence Quantum Yield of Core-Only InP Quantum Dots via a Simple Postsynthetic InF3 Treatment. *ACS Nano* **2024,** *18* (22), 14685-14695.
11. Almeida, G.; van der Poll, L.; Evers, W. H.; Szoboszlai, E.; Vonk, S. J. W.; Rabouw, F. T.; Houtepen, A. J., Size-Dependent Optical Properties of InP Colloidal Quantum Dots. *Nano Letters* **2023,** *23* (18), 8697-8703.
12. Li, H.; Zhang, W.; Bian, Y.; Ahn, T. K.; Shen, H.; Ji, B., ZnF2-Assisted Synthesis of Highly Luminescent InP/ZnSe/ZnS Quantum Dots for Efficient and Stable Electroluminescence. *Nano Letters* **2022,** *22* (10), 4067-4073.
13. Cerpentier, J.; Karadza, B.; van Avermaet, H.; Giordano, L.; Schiettecatte, P.; Hens, Z.; Meuret, Y., InP-based quantum dot on-chip white LEDs with optimal circadian efficiency. *Optics & Laser Technology* **2023,** *167*, 109839.
14. Karadza, B.; Schiettecatte, P.; Van Avermaet, H.; Mingabudinova, L.; Giordano, L.; Respekta, D.; Deng, Y.-H.; Nakonechnyi, I.; De Nolf, K.; Walravens, W.; Meuret, Y.; Hens, Z., Bridging the Green Gap: Monochromatic InP-Based Quantum-Dot-on-Chip LEDs with over 50% Color Conversion Efficiency. *Nano Letters* **2023,** *23* (12), 5490-5496.
15. Walukiewicz, W., Defects and Self-Compensation in Semiconductors. In *Wide-Gap Chalcopyrites*, Siebentritt, S.; Rau, U., Eds. Springer Berlin Heidelberg: Berlin, Heidelberg, 2006; pp 35-54.
16. Heinrich, M.; Domke, C.; Ebert, P.; Urban, K., Charged steps on III-V compound semiconductor surfaces. *Physical Review B* **1996,** *53* (16), 10894-10897.
17. Kabiraj, D.; Grötzschel, R.; Ghosh, S., Modification of charge compensation in semi-insulating semiconductors by high energy light ion irradiation. *Journal of Applied Physics* **2008,** *103* (5).
18. du Fossé, I.; ten Brink, S.; Infante, I.; Houtepen, A. J., Role of Surface Reduction in the Formation of Traps in n-Doped II–VI Semiconductor Nanocrystals: How to Charge without Reducing the Surface. *Chemistry of Materials* **2019,** *31* (12), 4575-4583.

19. du Fossé, I.; Lal, S.; Hossaini, A. N.; Infante, I.; Houtepen, A. J., Effect of Ligands and Solvents on the Stability of Electron Charged CdSe Colloidal Quantum Dots. *The Journal of Physical Chemistry C* **2021,** *125* (43), 23968-23975.

20. Boehme, S. C.; Wang, H.; Siebbeles, L. D. A.; Vanmaekelbergh, D.; Houtepen, A. J., Electrochemical Charging of CdSe Quantum Dot Films: Dependence on Void Size and Counterion Proximity. *ACS Nano* **2013,** *7* (3), 2500-2508.

21. Ashokan, A.; Mulvaney, P., Spectroelectrochemistry of Colloidal CdSe Quantum Dots. *Chemistry of Materials* **2021,** *33* (4), 1353-1362.

22. van der Stam, W.; Grimaldi, G.; Geuchies, J. J.; Gudjonsdottir, S.; van Uffelen, P. T.; van Overeem, M.; Brynjarsson, B.; Kirkwood, N.; Houtepen, A. J., Electrochemical Modulation of the Photophysics of Surface-Localized Trap States in Core/Shell/(Shell) Quantum Dot Films. *Chemistry of Materials* **2019,** *31* (20), 8484-8493.

23. Pu, C.; Dai, X.; Shu, Y.; Zhu, M.; Deng, Y.; Jin, Y.; Peng, X., Electrochemically-stable ligands bridge the photoluminescence-electroluminescence gap of quantum dots. *Nature Communications* **2020,** *11* (1), 937.

24. Vogel, Y. B.; Pham, L. N.; Stam, M.; Ubbink, R. F.; Coote, M. L.; Houtepen, A. J., Solvation Shifts the Band-Edge Position of Colloidal Quantum Dots by Nearly 1 eV. *Journal of the American Chemical Society* **2024,** *146* (14), 9928-9938.

25. Vogel, Y. B.; Stam, M.; Mulder, J. T.; Houtepen, A. J., Long-Range Charge Transport via Redox Ligands in Quantum Dot Assemblies. *ACS Nano* **2022,** *16* (12), 21216-21224.

26. Guyot-Sionnest, P., Charging colloidal quantum dots by electrochemistry. *Microchimica Acta* **2008,** *160* (3), 309-314.

27. Gudjonsdottir, S.; Koopman, C.; Houtepen, A. J., Enhancing the stability of the electron density in electrochemically doped ZnO quantum dots. *The Journal of Chemical Physics* **2019,** *151* (14), 144708.

28. Gudjonsdottir, S.; van der Stam, W.; Kirkwood, N.; Evers, W. H.; Houtepen, A. J., The Role of Dopant Ions on Charge Injection and Transport in Electrochemically Doped Quantum Dot Films. *Journal of the American Chemical Society* **2018,** *140* (21), 6582-6590.

29. Roest, A. L.; Germeau, A.; Kelly, J. J.; Vanmaekelbergh, D.; Allan, G.; Meulenkamp, E. A., Long-Range Transport in an Assembly of ZnO Quantum Dots: The Effects of Quantum Confinement, Coulomb Repulsion and Structural Disorder. *ChemPhysChem* **2003,** *4* (9), 959-966.

30. Stam, M.; du Fossé, I.; Infante, I.; Houtepen, A. J., Guilty as Charged: The Role of Undercoordinated Indium in Electron-Charged Indium Phosphide Quantum Dots. *ACS Nano* **2023,** *17* (18), 18576-18583.

31. Yu, W.; Richter, M. H.; Buabthong, P.; Moreno-Hernandez, I. A.; Read, C. G.; Simonoff, E.; Brunschwig, B. S.; Lewis, N. S., Investigations of the stability of etched or platinized p-InP(100) photocathodes for solar-driven hydrogen evolution in acidic or alkaline aqueous electrolytes. *Energy & Environmental Science* **2021,** *14* (11), 6007-6020.

32. Park, J.; Kim, T.; Kim, D., Charge Injection and Energy Transfer of Surface-Engineered InP/ZnSe/ZnS Quantum Dots. *Nanomaterials* **2023,** *13* (7), 1159.

33. Park, J.; Won, Y.-H.; Kim, T.; Jang, E.; Kim, D., Electrochemical Charging Effect on the Optical Properties of InP/ZnSe/ZnS Quantum Dots. *Small* **2020,** *16* (41), 2003542.

34. Crisp, R. W.; Kirkwood, N.; Grimaldi, G.; Kinge, S.; Siebbeles, L. D. A.; Houtepen, A. J., Highly Photoconductive InP Quantum Dots Films and Solar Cells. *ACS Applied Energy Materials* **2018,** *1* (11), 6569-6576.

35. Tessier, M. D.; Dupont, D.; De Nolf, K.; De Roo, J.; Hens, Z., Economic and Size-Tunable Synthesis of InP/ZnE (E = S, Se) Colloidal Quantum Dots. *Chemistry of Materials* **2015,** *27* (13), 4893-4898.

36. Hughes, K. E.; Stein, J. L.; Friedfeld, M. R.; Cossairt, B. M.; Gamelin, D. R., Effects of Surface Chemistry on the Photophysics of Colloidal InP Nanocrystals. *ACS Nano* **2019,** *13* (12),

4

14198-14207.

37. Gary, D. C.; Terban, M. W.; Billinge, S. J. L.; Cossairt, B. M., Two-Step Nucleation and Growth of InP Quantum Dots via Magic-Sized Cluster Intermediates. *Chemistry of Materials* **2015,** *27* (4), 1432-1441.

38. Ubbink, R. F.; Almeida, G.; Iziyi, H.; du Fossé, I.; Verkleij, R.; Ganapathy, S.; van Eck, E. R. H.; Houtepen, A. J., A Water-Free In Situ HF Treatment for Ultrabright InP Quantum Dots. *Chemistry of Materials* **2022,** *34* (22), 10093-10103.

39. Achorn, O. B.; Franke, D.; Bawendi, M. G., Seedless Continuous Injection Synthesis of Indium Phosphide Quantum Dots as a Route to Large Size and Low Size Dispersity. *Chemistry of Materials* **2020,** *32* (15), 6532-6539.

40. Janke, E. M.; Williams, N. E.; She, C.; Zherebetskyy, D.; Hudson, M. H.; Wang, L.; Gosztola, D. J.; Schaller, R. D.; Lee, B.; Sun, C.; Engel, G. S.; Talapin, D. V., Origin of Broad Emission Spectra in InP Quantum Dots: Contributions from Structural and Electronic Disorder. *Journal of the American Chemical Society* **2018,** *140* (46), 15791-15803.

41. Dümbgen, K. C.; Leemans, J.; De Roo, V.; Minjauw, M.; Detavernier, C.; Hens, Z., Surface Chemistry of InP Quantum Dots, Amine–Halide Co-Passivation, and Binding of Z-Type Ligands. *Chemistry of Materials* **2023,** *35* (3), 1037-1046.

42. Connelly, N. G.; Geiger, W. E., Chemical Redox Agents for Organometallic Chemistry. *Chemical Reviews* **1996,** *96* (2), 877-910.

43. Paul, A.; Borrelli, R.; Bouyanfif, H.; Gottis, S.; Sauvage, F., Tunable Redox Potential, Optical Properties, and Enhanced Stability of Modified Ferrocene-Based Complexes. *ACS Omega* **2019,** *4* (12), 14780-14789.

44. van der Stam, W.; du Fossé, I.; Grimaldi, G.; Monchen, J. O. V.; Kirkwood, N.; Houtepen, A. J., Spectroelectrochemical Signatures of Surface Trap Passivation on CdTe Nanocrystals. *Chemistry of Materials* **2018,** *30* (21), 8052-8061.

45. Houtepen, A. J.; Vanmaekelbergh, D., Orbital Occupation in Electron-Charged CdSe Quantum-Dot Solids. *The Journal of Physical Chemistry B* **2005,** *109* (42), 19634-19642.

46. Franceschetti, A.; Zunger, A., Optical transitions in charged CdSe quantum dots. *Physical Review B* **2000,** *62* (24), R16287-R16290.

47. Boehme, S. C.; Vanmaekelbergh, D.; Evers, W. H.; Siebbeles, L. D. A.; Houtepen, A. J., In Situ Spectroelectrochemical Determination of Energy Levels and Energy Level Offsets in Quantum-Dot Heterojunctions. *The Journal of Physical Chemistry C* **2016,** *120* (9), 5164-5173.

48. Allred, A. L., Electronegativity values from thermochemical data. *Journal of Inorganic and Nuclear Chemistry* **1961,** *17* (3), 215-221.

49. Bard, A. J.; Faulkner, L. R., *Electrochemical Methods: Fundamentals and Applications, 2nd Edition*. Wiley Textbooks: 2001.

50. Haynes, W. M., CRC Handbook of Chemistry and Physics, 95th Edition. 95th ed ed.; CRC Press: Hoboken, 2014.

51. Schiettecatte, P.; Giordano, L.; Cruyssaert, B.; Bonifas, G.; De Vlamynck, N.; Van Avermaet, H.; Zhao, Q.; Vantomme, A.; Nayral, C.; Delpech, F.; Hens, Z., Enhanced Surface Passivation of InP/ZnSe Quantum Dots by Zinc Acetate Exposure. *Chemistry of Materials* **2024,** *36* (12), 5996-6005.

52. Kroupa, D. M.; Vörös, M.; Brawand, N. P.; McNichols, B. W.; Miller, E. M.; Gu, J.; Nozik, A. J.; Sellinger, A.; Galli, G.; Beard, M. C., Tuning colloidal quantum dot band edge positions through solution-phase surface chemistry modification. *Nature Communications* **2017,** *8* (1), 15257.

53. Brown, P. R.; Kim, D.; Lunt, R. R.; Zhao, N.; Bawendi, M. G.; Grossman, J. C.; Bulović, V., Energy Level Modification in Lead Sulfide Quantum Dot Thin Films through Ligand Exchange. *ACS Nano* **2014,** *8* (6), 5863-5872.

54. Song, J. H.; Choi, H.; Pham, H. T.; Jeong, S., Energy level tuned indium arsenide colloidal quantum dot films for efficient photovoltaics. *Nature Communications* **2018,** *9* (1), 4267.

55.   Hendricks, M. P.; Campos, M. P.; Cleveland, G. T.; Jen-La Plante, I.; Owen, J. S., A tunable library of substituted thiourea precursors to metal sulfide nanocrystals. *Science* **2015,** *348* (6240), 1226-1230.

56.   Dhaene, E.; Billet, J.; Bennett, E.; Van Driessche, I.; De Roo, J., The Trouble with ODE: Polymerization during Nanocrystal Synthesis. *Nano Letters* **2019,** *19* (10), 7411-7417.

57.   Magde, D.; Wong, R.; Seybold, P. G., Fluorescence Quantum Yields and Their Relation to Lifetimes of Rhodamine 6G and Fluorescein in Nine Solvents: Improved Absolute Standards for Quantum Yields. *Photochemistry and Photobiology* **2002,** *75* (4), 327-334.
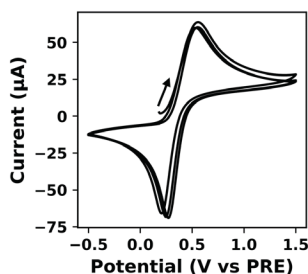
4

Appendix
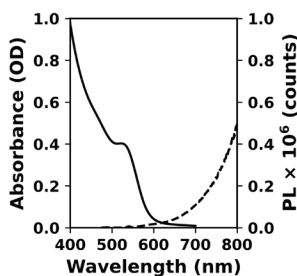
**Figure A4.1**: Absorbance (solid) and PL (dashed) of a core-only InP dispersion.

4

Figure A4.2: CV of ferrocene in 0.1 M TBAPF$_6$ in acetonitrile used to calibrate the Ag pseudoreference electrode at a scan rate of 30 mV/s. The black arrow indicates the starting point and the direction of the CV. The half wave potential ($E_{1/2}$) is estimated at 0.39 V.

The potential of the Ag pseudoreference electrode with respect to vacuum is calculated with the formula: $E_{abs} = - E_{Ag} -4.68$ (SCE $vs.$ vacuum) $– 0.40$ (ferrocene $vs.$ SCE) $+ E_{1/2}$. The pseudoreference electrode is established to be at -4.69 V $vs.$ vacuum.
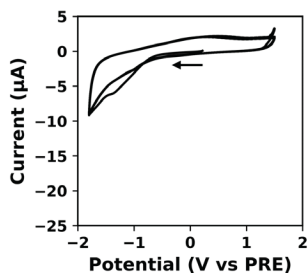
Figure A4.3: CV recorded between -1.8 and 1.5 V on a bare FTO substrate with a scan rate of 30 mV/s in 0.1 M TBA PF$_6$ in ACN as electrolyte. The black arrow indicates the starting point and the scan direction of the CV.

Original ligands

2DT
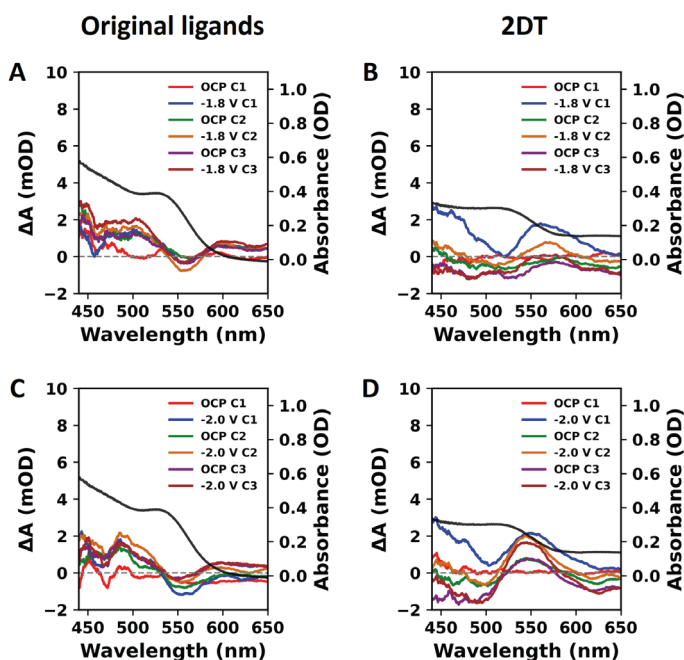
Figure A4.4: The absorbance and differential absorbance for QD films at OCP and the most negative potential for three consecutive scans are displayed in (A) and (C) for films with the original ligands and in (B) and (D) for films with the 2DT ligands.
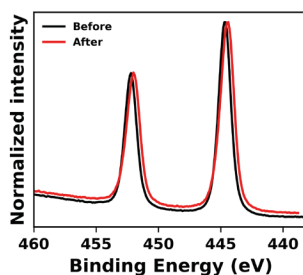
Figure A4.5: XPS spectrum of the In3d photoemission line for a core-only InP QD film before (black) and after (red) 10 minutes at -1.8 V.

109
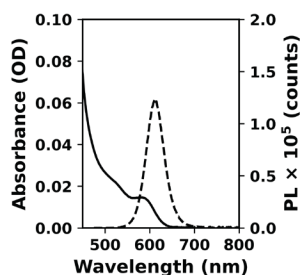
Figure A4.6: Absorbance (solid) and PL (dashed) of a core/shell/shell InP/ZnSe/ZnS dispersion. The PLQY was measured against the Fluorescein reference dye (92% in EtOH) and was found to be 63%.

4

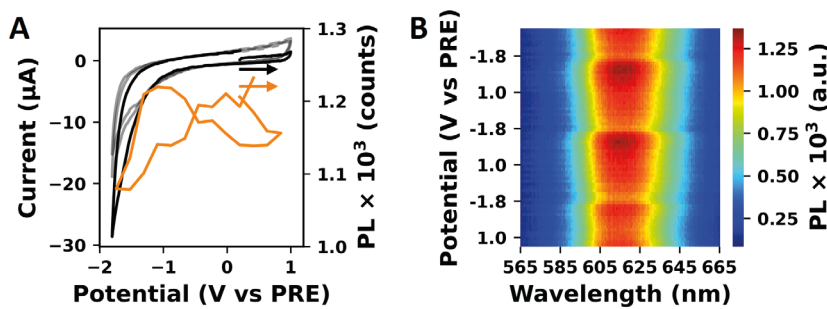**Figure A4.7**: Spectroelectrochemical measurements on an InP/ZnSe/ZnS QD film. The CV (A) is recorded between 1.0 V and -1.8 V, recorded at a scan rate of 100 mV/s starting at 0.2 V in 0.1 M TBA PF6 in ACN as electrolyte, the second and third scan are indicated in grey. The black arrow indicates the starting point and the direction of the CV and the orange arrow indicates the starting point and the direction the PL development during the CV. The PL development during the first scan is shown in orange. (B) is the corresponding 2D plot over the entire CV.
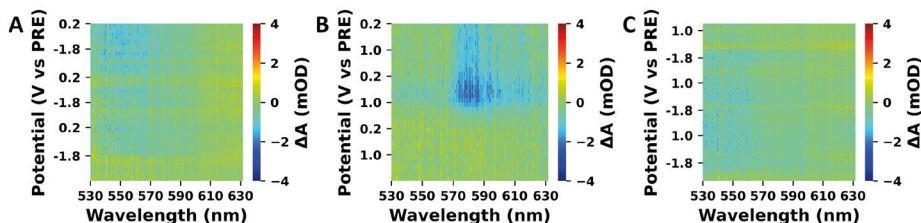
Figure A4.8: 2D plots of the differential absorbance (ΔA) for an InP/ZnSe/ZnS QD film scanned from OCP to -1.8 V (A), from OCP to +1.0 V (B) and from OCP to -1.8 V to +1.0 V (C).
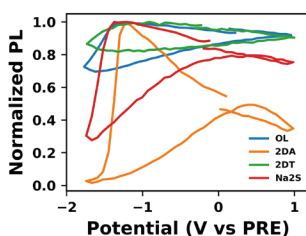
Figure A4.9: Normalized PL evolution during one scan for films with the original ligands (blue), 2DA ligands (orange), 2DT ligands (green) and Na$_2$S ligands (red).

4
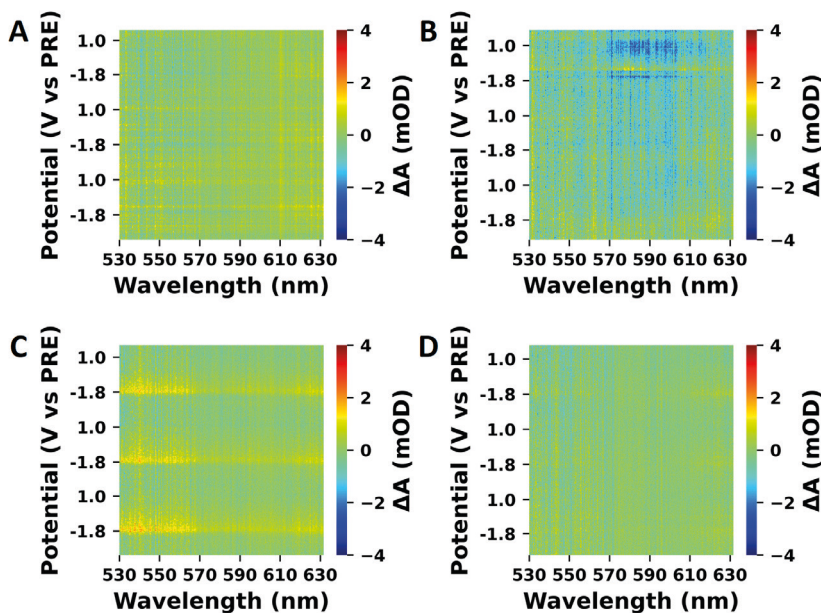
Figure A4.10: 2D plots of the differential absorbance (ΔA) for InP/ZnSe/ZnS QD films scanned between -1.8 V and +1.0 V with the original ligands (A), 2DT ligands (B), 2DA ligands (C) and Na$_2$S ligands (D).

Table A4.1: Negative and positive onset potentials for the decrease in PL for films with the original ligands, 2DA ligands, 2DT ligands and Na$_2$S ligands.

Ligand	Negative onset (V vs PRE)	Positive onset (V vs PRE)
OL	-1.33	-
2DA	-1.23	+0.47
2DT	-1.32	-
Na$_2$S	-1.37	+0.47

111

Summary

Quantum dots (QDs) play a central role in this thesis and can be described as semiconductor nanoparticles small enough for quantum confinement to occur. The quantum confinement effect results in the size dependance of several properties of the QDs, including the band gap energy. The band gap determines the eventual color of the light emitted by the QDs and observed by our eyes. This means that by simply varying the size of the QDs the color of the nanoparticles can be tuned. The size-dependent properties, combined with a high photoluminescence (PL) quantum yield (PLQY) and pure color emission, make QDs very attractive for incorporation in lighting applications. To comply to modern European regulations, InP-based QDs are developed, omitting the use of prohibited, toxic elements such as Cd and Pb. However, the understanding and quality of InP-based QDs lag behind those of Cd- and Pb-based QD materials, necessitating further investigation into the material properties. It has been observed that most problems and questions arise from the surface chemistry of InP QDs. Therefore, this thesis is dedicated to studying the surface of InP-based QDs and finding methods to improve the overall quality of InP-based QDs.

The main concepts of InP-based QDs are discussed in Chapter 1. First, the general electronic and optical properties of InP are reviewed and compared to other semiconductor materials. Then, the synthesis methods considered most standard are discussed and evaluated. The reviewed synthesis methods will come back in the following Chapters. The resulting QDs often demonstrate limited efficiency, and the phenomena causing this limited efficiency are discussed along with previously investigated solutions. The Chapter concludes with an overview of achieved and possible applications of InP-based QDs.

In Chapter 2, we investigate and optimize a simple postsynthetic treatment to achieve a near-unity PLQY on core-only InP QDs. Synthesized InP QDs have a PLQY of less than 1% and show mainly trap state emission. It is generally assumed that a significant portion of the efficiency quenching is caused by surface oxides and undercoordinated P atoms on the surface. Surface oxidation is prevented by performing the synthesis under strict inert conditions. Passivation of the undercoordinated P atoms can be achieved by providing Z-type ligands. A series of metal salts is tested as Z-type ligands on InP QDs in a treatment at 150 °C for 30 minutes in the presence of $In(PA)_3$. InF_3 is found as the most suitable Z-type ligand in these conditions boosting the PLQY to 70%. Optimization of the temperature and time of the treatment results in a PLQY of 93% for a treatment at 180 for 60 minutes while preventing significant broadening of the emission peak. The treatment is successfully applied to various sizes of InP QDs and to InP QDs obtained *via* different synthesis routes.

Density functional theory (DFT) calculations are used in Chapter 3 to investigate electron charging of InP core-only and InP/ZnSe QDs on an atomic scale. Two models were designed, one spherical and the other tetrahedral in shape, of InP QDs, passivated with Cl atoms mimicking surface ligands with the advantage of lower computational costs. An energy diagram with a bandgap clear of trap states is obtained for these QD models in the neutral state. The addition of one extra electron leads to the formation of a trap

state in both QD models, and it is found that undercoordinated In atoms are responsible for the formation of these trap states. InP/ZnSe core/shell models with all In atoms fully coordinated can be charged with electrons without the formation of trap states. These results show that undercoordinated In atoms should be avoided for InP-based QDs to be stable upon charging.

To elucidate the experimental effects of charging InP-based QDs, spectroelectrochemical experiments are performed on thin films of InP core-only and InP/ZnSe/ZnS QDs, and the results are described in Chapter 4. A dispersion of InP core-only QDs is dropcasted on an FTO substrate to create a thin film. The film is then placed in an electrochemical cell, and a cyclic voltammogram is recorded, cycling the potential between two maxima while recording the current. Simultaneously, the optical features of the QDs are probed by measuring the absorption. A current is measured while a negative potential is applied to the core-only QD film, but the absorption spectrum remains unchanged, indicating that injected charges are not stably injected into the conduction band of the QDs. Changing the surface ligands showed that the electrochemical reactions that occurred are coupled to the surface ligands, and no evidence was found that the negative potential resulted in the reduction of In from the QDs. Thin films made from InP/ZnSe/ZnS QDs showed a decrease in PL intensity during the spectroelectrochemical measurements without a change in absorption. This suggests that also for the InP/ZnSe/ZnS QDs, the charges do not remain in the conduction or valence band. We propose that once the film becomes conductive trap states located in the band gap are filled with injected charges, or that the injected charges induce electrochemical reactions leading to trap states. Both phenomena explain the change in PL without any changes in the absorption of the films.

Throughout these chapters, it has become clear that the surface of InP-based QDs plays a significant role in the properties of the QDs The pronounced influence of the surface on the final properties of QDs can be explained by their relatively high surface-to-volume ratio compared to bulk materials. Implementation of InP-based QDs in applications thus requires careful study and modification of the surface, whether it is to achieve high efficiency, create an electrochemically stable system, or successfully inject charges into the conduction or valence band.

Samenvatting

Kwantum stippen (KS) spelen een centrale rol in dit proefschrift en kunnen worden beschreven als nanodeeltjes van halfgeleidermateriaal welke klein genoeg zijn om kwantumopsluiting te laten plaatsvinden. Dit effect zorgt ervoor dat verschillende eigenschappen, waaronder de bandkloofenergie, afhankelijk zijn van de afmetingen van de KS. De bandkloofenergie bepaalt de uiteindelijke kleur van het licht dat door de KS wordt uitgezonden en door onze ogen wordt waargenomen. Eenvoudigweg betekent dit dat door de grootte van de KS te variëren, de kleur van de KS kan worden afgestemd. De combinatie van grootte-afhankelijke eigenschappen, een hoge fotoluminescentie (FL) kwantumopbrengst (FLKO) en een hoge kleur puurheid, maakt KS zeer aantrekkelijk voor verlichtingstoepassingen. Op InP-gebaseerde KS zijn ontwikkeld om te voldoen aan de moderne Europese regelgeving waarbij er geen verboden, toxische elementen zoals Cd en Pb gebruikt worden. Echter, de kennis en de kwaliteit van InP KS zijn nog niet zo goed als voor KS gemaakt van materialen gebaseerd op Cd en Pb, wat betekent dat verder onderzoek noodzakelijk is. Het is bekend dat de meeste problemen en vragen voor InP KS komen van de oppervlaktechemie van de KS. Dit proefschrift is daarom gewijd aan het bestuderen van het oppervlak van op InP-gebaseerde KS en het vinden van methoden om de algehele kwaliteit van de op InP-gebaseerde KS te verbeteren.

De belangrijkste concepten van op InP-gebaseerde KS worden besproken in Hoofdstuk 1. Eerst worden de algemene elektronische en optische eigenschappen van InP besproken en vergeleken met andere halfgeleidermaterialen. Vervolgens worden de meest gangbare synthesemethoden besproken en geëvalueerd. De besproken synthesemethoden zullen terugkomen in de volgende Hoofdstukken. De resulterende KS hebben vaak een zeer beperkte efficiëntie, en de fenomenen die verantwoordelijk zijn voor de beperkte efficiëntie, worden besproken samen met eerder onderzochte oplossingen. Het hoofdstuk eindigt met een overzicht van behaalde en toekomstige toepassingen van InP-gebaseerde KS.

In Hoofdstuk 2 wordt een eenvoudige postsynthese behandeling onderzocht en geoptimaliseerd om een FLKO van bijna 100% te bereiken op InP KS. Gesynthetiseerde InP KS hebben een FLKO van minder dan 1% en vertonen voornamelijk emissie van zogenaamde valkuil toestanden. Over het algemeen wordt aangenomen dat een aanzienlijk deel van de efficiëntievermindering wordt veroorzaakt door oxides en ondergecoördineerde P-atomen op het oppervlak. Oxidatie op het oppervlakte wordt voorkomen door de synthese uit te voeren onder strikt inerte omstandigheden. Passivatie van de ondergecoördineerde P-atomen kan worden bereikt door Z-type liganden aan te bieden. Een reeks metaalzouten is getest als Z-type liganden op InP KS in een behandeling bij 150 °C voor 30 minuten in aanwezigheid van $In(PA)_3$. InF_3 blijkt het meest geschikte Z-type ligand te zijn onder deze omstandigheden, wat de FLKO verhoogt naar 70%. Optimalisatie van de temperatuur en tijd van de behandeling resulteert in een FLKO van 93% voor een behandeling bij 180 °C voor 60 minuten, terwijl verbreding van de emissiepiek kan worden voorkomen. De behandeling is daarnaast ook succesvol toegepast op verschillende groottes van InP KS en op InP KS verkregen via verschillende

syntheseroutes.

In Hoofdstuk 3 worden computationele dichtheidsfunctionaaltheorie (DFT) berekeningen gebruikt om het opladen met extra elektronen van InP en InP/ZnSe KS op atomaire schaal te onderzoeken. Voor de InP KS zijn er twee modellen ontworpen, één bolvormig en de andere tetraëdrisch van vorm, gepassiveerd met Cl-atomen om oppervlakte-liganden na te bootsen met het voordeel van lagere computationele kosten. Een energiediagram met een bandkloof vrij van valkuil toestanden wordt verkregen voor deze modellen in de neutrale toestand. De toevoeging van één extra elektron leidt tot de vorming van een valkuil toestand in beide modellen en het blijkt dat ondergecoördineerde In-atomen verantwoordelijk zijn voor de vorming van deze valkuil toestanden. InP/ZnSe KS modellen met alle In-atomen volledig gecoördineerd kunnen worden opgeladen met elektronen zonder de vorming van valkuil toestanden. Deze resultaten tonen aan dat ondergecoördineerde In-atomen moeten worden vermeden voor InP-gebaseerde KS om stabiel te zijn bij oplading.

Om de experimentele effecten van het opladen van op InP-gebaseerde KS te onderzoeken, worden spectro-elektrochemische experimenten uitgevoerd op dunne films van InP en InP/ZnSe/ZnS KS en de resultaten zijn beschreven in Hoofdstuk 4. Een dispersie van InP KS wordt op een geleidend substraat gedruppeld en gedroogd om een dunne film te creëren. De film wordt vervolgens in een elektrochemische cel geplaatst en een cyclisch voltammogram is opgenomen, waarbij het potentiaal wordt gescand tussen twee maxima terwijl de stroom wordt opgenomen. Gelijktijdig worden de optische eigenschappen van de KS onderzocht door de absorptie te meten. Een stroom wordt gemeten wanner een negatieve potentiaal over de InP KS film wordt aangelegd, maar het absorptiespectrum blijft onveranderd, wat aangeeft dat geïnjecteerde ladingen niet stabiel in de geleidingsband van de KS worden geïnjecteerd. Verandering van de liganden op het oppervlakte toont aan dat de elektrochemische reacties die optreden gekoppeld zijn aan de oppervlakte liganden. Daarnaast is er geen bewijs gevonden dat de negatieve potentiaal resulteerde in de reductie van In uit de KS. Dunne films gemaakt van InP/ZnSe/ZnS KS toonden een afname in FL intensiteit tijdens de spectro-elektrochemische metingen zonder een verandering in absorptie. Dit wijst erop dat ook voor de InP/ZnSe/ZnS KS, de ladingen niet in de geleidings- of valentieband blijven. Het is onze hypothese dat zodra de film geleidend wordt, valkuil toestanden in de bandkloof worden gevuld met geïnjecteerde ladingen, of dat de geïnjecteerde ladingen elektrochemische reacties induceren die leiden tot valkuil toestanden. Beide fenomenen verklaren de verandering in FL zonder enige veranderingen in de absorptie van de films.

Door de Hoofdstukken heen is het duidelijk geworden dat het oppervlak van InP gebaseerde KS een zeer sterke rol speelt in de eigenschappen van de KS. De uitgesproken invloed van het oppervlak op de uiteindelijke eigenschappen van QDs kan worden verklaard door hun relatief hoge oppervlakte-tot-volume verhouding vergeleken met bulk materialen. Implementatie van InP gebaseerde KS in toepassingen vereist dus zorgvuldige studie en aanpassing van het oppervlak, of het nu is om hoge efficiëntie te bereiken, een elektrochemisch stabiel systeem te creëren, of succesvol ladingen in de geleidings- of valentieband te injecteren.

115

Acknowledgements

The most-read section of the average thesis is, in all likelihood, the acknowledgments. Whether this is due to the vanity of the reader or the collaborative nature of a thesis, is left for others to decide. What I do know is that my thesis would never have been completed solely through my own efforts. I am profoundly grateful to everyone who supported me in any way throughout this journey. Colleagues, friends and family, I've learned so much from you, and for that, I am deeply thankful.

First and foremost, I want to express my gratitude to my supervisor, **Arjan**. Thank you for entrusting me with this PhD position, even though I came from a different background. I appreciate the freedom I was given throughout my research, which allowed me to grow both as a scientist and as a person. Even more, I'm grateful for the moments when I could rely on your knowledge and expertise during our meetings. Often, I would enter those meetings feeling lost and confused by my results, and you would reassure me that things weren't as bad as they seemed. You taught me so much about quantum dots, spectroscopy, and "where electrons prefer to go". I have truly enjoyed our collaboration, our discussions about science, and our conversations about what really matters in life.

Tom, your wise counsel ensured that Arjan and I avoided getting stuck in the myriad of questions we encountered. Although we didn't have frequent scientific meetings, you played a key role in shaping this thesis. You encouraged us to plan publications and this thesis well in advance. I also want to thank you for the enjoyable conversations during lunch, at OM outings, and during your office walks.

Your vast knowledge of chemistry people has been invaluable for my PhD research, **Michael**. During your postdoc in the OM group, you contributed greatly to both scientific and non-scientific aspects of our work. You were always the go-to person for questions about chemicals, equipment, or data processing, and I eagerly took advantage of your expertise. I also thoroughly enjoyed our car rides to and from Delft, even if the mornings were often marked by mutual grumpiness. Thank you for all your help, for all the listening to my complaints and for advising on my experiments. I enjoyed all our conversations in the car, which ranged from light topics like sports to deeper, personal matters. I look forward to seeing you soon on the squash court, where we can bond over a drink and over our ever improving fitness!

Jence, we first met when you gave me a tour during my interview. Your open nature and friendliness immediately made me feel you would be a wonderful colleague, and you have far exceeded those expectations! Despite facing your own challenges, you were always willing to help when I needed support. I am immensely grateful for your assistance with my research, but even more so for the mental support, coffee breaks, and chats along the way. You made the OM group a fun place to work at and I'm sure you are doing the same at your new job.

Indy, I truly enjoyed sharing an office with you. Though we mostly met online, the times you were at TU Delft were always filled with special moments ranging from scientific discussions to playing frisbee with a mousepad. Thank you for your patience while teaching me DFT calculations, processing the resulting data, and helping me developing an appreciation for piano music. I'm especially grateful that we could share highs and lows outside of work, including music, gardening, baking, and complaining about people. You really helped me through difficult parts of this journey with your support and advise.

"Complaining works", is one of the most valuable non-scientific lessons I've learned from you, **Ferdinand**. This idea is part of a broader concept you taught me: that it's good to question the status quo. Thank you for helping me navigate computational challenges and for all the moments of laughter we shared.

Laurens, you've shown me the importance of maintaining curiosity and that there's always more to learn. I admire your inquisitive mindset, especially during the many OM meetings, where you would always ask insightful questions to better understand the findings of our research. Thank you for all your thoughtful questions and for the wonderful conversations!

Yan, thank you so much for sharing your scientific wisdom with me. I continue to be impressed by your approach to experiments and how you consistently bring them to successful completion—a true "experiment whisperer". Beyond that, you were a fantastic colleague, always ready to think along with my challenges. I'm deeply grateful for your support, our discussions (both scientific and non-scientific), and all the lunches we shared.

Reinout, it was a great privilege to work alongside you. You have an incredible analytical ability, and I was always grateful when you took the time to think along with me on my research. You are one of those scientists who thinks carefully before speaking, which results in well-thought-out arguments and discussions. I also thoroughly enjoyed our collaborations and the trips we made together to Germany, Switzerland, and Belgium. Wherever you work next, I'm confident you will be an incredible asset to the organization!

I've learned so much from you, **Hua**—though unfortunately, I can't repeat the Chinese words you taught me here, and you know why! Your scientific contributions to our group were impressive from day one, and for me, you will always be "the master of light." I'm certain you will excel in all the experiments you take on. You are a truly remarkable person, and I cherished every moment of our collaboration. I still owe you the recipe for my mother's apple pie, and I promise you will get it! Thank you for the laughter, the time we shared in the OM group, and the memories we created. I hope we'll continue to meet occasionally for lunch or drinks.

Present at both the beginning and the end of my PhD in different roles. **Jaco**, it was a privilege to be trained by you in the lab, and I've always admired your passion for physics, chemistry, and everything in between. You make science look effortless, but I know how much hard work lies behind it. Even after leaving the lab, you were always available to help with technical and scientific challenges. You're an amazing person, and I'm thrilled that you now live in Leiden. I look forward to enjoying your company, whether it's in the bouldering gym, over a delightful dinner, or in a laser lab.

117

Guilherme, you helped me create my very first quantum dots, which formed the foundation of this entire thesis. You assisted me with experimental design, execution, data processing, and critically analysing my results. I am incredibly grateful for your guidance and support throughout this journey.

Zimu, your perseverance continues to amaze me. Despite challenges like the Covid-19 pandemic and setbacks with your setup, you produced an outstanding thesis and secured a well-deserved postdoc position at Cambridge University. I've enjoyed our conversations about food and the importance that it takes in our lives. I'm sure you are be doing an amazing job in the lab you are working in now and I wish you the best on your future adventures.

Lara, after your work with us on InP QDs, you decided to switch to "the other side". I'm confident you'll do equally impressive work with the perovskite materials as you did with the quantum dots. Thank you for the enjoyable chats and coffee breaks we shared while both working on our writing. I appreciated our venting sessions, which left us both feeling lighter afterwards. I wish you all the best with your continued research into perovskites!

Your kindness and positive energy have made this PhD journey much more manageable, **Jasmeen**. It was a pleasure to be part of the same group as you. I've always enjoyed discussing both science and various other topics with you, and I'm deeply impressed by how quickly you've improved in both the Dutch language and the art of small talk.

Maryam, your guidance was essential at the beginning of my PhD, helping me in the lab and spending countless hours with me in the cleanroom. You also reassured me not to stress about my slow progress in the beginning, reminding me that things naturally pick up later—and you were absolutely right! Thank you for all the support and guidance you provided.

Deepika, our shared moments of venting about the challenges of wrapping up a PhD, drawing analogies between Harry Potter and this PhD journey, and taking short office breaks have been invaluable in keeping me motivated to tackle experiments and writing. Thank you for being my office companion through it all.

Solrun, despite being in the final stages of your own PhD and dealing with a pandemic, you still found time to help me get started with mine. Thank you for your guidance in the lab, repairing electrochemical caps, and working with the spectroelectrochemical setup. Your help during such a challenging time was greatly appreciated.

A special word of thanks goes to the team that makes research possible at TU Delft. **Adinda**, I could always come to you with my questions, and I truly enjoyed our conversations about vacations, cookies, and horses. It was a pleasure working with you, and I am grateful for all your help. **Bahiya**, thank you so much for your solutions to the various lab problems we encountered. Your energy and determination in tackling challenges and always finding solutions are inspiring. It was a delight to chat with you, and I am thankful for our collaboration. **Nick** and **Ruben**, our previous lab managers, thank you for your assistance both in and outside the lab. **Jos**, you are known both within and outside the OM group

for your immense knowledge and expertise. It was a privilege to work with you, and I'm grateful for your support. You were always willing to help and brainstorm about solutions, and when there were no pressing problems, I enjoyed our conversations immensely. **John**, without your contributions to the spectroelectrochemistry setup, Chapter 4 likely wouldn't exist. Thank you for your help with the setup and for repairing the disconnected cables of the electrochemical cells. **Pierre**, although we didn't work together extensively, you left a lasting impression. Your positive energy and curiosity are truly inspiring. I look forward to hearing more about your adventures as a teacher in China, penguin weigher, Antarctic explorer, and all your other endeavours. **Wiel**, the list of ways you've supported the OM group could in itself form a thesis. Apart from your help with the TEM, gloveboxes, and the electrochemistry setup, I enjoyed our discussions about science, the OM group, and raising kids. **Bart**, thank you for all your help with the XPS measurements. Your friendly and helpful nature made working with you a pleasure. **Marcel**, although we didn't conduct research together, I greatly appreciate your positive mindset and enthusiasm for science, which contributed to this thesis. I enjoyed hearing about your theatre performances and discussing our volleyball matches. I still hope we will play against each other one day.

This thesis would not have taken its current form without the contributions of the students I had the privilege of supervising during my PhD. **Mourijn**, you worked incredibly hard on the synthesis of InP-based QDs. The sheer number of syntheses you performed is impressive, and the results you obtained significantly enhanced our understanding of QDs. It was a pleasure to work with you and see how quickly you became independent. **Irene**, I remember how happy you were to finally say goodbye to the glovebox after spending so much time working in it. I hope your memories aren't solely filled with negative thoughts about the gloveboxes! You worked extremely hard on synthesizing QDs, creating thin films, and electrochemically charging these QD films. Your work was pivotal for Chapter 4. **Colin**, you took on a very challenging project, working on the synthesis of ZnSe/ZnS QDs and attempting to charge them together with me and Jence. I enjoyed diving into this project with you and appreciated how quickly you picked up knowledge about our research. **Niels**, you also worked on creating InP-based QDs for electrochemical charging experiments. Despite the restrictions on lab access due to the pandemic, you managed your lab work efficiently and achieved outstanding results. **Jitske**, you perhaps tackled the most challenging project of all. Your task was to develop Python simulations for electrochemical measurements, all while working remotely due to Covid-19. You worked incredibly hard and you made the most of it under the given circumstances. Thank you all for working with me and contributing to my research. I thoroughly enjoyed collaborating with each of you and am deeply grateful for all that I learned from you.

Of course, the entire OM group contributed to this thesis, not only through critical questions during the Friday afternoon discussions but perhaps more importantly by creating an incredibly welcoming, safe, and supportive work environment. I would like to thank everyone mentioned above, as well as the following individuals who, although I worked with them less directly, contributed to the positive atmosphere in the OM group: **Goutam, Hamit, Jiashang, Jin, Katerina, Lennart, Magnus, María, Michelle, Nisha, Reinder, and Valentina**.

My heartfelt thanks go to my amazing friends in Leiden and the surrounding areas. **Anne, Stan, Marije, Martijn, Samantha, Vincent, and Huub**, you are incredible people, and I am so grateful to have you in my life and for all the support you've given me in so many ways: game nights, dinners, concerts, weekend trips, co-working sessions, listening to my complaints about my PhD, volleyball matches, bouldering (reluctantly, for some of you), coffee dates, parties, and all the other fun and memorable adventures we've shared. Knowing I could rely on you when I needed to was truly comforting!

Amaya, Mirjam, and Rafael, you've stuck with me as friends since we started our bachelor's program. Thank you for our regular catch-ups, lovely dinners, and all the support throughout my PhD.

Sports have always been an essential part of my life for relaxation and recharging. To my teammates, volleyball friends, and bouldering friends—**Bart, Ben, Cas, Casper, Christiane, Coen, Daphne, Emy, Friso, Govert, Hessel, Jaap, Jaime, Jasper, Jesse, Jessica, Jessy, Jonathan, Joris, Koen, Lars, Laura, Lieke, Maartje, Maurice, Max, Niels, Olivier, Pjotr, Rogier, Sietse, Sjoerd, Tim, Tom E., and Tom N.**—thank you for the exciting matches, fun post-game drinks, and all your support during my PhD.

A special word of thanks goes to our cat, **Marley**. Animals naturally understand emotions better and never ask tough questions!

Of course, I also want to thank my family, especially **Leon** and my parents. **Leon**, you have always been my role model. Thanks to you, I learned to explore—first with blocks and LEGO, now with atoms and molecules. As kids, we said we wanted to be inventors, and I think we've both achieved that in our own ways. Thank you for everything you've taught me, as a child and as an adult, and for always being there when I need you.

Leo and Marion, because of you, I had the opportunity to study and, ultimately, pursue a PhD. I'm grateful for all your support, for listening to my scientific stories, and for being amazing parents.

Last but certainly not least, my deepest gratitude goes to **Melanie**. You were there at every step of my PhD journey and witnessed all the highs and lows. Thank you for reassuring me when doubts crept in, for discussing my results, and for giving me the gentle push I needed when my motivation faltered. You made sure that the achievements I made during my PhD were acknowledged as I was too often focussed on the things that still had to be done. Sharing this journey with you—through both of our PhDs—has been invaluable. I'm deeply grateful for the open conversations we had about our research and the mutual support we provided each other. Your curious nature, patience, and attentive ear make you the perfect partner for me. I'm profoundly thankful that you have always been there for me, and want to continue to be there for me. You are my rock, and I couldn't have done this without you.

List of Publications

Yan B. Vogel, Maarten Stam, Jence T. Mulder, Arjan J. Houtepen. "Long-Range Charge Transport via Redox Ligands in Quantum Dot Assemblies". *ACS Nano* 2022**,** *16* (12), 21216-21224.

Maarten Stam, Indy du Fossé, Ivan Infante, Arjan J. Houtepen. "Guilty as Charged: The Role of Undercoordinated Indium in Electron-Charged Indium Phosphide Quantum Dots". *ACS Nano* 2023**,** *17* (18), 18576-18583.

Guilherme Almeida, Reinout F. Ubbink, Maarten Stam, Indy du Fossé, Arjan J. Houtepen. "InP colloidal quantum dots for visible and near-infrared photonics". *Nature Reviews Materials* 2023**,** *8* (11), 742-758.

Maarten Stam, Guilherme Almeida, Reinout Ubbink, Lara M. van der Poll, Yan B. Vogel, Hua Chen, Luca Giordano, Pieter Schiettecatte, Zeger Hens, Arjan J. Houtepen. "Near-Unity Photoluminescence Quantum Yield of Core-Only InP Quantum Dots via a Simple Postsynthetic InF_3 Treatment". *ACS Nano* 2024**,** *18* (22), 14685-14695.

Yan B. Vogel, Le N. Pham, Maarten Stam, Reinout F. Ubbink, Michelle L. Coote, Arjan J. Houtepen. "Solvation Shifts the Band-Edge Position of Colloidal Quantum Dots by Nearly 1 eV". *Journal of the American Chemical Society* 2024**,** *146* (14), 9928-9938.

Curriculum Vitae

Maarten Stam was born on the 3rd of March 1996 in the town of Oud-Beijerland, The Netherlands. In 2014, he started the bachelor programme Molecular Science and Technology, a joint degree between Leiden University and Delft University of Technology, and he was awarded the scholarship "Topsector Chemiebeurs". After the completion of the thesis project entitled "The immobilization of a Ni(cyclam)$^{2+}$ complex on a gold electrode for the electrocatalytic reduction of CO_2", he graduated cum laude. Subsequently, he started the master's programme Chemistry at Leiden University in 2017. By defending his master's thesis with the title "Bridging the gap between heterogeneous and homogeneous catalysis by immobilizing catalysts on electrodes for reduction of O_2", he obtained his master's degree. In 2020, Maarten joined the Optoelectronic Materials group at Delft University of Technology to begin the journey of his PhD project under the supervision of Prof. Dr. Arjan Houtepen and Dr. Tom Savenije.

Outside the office, Maarten spends his time on the volleyball court or in the bouldering hall, enjoying both the physical and mental challenges from both sports. Besides these activities, he enjoys reading a good book, gaming and playing board games with friends.